CHARACTERIZATION AND TRANSPORT PROPERTIES OF PVA–LiBOB BASED POLYMER ELECTROLYTES WITH APPLICATION IN DYE SENSITIZED SOLAR CELLS

IKHWAN SYAFIQ BIN MOHD NOOR

FACULTY OF SCIENCE
UNIVERSITY OF MALAYA
KUALA LUMPUR

2016

CHARACTERIZATION AND TRANSPORT PROPERTIES OF PVA–LiBOB BASED POLYMER ELECTROLYTES WITH APPLICATION IN DYE SENSITIZED SOLAR CELLS

IKHWAN SYAFIQ BIN MOHD NOOR

THESIS SUBMITTED IN FULFILLMENT OF THE REQUIREMENT FOR THE DEGREE OF DOCTOR OF PHILOSOPHY

FACULTY OF SCIENCE
UNIVERSITY OF MALAYA
KUALA LUMPUR

2016

UNIVERSITY OF MALAYA
ORIGINAL LITERARY WORK DECLARATION

Name of Candidate : **Ikhwan Syafiq bin Mohd Noor**

Registration/Matric No : **SHC130022**

Name of Degree : **Doctor of Philosophy**

Title of Project Paper/Research Report/Dissertation/Thesis (“this Work”):

Characterization and Transport Properties of PVA–LiBOB Based Polymer Electrolytes with Application in Dye Sensitized Solar Cells

Field of Study : **Experimental Physics**

I do solemnly and sincerely declare that:

(1) I am the sole author/writer of this Work;
(2) This Work is original;
(3) Any use of any work in which copyright exists was done by way of fair dealing and for permitted purposes and any excerpt or extract from, or reference to or reproduction of any copyright work has been disclosed expressly and sufficiently and the title of the Work and its authorship have been acknowledged in this Work;
(4) I do not have any actual knowledge nor do I ought reasonably to know that the making of this work constitutes an infringement of any copyright work;
(5) I hereby assign all and every rights in the copyright to this Work to the University ofMalaya (“UM”), who henceforth shall be owner of the copyright in this Work and that any reproduction or use in any form or by any means whatsoever is prohibited without the written consent of UM having been first had and obtained;
(6) I am fully aware that if in the course of making this Work I have infringed any copyright whether intentionally or otherwise, I may be subject to legal action or any other action as may be determined by UM.

Candidate’s Signature Date:

Subscribed and solemnly declared before,

Witness’s Signature Date:

Name:

Designation:

ABSTRACT

The objectives of this work are to (i) produce high conducting solid and gel poly(vinyl alcohol) (PVA) based polymer electrolytes incorporated with lithium bis(oxalato)borate (LiBOB) salt, (ii) determine and analyse the transport properties of charge carriers of solid and gel PVA–based electrolyte and (iii) study the influence of LiBOB–TBAI and LiBOB–TBAI–BMII gel electrolyte on the performance of dye sensitized solar cells (DSSCs). Three electrolyte systems were prepared i.e. PVA–LiBOB solid and gel electrolytes, PVA–LiBOB–TBAI–I_2–DMF and PVA–LiBOB–TBAI–BMII–I_2–DMF gel electrolytes. The highest room temperature conductivity (σ) obtained for PVA–LiBOB solid electrolyte was 2.83×10^{-4} S cm^{-1} with 60 wt.% PVA: 40 wt.% LiBOB. Mobility (μ) and number density (n) was 9.58×10^{-7} cm^2 V^{-1} s^{-1} and 1.85×10^{21} cm^{-3}, respectively. In gel form the σ of this electrolyte with 60 wt.% PVA–40 wt.% LiBOB (B0 electrolyte) is enhanced to 7.31×10^{-3} S cm^{-1}. μ and n was 8.41×10^{-5} cm^2 V^{-1} s^{-1} and 5.42×10^{20} cm^{-3}, respectively. In order to use these electrolytes in DSSC, tetrabutylammonium iodide (TBAI) and iodine (I_2) have been added in B0 electrolyte to generate redox process. The electrolyte with composition 17.53 wt.% PVA–1.75 wt.% LiBOB–9.93 wt.% TBAI–0.68 wt.% I_2–70.11 wt.% DMF (B5 electrolyte) exhibits σ of 5.13×10^{-3} S cm^{-1} and the DSSC utilizing this electrolyte exhibits the highest efficiency of 6.11%. The values of μ and n obtained were 9.58×10^{-5} cm^2 V^{-1} s^{-1} and 3.35×10^{20} cm^{-3}, respectively. In a further attempt to increase solar efficiency, 1–butyl–3–methylimidazolium iodide (BMII) was added to B5 electrolyte and efficiency becomes 7.28% when added with 9 wt.% BMII. The conductivity is enhanced to 7.52×10^{-3} S cm^{-1} and μ is 9.52×10^{-5} cm^2 V^{-1} s^{-1} and n is 4.93×10^{20} cm^{-3}. Conductivity for all electrolytes prepared in this work increased with increasing temperature. This work also reports the significance of Li$^+$ in determining how the performance of the DSSC can be controlled.

ABSTRAK

Objektif kajian ini adalah untuk (i) menghasilkan elektrolit pepejal dan gel berkekonduksian tinggi berasaskan poli(vinil alkohol) (PVA) kompleks dengan garam lithium bis(oxalato)borate (LiBOB), (ii) menentukan dan menganalisa sifat pengangkutan pembawa cas untuk PVA–elektrolit polimer pepejal dan gel, dan (iii) mengkaji pengaruh LiBOB–TBAI dan LiBOB–TBAI–BMII elektrolit gel terhadap prestasi pewarna pemeka sel suria (DSSCs). Tiga sistem elektrolit telah dihasilkan iaitu PVA–LiBOB elektrolit pepejal dan gel, PVA–LiBOB–TBAI–I_2–DMF dan PVA–LiBOB–TBAI–BMII–I_2–DMF elektrolit gel. Kekonduksian (σ) optimum pada suhu bilik untuk PVA–LiBOB elektrolit pepejal adalah 2.83×10^{-4} S cm^{-1} dengan 60 wt.% PVA:40 wt.% LiBOB. Mobiliti (μ) dan ketumpatan ion bebas (n) masing-masing adalah 9.58×10^{-7} cm^{2} V^{-1} s^{-1} dan 1.85×10^{21} cm^{-3}. Dalam bentuk gel, σ elektrolit dengan 60 wt.% PVA–40 wt.% LiBOB (elektrolit B0) meningkatkan kepada 7.31×10^{-3} S cm^{-1}. μ dan n masing–masing adalah 8.41×10^{-5} cm^{2} V^{-1} s^{-1} dan 5.42×10^{20} cm^{-3}. Untuk menggunakan elektrolit–elektrolit ini dalam DSSC, tetrabutylammonium iodide (TBAI) dan iodine (I_2) telah ditambah ke dalam elektrolit B0 untuk menghasilkan proses redox. Elektrolit dengan komposisi 17.53 wt.% PVA–1.75 wt.% LiBOB–9.93 wt.% TBAI–0.68 wt.% I_2–70.11 wt.% DMF (elektrolit B5) mempamerkan σ 5.13×10^{-3} S cm^{-1} dan DSSC dengan electrolit ini mempamerkan kecekapan tertinggi iaitu 6.11%. Nilai μ dan n diperolehi masing-masing adalah 9.58×10^{-5} cm^{2} V^{-1} s^{-1} dan 3.35×10^{20} cm^{-3}. Dalam usaha meningkatkan kecekapan solar, BMII ditambah kepada elektrolit B5 dan kecekapan menjadi 7.28% untuk 9 wt.% BMII. σ meningkat kepada 7.52×10^{-3} S cm^{-1} dan μ ialah 9.52×10^{-5} cm^{2} V^{-1} s^{-1} dan n ialah 4.93×10^{20} cm^{-3}. Kekonduksian kesemua elektrolit yang dihasilkan dalam kerja ini meningkat dengan peningkatan suhu. Kerja ini juga melaporkan kepentingan Li^{+} dalam menentukan bagaimana prestasi DSSC boleh dikawal.

ACKNOWLEDGEMENT

بِسْمِ ٱللَّهِ ٱلرَّحْمَٰنِ ٱلرَّحِيمِ

In the name of Allah, Most Gracious, Most Merciful. Salawat and salaam to the beloved Prophet Muhammad SAW. Alhamdulillah, I am very thankful to Allah for giving me strength, patience and health in completing this work.

I would like to express my infinite appreciation and gratitude to my supervisor, Professor Dr. Abdul Karim bin Haji Mohd Arof for his guidance and encouragement in completing this work. He was my mentor who is full with knowledge and never stingy in sharing knowledge. He guides me to be a good researcher and shed a light towards research field. I would like to extend my thanks to my co–supervisor, Dr. Siti Rohana binti Majid for his guidance and support in making sure I kept an interest in these research studies.

I would like to thank my parents (Mohd Noor bin Ali and Norsidah binti Haron) for their prayers and encouragement until this thesis is complete. I am very grateful to have parents who always supported me in achieving my ambition to get a PhD degree. I am thankful also to my sibling for their support.

To all my lab mates in Centre for Ionics University of Malaya (CIUM), thank you for the help, support and encouragement in completing this research study. The golden moments are the knowledge sharing and discussion we made to keep research expended.

Last but not list, I would like to thanks University of Malaya for giving me a sponsorship (Skim Biasiswa Universiti Malaya) during my studies for three years.

TABLE OF CONTENTS

CHAPTER 1 : INTRODUCTION TO THE THESIS

CHAPTER 2 : LITERATURE REVIEW

CHAPTER 3 : EXPERIMENTAL METHODS

CHAPTER 4 : RESULTS FOR PVA–LiBOB SOLID POLYMER ELECTROLYTE SYSTEM

CHAPTER 5 : RESULTS FOR PVA–LiBOB–TBAI–I_2–DMF GEL POLYMER ELECTROLYTE SYSTEM

CHAPTER 6 : RESULTS FOR PVA–LiBOB–TBAI–BMII–I_2–DMF GEL POLYMER ELECTROLYTE SYSTEM

CHAPTER 7 : RESULTS FOR DYE SENSITIZED SOLAR CELLS

LIST OF FIGURES

LIST OF TABLES

LIST OF SYMBOLS AND ABBREVATIONS

CPE	:	Constant phase element
DSSC	:	Dye sensitized solar cell
EIS	:	Electrochemical impedance spectroscopy
FTIR	:	Fourier transform infrared spectroscopy
GPE	:	Gel polymer electrolyte
SPE	:	Solid polymer electrolyte
wt.%	:	Weight percent
C	:	Bulk geometrical capacitance
C_e	:	Electrical double layer (EDL) capacitance
D	:	Diffusion coefficient of charge carriers
d	:	Sample thickness
e	:	Elementary charge
FF	:	Fill factor
I	:	Iodide
I_3	:	Triiodide
J_{opt}	:	Optimum current density
J_{sc}	:	Short circuit current density
k_b	:	Boltzmann constant
M_w	:	Molecular weight
n	:	Number density of charge carriers
P_{in}	:	Incident power density
R_b	:	Bulk resistance
T	:	Temperature
V_{oc}	:	Open circuit voltage
V_{opt}	:	Optimum voltage
Z'	:	Real impedance
Z''	:	Negative imaginary impedance
ε_o	:	Vacuum permittivity
ε_r	:	Dielectric constant
η	:	Solar conversion efficiency
λ	:	Electrical double layer thickness
μ	:	Mobility of charge carriers
σ	:	Ionic conductivity
ω	:	Angular frequency
AN	:	Acetonitrile
BMII	:	1–butyl–3–methylimidazolium iodide
CNT	:	Carbon nanotube
CoS_2	:	Cobalt sulfide
CoSe	:	Cobalt selenide
$Cu(NO_3)_2$	:	Copper(II) nitrate
CuS	:	Copper sulfide
DMC	:	Dimethyl carbonate
DMF	:	Dimethylformamide
EC	:	Ethylene carbonate
EMIDCN	:	1–ethyl–3–methylimidazolium dicyanamide
EMITFO	:	1–ethyl–3–methylimidazolium trifluoromethanesulfonate
EMITFSI	:	1–ethyl–3–methylimidazolium bis(trifluoromethylsulfonyl)imide
HMII	:	1–hexyl–3–methylimidazoulium iodide

K34 : Butyl–bis(3–methylimidazolium)diiodide
K35 : Octyl–bis(3–methylimidazolium)diiodide
K36 : Triethyleneglycol–bis(3–methylimidazolium)diiodide
KI : Potassium iodide
KOH : Potassium hydroxide
$LiAsF_4$: Lithium arsenicfluoride
$LiBF_4$: Lithium tetrafluoroborate
LiBOB : Lithium bis(oxalato)borate
$LiCF_3SO_3$: Lithium trifluoromethanesulfonate
$LiClO_4$: Lithium perchlorate
LiI : Lithium iodide
$LiN(SO_2CF_3)_2$: Lithium bis(trifluoromethanesulphonyl)imide
Mo_2C : Molybdenum carbide
Mo_2N : Molybdenum nitride
MoO_2 : Molybdenum(IV) oxide
MoS_2 : Molybdenum disulfide
MPN : 3–methoxy propyonitrile
NBB : N–Butylbenzimidazole
NbN : Niobium nitride
NH_4Br : Ammonium bromide
NH_4Cl : Ammonium chloride
NH_4I : Ammonium iodide
NH_4NO_3 : Ammonium nitrate
$NiCoSe_2$: Nickel cobalt sulfide
$NiSe_2$: Nickel diselenide
PAN : Poly(acrylonitrile)
PC : Propylene carbonate
PEO : Poly(ethylene oxide)
PMII : 1–methyl–3–propylimidazolium iodide
PMMA : Poly(methyl methacrylate)
Pt : Platinum
PVA : Poly(vinyl alcohol)
PVAc : Poly(vinyl acetate)
PVC : Poly(vinyl chlorid)
PVDF : Poly(vinylidene fluoride)
PVDF–HFP : Poly(vinylidenefluoride–hexafluoropropylene)
SnO_2 : Tin dioxide
TBAI : Tetrabutylammonium iodide
TBP : *Tert*–butyl pyridine
TEGDI : Tetraethyleneglycol–bis(3–methylimidazolium)diiodide
TiC : Titanium carbide
TiN : Titanium nitride
TiO_2 : Titanium dioxide
TMAI : Tetramethylammonium iodide
TPAI : Tetrapropylammonium iodide
V_2O_3 : Vanadium(III) oxide
VC : Vanadium carbide
WC : Tungsten carbide
WS_2 : Tungsten(IV) sulfide
ZnO : Zinc oxide

LIST OF APPENDICES

CHAPTER 1 : INTRODUCTION TO THE THESIS

1.1. Introduction

Polymer electrolyte is an ionic conductor used in electrochemical devices. To obtain good performance from electrochemical devices, the polymer electrolyte membrane must have excellent–properties such as good ionic conductivity, thermal, mechanical and electrochemical stabilities. Among all these properties, ionic conductivity is the main focus in this work.

The ionic conductivity (σ) of a polymer electrolyte is given by:

$$\sigma = n\mu e \tag{1.1}$$

where n is number density and μ is the mobility of charge carriers, and e is the elementary charge. It can be seen from equation (1.1) that n and μ are two important parameters that control the conductivity of polymer electrolytes. Thus, it is essential that n and μ quantitatively be determined. Knowledge of these parameters can shed some light on the mechanism of ion transport in these polymer membranes and how the ions indirectly influence the performance of electrochemical devices.

Dye sensitized solar cells (DSSCs) are among the many electrochemical devices that have received much attention due to their environmental friendliness, easy fabrication, ability to exhibit high solar energy efficiency and low cost (O'regan & Grätzel, 1991). A common DSSC consists of an electrolyte sandwiched between titanium dioxide (TiO_2) photoanode that has been soaked with a dye and a platinum (Pt) counter electrode. The electrolyte must contain a redox mediator for regeneration of oxidized dyes (Grätzel, 2003). The most preferable redox couple is I^-/I_3^- because their rate of recombination with electrons injected from the sensitizing dye is slow (Arof *et al.*, 2013).

The efficiency of DSSCs is known to increase on using polymer electrolytes containing binary iodide salts. According to Arof *et al.* (2013), a DSSC consisting of a PVA–based gel polymer electrolyte with 59.6 wt.% KI–40.4 wt.% Pr_4NI salt composition exhibited the highest efficiency of 3.27% under 1 Sun illumination at room temperature. Under similar conditions, Dissanayake *et al.* (2012) have also reported that DSSCs utilizing PAN–based gel electrolyte with 16.6 wt.% KI–83.4 wt.% Pr_4NI binary salt composition showed an efficiency of 5.36%. The mixed cation effect resulted in the high efficiency of the DSSC (Shi *et al.*, 2011). The size of cation plays an important role in intercalating into the TiO_2 mesopores. The small sized cations (e.g. Li^+ and K^+) can easily enter the mesoporus TiO_2 semiconducting layer of the photoanode and get adsorbed on the TiO_2 surface compared to the bigger sized cations (e.g. Pr_4N^+). The cations with smaller size will accumulate at the surface of TiO_2 thus shifting the conduction band of TiO_2 towards the redox potential of the I^-/I_3^- mediators. This increases the energy difference between the conduction band and the excited state of the dye resulting in the increase in the electron injection rate that leads to higher short circuit current. On the other hand, iodide salts with larger cations dissociate easily due to low lattice energy giving more free iodide ions that helps complete the circuit faster. Increase in mobile iodides as well as high iodide mobility can facilitate greater current flow when the iodide ions transfer electrons to the oxidized dye molecules from the counter electrode for dye regeneration.

Binary iodide salts added to the polymer electrolyte consist of a small and a big cations to enhance the performance of DSSCs. However, the effect of cation cannot be understood clearly due to the presence of I^- ions coming from both iodide salts. As far as we are aware, there are no reports on DSSCs employing double salts that incorporate an iodide and a non–iodide salt. Thus, in this work, a non–iodide salt will used in the electrolyte to provide the smaller cations without producing I^- ions simultaneously. The small cations from the non–iodide salt are expected to modify the surface states of the photoanode semiconducting layer and increase the current density of the DSSC by increasing electron injection into the conduction band of the semiconductor (Dissanayake *et al.*, 2012).

1.2. Objectives of the Thesis

Poly(vinyl alcohol) or PVA was used in this work as the polymer host. The objectives of this work are summarized as below:

- to produce new solid polymer electrolytes based on PVA–LiBOB complexes.
- to enhance PVA–LiBOB solid electrolyte conductivity by changing it into gel form, as well as incorporating the electrolyte with an iodide salt and an ionic liquid.
- to determine and analyse the transport properties of charge carriers of PVA–based solid and gel polymer electrolyte.
- to ensure that the electrolyte is usable for dye–sensitized solar cell application (DSSC) by adding I_2 crystals so as to form the I^-/I_3^- redox couple.
- to investigate whether a non–iodide salt e.g. LiBOB can affect performance of the DSSCs.
- to study the influence of ionic liquid on the performance of DSSCs.

1.3. Scope of the Thesis

This thesis consists of nine chapters. The first chapter begins with an introduction to the scope of work. Chapter 2 gives an overview of polymer electrolytes which comprises solid and gel electrolytes, selection and properties of materials used, and an inexhaustive review about DSSCs as well as its working principle. Chapter 3 describes the details of sample preparations and characterizations such as fourier transform infrared (FTIR) spectroscopy, electrochemical impedance spectroscopy (EIS) and DSSC fabrications.

Chapter 4 presents characterization results from infrared and impedance spectroscopies. FTIR studies prove the formation of polymer–salt complexes and evaluate the percentage of free and contact ions from which the number density, mobility and diffusion coefficient will be determined and deconvoluted to determine the percentage of free ions can be obtained. From EIS studies, the composition giving the highest ionic conductivity can be determined and the transport parameters similar to that obtained from FTIR studies can also be obtained, but purely from impedance data.

Chapter 5 describes the results obtained from characterization of PVA–LiBOB–TBAI–I_2–DMF gel polymer electrolyte system. Studies investigate the complexation of polymer–salt, polymer–salt–plasticizer, and deconvolution of the bands corresponding to free and contact ions following results based on FTIR. EIS study will reveal how the ionic conductivity varies with composition and temperature. Transport parameters such as mobility, diffusion coefficient and concentration of mobile ions at room and varied temperatures will also be determined.

The results obtained from characterization of PVA–LiBOB–TBAI–BMII–I_2–DMF gel polymer electrolyte system will be displayed in Chapter 6. Infrared spectroscopic studies investigate the complexation of polymer–salt–ionic liquid and polymer–salt–plasticizer–ionic liquid, and deconvolution of bands corresponding to free and contact ions to determine their concentration. As with other systems, from impedance study, variation with electrolyte composition and temperature can be determined. Transport parameters such as concentration of mobile species, their diffusion coefficient and mobility at room and elevated temperatures will also be evaluated.

In order to achieve another objective of the present work, Chapter 7 describes the performance of DSSCs fabricated using the polymer electrolyte prepared. Chapter 8 discusses all results obtained and Chapter 9 concludes the thesis with some suggestions for future work that will help to increase the body of knowledge in the vast literature on polymer electrolytes and DSSCs.

CHAPTER 2 : LITERATURE REVIEW

2.1. Introduction

In this chapter, the introduction of the polymer and polymer electrolytes will be described briefly. The basic properties of polymer electrolytes and classification of polymer electrolytes will be explained. In this work, poly(vinly alcohol) or PVA in short was chosen as the polymer host for the polymer electrolyte systems. PVA will be added with salts to generate conductivity and ionic liquid to enhance conductivity of the complexes. The properties and choice of materials used in this work will be explained in detail. The polymer electrolytes prepared will be used in DSSCs and the basic working principle of the solar cells will also be discussed in this chapter.

2.2. Polymer

Polymer is a large molecule consisting of small repeat units called monomer that are being held together by covalent bonds. The process of reacting monomers together in a chemical reaction to form polymer chains is called polymerization. Usually a polymer consists of a long chain of molecules with very high molecular weight.

Polymers can be classified into three types which are natural, synthetic and semi–synthetic polymers. Natural or biopolymers are polymers that can be obtained from living organisms such as animals and plants. Cellulose (Shuhaimi *et al*., 2012), starch (Khiar & Arof, 2010), chitin (Osman & Arof, 2003), protein (Parthasarathy *et al*., 2007), gellan gum (Noor *et al*., 2012), deoxyribonucleic (DNA) (Leones *et al*., 2015) and ribonucleic acid (RNA) (Zgârian *et al*., 2015) are examples of natural polymers in which the monomeric units are sugar, amino acid and nucleotide, respectively.

Biopolymers are renewable because they are made from plant materials which can be continuously grown. Also, some of these polymers are biodegradable.

Synthetic polymers are human–made polymers prepared in the laboratories. Poly(vinyl alcohol) (Kadir *et al*., 2010), poly(vinyl chloride) (Ramesh *et al*., 2002), polypropylene (Young *et al*., 2014), polystyrene (Lim *et al*., 2012), poly(tetrafluoro-ethylene) (Rofaiel *et al*., 2012), nylon (Grondin *et al*., 1995) and nafion (Zaidi, 2009) are examples of synthetic polymers. Most of the synthetic polymers consist of carbon–carbon backbone. Some of them have other elements such as oxygen, sulfur and nitrogen that are attached along the backbone. Synthetic polymers are widely used as a variety of consumer products in daily life such as packaging bag (MacDonald *et al*., 1999) and home furniture (LaBlance, 2003).

Semi–synthetic polymer is mostly derived from natural polymer by subjecting them to some chemical processes. As an example, on acetylation cellulose with acetic anhydride in a sulphuric acid environment produces cellulose diacetate polymer (Yoshikawa *et al*., 1999). Vulcanized rubber and nitrocellulose are also examples of semi–synthetic polymers (Flory, 1944).

2.3. Polymer Electrolyte

Polymer electrolyte is defined as a material formed by complexation or interaction between polymer and salt which has the ability to present ionic conductivity from the movement of free ions. The heteroatom (O, N and S) in the backbone of the polymer will form a dative bond with an ionizing group i.e. the cation of a salt. These electron donating heteroatoms solvates cations. Under the action of an electric field, the cations will hop from one donor to another donor site.

Polymer electrolyte was first discovered by Peter V. Wright in 1975 (Wright, 1975). He found that poly(ethylene) oxide or PEO can form complexes with sodium and potassium salts. PEO acts as a polymer host to produce solid electrical conducting polymer–salt complexes. Three years later, Michel Armand discovered that a lithium salt could dissolve in a solvating PEO polymer matrix to form PEO/lithium solid polymer electrolyte complexes with a good conductivity (Armand *et al*., 1979). Since then, many polymer electrolyte systems have been investigated. Polymer electrolytes have drawn attention of many researchers due to the possible applications in dye sensitised solar cells (O'regan & Grätzel, 1991), batteries (Sumathipala *et al*., 2007), supercapacitors (Shuhaimi *et al*., 2012) and electrochromic devices (Singh *et al*., 1995).

Before the presence of polymer electrolyte, liquid electrolyte was widely used in electrochemical devices. Liquid electrolyte faces several problems such as:

- easy to leak from an electrochemical device,
- not portable. This is because liquid electrolyte is bulk fluid and hence the device will be difficult to move from one position to another,
- easily corrode the electrodes of the device,
- produce low energy and power density when used in electrochemical devices,
- limited temperature range. The boiling point of the solvent used limits the temperature range of device operation.

Due to the disadvantages of liquid electrolyte, efforts have been geared towards replacing them with polymer electrolytes that have advantages as listed below:

- polymer electrolytes (PEs) have excellent design flexibility,
- PEs have satisfactory chemical, mechanical, thermal and electrochemical stabilities,

- PEs are able to form good contact with electrodes,
- PEs have good safety feature.

In electrochemical device application, the conductivity of an electrolyte used must be high. Unfortunately, the conductivity of polymer electrolyte is at least 100 to 1000 times less than in a liquid electrolyte. Although higher conductivity is preferable, polymer electrolyte with conductivity of ~10^{-4} S cm^{-1} has been shown to be sufficient for application in thin film electrochemical cells (Singh *et al.*, 1995; Sumathipala *et al.*, 2007; Shuhaimi *et al.*, 2012). For device applications, a polymer electrolyte should possess:

- high room temperature conductivity ($\sigma \geq 10^{-4}$ S cm^{-1}),
- good chemical, thermal, mechanical and electrochemical stabilities,
- good compatibility with the electrode materials,
- low activation energy for ionic conduction,
- no phase change in the operating temperature regime,
- low glass transition temperature (T_g) as well as low degree of crystallinity for ionic conductivity.

PEs can be classified as (i) dry or solid polymer electrolytes, (ii) gel electrolytes and (iii) composite electrolytes. Attempts to produce a polymer electrolyte with conductivity equivalent to that of liquids, as well as good chemical, thermal, mechanical and electrochemical properties are still ongoing worldwide. In this work, we focus on solid and gel polymer electrolyte systems.

2.3.1. Solid Polymer Electrolyte (SPE)

Solid polymer electrolyte is defined as a solvent–free polymer salt system, where the ion conduction takes place in a phase formed by dissolving salt with low lattice energy in a high or low molecular weight polar polymer matrix.

Solid polymer electrolyte is generally produced by solution casting technique in the form of thin films (Tipton *et al.*, 1994; Singh *et al.*, 1995; Rajendran & Uma, 2000; Ramesh *et al.*, 2002). Solid polymer electrolyte has the ability to present high ionic conductivity and functions in a similar manner like liquid electrolytes (Kalaignan *et al.*, 2006; Hema *et al.*, 2009a; Hema *et al.*, 2009b; Hema *et al.*, 2010). The advantages of solid polymer electrolyte are due to their unique properties:

- can be used to make smaller and space saving devices,
- light weight,
- good processibility and flexibility,
- pressure resistant,
- relatively high room temperature ionic conductivity ($\sigma \geq 10^{-4}$ S cm^{-1}),
- safe since it is not volatile.

Table 2.1 lists the room temperature conductivity obtained by several solid polymer electrolytes. The room temperature conductivity of solid polymer electrolyte can reach as high as 10^{-3} S cm^{-1}. This imply that solid polymer electrolytes can attain the characteristics of liquid electrolytes and at the same time be able to resolve problems encountered from the liquid electrolytes such as leakage, flexibility, corrosion and safety.

Table 2.1: Room temperature conductivity (298 K) of several solid polymer electrolytes.

Solid polymer electrolyte	**Conductivity, σ (S cm^{-1})**	**Reference**
$80PEO:20NH_4I$ (in mole %)	1.00×10^{-5}	(Maurya *et al.*, 1992)
$85PVA:15NH_4Cl$ (in mole %)	1.00×10^{-5}	(Hema *et al.*, 2009a)
$70PVA:30Cu(NO_3)_2$ (in wt.%)	1.60×10^{-5}	(Ramya *et al.*, 2005)
$35PVC:65LiCF_3SO_3$ (in wt.%)	2.40×10^{-5}	(Subban *et al.*, 2005)
$60PVA:40LiClO_4$ (in wt.%)	3.22×10^{-5}	(Lim *et al.*, 2014)
$PVDF:LiCF_3SO_3$	3.40×10^{-5}	(Mohamed & Arof, 2004)
PEO:KI	8.36×10^{-5}	(Kalaignan *et al.*, 2006)
$70PAN:30NH_4I$ (in wt.%)	1.49×10^{-4}	(Jyothi *et al.*, 2014)
$74PAN:26LiCF_3SO_3$ (in wt.%)	3.04×10^{-4}	(Osman *et al.*, 2011)
$75PVA:25NH_4Br$ (in mole %)	5.70×10^{-4}	(Hema *et al.*, 2009a)
PVA:KI	5.89×10^{-4}	(Said *et al.*, 2015)
$75PVA:25LiCF_3SO_3$ (in mole %)	7.06×10^{-4}	(Malathi *et al.*, 2010)
60PVA:40KOH (in wt.%)	8.50×10^{-4}	(Mohamad *et al.*, 2002)
$PEO:LiI:I_2$	2.00×10^{-3}	(Trang *et al.*, 2013)
$75PVA:25NH_4I$ (in mole %)	2.50×10^{-3}	(Hema *et al.*, 2009a)
$80PVA:20NH_4NO_3$ (in mole %)	7.50×10^{-3}	(Hema *et al.*, 2010)

A lot of attention is given to solid electrolytes in the hope that it may replace liquid electrolytes in devices such as DSSCs. Table 2.2 lists some of solid polymer electrolytes, their conductivity and solar conversion efficiency (η) obtained in the respective DSSCs. In Table 2.2, it can be seen that the DSSC fabricated using solid polymer electrolyte can achieve solar conversion efficiency up to 2%. This proves that solid polymer electrolyte is able to perform in electrochemical devices like DSSC. The research is still on going to improve the performance of solid polymer electrolyte in electrochemical devices especially in dye sensitized solar cell.

Table 2.2: Solar conversion efficiency, η values for DSSC fabricated with some solid polymer electrolyte measured under 100 mW cm^{-2} light illumination.

Solid polymer electrolyte	**Conductivity, σ (S cm^{-1})**	**DSSC**	**Reference**
PVDF:KI:I_2	–	TiO_2/N3 dye/SPE/Pt η = 0.39%	(Anandan *et al.*, 2006)
PEO:NaI:I_2	3.46×10^{-6}	TiO_2/N719 dye/SPE/Pt η = 0.74%	(Singh *et al.*, 2011)
PEO:LiI:I_2	2.00×10^{-3}	TiO_2/N719 dye/SPE/Pt η = 1.98%	(Trang *et al.*, 2013)
PEO:KI:I_2	8.36×10^{-5}	TiO_2/N719 dye/SPE/Pt η = 2.04%	(Kalaignan *et al.*, 2006)

2.3.2 Gel Polymer Electrolyte (GPE)

The low ionic conductivity value ($\sigma \leq 10^{-3}$ S cm^{-1}) of solid polymer electrolyte at room temperature has changed the research to gel polymer electrolytes. Gel polymer electrolyte is defined as a solvent swollen polymer network (Karuppasamy *et al.*, 2015). The solvent is encaged in the polymer matrix and therefore leakage can be prevented (Dissanayake *et al.*, 2012). Gel polymer electrolyte is in a state between that of liquid and solid polymer electrolytes. To form this type of electrolyte, plasticizers are used. Ionic conduction takes place through the liquid, which has been trapped in the polymer host. This may indirectly increase the ionic mobility thus improving ionic conductivity of the electrolyte.

Gel polymer electrolyte serves as an alternative to both solid and liquid electrolytes. Gel polymer electrolytes have the advantages of:

- relatively high room temperature ionic conductivity ($\sigma \geq 10^{-3}$ S cm^{-1}),

- non–leakage,
- forming good contact with electrode,
- being flexible with no shape restrictions,
- good chemical, thermal and electrochemical stabilities,
- high energy and power density when used in devices,
- safe.

The addition of a solvent which acts as a plasticizer into the solid polymer electrolyte has changed its mechanical properties. The solid polymer electrolyte now becomes jelly and in this state is known as gel polymer electrolyte. The solid electrolyte conductivity is improved when it is converted to a gel polymer electrolyte. Table 2.3 compares solid and gel polymer electrolyte ionic conductivity at 298 K (room temperature).

Table 2.3: Comparison of room temperature (298 K) conductivity between several solid and gel polymer electrolytes.

Solid polymer electrolyte		**Gel polymer electrolyte**	
Electrolyte [reference]	**Conductivity, σ (S cm^{-1})**	**Electrolyte [reference]**	**Conductivity, σ (S cm^{-1})**
PMMA:$LiClO_4$ [(Shukla & Thakur, 2009)]	7.00×10^{-8}	PMMA:EC:PC:$LiClO_4$ [(Van Schalkwijk & Scrosati, 2002)]	7.00×10^{-4}
PAN:$LiClO_4$ [(Yang *et al.*, 1996)]	6.51×10^{-7}	PAN:EC:PC:$LiClO_4$ [(Song *et al.*, 1999)]	1.70×10^{-3}
		PAN:EC:DMC:$LiClO_4$ [(Van Schalkwijk & Scrosati, 2002)]	3.90×10^{-3}
PVA:KI [(Said *et al.*, 2015)]	5.89×10^{-4}	PVA:KOH:KI [(Yu *et al.*, 2011)]	1.27×10^{-2}
		PVA:EC:PC:KI [(Aziz *et al.*, 2014)]	1.29×10^{-2}

Table 2.3, continued…

PAN:$LiCF_3SO_3$ [(Osman *et al.*, 2011)]	3.04×10^{-4}	PAN:EC:PC:$LiCF_3SO_3$ [(Chowdari & Wang, 2000)]	1.20×10^{-3}
PMMA:$LiCF_3SO_3$ [(Ramesh & Wong, 2009)]	9.88×10^{-4}	PMMA:EC:PC:$LiCF_3SO_3$ [(Rajendran & Uma, 2000)]	5.50×10^{-3}

From Table 2.3, the conductivity of solid electrolyte can increase up to four magnitude orders when converted to gel. The conductivity is equivalent to that exhibited by liquid electrolytes. This is the advantage of gel polymer electrolytes which can possess high ionic conductivity similar like liquid electrolytes and at the same time have properties of solid polymer electrolyte which are non–leakage, no shape restriction and safe.

The good properties of gel polymer electrolyte make it widely used in electrochemical devices such as DSSC. Table 2.4 lists some of the gel polymer electrolytes with the η obtained in the respective DSSCs. From Table 2.4, DSSCs fabricated using gel polymer electrolytes can achieve solar conversion efficiency up to 7.3%. This high solar conversion efficiency obtained by gel polymer electrolyte is comparable to DSSC with liquid electrolyte which reported by O'regan & Grätzel (1991). This shows that gel electrolytes can replace liquid electrolytes in DSSCs. The study is still ongoing by many researchers around the world to improve the performance of polymer gel electrolyte in electrochemical devices, especially in dye sensitized solar cells.

Table 2.4: Solar conversion efficiency, η values for DSSC fabricated with some gel polymer electrolyte measured under 100 mW cm^{-2} light illumination.

Gel polymer electrolyte	**Conductivity, σ (S cm^{-1})**	**DSSC**	**Reference**
PAN:EC:PC:TPAI:I_2	2.40×10^{-3}	TiO_2/N719 dye/Electrolyte/Pt η = 4.47%	(Dissanayake *et al.*, 2012)
PAN:EC:PC:KI:I_2	4.40×10^{-3}	TiO_2/N719 dye/Electrolyte/Pt η = 4.98%	(Dissanayake *et al.*, 2012)
PVDF-HFP:AN:TPAI:I_2	–	TiO_2/N3 dye/Electrolyte/Pt η = 5.33%	(Lee *et al.*, 2009)
PAN:EC:PC:KI:TPAI:I_2	2.70×10^{-3}	TiO_2/N719 dye/Electrolyte/Pt η = 5.36%	(Dissanayake *et al.*, 2012)
PVA:EC:PC:KI:TBAI:I_2	5.27×10^{-3}	TiO_2/N3 dye/Electrolyte/Pt η = 5.80%	(Aziz *et al.*, 2015)
PVDF-HFP:AN:TBAI:I_2	–	TiO_2/N3 dye/Electrolyte/Pt η = 6.74%	(Lee *et al.*, 2009)
PAN:EC:PC:TBAI:I_2	4.33×10^{-3}	TiO_2/N719 dye/Electrolyte/Pt η = 7.27%	(Ileperuma *et al.*, 2011)

2.4. Poly(vinyl alcohol) or PVA

Poly(vinly alcohol) or PVA is a hydrophilic synthetic polymer. It has the chemical formula of $[CH_2CH(OH)]_n$ and molecular structure of the monomer is as shown in Figure 2.1. Poly(vinyl alcohol) was discovered by Herrmann and Wolfram in 1924 (Herrmann & Wolfram, 1928). The preparation of PVA is different from other vinyl polymers. PVA was not prepared by polymerization of the corresponding monomer (vinyl alcohol). Herrmann and Wolfram found that the hydrolyzing poly(vinyl acetate) or PVAc in ethanol with the present of aqueous sodium hydroxide (NaOH) as catalyst produced PVA and methyl acetate. During the hydrolysis process, the acetate groups in PVAc are hydrolyzed by ester interchange with methanol and replaced by hydroxyl groups in the polymer chain in the presence of catalyst. Figure 2.2 shows the hydrolysis step to prepare PVA from PVAc in the presence of sodium hydroxide as the catalyst.

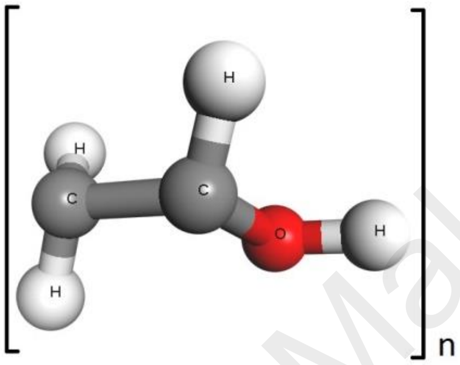

Figure 2.1: Molecular structure of poly(vinyl alcohol) (PVA) polymer.

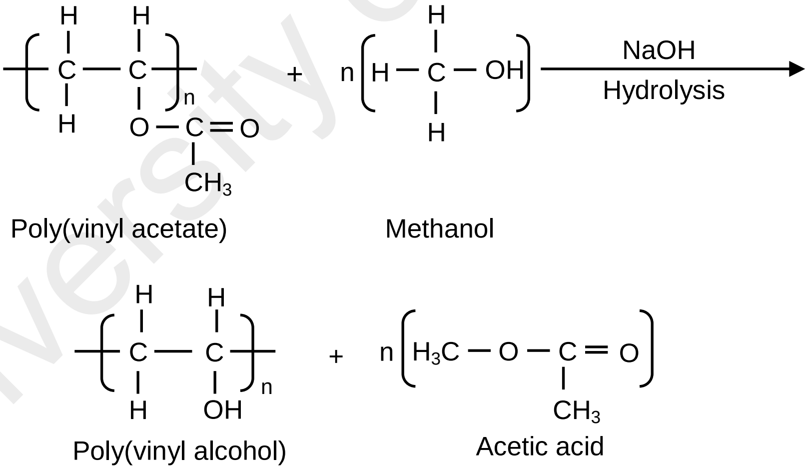

Figure 2.2: Hydrolysis step to prepare poly(vinyl alcohol).

Poly(vinyl alcohol) can be classified as fully hydrolyzed and partially hydrolyzed. The degree of hydrolysis depends on the degree of replacement of acetate group with hydroxyl groups and the degree of polymerization. The fully hydrolyzed PVA still contains 1 to 2 mole% of acetate group in the polymer chain while partially hydrolyzed PVA still maintains 10 to 20 mole% of acetate group.

Poly(vinyl alcohol) is in the form of a white or cream colored granular powder. It has several advantages such as:

- non–toxic,
- non–carcinogenic,
- bio–adhesive,
- odorless,
- malleable,
- transparent,
- has good durability,
- low cost.

These features make the PVA an attractive polymer. PVA has been used widely in different areas of science and technology such as:

- finishing agent and textile sizing (Han & Gu, 2008),
- photosensitive coatings (Brinkman *et al*., 1991),
- emulsifier (Blehn & Ernsberger, 1948),
- food packaging application (Tripathi *et al*., 2009),
- adhesives for leather, textiles, wood and paper (Hayashi & Moriya, 1976; Xiaomei *et al*., 2012).

In the field of polymer electrolytes, PVA has been widely utilized as a polymer matrix for ion transport (Hema *et al.*, 2009a; Hema *et al.*, 2010; Malathi *et al.*, 2010). This is because PVA has the following properties:

- able to withstand high electric fields (>1000kV mm^{-1}) (Subba Reddy *et al*., 2006),
- high dielectric constant, $\varepsilon_r = 8.1$ (Singh & Gupta, 1998),

- good charge storage capacity (Malathi *et al*., 2010),
- dopant–dependent electrical and optical properties (Malathi *et al*., 2010).

Table 2.5 lists the dielectric constant of some polymer at room temperature (298 K). It can be seen that among the entire polymers listed in Table 2.5, PVA has the higher relative dielectric constant i.e. ε_r = 8.1. High relative dielectric constant is important in choosing a polymer host in polymer electrolyte. A polymer host with a high relative dielectric constant assists to dissociate the doping salt thus increasing the number of free ion for transport in polymer electrolyte. In addition, the high dielectric constant possessed by polymer host enables it to hold the ions for long period of time with large quantities of ions.

Table 2.5: Dielectric constant at 298 K for some polymer.

Polymer	**Dielectric constant, ε_r**	**Reference**
Poly(tetrafluoroethylene)	1.9	(Barber *et al.*, 2009)
Poly(ethylene)	2.3	(Lanza & Herrmann, 1958)
Poly(styrene)	2.6	(Barber *et al.*, 2009)
Poly(imide)	2.8	(Ahmad, 2012)
Poly(arylene ether)	2.9	(Barber *et al.*, 2009)
Poly(ethylene oxide)	4.5	(Albinsson, 1994)
Poly(vinyl chloride)	4.5	(Albinsson, 1994)
Poly(propylene oxide)	5.0	(Tipton *et al.*, 1994)
Poly(acrylonitrile)	5.0	(Thünemann, 2000)
Poly(vinylidene fluoride)	6.0	(Ahmad, 2012)
Poly(vinyl acetate)	7.8	(Albinsson, 1994)
Poly(vinyl alcohol)	8.1	(Singh & Gupta, 1998)

PVA has a hydroxyl (OH) group attached to methane carbon in their polymer chain. This OH group can be a source for the creation of hydrogen bond, thus help the formation of polymer complexes. Salts such as lithium trifluoromethanesulfonate ($LiCF_3SO_3$) added into PVA can easily dissociate due to the high relative dielectric constant of PVA. The free cations from salt will create a dative bond with electrons donating atom (i.e. oxygen) in the hydroxyl group of PVA to form the polymer–salt complexes.

Many studies have been done using PVA as a polymer host in polymer electrolyte. The important aspect to be focused in polymer electrolyte is conductivity. High conductivity value is needed by the polymer electrolyte to makes it shows a good performance when used in electrochemical devices. Table 2.6 lists some reports using PVA and other polymer as a polymer host in polymer electrolyte with their respective conductivity values obtained at room temperature (298 K).

Table 2.6: Conductivity values of some polymer electrolytes measured at room temperature (298 K).

Electrolyte	**Conductivity, σ (S cm^{-1})**	**Reference**
Polymer–$LiClO_4$ complexes		
PMMA:$LiClO_4$	7.00×10^{-8}	(Shukla & Thakur, 2009)
85PEO:15$LiClO_4$ (in mole %)	3.98×10^{-7}	(Karmakar & Ghosh, 2012)
80PAN:20$LiClO_4$ (in mole %)	6.51×10^{-7}	(Yang *et al.*, 1996)
PVC:$LiClO_4$	1.20×10^{-6}	(Rahman *et al.*, 2004)
60PVA:40$LiClO_4$ (in wt.%)	3.22×10^{-5}	(Lim *et al.*, 2014)
Polymer–$LiCF_3SO_3$ complexes		
70PEO:30$LiCF_3SO_3$ (in mole %)	1.63×10^{-6}	(Karan *et al.*, 2008)
35PVC:65$LiCF_3SO_3$ (in wt.%)	2.40×10^{-5}	(Subban *et al.*, 2005)
PVDF:$LiCF_3SO_3$	3.40×10^{-5}	(Mohamed & Arof, 2004)
65PMMA:35$LiCF_3SO_3$ (in wt.%)	9.88×10^{-5}	(Ramesh & Wong, 2009)
74PAN:26$LiCF_3SO_3$ (in wt.%)	3.04×10^{-4}	(Osman *et al.*, 2011)
75PVA:25$LiCF_3SO_3$ (in mole %)	7.06×10^{-4}	(Malathi *et al.*, 2010)
Polymer–NH_4I complexes		
70PVC:30NH_4I (in wt.%)	4.60×10^{-7}	(Deraman *et al.*, 2012)
80PEO:20NH_4I (in mole %)	1.00×10^{-5}	(Maurya *et al.*, 1992)
70PAN:30NH_4I (in wt.%)	1.49×10^{-4}	(Jyothi *et al.*, 2014)
75PVA:25NH_4I (in mole %)	2.50×10^{-3}	(Hema *et al.*, 2009a)

Table 2.6, continued…

Polymer–KOH complexes		
70PEO:30KOH (in wt.%)	2.10×10^{-8}	(Mohamad *et al.*, 2008)
60PVA:40KOH (in wt.%)	8.50×10^{-4}	(Mohamad *et al.*, 2002)
PVA–salt complexes		
85PVA:15NH_4Cl (in mole %)	1.0×10^{-5}	(Hema *et al.*, 2009a)
70PVA:30$Cu(NO_3)_2$ (in wt.%)	1.6×10^{-5}	(Ramya *et al.*, 2005)
75PVA:25NH_4Br (in mole %)	5.7×10^{-4}	(Hema *et al.*, 2009a)
80PVA:20NH_4NO_3 (in mole %)	7.5×10^{-3}	(Hema *et al.*, 2010)

In Table 2.6, it can be seen that PVA–$LiClO_4$ complexes exhibited the highest conductivity compared to the other polymer–$LiClO_4$ complexes. The same result can be seen to occur in polymer–$LiCF_3SO_3$, polymer–KOH and polymer–NH_4I systems where the PVA based polymer electrolyte showed the highest conductivity among the other polymer hosts. As can be seen in Table 2.6, the ambient conductivity values of PVA based solid polymer electrolyte is 10^{-5} S cm^{-1} and can increase up to 7.5×10^{-3} S cm^{-1}. This shows that PVA is the better material for use as a polymer host.

In this work, 80% hydrolyzed PVA has been chosen as the host. Every *et al.* (1998) has measured the conductivity of PVA with 99% and 88% hydrolyzed complexes with $LiCF_3SO_3$. They reported that the conductivity of polymer electrolyte for PVA with 88% hydrolyzed is higher than 99% hydrolyzed. Thus, it is better to use PVA with a lower degree of hydrolysis.

2.5. Lithium bis(oxalato)borate (LiBOB)

Lithium bis(oxalato)borate or LiBOB is a prominent salt that belongs to a family of thermally stable chelatoborate salts. It has the chemical formula of $LiB(C_2O_4)_2$ and molecular structure as shown in Figure 2.3. The molecular weight, M_w of LiBOB is 193.79 g mol^{-1}.

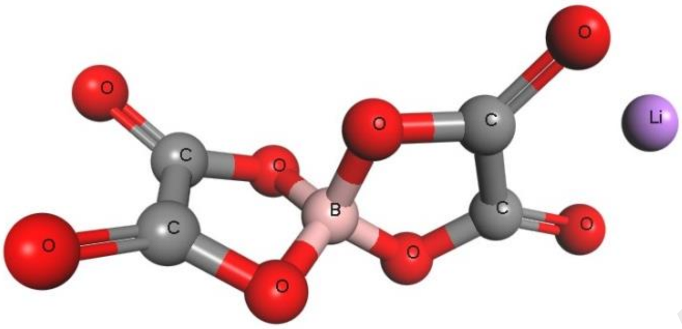

Figure 2.3: Molecular structure of lithium bis(oxalato)borate (LiBOB) salt.

LiBOB salt was first introduced in 1999 (Lischka *et al.*, 1999). Since then, LiBOB salt has been used widely in the field of polymer electrolytes and much attention has been given in battery applications. LiBOB salt has the following features:

- low cost (Xu *et al.*, 2002),
- high thermal stability up to 575 K (Wang *et al.*, 2006),
- environmental compatibility (Wang *et al.*, 2006),
- no production of harmfull gases and/or other undesired compounds upon contact with occasional water impurities (Xu *et al.*, 2005),
- wide electrochemical window (Xu *et al.*, 2005),
- high conductivity in various aprotic solvents (Kufian *et al.*, 2012),
- ability to form solid electrolyte interface (SEI) layer in electrodes (Xu *et al.*, 2002),
- high solvating ability (Karuppasamy *et al.*, 2015),
- less hygroscopic nature (Karuppasamy *et al.*, 2015).

In polymer electrolyte, salt is added into the polymer host to provide the charge carrier for ion conduction. LiBOB salt is the prominent salt to use in polymer electrolyte due to their low lattice energy of 496 kJ mol^{-1} (Holomb *et al.*, 2006) as well as the good features mentioned above. Low lattice energy results in weak interaction between cation and anion, thus increase the potential of LiBOB salt to dissociate into free ions. Arof and his co-workers (Arof *et al.*, 2014a) reported that ~72% of LiBOB free ions was obtained when 50 wt.% of LiBOB salt was incorporated into 50 wt.% PAN polymer as determined from FTIR deconvolution of the appropriate bands. Kufian *et al.* (2012) reported that ~71% of LiBOB free ions was dissociated in 0.6 M LiBOB in EC:PC as determined from FTIR deconvolution. This illustrated that LiBOB salt has potential to dissociate a large number of free ions when it incorporated into polymer electrolytes. A large numbers of free ions in polymer electrolyte will result in high ionic conductivity. Table 2.7 lists the conductivity at room temperature of some solid, gel and liquid electrolytes.

Table 2.7: Conductivity values of some solid polymer, gel polymer and liquid electrolytes at room temperature (298 K).

Electrolyte	**Conductivity, σ (S cm^{-1})**	**Reference**
Solid polymer electrolyte		
85PEO:15LiClO$_4$ (in mole %)	3.98×10^{-7}	(Karmakar & Ghosh, 2012)
70PEO:30LiCF$_3$SO$_3$ (in mole %)	1.63×10^{-6}	(Karan *et al.*, 2008)
50PEO:1LiBOB (in mole %)	7.00×10^{-5}	(Appetecchi *et al.*, 2004)
80PAN:20LiClO$_4$ (in mole %)	6.51×10^{-7}	(Yang *et al.*, 1996)
50PAN:50LiBOB (in wt.%)	2.55×10^{-5}	(Arof *et al.*, 2014b)
74PAN:26LiCF$_3$SO$_3$ (in wt.%)	3.04×10^{-4}	(Osman *et al.*, 2011)
Gel polymer electrolyte		
PMMA:EC:PC:LiClO$_4$	7.00×10^{-4}	(Van Schalkwijk & Scrosati, 2002)
PMMA:EC:PC:LiN(SO$_2$CF$_3$)$_2$	7.00×10^{-4}	(Van Schalkwijk & Scrosati, 2002)
PMMA:EC:PC:LiAsF$_4$	8.00×10^{-4}	(Van Schalkwijk & Scrosati, 2002)
PMMA:EC:PC:LiBOB	1.11×10^{-3}	(Kufian *et al.*, 2012)

Table 2.7, continued…

Liquid electrolyte		
EC:PC:$LiClO_4$	2.20×10^{-3}	(Croce *et al*., 1998)
EC:PC:$LiCF_3SO_3$	2.80×10^{-3}	(Perera & Dissanayake, 2006)
EC:PC:LiBOB	4.80×10^{-3}	(Kufian *et al*., 2012)
PC:$LiCF_3SO_3$	1.70×10^{-3}	(Moseley & Garche, 2014)
PC:$LiBF_4$	3.40×10^{-3}	(Moseley & Garche, 2014)
PC:LiBOB	4.14×10^{-3}	(Xu *et al*., 2003)
EC:DMC:$LiBF_4$	4.90×10^{-3}	(Moseley & Garche, 2014)
EC:DMC:LiBOB	7.50×10^{-3}	(Moseley & Garche, 2014)

In Table 2.7, it can be seen that incorporation of LiBOB salt with PEO polymer revealed conductivity of 7.00×10^{-5} S cm^{-1} compared to the PEO polymer complexes with $LiClO_4$ and $LiCF_3SO_3$ salts. The incorporation of LiBOB salt into PAN polymer revealed a conductivity of 2.55×10^{-5} S cm^{-1} which is higher than PAN–$LiClO_4$ solid polymer electrolyte. Of course, this table is inexhaustive in data, but it serves to show the strength of the LiBOB salt.

For gel polymer electrolyte system in Table 2.7, PMMA–EC–PC–LiBOB exhibits room temperature conductivity of 1.11×10^{-3} S cm^{-1} compared to the PMMA–based gel polymer electrolyte complexes with $LiClO_4$, $LiN(SO_2CF_3)_2$ and $LiAsF_4$. The same result is also observed in liquid electrolyte systems shown in Table 2.7. Liquid electrolytes that consist of LiBOB salt exhibits the highest room temperature conductivity compared with the liquid electrolytes that consist of other salts.

Based on the conductivity values of electrolytes listed in Table 2.7, it may be inferred that a particular mass of LiBOB salt has potential to dissociate into a large number of charge carriers and revealed high ionic conductivity value. High ionic conductivity is important in polymer electrolytes to ensure good performance when used in electrochemical devices. Thus LiBOB salt is best suited for use as charge supplier from lithium salt in a polymer electrolyte.

In this work, LiBOB salt was chosen as ion supplier for polymer electrolyte due to the high ionic conductivity that can obtained when incorporated with several polymers as well as the good properties of the salt.

2.6. Tetrabutylammonium Iodide (TBAI)

Tetrabutylammonium iodide (TBAI) is a quaternary ammonium salt with an iodide counterion. It has the chemical formula of $C_{16}H_{36}NI$ and molecular structure as shown in Figure 2.4. The molecular weight, M_w of TBAI is 369.37 g mol^{-1}.

TBAI salt is commonly used in polymer electrolyte as iodide supplier that generates the redox process in dye sensitized solar cell application. In DSSC, iodide ions are important for their role in transporting electrons from the counter electrode to the photoanode ionized dye. The rate of redox process can enhanced by having a large number of iodide ions in the polymer electrolyte and thus helps in increase the solar conversion efficiency of DSSC.

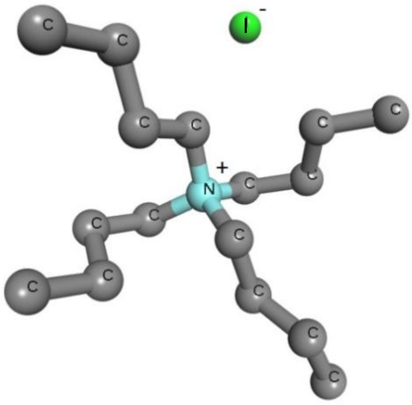

Figure 2.4: Molecular structure of tetrabutylammonium iodide (TBAI) salt.

Table 2.8 lists the solar conversion efficiency, η values for DSSC fabricated with several polymer electrolytes measured under 100 mW cm^{-2} light illumination. The DSSC with electrolyte consisting of TBAI salt obtained the highest solar conversion efficiency. This is because TBAI salt has a big cation. This enables the salt to be easily dissociated and form free TBA$^+$ and I$^-$.

From Table 2.8, the solar conversion efficiency of 7.27% was achieved for DSSC using PAN–EC–PC–TBAI–I_2 gel polymer electrolyte. The DSSC using PAN–EC–PC–I_2 gel polymer electrolyte consisting of TPAI and KI revealed the solar conversion efficiency of 4.47% and 4.98%, respectively. The large difference in efficiency obtained for DSSC using gel polymer electrolyte consisting of TBAI salt prove that TBAI salt help to increase the solar conversion efficiency and it is a suitable salt to choose in DSSC.

Table 2.8: Solar conversion efficiency, η values for DSSC fabricated with polymer electrolyte measured under 100 mW cm^{-2} light illuminations.

Polymer electrolyte	**Conductivity, σ (S cm^{-1})**	**DSSC**	**Reference**
PVDF–HFP:PC:NH_4I:I_2	–	TiO_2/N3 dye/Electrolyte/Pt η = 1.83%	(Lee *et al.*, 2009)
PVDF–HFP:PC:TPAI:I_2	–	TiO_2/N3 dye/Electrolyte/Pt η = 3.19%	(Lee *et al.*, 2009)
PVDF–HFP:PC:TBAI:I_2	–	TiO_2/N3 dye/Electrolyte/Pt η = 3.57%	(Lee *et al.*, 2009)
PVDF–HFP:AN:NH_4I:I_2	–	TiO_2/N3 dye/Electrolyte/Pt η = 2.34%	(Lee *et al.*, 2009)
PVDF–HFP:AN:TPAI:I_2	–	TiO_2/N3 dye/Electrolyte/Pt η = 5.33%	(Lee *et al.*, 2009)

Table 2.8, continued…

PVDF–HFP:AN:TBAI:I_2	–	TiO_2/N3 dye/Electrolyte/Pt η = 6.74%	(Lee *et al.*, 2009)
PAN:EC:PC:TPAI:I_2	2.40×10^{-3}	TiO_2/N719 dye/Electrolyte/Pt η = 4.47%	(Dissanayake *et al.*, 2012)
PAN:EC:PC:KI:I_2	4.40×10^{-3}	TiO_2/N719 dye/Electrolyte/Pt η = 4.98%	(Dissanayake *et al.*, 2012)
PAN:EC:PC:TBAI:I_2	4.33×10^{-3}	TiO_2/N719 dye/Electrolyte/Pt η = 7.27%	(Ileperuma *et al.*, 2011)
PVA:EC:PC:KI:TMAI:I_2	1.29×10^{-2}	TiO_2/N3 dye/Electrolyte/Pt η = 3.45%	(Aziz *et al.*, 2013b)
PVA:EC:PC:KI:TPAI:I_2	9.72×10^{-3}	TiO_2/N3 dye/Electrolyte/Pt η = 3.12%	(Aziz *et al.*, 2013a)
PVA:EC:PC:KI:TBAI:I_2	5.27×10^{-3}	TiO_2/N3 dye/Electrolyte/Pt η = 5.80%	(Aziz *et al.*, 2015)

In Table 2.8, it is observed that the DSSC fabricated with PVA–EC–PC–KI–TBAI–I_2 gel electrolyte exhibited the highest efficiency of 5.80% compared to DSSC fabricated with PVA–EC–PC–KI–TMAI–I_2 and PVA–EC–PC–KI–TPAI–I_2 gel polymer electrolytes. This shows that TBAI has played a good role as a second salt in improving the solar conversion efficiency of DSSC.

In this study, TBAI salt has been chosen as a second salt in PVA–LiBOB polymer electrolyte system. The addition of TBAI salt is to generate the redox process in PVA–LiBOB polymer electrolyte system for DSSC application.

2.7. 1–butyl–3–methylimidazolium Iodide (BMII) Ionic Liquid

Ionic liquid is a salt in which the cations and anions weakly interact with each other, resulting in a liquid state at room temperature. Ionic liquid has attracted significant attention due to the following properties like (An *et al.*, 2011):

- high ionic conductivity,
- high thermal stability,
- non–flammable,
- non–volatile,
- wider electrochemistry window,
- electrochemical stability,
- safety.

Due to the unique features of ionic liquid, it can be used as electrolytes for electrochemical device application including DSSCs.

Ionic liquid is in the liquid state at room temperature. It has been added into polymer electrolytes and plays its role as plasticizer to increase the ionic conductivity, so that the polymer electrolyte can perform better in electrochemical devices. Table 2.9 lists the conductivity of some polymer electrolytes at room temperature with and without ionic liquid, and their corresponding solar conversion efficiency values.

In Table 2.9, the room temperature conductivity of PEO–PMII ionic liquid complexes is higher than PEO–KI complexes. The conductivity difference is about two magnitude order. The higher conductivity obtained by PEO–PMII ionic liquid complexes is due to high amount of charge carriers in that electrolyte compared with PEO–KI complexes.

From Table 2.9, it is observed that the room temperature conductivity of polymer electrolyte with ionic liquid is higher than polymer electrolyte without ionic liquid treated. Ionic liquid can increase the conductivity of polymer electrolytes up to two magnitude order. This showed ionic liquid can provide more charge carriers in polymer electrolyte and thus exhibit higher ionic conductivity compared to the polymer electrolyte without ionic liquid added.

Due to the large amount of charge carriers produced by ionic liquid, the polymer electrolytes with ionic liquid added exhibits good performance in DSSCs. As can be seen from some results tabulated in Table 2.9, PEO polymer with PMII ionic liquid revealed solar conversion efficiency of 0.81% which is higher by 0.8% than PEO polymer complexes with KI salt. The addition of ionic liquid into polymer–salt complexes is seen to increase the solar conversion efficiency by ~2%. This shows that ionic liquid is useful in polymer electrolytes to enhance ionic conductivity and also improve the performance of the device when the electrolytes are applied in electrochemical devices.

Table 2.9: Solar conversion efficiency, η values for DSSC fabricated with polymer electrolyte consisting ionic liquid under 100 mW cm^{-2} light illumination with corresponding room temperature conductivity.

Polymer electrolyte	**Conductivity, σ (S cm^{-1})**	**DSSC**	**Reference**
PEO–KI complexes			
PEO:KI:I_2	1.87×10^{-6}	TiO_2/N719 dye/Electrolyte/Pt η = 0.01%	(Singh *et al.*, 2008a)
PEO:PMII:I_2	3.56×10^{-4}	TiO_2/N719 dye/Electrolyte/Pt η = 0.81%	(Singh *et al.*, 2008a)

Table 2.9, continued…

PEO:KI:I_2:EMITFSI	8.80×10^{-5}	TiO_2/N719 dye/Electrolyte/Pt η = 1.75%	(Singh *et al.*, 2008b)
PEO:KI:I_2:EMIDCN	4.72×10^{-4}	TiO_2/N719 dye/Electrolyte/Pt η = 2.00%	(Pramod *et al.*, 2009)
PEO–NaI complexes			
PEO:NaI:I_2	2.02×10^{-6}	TiO_2/N719 dye/Electrolyte/Pt η = 0.76%	(Pramod *et al.*, 2011)
PEO:NaI:I_2:EMITFO	4.72×10^{-5}	TiO_2/N719 dye/Electrolyte/Pt η = 2.45%	(Pramod *et al.*, 2011)
Chitosan–NH_4I complexes			
Chitosan:NH_4I:I_2	3.73×10^{-7}	TiO_2/N719 dye/Electrolyte/Pt η = 0.29%	(Buraidah *et al.*, 2010)
Chitosan:NH_4I:I_2:EC	7.34×10^{-6}	TiO_2/N719 dye/Electrolyte/Pt η = 0.51%	(Buraidah *et al.*, 2010)
Chitosan:NH_4I:I_2:BMII	8.47×10^{-4}	TiO_2/N719 dye/Electrolyte/Pt η = 1.24%	(Buraidah *et al.*, 2010)

BMII = 1–butyl–3–methylimidazolium iodide, PMII = 1–methyl–3–propylimidazolium iodide, EMITFSI = 1–ethyl–3–methylimidazolium bis(trifluoromethylsulfonyl)imide, EMIDCN = 1–ethyl–3–methylimidazolium dicyanamide and EMITFO = 1–ethyl–3–methylimidazolium trifluoromethane–sulfonate.

In this work, the polymer electrolytes prepared will be used in dye sensitized solar cell application. In DSSC, iodide ions are essential to generate redox process and a large amount of iodide charge carriers could increase the solar conversion efficiency of the DSSC. Thus, iodide–based ionic liquid is necessary in this work. 1–butyl–3–methylimidazolium iodide (BMII) ionic liquid has been selected as plasticizer. BMII ionic liquid has a chemical formula of $C_8H_{15}N_2I$ and molecular structure as shown in Figure 2.5. The molecular weight, M_w of BMII is 266.12 g mol^{-1}.

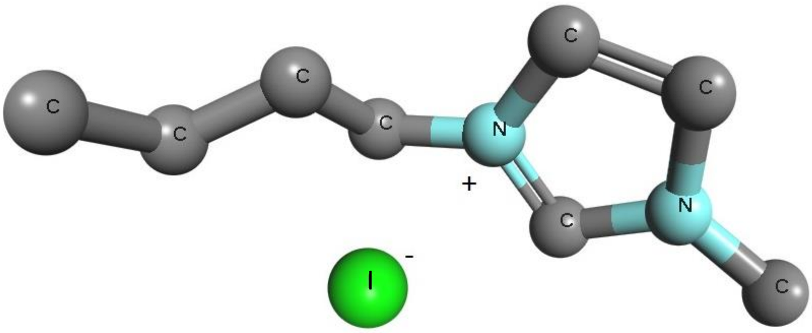

Figure 2.5: Molecular structure of 1–butyl–3–methylimidazolium iodide (BMII) ionic liquid.

Table 2.10 shows solar conversion efficiency, η values for DSSC fabricated with electrolytes composed of several ionic liquids measured under 100 mW cm^{-2} light illuminations. It can be seen that the DSSC fabricated with electrolyte consisting of BMII ionic liquid resulting higher solar conversion efficiency compared to DSSCs fabricated with electrolyte with other ionic liquids. This shows that BMII ionic liquid can perform better in DSSC. In this study, BMII ionic liquid will be added into polymer–salt complexes to increase the conductivity as well as improve the DSSC performance.

Table 2.10: Solar conversion efficiency, η values for DSSC fabricated with electrolyte containing ionic liquid measured under 100 mW cm^{-2} light illumination.

Electrolyte	DSSC	Reference
HMII:I_2:NBB	TiO_2/Z907 dye/electrolyte/Pt η = 3.36%	(Cao *et al.*, 2008)
BMII:I_2:NBB	TiO_2/Z907 dye/ electrolyte /Pt η = 5.31%	(Cao *et al.*, 2008)
K35:LiI:I_2:TBP:MPN	TiO_2/Z907 dye/ electrolyte /Pt η = 4.45%	(Zafer *et al.*, 2009)
TEGDI:LiI:I_2:TBP:MPN	TiO_2/Z907 dye/ electrolyte /Pt η = 4.65%	(Zafer *et al.*, 2009)
K36:LiI:I_2:TBP:MPN	TiO_2/Z907 dye/ electrolyte /Pt η = 5.16%	(Zafer *et al.*, 2009)

Table 2.10, continued…

K34:LiI:I_2:TBP:MPN	TiO_2/Z907 dye/ electrolyte /Pt η = 5.60%	(Zafer *et al.*, 2009)
BMII:LiI:I_2:TBP:MPN	TiO_2/Z907 dye/ electrolyte /Pt η = 5.64%	(Zafer *et al.*, 2009)

2.8. Dimethylformamide (DMF)

Dimethylformamide or DMF is an organic solvent with formula structure of C_3H_7NO. It has the molecular weight, M_w of 73.09 g mol^{-1}. It was prepared by reaction of dimethylamine with carbon monoxide or by combining methyl formate and dimethylamine (Weissermel & Arpe, 1978).

DMF has attractive properties like colorless, odorless and low volatility. These properties make DMF suitable to be used in the production of acrylic fiber and plastics (Li & Hsieh, 2005). Besides that, it is also has been used in the manufacture of synthetic leathers, adhesive, surface coatings fiber and films (Bipp & Kieczka, 2000).

In polymer electrolyte, DMF has been used as a plasticizer to improve the conductivity (Reddy *et al.*, 1999; Jacob & Arof, 2000). The high dielectric constant value (ε_r = 36.7) of DMF helps to dissociate more salt into ions (Pandey *et al.*, 2013). The addition of large amount of DMF in solid polymer electrolyte makes the solid state turn into gel type. The high boiling point (T_b = 427 K) of DMF keeps this plasticizer trapped in gel polymer electrolyte (Song *et al.*, 1999).

In this work, LiBOB salt has been used to incorporate with PVA polymer. LiBOB salt is sensitive to many solvents, thus an appropriate solvent should be used to dissolve the salt. DMF is found to be a convenient solvent for LiBOB salt (Xu &

Angell, 2001). Thus, DMF has been chosen as a solvent to dissolve LiBOB salt with PVA polymer. In addition, DMF has been used as a plasticizer due to their high dielectric constant. An amount of DMF was added into PVA–LiBOB solid polymer electrolyte to change their state from solid to gel form in order to increase the conductivity and get good DSSC performance.

2.9. Dye Sensitized Solar Cell (DSSC)

Dye sensitization was discovered by Hermann Wilhelm Vogel in 1873 (Peter, 2007) when he found that photographic films become more sensitive to light at longer wavelengths when green dye was added to silver halide photographic emulsions. This observation led to the making of new kinds of emulsions which were sensitive to all wavelengths in the visible. One year later, Sir William de Wiveleslie Abney successfully achieved sensitization of photographic emulsion from the violet to the infrared region of the spectrum. In 1887, Moser brought the concept of dye enhancement from photography to photoelectrochemistry (Moser, 1887). He used erythrosine dye on silver halide electrode after observing that dye enhancement was able to amplify the photoelectric current and generate voltage.

The finding by Moser had high impact to research carried out around the world. In 1964, Namba and Hishiki showed the effect of dye in photoelectrochemistry using zinc oxide (ZnO) semiconductor electrode (Namba & Hishiki, 1965). The dye sensitized the ZnO and enabled photoconductivity to occur. In 1965, Nelson suggested that to achieve maximum efficiency, the dye should be adsorbed as a closed packed monolayer on the semiconductor electrodes which increase the number of effective sensitizers (Nelson, 1965). If the dye adsorbed as multilayers, there is a reduction in the number of effective sensitizers, thus reducing the efficiency. During this time, it is still unclear whether the sensitization process involved electrons or energy transfer from dye to semiconductor (Bourdon, 1965). Bourdon reported that if the electron is provided by the dye, one has an electron transfer but if the electron is provided by a donor level at the crystal surface of the dye, one has an energy transfer. Figure 2.6 shows the schematic diagram of the mechanism for sensitization taken the electron or energy transfer in photographic semiconductor colloid particles reported by Bourdon.

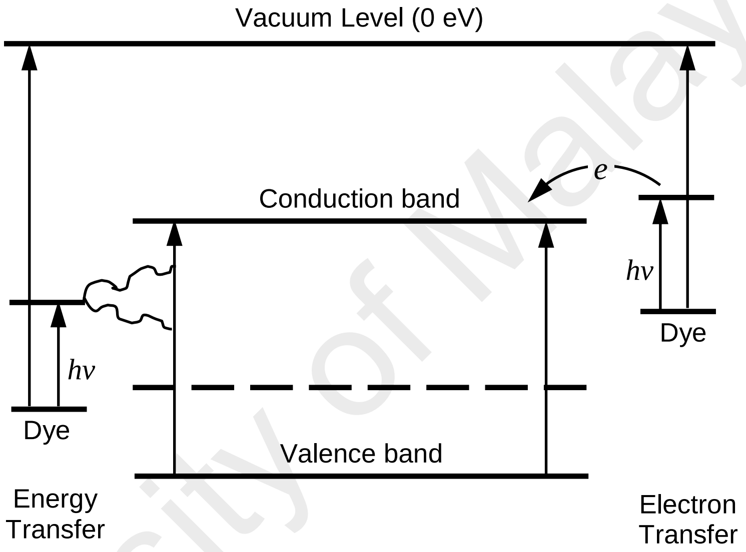

Figure 2.6: Schematic diagram of mechanism for sensitization taken the electron or energy transfer in photographic semiconductor colloid particles.

A few years later, Gerischer, Tributsch and Hauffe showed that it is electron injection from the excited dye molecule that took part in the sensitization process (Gerischer & Tributsch, 1968; Hauffe *et al.*, 1970). Application for solar energy conversion was not yet possible at that time because sensitization by single–crystal electrode was only able to generate very small photocurrents. This is because light absorption by the monolayer dye on the semiconductor surface is very weak. In 1976, Tsubomura and his coworkers showed that the photocurrent generated in a photocell can be increased by replacing the flat surface of a single–crystal ZnO electrode with a porous microcrystalline ZnO layer (Tsubomura *et al*., 1976). The porous ZnO layer has a larger surface area and thus the dye is adsorbing on a larger surface area of the electrode. This leads to increased light absorption at the semiconductor electrode, thus enhancing the photocell efficiency. Several decades ago, (O'regan & Grätzel, 1991) achieved a high light to electricity conversion efficiency of 7.1% under AM1.5 solar light illumination. The photoelectrochemical solar cell or also known as dye sensitized solar cell (DSSC) fabricated by the researchers used a porous layer of titanium dioxide (TiO_2) sensitized by a strongly absorbing ruthenium dye. Since then, many attempts were carried out to improve efficiency of DSSC in terms of semiconductor modification use of new organic dyes and high conducting electrolytes. The goal in DSSC research is to compete with the conventional photovoltaics with the hope that someday DSSCs may be used as an energy source.

Fabrication of a dye sensitized solar cells starts with two sheets of fluorine–doped tin oxide (FTO) or indium doped tin oxide (ITO) substrates. One plate was coated with a thin nano–sized porous semiconductor layer. The nano–sized semiconductor particles is about 20 to 40 nm that can provide a larger surface area to volume ratio for adherence of the dye. This can also result in larger optical absorption and larger photocurrent. There are several types of semiconductors use for as photoanode in DSSC. These include TiO_2, ZnO and SnO_2 and the most widely used is TiO_2. The TiO_2 paste was sintered at 450°C to produce a mesoporous layer of thickness ≈10 μm with a porosity of around 50% (Peter, 2007). There are three types of porosity which is microporous, mesoporous and macroporous. Micropores have a very small size up to 2 nm. Mesopores have a pore between 2 and 50 nm while macropores have a pore size more than 50 nm. Macroporous semiconductor with large pores size provides a large surface area for dye to adhere. It also provides a large amount of light to be absorped but would bring about an unwanted back scattering of light which could prevent the light from penetrating the dye molecules in a middle region. Microporous semiconductor with very small pore size can minimize the light loss due to such back scattering but less dye will adhere at the porous semiconductor. Semiconductor with large porosity and large light absorption is needed in DSSC so that more dye molecules can enter the semiconductor pores thus many electrons can be injected into the semiconductor. Hence, mesoporous semiconductor is the best for use in DSSC because of its size in between the microporous and macroporous. It can provide a large surface area for dye to adhere and also minimize the light loss due to back scattering. To enable the dye to adhere on the TiO_2 surface and the walls of the pores, the TiO_2 electrode was then soaked in the dye solution. The dye will be adsorbed on the TiO_2 electrode.

The second plate was coated with platinum (Pt) by sputtering, electrochemical deposition or spin coating the Pt paste (Pt catalyst T/SP) and heated at 450°C. Platinum acts as counter electrode in DSSC operation. There are other types of counter electrode such as carbon nanostructures, activated carbon, CNTs, graphene, ternary metal selenides ($NiSe_2$, $NiCoSe_2$, CoSe), metal sulfides (MoS_2, CoS_2, CuS, WS_2), metal oxides (V_2O_3, ZnO, SnO_2, MoO_2), metal carbides (TiC, VC, WC, Mo_2C) and metal nitrides (Mo_2N, NbN, TiN) that can be used in DSSC but platinum is more favorable due to its perfect stability and high catalytic properties (Thomas *et al*., 2014). A polymer electrolyte consisting of iodide/triiodide (I^-/I_3^-) redox mediator is then sandwiched between the two plates. Figure 2.7 shows the schematic diagram of DSSC fabrication with a polymer electrolyte.

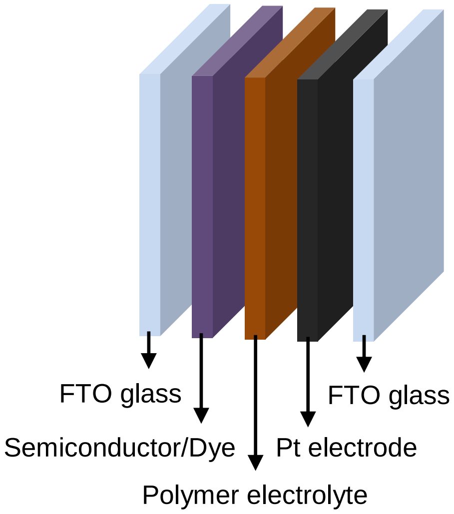

Figure 2.7: Schematic diagram of DSSC fabrication.

The operation of a DSSC is shown schematically in Figure 2.8. Generation of a photocurrent in the DSSC occurs when light (photon) is absorbed by the sensitizing dye. Semiconductor nanoparticles play an important role to allow the light to pass through to the dye which adheres at the mesoporous semiconductor. Thus, a semiconductor nanoparticles with large energy gap as well as large optical absorption is needed in DSSC. TiO_2 semiconductor is reported to have high energy gap of 3.2 eV (Grätzel, 1999). This feature makes TiO_2 widely used as metal oxide in DSSC. Upon absorption of photons, the solar energy absorbed by the dye is the same as the energy gap between highest occupied molecular orbitals (HOMO) and lowest unoccupied molecular orbital (LUMO). This leads to the formation of electronically excited dye molecule, $S*$ (i.e. an electronic transition from the HOMO to the LUMO). The dye molecules, $S°$ are excited from HOMO to LUMO states. This excitation process is represented by equation (2.1).

$$S° + hv \rightarrow S* \tag{2.1}$$

The excited dye, $S*$ releases an electron, e^{-} and this electron is injected from the LUMO level into the conduction band of the wide bandgap nanostructured semiconductor TiO_2.

The dye molecule is now in an oxidized state, S^+. This process was represented by equation (2.2) below:

$$S^* \rightarrow e^-_{(TiO_2)} + S^+ \tag{2.2}$$

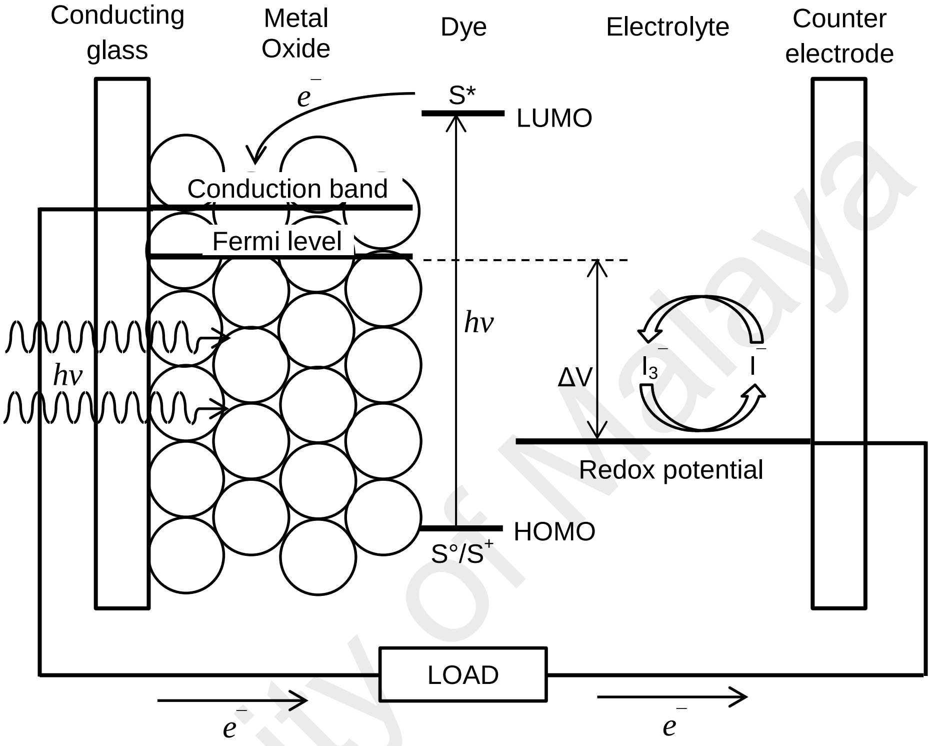

Figure 2.8: Schematic diagram of operation of dye sensitized solar cells.

The charge transfer occurs via the TiO_2–dye interfacial bond due to a strong electronic coupling between dye and TiO_2 (Thomas *et al.*, 2014). An electron is transferred from the dye metal to the π^* orbital of the surface anchoring carboxylated bipyridyl ligand from where it is released within 50 fs into the conduction band of TiO_2, generating electric charges with unit quantum yield (Grätzel, 1999). The injected electrons 'random walk' through the interconnected oxide particles network until they reach the conducting oxide glass substrate (FTO or ITO). The electron then passes through a load where work is done until it reaches the counter electrode (C.E.). The electron from counter electrode recombines with the oxidized dye molecule via an I^-/I_3^- redox process in the electrolyte. The I_3^- ion in the electrolyte accepts the electron from the external load at the counter electrode and is reduced to I^- ion. The reduction process here is show in equation (2.3).

$$\frac{1}{2}I_3^- + e^-_{(C.E.)} \rightarrow \frac{3}{2}I^- + C.E. \tag{2.3}$$

This I^- ion then regenerates the oxidized dye molecules, S^+ by returning the electron and itself is oxidized to I_3^- ion again. The process is shown in equation (2.4).

$$S^+ + \frac{3}{2}I^- \rightarrow S + \frac{1}{2}I_3^- \tag{2.4}$$

This process occurs continuously. The regenerative cycle is completed by the conversion of I_3^- to I^- ions.

For DSSC commercialization, aging is a major factor to be taken into account as this factor affects the performance of solar cells. Dirt and weather conditions (temperature, solar irradiation intensity and humidity) are the aging factors of DSSC. The use of polymer electrolyte in DSSCs that is more conductive at different temperatures gives the advantages to the DSSC to slow down the aging factor. In addition, the ability of DSSC to be more efficient at lower than 1 Sun solar intensities makes it more robust for use in daily life. The perfect sealing process can prevent humidity from deteriorating the device.

2.10. Summary

Introduction about polymer and polymer electrolytes have been done briefly in this chapter. The classification of polymer electrolyte and their properties have also been discussed. The reason for choosing PVA polymer, LiBOB salt, TBAI salt and

1–butyl–3–methylimidazolium iodide (BMII) ionic liquid for this work has been explained in detail. The electrolytes prepared in this work have been used in DSSC application. The basic operation principle of DSSC was also explained.

CHAPTER 3 : EXPERIMENTAL METHODS

3.1. Introduction

In this investigation, PVA was used as the polymer matrix. Lithium bis(oxalato)borate or LiBOB and tetrabutylammonium iodide (TBAI) salts have been used to provide the charge carriers in the electrolyte. Dimethylformamide (DMF) was the solvent used to dissolve the polymer and salts, and also to act as a plasticizer. 1–butyl–3–methylimidazolium iodide (BMII) ionic liquid (IL) was added in the electrolyte to provide the extra charge carriers. Two types of electrolytes have been prepared, namely solid polymer electrolyte (SPE) and gel polymer electrolyte (GPE). All electrolytes prepared were characterized using fourier transform infrared (FTIR) spectroscopy and electrochemical impedance spectroscopy (EIS). The first electrolyte system was PVA–LiBOB solid polymer electrolytes. The highest conducting electrolyte in the first system was added with TBAI salt and 2 g DMF to form the second electrolyte system i.e. PVA–LiBOB–TBAI–I_2–DMF gel polymer electrolyte. All electrolytes prepared in the second system were used as a medium for charge transfer in dye sensitized solar cells (DSSCs). *J–V* measurements were done to determine the efficiency of the DSSC. The electrolyte with highest solar conversion efficiency in the second system was added with different amounts of BMII ionic liquid to form the third electrolyte system i.e. PVA–LiBOB–TBAI–I_2–BMII–DMF gel polymer electrolytes. All electrolytes in the third system were also used in DSSC fabrication.

3.2. Electrolyte Preparation

3.2.1. PVA–LiBOB Solid Polymer Electrolytes

PVA–LiBOB in liquid form were solution cast to form solid polymer electrolytes. The PVA–LiBOB electrolyte compositions are as listed in Table 3.1. Desired amounts of LiBOB salt (Chemetall) were dissolved in 10 mL DMF (Aldrich) in a closed container. LiBOB salt is moisture sensitive. The mixture was stirred at 298 K (room temperature) for 1 h in a dry box. A mass of 0.5 g PVA (Aldrich, average molecular weight of 10,000 g mol^{-1}, 80% hydrolyzed) was added into the LiBOB–DMF solution and continuously stirred at 363 K for 4 h in the dry box. The homogenous solutions were cast into glass containers and dried at 333 K under vacuum for 12 h for removal of remaining solvents and to form films. Figure 3.1 shows the PVA–LiBOB solid polymer electrolytes that have been prepared.

Table 3.1: Composition and designation of PVA–LiBOB solid polymer electrolytes system.

Designation	**PVA (g)**	**LiBOB (g)**	**PVA : LiBOB (wt.% : wt.%) composition**
A0	0.5000	0	100 : 0
A1	0.5000	0.0556	90 : 10
A2	0.5000	0.1250	80 : 20
A3	0.5000	0.2143	70 : 30
A4	0.5000	0.3333	60 : 40
A5	0.5000	0.5000	50 : 50

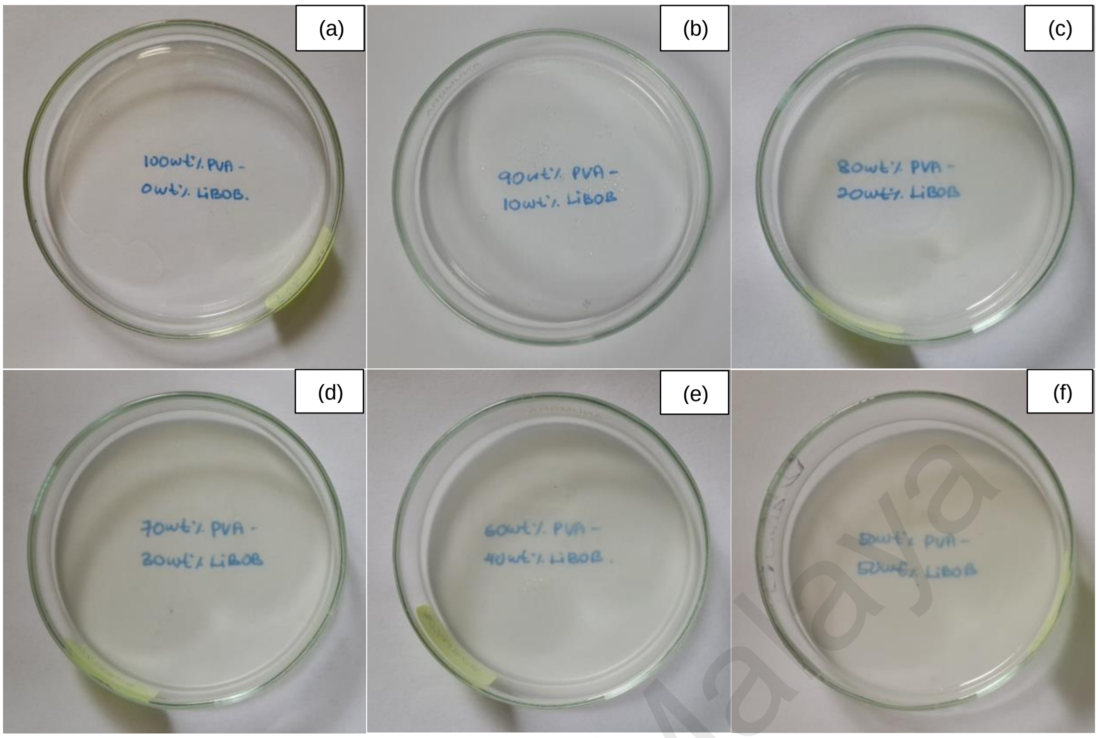

Figure 3.1: (a) A0, (b) A1, (c) A2, (d) A3, (e) A4 and (f) A5 electrolyte prepared by solution cast technique.

3.2.2. PVA–LiBOB–TBAI–I_2–DMF Gel Polymer Electrolytes

In the second electrolyte system, a second salt, tetrabutylammonium iodide (TBAI) was introduced into the highest conducting electrolyte in the first system. In this case, it is the electrolyte with composition 60 wt.% PVA–40 wt.% LiBOB (A4 electrolyte). The amount of LiBOB and TBAI salts were varied, but the total salt composition, which is 40 wt.% was maintained following the highest salt composition in first electrolyte system. In this work, TBAI salt was used to generate the redox process in the dye sensitized solar cells (DSSCs). LiBOB salt was used to provide cations for attachment to the DSSC photoanode that should be able to modify the surface states of the TiO_2 semiconducting layer and the walls of its pores in order to increase the rate of electron injection from the excited state of the dye into the TiO_2 conduction band. Hence, the solar conversion efficiency of the DSSC will increase.

Table 3.2 shows the electrolyte composition and their designations. In preparing the PVA–LiBOB–TBAI–I_2–DMF gel polymer electrolytes, desired amounts of LiBOB and TBAI (Aldrich) salts were dissolved in 2 g of DMF and stirred in a closed container for 2 h at room temperature (298 K). A 2 g mass of DMF was used as it resulted in a good gel by visual observation. A higher amount would lead to a more liquid electrolyte. The total amount of LiBOB and TBAI salts was maintained at 0.3333 g. A 0.5 g mass of PVA was then added into the LiBOB–TBAI–DMF homogenous solution and continuously stirred at 363 K for 4 h. Heating was stopped after the mixture has become viscous and gel–like. The gel electrolyte was cooled to room temperature. While cooling, I_2 (Aldrich) was added into the gel. Stirring was continued until the gel electrolyte reached ambient temperature. The amount of iodine added was equivalent to 10 mole% of the total number of mole of TBAI salt in the electrolytes. The homogenous gel polymer electrolytes were placed in a desiccator overnight before being used for characterizations. Figure 3.2 shows the PVA–LiBOB–TBAI–I_2–DMF gel polymer electrolytes that were prepared.

Table 3.2: Composition and designation of PVA–LiBOB–TBAI–I_2–DMF gel polymer electrolytes system.

Designation	**PVA (g)**	**LiBOB (g)**	**TBAI (g)**	**I_2 (g)**	**DMF (g)**	**LiBOB : TBAI (wt.% : wt %) composition**	**PVA : LiBOB : TBAI : I_2 : DMF (wt.% : wt.% : wt.% : wt.% : wt.%) composition**
B0	0.5000	0.3333	0	0	2.0000	100 : 0	17.65 : 11.76 : 0 : 0 : 70.59
B1	0.5000	0.2500	0.0833	0.0057	2.0000	75 : 25	17.61 : 8.81 : 2.93 : 0.20 : 70.45

Table 3.2, continued…

B2	0.5000	0.1667	0.1667	0.0115	2.0000	50 : 50	17.58 : 5.86 : 5.86 : 0.40 : 70.30
B3	0.5000	0.0833	0.2500	0.0172	2.0000	25 : 75	17.54 : 2.92 : 8.77 : 0.60 : 70.16
B4	0.5000	0.0667	0.2666	0.0183	2.0000	20 : 80	17.53 : 2.34 : 9.35 : 0.64 : 70.14
B5	0.5000	0.0500	0.2833	0.0195	2.0000	15 : 85	17.53 : 1.75 : 9.93 : 0.68 : 70.11
B6	0.5000	0.0333	0.3000	0.0206	2.0000	10 : 90	17.52 : 1.17 : 10.51 : 0.72 : 70.08
B7	0.5000	0	0.3333	0.0229	2.0000	0 : 100	17.51 : 0 : 11.67 : 0.8 : 70.02

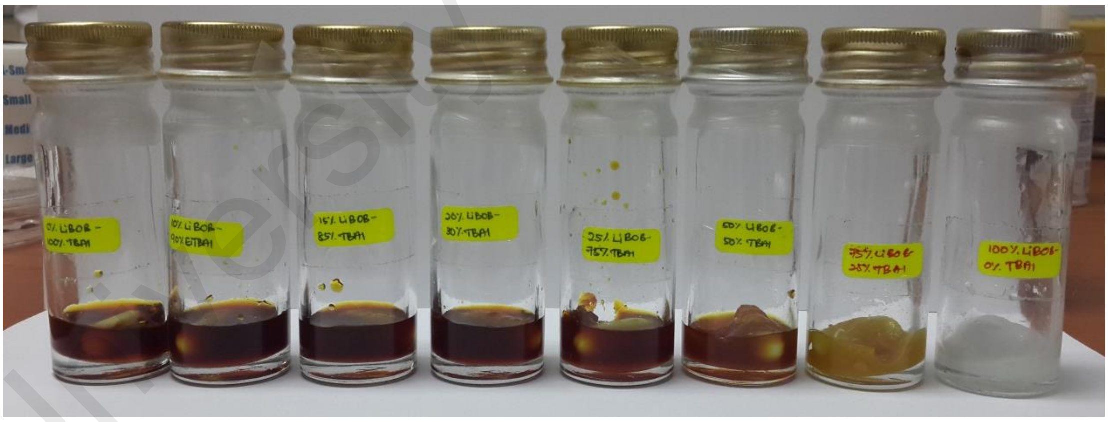

Figure 3.2: PVA–LiBOB–TBAI–I_2–DMF gel polymer electrolytes prepared in a closed container.

3.2.3. PVA–LiBOB–TBAI–BMII–I_2–DMF Gel Polymer Electrolytes

In this electrolyte system, an ionic liquid (IL) was added to the electrolyte of the second system that revealed the highest DSSC efficiency with the aim to enhance the efficiency of DSSC obtained. 1–butyl–3–methylimidazolium iodide (BMII) ionic liquid (IL) was used. The ionic liquid is to provide the extra charge carriers, especially the iodide anion. The electrolyte with composition 17.53 wt.% PVA–1.75 wt.% LiBOB–9.93 wt.% TBAI–0.68 wt.% I_2–70.11 wt.% DMF (B5 electrolyte) was chosen due to high solar to electrical conversion efficiency given by this electrolyte from the second electrolyte system. In preparing the PVA–LiBOB–TBAI–BMII–I_2–DMF gel polymer electrolytes, 0.05 g of LiBOB and 0.2833 g of TBAI salts were dissolved in 2 g of DMF and stirred in a closed container for 2 h at room temperature (297 K). It was also observed that 1 g DMF could not dissolve the salts completely. The homogenous LiBOB–TBAI–DMF solution was then be added with 0.5 g of PVA and stirred continuously at 363 K for 4 h. The amounts of BMII listed in Table 3.3 were added into the viscous and gel–like PVA–LiBOB–TBAI–DMF electrolyte and stirred continuously at the same temperature (363 K) for 1 h. The heating was then stopped and 0.0195 g of iodine was added into the gel electrolyte. The gel electrolyte was continuously stirred until the temperature reached room temperature. The homogenous gel electrolytes (shown in Figure 3.3) were placed in a desiccator overnight before further characterizations.

Table 3.3: Composition and designation of PVA–LiBOB–TBAI–BMII–I_2–DMF gel polymer electrolytes system.

Designation	**PVA (g)**	**LiBOB (g)**	**TBAI (g)**	**BMII (g)**	**I_2 (g)**	**DMF (g)**	**PVA : LiBOB : TBAI BMII : I_2 : DMF (wt.% : wt.% : wt.% wt.% : wt.% : wt.%) composition**
C0	0.5000	0.0500	0.2833	0	0.0195	2.0000	17.53 : 1.75 : 9.93 : 0 : 0.68 : 70.11
C1	0.5000	0.0500	0.2833	0.0288	0.0195	2.0000	17.35 : 1.74 : 9.83 : 1 : 0.68 : 69.41

Table 3.3, continued…

C2	0.5000	0.0500	0.2833	0.0882	0.0195	2.0000	17 : 1.7 : 9.63 : 3 : 0.66 : 68
C3	0.5000	0.0500	0.2833	0.1501	0.0195	2.0000	16.65 : 1.67 : 9.43 : 5 : 0.65 : 66.6
C4	0.5000	0.0500	0.2833	0.2147	0.0195	2.0000	16.3 : 1.63 : 9.24 : 7 : 0.64 : 65.2
C5	0.5000	0.0500	0.2833	0.2821	0.0195	2.0000	15.95 : 1.59 : 9.04 : 9 : 0.62 : 63.8

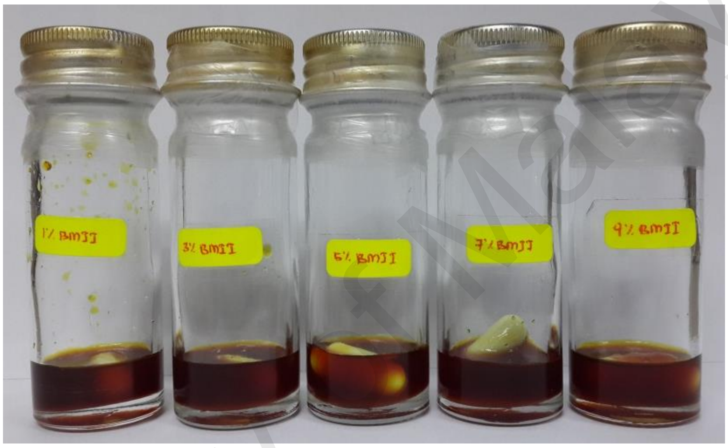

Figure 3.3: PVA–LiBOB–TBAI–BMII–I_2–DMF gel polymer electrolytes prepared in a closed container.

3.3. Sample Characterizations

3.3.1. Fourier Transform Infrared (FTIR) Spectroscopy

FTIR spectroscopy was used to determine the formation of polymer–salt complexes or interaction between salt and polymer. The Thermo Scientific model Nicolet iS10 spectrometer was used to obtain the spectra for all samples. The electrolyte was placed on the detector of the FTIR spectrometer and the spectrum recorded between 4000 and 650 wavenumbers at 4 cm^{-1} resolution in the transmittance mode at room temperature (297 K). From the FTIR spectrum, the functional group of the materials in the electrolyte can be determined. This is because each functional group vibrates at their own frequency. The interaction of salt and polymer in the electrolyte can be observed from the shifting of the IR band or the change in intensity of the FTIR spectra.

In this work, LiBOB salt was used as charge supplier in the electrolyte. Following Holomb *et al.* (2006), BOB^{-} anion band is located at 1804 cm^{-1}. Contact ion bands are located at 1812, 1817 and 1828 cm^{-1} in the spectrum. Figure 3.4 shows the structure of BOB^{-} anions and contact ions as reported by Holomb *et al.* (2006). Figure 3.5 shows the IR spectra of 1.0 and 0.5 M LiBOB in poly(propylene glycol) (PPG).

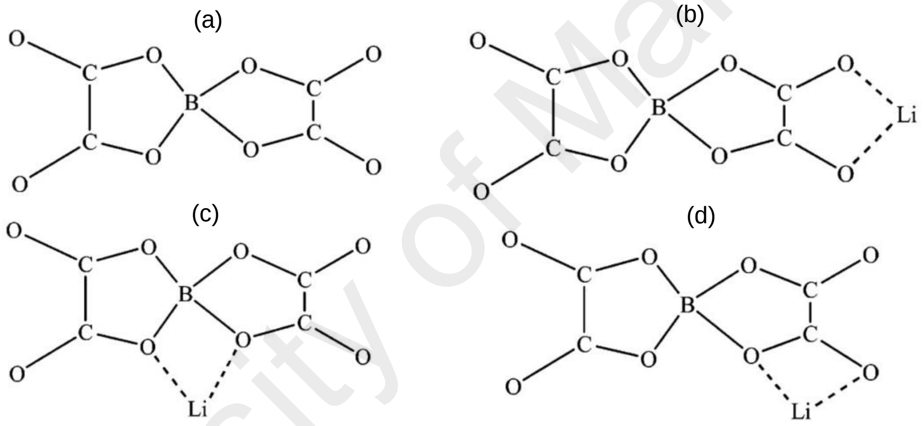

Figure 3.4: Structure of (a) BOB^{-} anions and (b,c,d) LiBOB contact ions with different model. (Holomb *et al*., 2006).

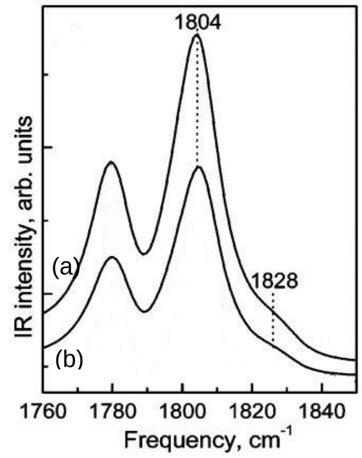

Figure 3.5: FTIR spectra of (a) 1 and (b) 0.5 M LiBOB in PPG. (Holomb *et al*., 2006).

Based on Figure 3.5, the bands of interest in this work should be between 1850 and 1760 wavenumbers since the free and contact ion bands are within this region (Holomb *et al.*, 2006). In order to determine the free and contact ion of LiBOB salt, the FTIR spectrum of this band was deconvoluted. This is because the FTIR spectrum of an electrolyte is an integrated result from the overlaps of many different vibration bands. Thus, deconvolution is the best method and widely used to find the peaks that build the band. Before deconvolution, we convert the spectrum in the region under consideration into the absorbance mode. The deconvolution procedure has been explained in Arof *et al*. (2014a). The peak close to 1804 cm^{-1} was assigned to free ions and that close to 1812, 1817 and 1828 cm^{-1} were assigned to contact ions. The equations (3.1) and (3.2) were used to calculate the percentage of free and contact ions.

$$\text{Percentage of free ions }(\%) = \frac{A_f}{A_f + A_c} \times 100\% \tag{3.1}$$

and

$$\text{Percentage of contact ions }(\%) = \frac{A_c}{A_f + A_c} \times 100\% \tag{3.2}$$

The area under the peak representing free ions is denoted as A_f and that for contact ions is A_c.

3.3.2. Electrochemical Impedance Spectroscopy (EIS)

Electrochemical impedance spectroscopy was performed to study the electrical properties of polymer electrolyte. In this method, a small sinusoidal potential (0.01 V) was applied across the sample and current through the sample measured for every operating frequency, impedance was obtained. The applied voltage was 10 mV to ensure that the voltage and current cross and trough the sample respectively is linearly related. According to (Macdonald & Johnson, 2005), the amplitude of the applied voltage must be less than the thermal voltage, V_T. The equation of V_T is as follows:

$$V_T = \frac{RT}{F} = \frac{kT}{e} \tag{3.3}$$

Here, *R* is the gas constant, *T* absolute temperature, *F* Faraday constant, *k* Boltzmann constant and *e* is elementary charge. Hence, if the impedance of the sample was measured at room temperature (298 K), then maximum $V_T = 25\,\mathrm{mV}$ and the applied voltage should not exceed this value.

In this work, the HIOKI 3532–50 LCR Hi–Tester was used to measure impedance from 50 Hz to 1 MHz. The samples (diameter 2.2 cm) were placed in between two 2 cm diameter stainless steel electrodes. In measuring impedance for gels, the electrolyte was put in a coin cell with surface area of 2 cm^2 and 0.26 cm thickness. Impedance measurements were carried out from 298 to 393 K. From a plot of negative imaginary impedance (*Z''*) versus real impedance (*Z'*), the bulk resistance, R_b was obtained. The ionic conductivity, σ of the sample was calculated using the equation below:

$$\sigma = \frac{d}{A \times R_b} \tag{3.4}$$

Here, *d* is the sample thickness and *A* is the electrode/electrolyte contact area. Figure 3.6 showed that the Nyquist plots may consists of a tilted semicircle and a tilted spike, or only a tilted spike.

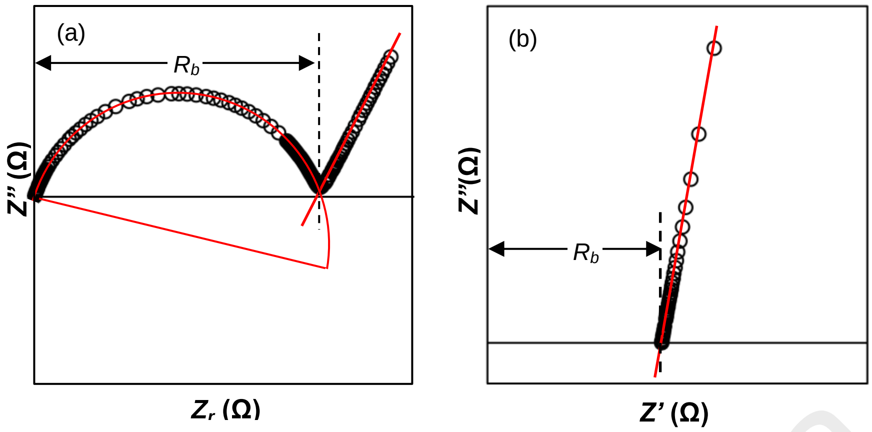

Figure 3.6: Schematic diagram to determine R_b from Nyquist plot consisting of (a) depressed semicircle and tilted spike and (b) only tilted spike.

Electrochemical impedance spectroscopy enables the transport properties of a polymer electrolyte to be studied (Bandara & Mellander, 2011; Bandara *et al.*, 2011; Arof *et al.*, 2014a). The fundamental property of an electrolyte is conductivity (σ), which in principle is the product of ion number density (n) and its mobility (μ) with the elementary charge (e). Knowing n and μ quantitatively is very useful. (Bandara & Mellander (2011) have shown that these parameters can be determined from impedance measurements. According to these authors, during impedance measurements, a polymer electrolyte is placed in between two blocking electrodes. In this configuration, the polymer electrolyte–blocking electrode configuration can be represented as shows in Figure 3.7(a). The equivalent circuit of the configuration can be represented as shown in Figure 3.7(b) and the real part of the impedance of this circuit is given by:

$$Z' = \frac{R}{1+(\omega RC)^2} \tag{3.5}$$

and its imaginary impedance as

$$Z'' = \frac{\omega R^2 C}{1+(\omega RC)^2} + \frac{2}{\omega C_e} \tag{3.6}$$

Here, *ω* is angular frequency. *C* is the bulk geometrical capacitance and C_e is the electrical double layer (EDL) capacitance. *R* is the bulk resistance of the polymer electrolyte.

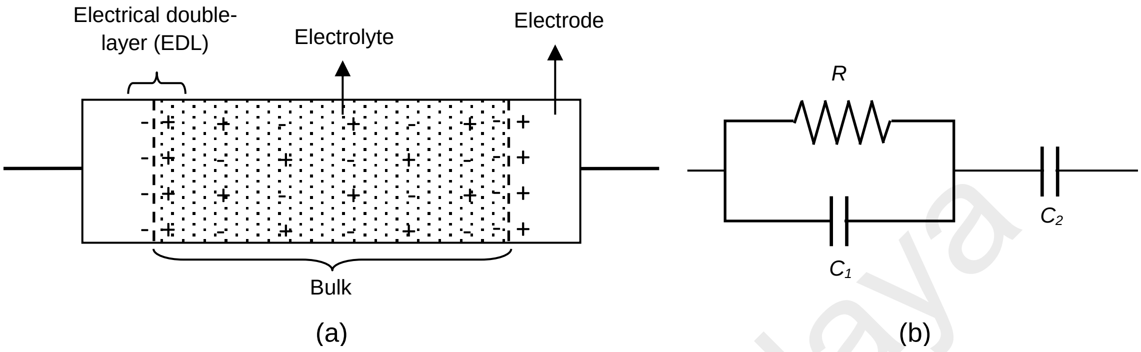

Figure 3.7: (a) Schematic diagram of polarization in polymer electrolyte with (b) its equivalent circuit configuration.

Plotting –*Z”* versus *Z’* using equations (3.5) and (3.6) gives a Nyquist plot as shown in Figure 3.8. The vertical spike implies a perfect capacitor and is represented by the second term on the right hand side of equation (3.6). The factor 2 in the second term on the right hand side of equation (3.6) takes into account the two EDLs formed at electrolyte/electrode interface.

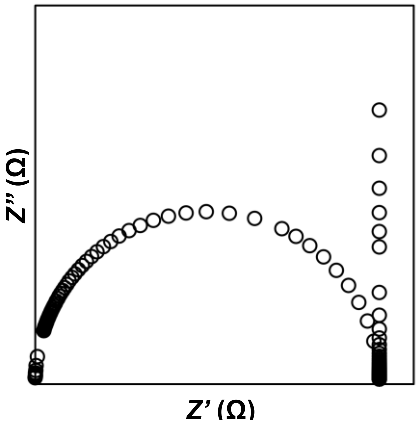

Figure 3.8: Nyquist plot of polymer electrolyte obtained using equation (3.5) and (3.6).

For a polymer electrolyte of thickness d with electrode/electrolyte contact area A, the C_e, C and R parameters are given by:

$$C_e = \frac{\varepsilon_r \varepsilon_o A}{\lambda} \tag{3.7}$$

$$C = \frac{\varepsilon_r \varepsilon_o A}{d} \tag{3.8}$$

$$R = \frac{d}{\sigma A} \tag{3.9}$$

Here ε_r is dielectric constant of the electrolyte, ε_o is vacuum permittivity (8.85×10^{-14} F cm^{-1}) and λ is electrical double layer thickness.

The dissipative loss curve following the broadband dielectric response (BDR) or Bandara–Mellander (B–M) approach is given by the equation below:

$$\tan(\phi) = \frac{\omega \tau_2 \sqrt{\delta}}{1 + (\omega \tau_2)^2} \tag{3.10}$$

and its maximum value is given by

$$[\tan(\phi)]_{\max} = \frac{\sqrt{\delta}}{2} \tag{3.11}$$

In equation (3.10), ω is angular frequency, $\tau_2 (= 1/\omega_2)$ is a time constant corresponding to the maximum dissipative loss curve. Here ω_2 is the angular frequency corresponding to the minimum in imaginary impedance, Z''. $\delta = d/\lambda$. From the B–M approach, diffusion coefficient (D), mobility (μ) and number density (n) of the free ions are given by:

$$D = \frac{d^2}{4\tau_2 \delta^2} \tag{3.12}$$

$$\mu = \frac{ed^2}{4kT\tau_2\delta^2} \tag{3.13}$$

$$n = \frac{4\sigma kT\tau_2\delta^2}{e^2d^2} \tag{3.14}$$

The value of D, μ and n in equations (3.12), (3.13) and (3.14) are dependent on the EDL layer.

Impedance measurements normally generate complex impedance plots comprising (i) a tilted semicircle, (ii) a tilted spike or (iii) a tilted semicircle with a tilted spike. This is not the same as the complex impedance plot adopted by (Bandara & Mellander, 2011) in developing equations (3.12), (3.13) and (3.14). They have assumed that the ions have a single relaxation time. A complex impedance plot comprising a depressed or tilted semicircle can be represented by an equivalent circuit comprising a constant phase element (CPE) and a resistor in parallel connection (Teo *et al*., 2012). The CPE is a “leaky capacitor”. A tilted or depressed spike can be represented by a CPE (Linford, 1988). A tilted semicircle with an inclined (tilted) spike can be represented by a resistor and CPE in parallel connection that is connected in series with another CPE as depicted in Figure 3.9. The depressed semicircle represents the bulk material while the tilted spike represents the electrical double layer.

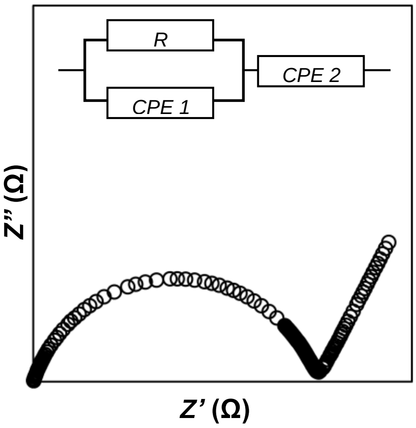

Figure 3.9: Experimental Nyquist plot of polymer electrolyte obtained from impedance spectroscopy and (inset) the corresponding equivalent circuit.

The real and negative imaginary parts of the complex impedance of a "leaky capacitor" or CPE is given by the equations below (Linford, 1988):

$$Z' = \frac{\cos\left(\frac{\pi p}{2}\right)}{k^{-1}\omega^{p}} \tag{3.15}$$

and

$$Z'' = \frac{\sin\left(\frac{\pi p}{2}\right)}{k^{-1}\omega^{p}} \tag{3.16}$$

For an equivalent circuit representing a complex impedance plot consisting of a depressed semicircle and tilted spike:

$$Z' = \frac{R + R^2 k_1^{-1}\omega^{p_1}\cos\left(\frac{\pi p_1}{2}\right)}{1 + 2Rk_1^{-1}\omega^{p_1}\cos\left(\frac{\pi p_1}{2}\right) + R^2 k_1^{-2}\omega^{2p_1}} + \frac{\cos\left(\frac{\pi p_2}{2}\right)}{k_2^{-1}\omega^{p_2}} \tag{3.17}$$

and

$$Z'' = \frac{R^2 k_1^{-1}\omega^{p_1}\sin\left(\frac{\pi p_1}{2}\right)}{1 + 2Rk_1^{-1}\omega^{p_1}\cos\left(\frac{\pi p_1}{2}\right) + R^2 k_1^{-2}\omega^{2p_1}} + \frac{\sin\left(\frac{\pi p_2}{2}\right)}{k_2^{-1}\omega^{p_2}} \tag{3.18}$$

According to (Linford, 1988), the inverse of k_1 i.e. k_1^{-1} in the equation (3.17) and (3.18) corresponds to bulk geometrical capacitance and k_2^{-1} is the double layer capacitance, which has the same representation as the capacitance C_e in the impedance equation used by (Bandara & Mellander, 2011). *R* is bulk resistance of the electrolyte. p_1 is a fraction of a $\pi/2$ angle i.e. $p_1\pi/2$, is the angle between the diameter of the depressed semicircle and *Z"* axis. p_2 is the skew parameter that controls the degree of the inclination of the tilted spike from the *Z'* axis and is the fraction of a right angle that is $p_2\pi/2$, the angle between the inclined spike and the *Z'* axis. A clearer explanation is given in Figure 3.10. p_1 and p_2 has value between 0 and 1.

If the complex impedance plot comprises of a depressed semicircle and a tilted spike, equations (3.17) and (3.18) should fit the plot with the appropriate value of the terms in the equation. The values of *R*, p_1 and p_2 can be determined from the complex impedance plot as shown in Figure 3.10. The values of k_1^{-1} and k_2^{-1} had to be obtained by trial and error until the experimental plot is fitted. The values of k_1^{-1} and k_2^{-1} are normally in the picofarad and microfarad range, respectively.

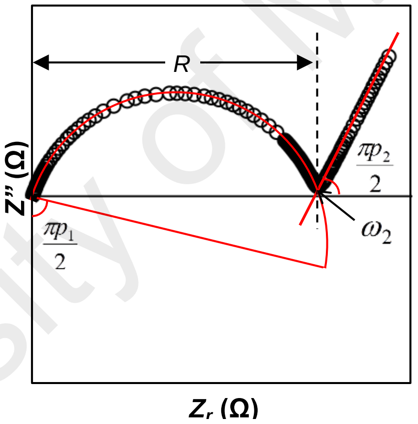

Figure 3.10: Typical Nyquist plot for polymer electrolyte.

If the experimental Nyquist plot obtained consists only tilted spiked, a depressed semicircle part in Figure 3.10 should be ignored. A Nyquist plot that takes the shape of only tilted spiked can be represented by an equivalent circuit comprising a resistor and constant phase element connected in series [refer appendix 2]. Hence, *Z'* and *–Z''* of tilted spiked complex impedance plot can be given by the equations below:

$$Z' = R + \frac{\cos\left(\frac{\pi p_2}{2}\right)}{k_2^{-1}\omega^{p_2}} \tag{3.19}$$

and

$$Z'' = \frac{sin\left(\frac{\pi p_2}{2}\right)}{k_2^{-1}\omega^{p2}} \tag{3.20}$$

In equation (3.19) and (3.20), the values of R and p_2 can be determined from the complex impedance plot shown in Figure 3.10 in order to fit the tilted spike Nyquist plot. The values of k_2^{-1} can be estimated in the microfarad range.

From (Bandara & Mellander, 2011), diffusion coefficient (*D*) of charge carriers in the electrolyte is defined by:

$$D = \frac{\lambda^2}{\tau_2} \tag{3.21}$$

Since capacitance k_2^{-1} is equivalent to capacitance C_e, equation (3.7) can be written as:

$$k_2^{-1} = \frac{\varepsilon_r \varepsilon_o A}{\lambda} \tag{3.22}$$

Hence,

$$\lambda = k_2 \varepsilon_r \varepsilon_o A \tag{3.23}$$

The diffusion coefficient (*D*) in equation (3.21) can be substituted using equation (3.23) to obtain:

$$D = \frac{(k_2 \varepsilon_r \varepsilon_o A)^2}{\tau_2} \tag{3.24}$$

The mobility (μ) of charge carriers can be evaluated from the Nernst–Einstein relation,

$$\mu = \frac{eD}{k_b T} \tag{3.25}$$

where k_b is 1.38×10^{-23} J K^{-1}, T is absolute temperature in Kelvin and e is 1.602×10^{-19} C. Upon substituting equation (3.24) into equation (3.25), we obtain:

$$\mu = \frac{e\left(k_2 \varepsilon_r \varepsilon_o A\right)^2}{k_b T \tau_2} \tag{3.26}$$

Since conductivity (σ) is given by

$$\sigma = n\mu e \tag{3.27}$$

The number density of charge carriers (n) can be obtained as:

$$n = \frac{\sigma k_b T \tau_2}{\left(e k_2 \varepsilon_r \varepsilon_o A\right)^2} \tag{3.28}$$

Thus using equations (3.24), (3.26) and (3.28), the diffusion coefficient (D), mobility (μ) and concentration of mobile ions (n) in electrolyte can be determined from the complex impedance plot. These equations was developed by Arof *et al*. (2014a) which is not dependent on the value of δ. This method is advantageous over the B–M method if the plot of loss tangent (tan δ) versus log ω does not exhibit a peak. Although the equations depend on the value of ε_r, transforming the impedance data into the permittivity formalism and plotting log ε' versus frequency will enable the value to be obtained. Equation below was used to plot the log ε' versus log frequency.

$$\varepsilon' = \frac{Z''}{\left(Z'^2 + Z''^2\right)}\left(\frac{d}{\omega \varepsilon_o A}\right) \tag{3.29}$$

The ε_r value to be inserted in the equations developed by Arof *et al*. (2014a) and is taken at the highest frequency where ε'appears constant.

3.4. Dye Sensitized Solar Cell (DSSC) Fabrication and Characterization

3.4.1. TiO_2/Dye Electrode Preparation

In preparing the photoanode, fluorine doped tin oxide (FTO) glass has been used as a current collector due to its good conductivity and transparency. The 1 cm × 2 cm FTO glass was first cleaned with detergent and rinsed with water and ethanol. The FTO glass was then immersed into propan–2–ol solution and heated at 353 K for 1 h to remove impurities. The glass was then removed from the solution and left to dry at ambient temperature. The FTO glass was then coated with two layers of TiO_2. The first layer of TiO_2 was prepared by grinding 0.5 g of TiO_2 (Degussa P–90) powder in 2 mL of HNO_3 (pH = 1) for 30 min before being spin coated on the dried and cleaned FTO glass at 2350 rpm for 45 second. The coated electrode was then sintered at 723 K for 45 min and then allowed to cool to room temperature. The second layer of TiO_2 was coated on the first layer electrode using the mixture of 0.5 g TiO_2 (Degussa P–25) powder, 2 mL of HNO_3 (pH = 1), 0.1 g poly(ethylene glycol) or PEG and 2 drops (0.1 g) surfactant. The mixture was then ground and the paste obtained was spread on the first layer TiO_2 electrode using the doctor blade method. The electrode was then sintered at 723 K for 45 min and then allowed to cool to room temperature. Figure 3.11 shows the double layer TiO_2 photoanode that has been prepared.

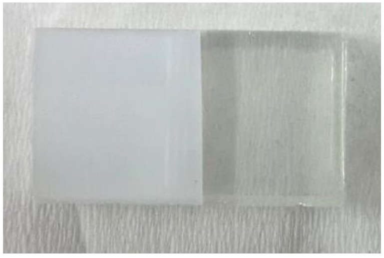

Figure 3.11: Double layer TiO_2 photoanode.

The TiO_2 layers were then immersed in a ruthenium 535–bis TBA (N719) dye solution diluted with ethanol to 0.3 mM for 24 h. The FTO/TiO_2/dye photoanode was then washed with ethanol to remove the unbound TiO_2 particles and unabsorbed dye before being used in DSSC fabrication.

3.4.2. Platinum (Pt) Counter Electrode Preparation

Platinum was used as the counter electrode. In preparing the platinum electrode, fluorine doped tin oxide (FTO) glass has been used as a current collector because of its low surface resistivities (7 Ω sq^{-1}). The 1 cm × 2 cm of FTO glass was first cleaned with detergent and rinsed with water and ethanol. The FTO glass was then immersed into propan–2–ol solution and heated at 353 K for 1 h to remove impurities. After that, the glass was taken out from the solution and left to dry at ambient temperature. The FTO glass was then placed on a hot plate and heated at 423 K. A commercial platinum solution Plastisol (Solaronix) was coated on the FTO glass drop by drop until the whole surface was covered. The electrode was then placed in a furnace and sintered at 723 K for 45 min after which it was allowed to cool to room temperature. Figure 3.12 shows the platinum electrode that has been prepared.

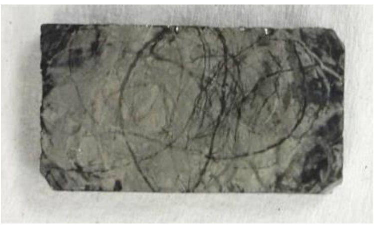

Figure 3.12: Platinum electrode.

3.4.3. DSSC Fabrication and *J–V* Characteristics

In this work, PVA–LiBOB–TBAI–I_2–DMF and PVA–LiBOB–TBAI–BMII–I_2–DMF gel polymer electrolytes (GPE) were used as a medium for charge transport in DSSCs. The GPE was sandwiched between TiO_2/dye photoanode and platinum (Pt) counter electrode in the configuration of FTO/TiO_2/Dye/GPE/Pt/FTO as shown in Figure 3.13.

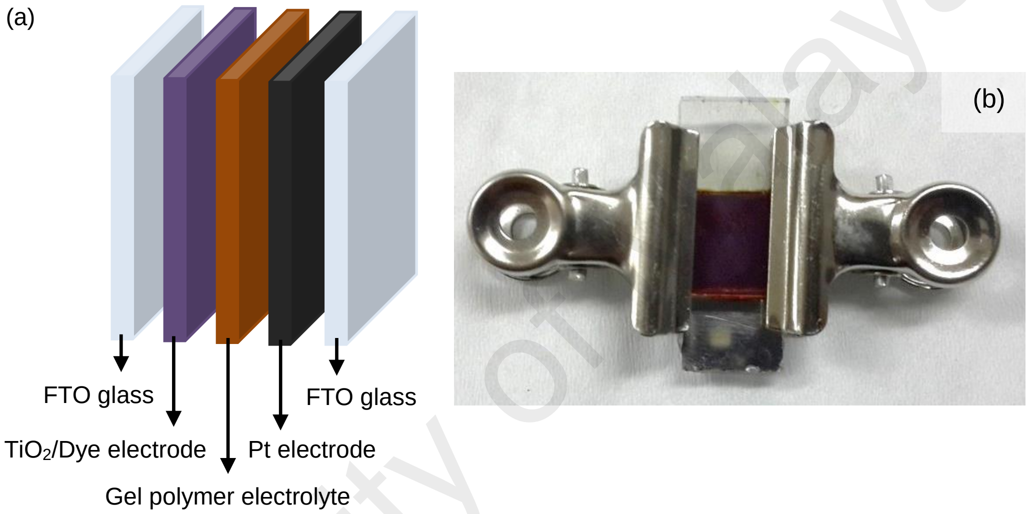

Figure 3.13: (a) Schematic diagram of DSSC fabrication and (b) the DSSC cell prepared in the lab.

The DSSC of 0.196 cm^2 window size was exposed to Orial LCS 100 (Xenon bulb 100W) light source with illumination of 1000 W m^{-2} at room temperature. In this work, N719 dye was used as sensitizer where the maximum range of UV–visible absorption is at 700 nm (Wang *et al.*, 2004). Thus no optical filters are needed to filter the IR irradiation coming from the source. The TiO_2 photoanode was connected to the counter/reference electrode wire while the platinum electrode was connected to the working electrode wire. All the electrode wires were connected to an Autolab potentiostat–galvanostat and the photocurrent density–voltage (*J–V*) characteristics of the DSSC measured. Figure 3.14 shows an example of *J–V* curve obtained from DSSC fabricated with 14.48 wt.% PVA–21.72 wt.% EC–28.96 wt.% PC–21.29 wt.% KI–9.12 wt.% TMAI–4.42 wt.% I_2 gel polymer electrolyte (Aziz *et al.*, 2013b).

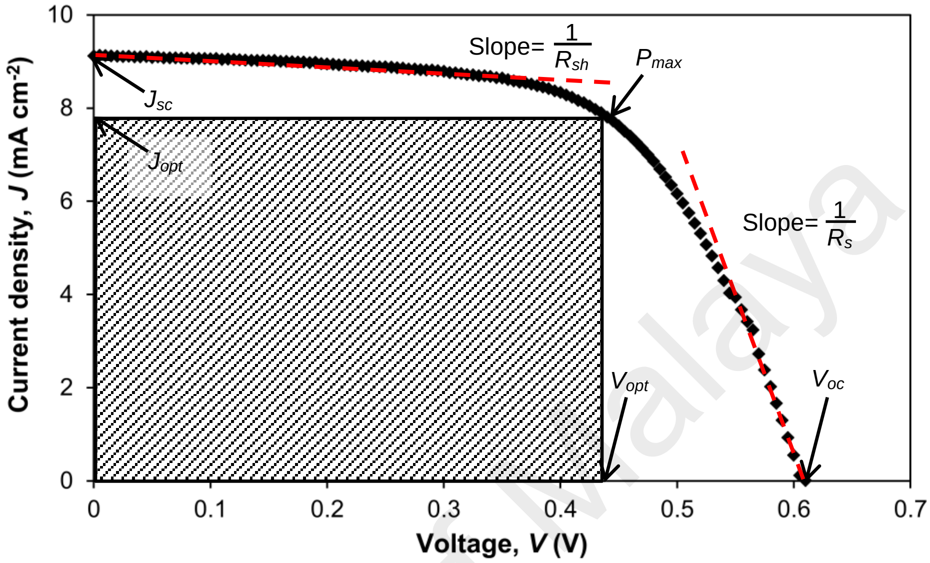

Figure 3.14: Photocurrent density–voltage (*J–V*) curve of DSSC (Aziz *et al.*, 2013b).

From the *J–V* plot, the current density, J_{opt} and voltage, V_{opt} at maximum power output were obtained and used in equation (3.30) to calculate the fill factor, *FF*.

$$FF(\%) = \frac{J_{opt}V_{opt}}{J_{sc}V_{oc}} \times 100\% \tag{3.30}$$

In equation (3.30), J_{sc} is the short circuit current density at zero voltage ($V = 0$). The V_{oc} is the open–circuit voltage when the contacts are isolated ($J = 0$). The *FF* value was then used to calculate the overall energy conversion efficiency, η of the cell using equation (3.31).

$$\eta(\%) = \frac{J_{sc}V_{oc}FF}{P_{in}} \times 100\% \tag{3.31}$$

Here, P_{in} is the total incident power density on to the cell.

The *J*–*V* plot of DSSC in Figure 3.14 can be represented by the equivalent circuit as shown in Figure 3.15 (Yang *et al.*, 2012). In Figure 3.15, I_{ph} is the ideal photocurrent, C_1 is capacitance element and R_{sh} is the shunt resistance. The sum of charge transfer resistance at Pt/electrode interface (R_1), diffusion of redox couple (R_2) and ohmic serial resistance (R_3) are the series resistance, R_s. The value of R_{sh} and R_s can be estimated by the inverse of tangent slope near the J_{sc} and V_{oc}, respectively as shown in Figure 3.14. Based on Figure 3.14, it can be seen that R_{sh} and R_s control the *FF* of DSSC. Higher R_{sh} and/or lower R_s can increase the *FF*, thus the efficiency of DSSC may increase.

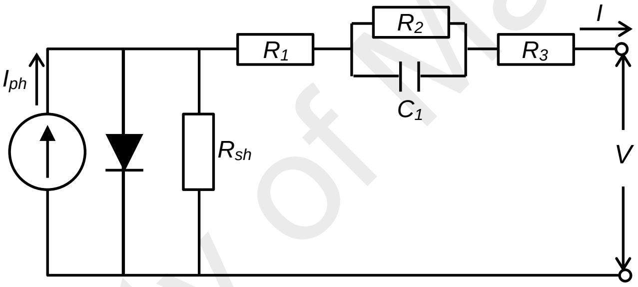

Figure 3.15: Equivalent circuit based on *J*–*V* characteristics of DSSC.

3.5. Summary

Two types of polymer electrolytes namely solid polymer electrolyte and gel polymer electrolyte have been prepared in this work. Three electrolyte systems were prepared, which is PVA–LiBOB solid polymer electrolyte (system 1), PVA–LiBOB–TBAI–I_2–DMF (system 2) and PVA–LiBOB–TBAI–BMII–I_2–DMF (system 3). All electrolytes were characterized using fourier transform infrared and electrochemical impedance spectroscopies. The electrolyte in system 2 and 3 were used in DSSC devices and characterized.

CHAPTER 4 : RESULTS FOR
PVA–LiBOB SOLID POLYMER ELECTROLYTE SYSTEM

4.1. Introduction

In this chapter, the solution cast technique was used to prepare PVA–LiBOB complexes. The electrolyte prepared was characterized by FTIR spectroscopy and analyzed using EIS for electrical properties. FTIR will discuss the complexation between the polymer and salt, and the vibrational bands corresponding to free and contact ions were deconvoluted to determine the percentage of free ions in the conducting membranes. EIS will discuss the changes in ionic conduction for polymer–salt electrolyte system at ambient and elevated temperatures. The transport properties of charge carriers of each electrolyte were also determined.

4.2. Fourier Transform Infrared (FTIR) Spectroscopy

To prove that PVA and LiBOB has formed a complex, FTIR studies were performed to observed the wavenumber shift of the relevant functional group of the polymer. In PVA this functional group is the OH group. The FTIR spectrum in transmittance mode for LiBOB salt, PVA and PVA–LiBOB complexes from 3700 to 3000 cm^{-1} and 1900 to 800 cm^{-1} are shown in Figure 4.1(a) and (b).

In LiBOB salt infrared spectrum, the band at 1803 cm^{-1} is assigned to C=O out–of–phase vibrations (Holomb *et al.*, 2006). In A0 electrolyte infrared spectrum, the band at 3322 cm^{-1} is assigned to OH band (Buraidah & Arof, 2011). The vibrational frequency at 1732 and 1659 cm^{-1} are assigned to C=O (Malathi *et al.*, 2010) and C=C (Somani *et al.*, 2003) acetate group vibrations, respectively. Since the PVA used is only

80% hydrolyzed, residues of incomplete hydrolysis can still be observed in the form of C=O and C=C bonds. The band at 1093 wavenumber has been assigned to C–O stretching of PVA (Buraidah & Arof, 2011).

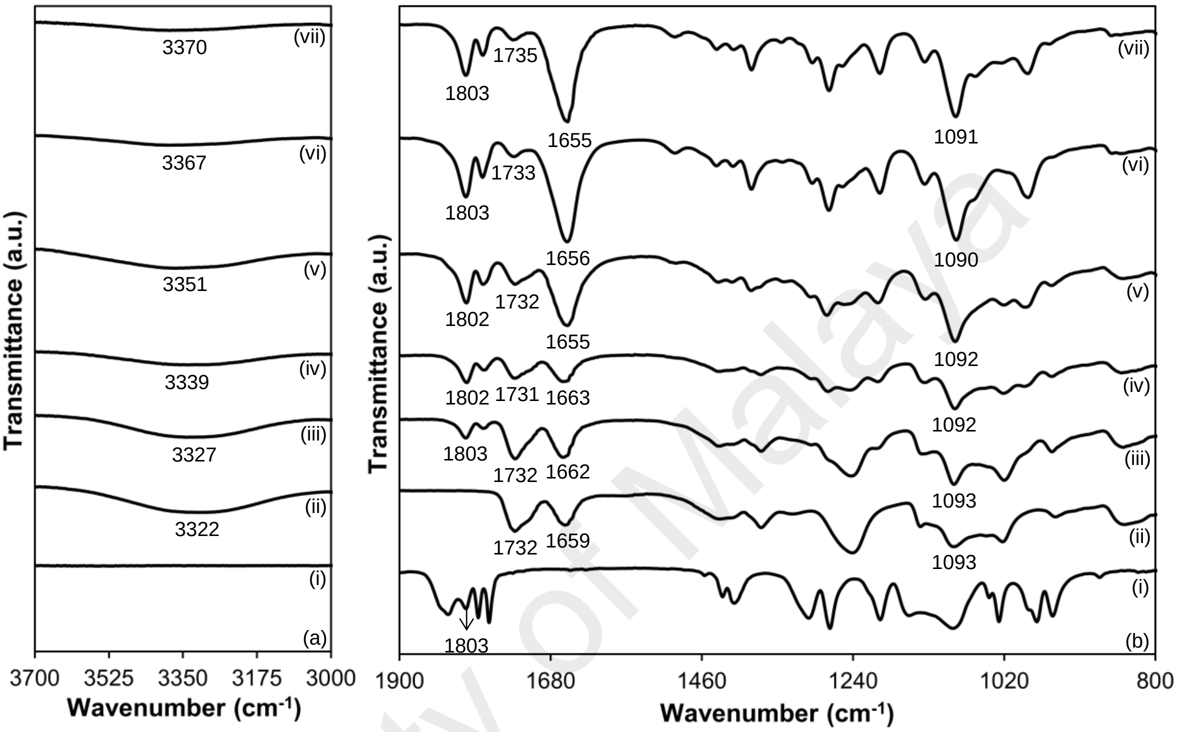

Figure 4.1: FTIR spectra of (i) LiBOB salt, (ii) A0 (PVA only), (iii) A1, (iv) A2, (v) A3, (vi) A4 and (vii) A5 electrolytes between (a) 3700 and 3000, and (b) 1900 and 800 wavenumber.

Addition of LiBOB salt into PVA polymer is observed to show all the vibration modes of PVA and LiBOB. In PVA–LiBOB complexes infrared spectrum, the vibrational band shown at 3327, 3339, 3351, 3367 and 3370 wavenumbers are corresponding to hydroxyl group of PVA. The band at 1802 and 1803 wavenumbers are assigned to C=O out–of–phase vibrations in LiBOB. The vibrational frequencies at 1731, 1732, 1733 and 1735 cm^{-1} are assigned to C=O vibrations of PVA acetate group. The band corresponding to C=C vibration modes of acetate group of PVA are shown at 1655, 1656, 1662 and 1663 wavenumbers. The vibrational frequencies at 1090, 1091, 1092 and 1093 cm^{-1} are assigned to C–O stretching of PVA.

Figure 4.2 shows the FTIR spectrum in transmittance mode for PVA and its complexes between 3700 and 3000 wavenumbers (hydroxyl region). Li^+ from the salt is expected to interact weakly with the lone pair electrons of the hydroxyl group oxygen in PVA. Hema *et al*. (2009b) have also reported the polymer and salt interaction can be observed from the band shift. From Figure 4.2, it can be observed that the OH band of A0 electrolyte (pure PVA) has shifted from 3322 cm^{-1} to higher wavenumbers as LiBOB salt is added indicating the occurrence of complexation between PVA and LiBOB.

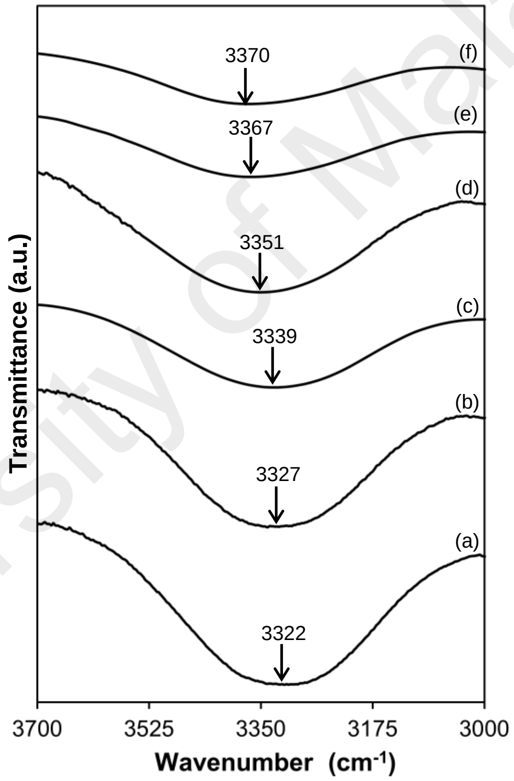

Figure 4.2: FTIR spectra between wavenumbers band of 3700 and 3000 of (a) A0, (b) A1, (c) A2, (d) A3, (e) A4 and (f) A5 electrolytes.

PVA is a hydrophilic polymer and therefore it easily absorbs water (Morita *et al.*, 2000). It is because PVA contains polar or charged functional group (hydroxyl group) which renders it to hold large amounts of water in their polymer network. In polymer electrolyte, the contamination of water should be avoided. Ping *et al.*, (2001) reported that the infrared spectrum of PVA membrane with water shows the hydroxyl group of water at 3280 and 3400 wavenumber. This indicates that the infrared spectrum of electrolytes prepared in this system might be overlapped with the hydroxyl band of water. Thus, the band between 3700 and 3000 wavenumber was deconvoluted to confirm that all electrolytes prepared is not contaminated with water. Figure 4.3 shows the deconvolution of hydroxyl region of PVA–LiBOB solid polymer electrolyte system between 3700 and 3000 wavenumber.

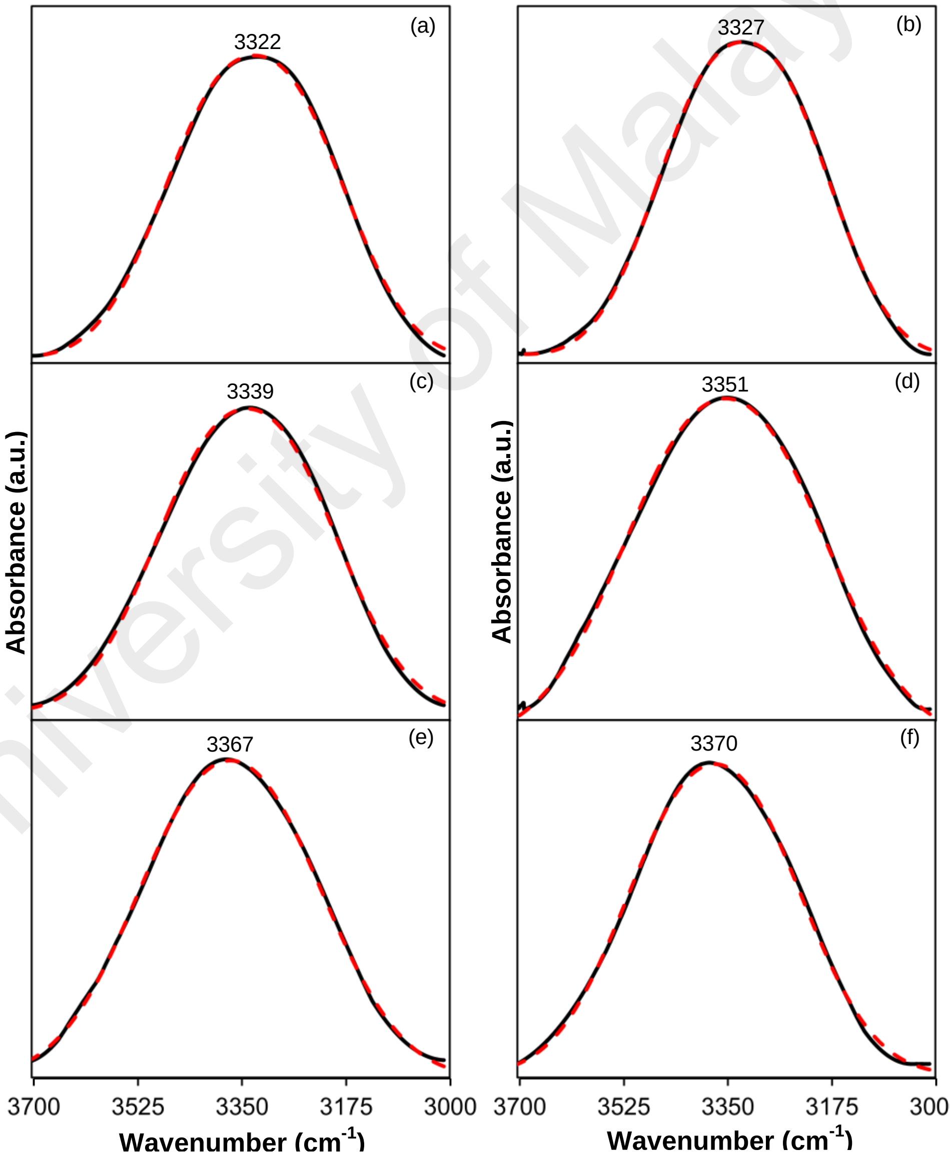

Figure 4.3: Deconvolution of the band between 3700 and 3000 cm^{-1} of (a) A0, (b) A1, (c) A2, (d) A3, (e) A4 and (f) A5 electrolytes. Line (—) due to original spectrum and line (---) due to fitted spectrum.

It is observed that only one deconvoluted peak appeared which can be assigned to the hydroxyl group of PVA in all electrolytes. Based on this observation, it is confirmed that there is no water contamination in the PVA–LiBOB solid polymer electrolytes prepared.

The occurrence of ion dissociation and association can be quantified from FTIR studies (Hou *et al.*, 2003; Chen *et al.*, 2011; Kufian *et al.*, 2012; Sim *et al.*, 2012). According to Holomb *et al.*, (2006), peaks at 1804 and 1828 wavenumber in the LiBOB FTIR spectrum is due to free ions (resulting from dissociation of ions) and ion pairs (due to association of ions), respectively. By fitting the investigated band in the Gaussian/Lorentzian mode, several peaks as shown in Figure 4.4 can be observed. However, only three peaks at 1802, 1812 and 1826 cm^{-1} are of prime concern. This is because as reported by Holomb *et al.*, (2006), ion pairs of LiBOB are observed at 1812 cm^{-1} in the FTIR spectrum for three different $Li^+\cdots BOB^-$ ion–pair models. Thus, in the present work depicted in Figure 4.4, the peak at 1802 cm^{-1} represents mobile ions and at 1812 and 1826 cm^{-1} represent ion pairs. The band at 1778 cm^{-1} is assigned to C=O out–of–phase vibrations of LiBOB (Holomb *et al*., 2006).

The area under peaks that correspond to free or mobile ions and ion pairs were calculated using equations (3.1) and (3.2). The variation in the areas expressed in percent against LiBOB concentration is illustrated in Figure 4.5. The free ion percentage increased until a maximum of 75.11% at 40 wt.% LiBOB salt concentration. The percentage area of ion pairs decreased to 24.89%. Beyond 40 wt.% LiBOB salt concentration, the percentage of free ion area decreased to 65.81% and can be attributed to ion association and this is confirmed by the increase in percentage area of ion pairs.

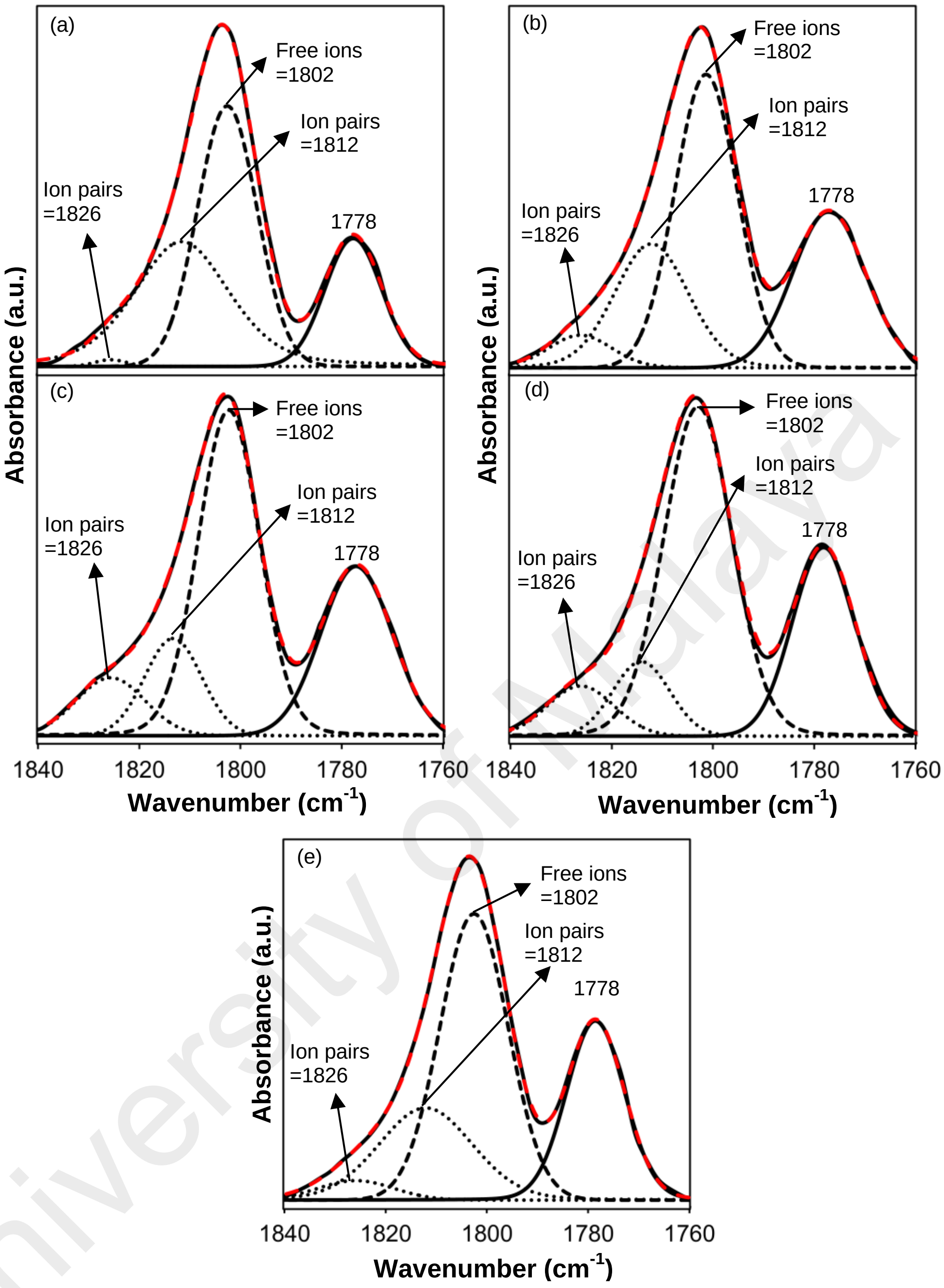

Figure 4.4: Deconvolution of the band between 1840 and 1760 cm^{-1} of (a) A1, (b) A2, (c) A3, (d) A4 and (e) A5 electrolytes. Area under line (---) due to free ions and line (·····) due to ion pairs. Line (—) refer to original spectrum and line (---) refer to fitted spectrum.

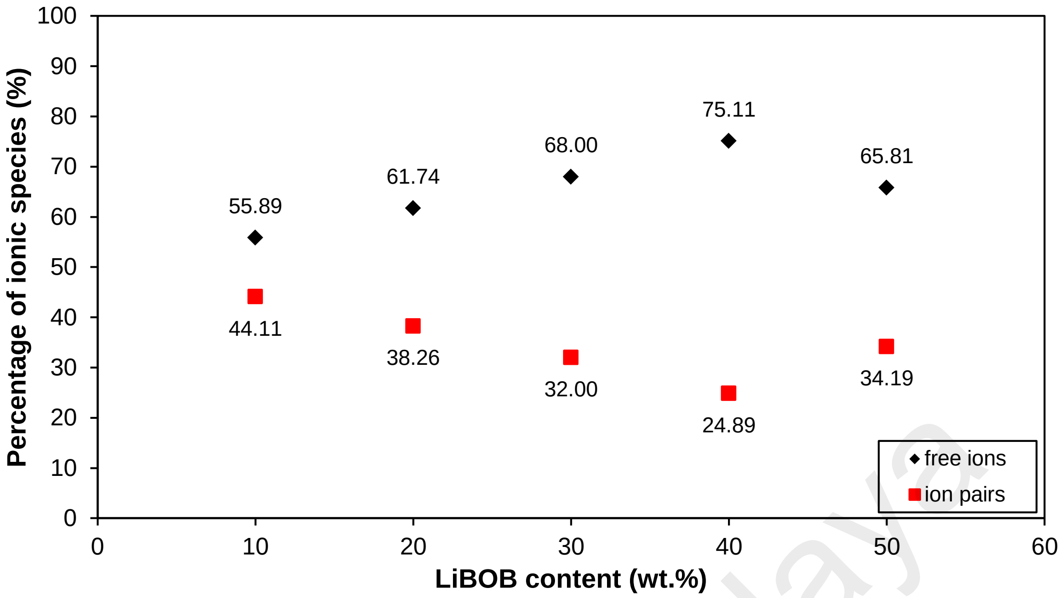

Figure 4.5: Area percentage of free ions and ion pairs for PVA–LiBOB solid polymer electrolytes at various concentrations.

It is reported that Petrowsky & Frech (2008) have used the FTIR method to determine mobility and concentration of the mobile ions for liquid electrolytes while (Ericson *et al.*, 2000) have calculated the two parameters for gel polymer electrolytes. The transport properties of charge carriers determined by FTIR method was also proven by Arof and his co–workers for solid polymer electrolyte (Abdul Rahaman *et al.*, 2014; Arof *et al.*, 2014a). Based on information obtained from FTIR spectroscopy, the values of number density (*n*), mobility (μ) and diffusion coefficient (*D*) of charge carriers for PVA–LiBOB solid polymer electrolyte system were calculated using equation below (Arof *et al.*, 2014a):

$$n = \frac{M \times N_A}{V_{Total}} \times \text{free ions (\%)} \times 2 \qquad (4.1)$$

$$\mu = \frac{\sigma V_{Total}}{2eMN_A \times \text{free ions (\%)}} \qquad (4.2)$$

$$D = \frac{k_b T \sigma V_{Total}}{2e^2 M N_A \times \text{free ions (\%)}} \tag{4.3}$$

In equation (4.1), M is the number of moles of salt used in each electrolyte, N_A is Avogadro's number (6.02×10^{23} mol^{-1}), V_{Total} is total volume of electrolyte, free ions (%) is the percentage of ion dissociation obtained from FTIR deconvolution in Figure 4.4 and constant 2 represents two moles of dissociated cation and anion, given in chemical equation below:

$$LiBOB \Leftrightarrow Li^+ + BOB^- \tag{4.4}$$

In equation (4.2), σ is dc conductivity and e is electron charge (1.602×10^{-19} C). k_b and T in equation (4.3) is Boltzmann constant (1.38×10^{-23} J K^{-1}) and absolute temperature, respectively. Table 4.1 lists the values of V_{Total}, free ions (%), n, μ and D of PVA–LiBOB solid polymer electrolyte obtained using FTIR method at room temperature.

Table 4.1: Values of V_{Total}, free ions (%), n, μ and D of PVA–LiBOB solid polymer electrolyte obtained using FTIR method at room temperature (298 K).

Electrolyte	V_{Total} **(cm^3)**	**Free ions (%)**	n **($\times10^{20}$ cm^{-3})**	μ **($\times10^{-7}$ cm^2 V^{-1} s^{-1})**	D **($\times10^{-9}$ cm^2 s^{-1})**
A1	0.490	55.89	3.943	0.278	0.714
A2	0.576	61.74	8.319	1.315	3.378
A3	0.688	68.00	13.159	2.277	5.849
A4	0.837	75.11	18.587	9.516	24.440
A5	1.045	65.81	19.563	3.809	9.782

4.3. Electrical Impedance Spectroscopy (EIS)

4.3.1. Ionic Conductivity of PVA–LiBOB Solid Polymer Electrolyte.

EIS was performed to study the electrical properties of polymer electrolyte. Figure 4.6 shows the Nyquist plots for PVA–LiBOB system at room temperature (298 K). The value of bulk resistance, R_b and thickness, *d* of each electrolyte are listed in Table 4.2. The effect of salt concentration on ionic conductivity of the PVA–LiBOB electrolytes at 298 K is depicted in Figure 4.7.

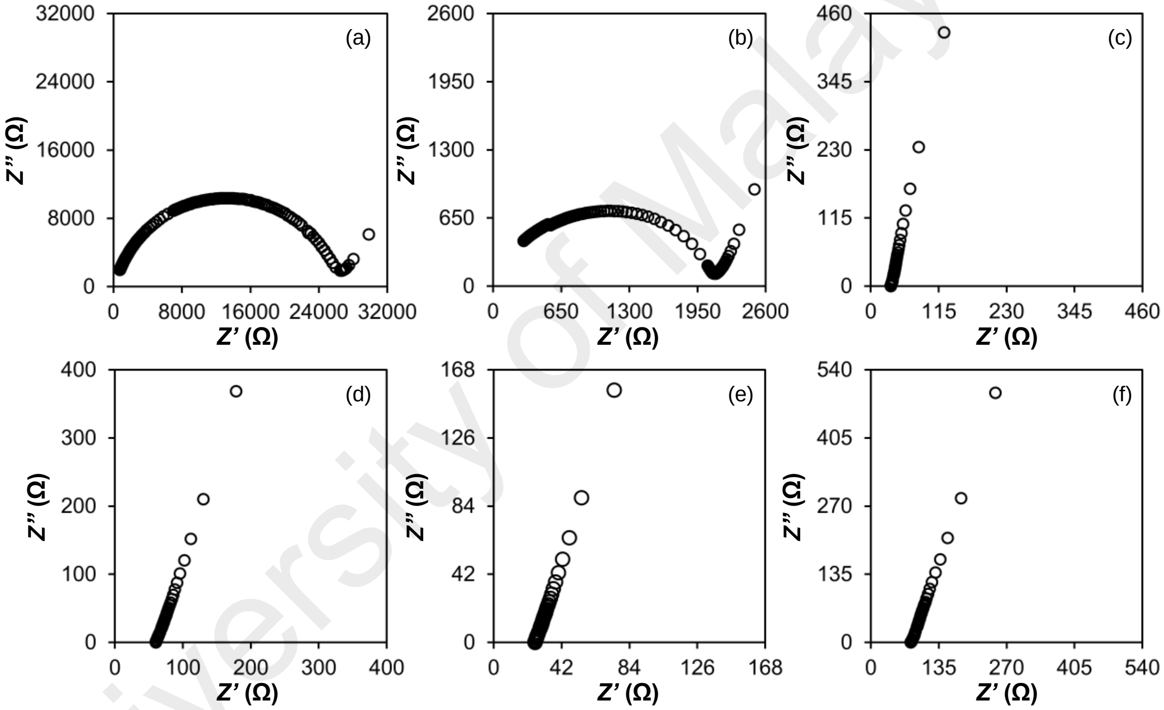

Figure 4.6: Nyquist plot of (a) A0, (b) A1, (c) A2, (d) A3, (e) A4 and (f) A5 solid polymer electrolyte at room temperature.

Table 4.2: The *d* and R_b values of PVA–LiBOB solid polymer electrolyte obtained in Figure 4.6.

Electrolyte	***d* (cm)**	**R_b (Ω)**
A0	0.0268	26200.0
A1	0.0117	2120.0
A2	0.0019	34.5
A3	0.0092	61.0
A4	0.0227	25.5
A5	0.0300	80.0

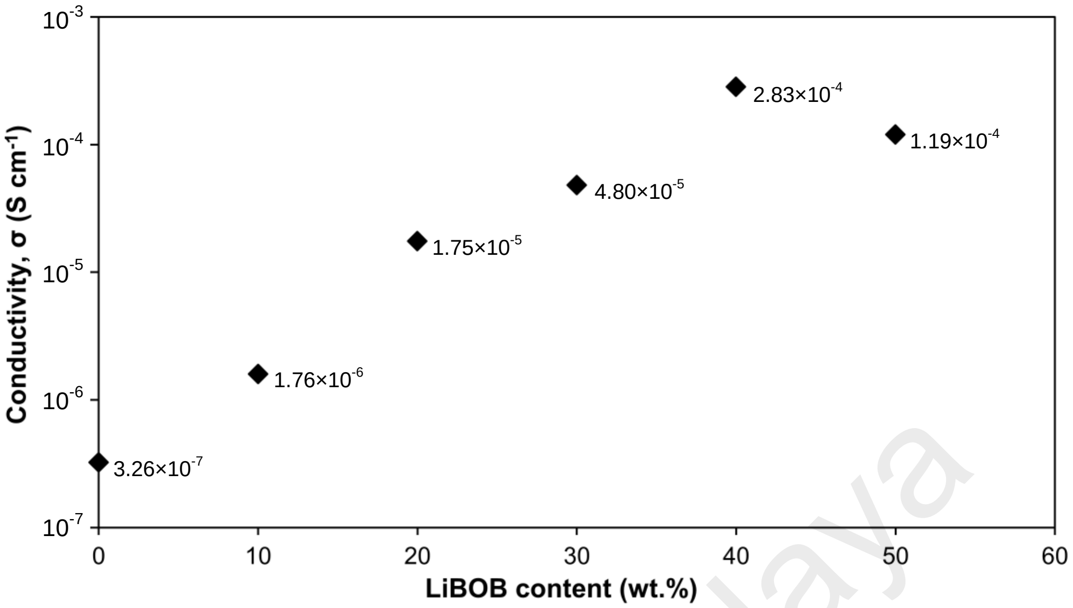

Figure 4.7: Ionic conductivity of PVA–LiBOB solid polymer electrolyte system at room temperature.

As illustrated in Figure 4.7, pure PVA (A0 electrolyte) has conductivity of 3.26×10^{-7} S cm^{-1}. On addition of 10 wt.% LiBOB salt (A1 electrolyte), conductivity increased by about one magnitude order to 1.76×10^{-6} S cm^{-1}. The conductivity increased gradually with increasing LiBOB salt in the electrolyte until the conductivity reached a maximum of 2.83×10^{-4} S cm^{-1} at 40 wt.% salt concentration and beyond the A4 electrolyte composition, conductivity decreased.

The dependence of conductivity on temperature for the PVA–LiBOB electrolytes is displayed in Figure 4.8. The conductivity for all samples was temperature assisted from 298 to 393 K. From Figure 4.8, the conductivity–temperature dependence of this system is observed to form a quadratic shape, which suggests that σ and T obey the VTF relationship. The VTF equation is given by:

$$\sigma T^{1/2} = A\exp\left[\frac{-E_a}{k_b(T-T_o)}\right] \tag{4.5}$$

In equation (4.5), A is the pre–exponential factor, E_a is the pseudoactivation energy of ion transport, k_b is Boltzmann constant, T is absolute temperature and T_o is the ideal glass transition temperature when the entropy is zero. T_o was determined by trial and error to make the conductivity–temperature relationship depicted by the plot of log $\sigma T^{1/2}$ versus 1000/(T–T_o) appear as linear as possible (Figure 4.9). Table 4.3 listed the values of T_o, T_g, $|T_g$–$T_o|$, regression (R^2) and E_a obtained from VTF plot in Figure 4.9.

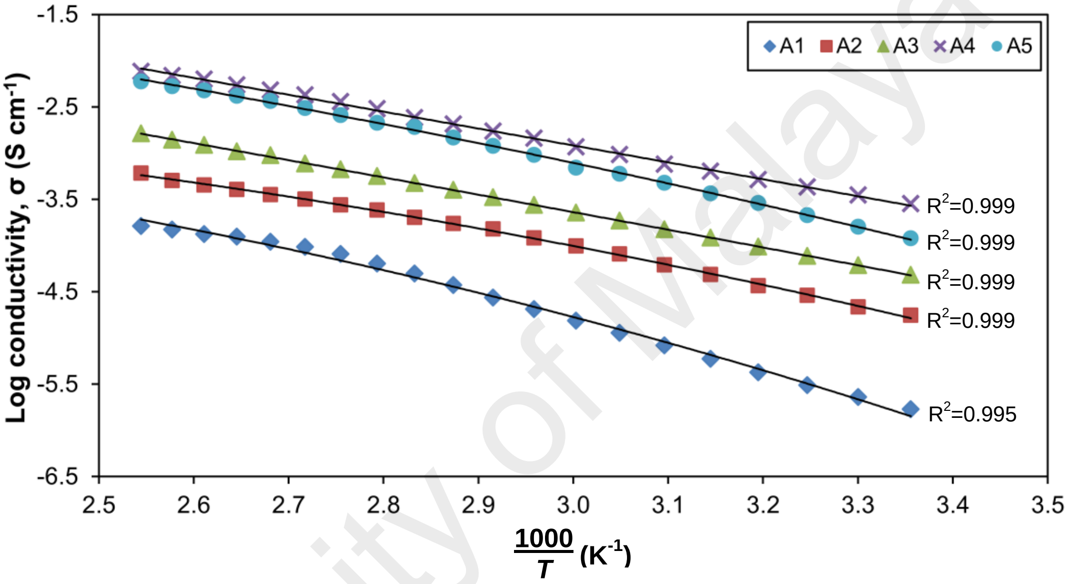

Figure 4.8: Conductivity–temperature dependence of PVA–LiBOB solid polymer electrolyte.

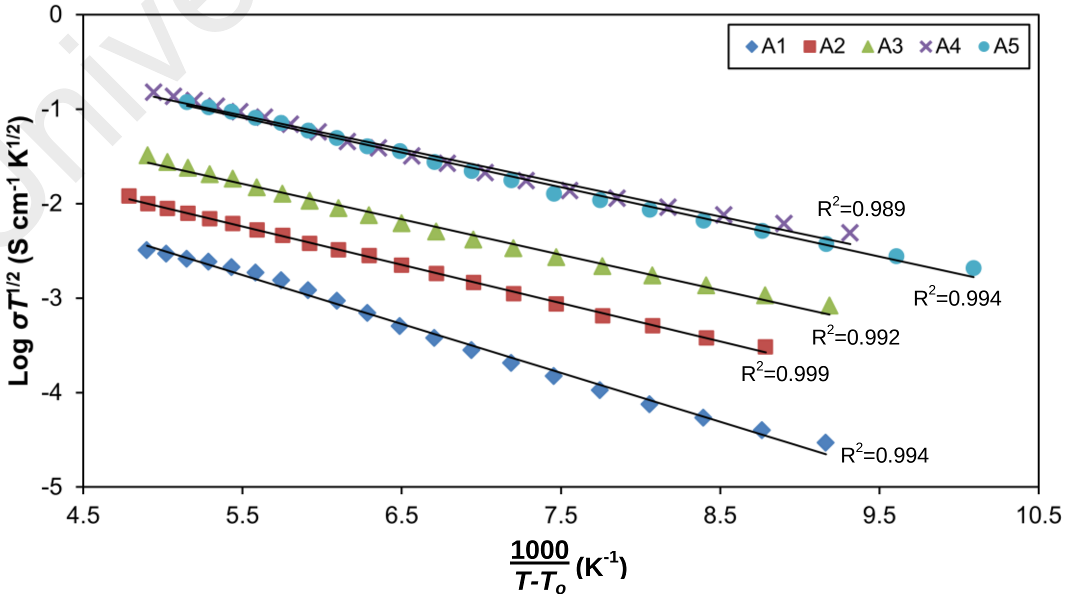

Figure 4.9: VTF plot of conductivity–temperature dependence of PVA–LiBOB electrolyte.

Table 4.3: The T_o, T_g, $|T_g–T_o|$, R^2 (regression) and E_a values of PVA–LiBOB solid polymer electrolyte system.

Electrolyte	T_o (K)	T_g (K)	$\|T_g–T_o\|$ (K)	R^2	E_a (meV)
A1	188.88	308.88	120	0.994	102.70
A2	184.18	304.18	120	0.999	80.54
A3	189.15	264.15	75	0.992	74.55
A4	190.67	240.67	50	0.989	70.76
A5	198.91	248.91	50	0.994	72.94

In Table 4.3, T_g values for each electrolytes was taken from (Noor *et al*., 2013). From Table 4.3, the value of $|T_g–T_o|$ for each electrolyte is between 120 and 50 K. This is in agreement with the VTF law where the T_o is 50 K lower than T_g (Garca-Coln *et al*., 1989).

4.3.2. Room Temperature Transport Properties of Charge Carriers of PVA–LiBOB Solid Polymer Electrolyte

Basically, conductivity (σ) of polymer electrolytes can be described by:

$$\sigma = n\mu e \tag{4.6}$$

where n is the number density of free ions that contribute to conductivity, μ is ionic mobility and e is elementary charge. It can be seen from equation (4.6) that n and μ are two important parameters that control the conductivity of polymer electrolyte. Thus, it will be useful if n and μ can be determined quantitatively. Based on the method proposed by (Arof *et al*., 2014a) or for simplicity referred to as the Arof–Noor (A–N) method, the concentration (in cm^{-3}) and mobility of the free ions in PVA–LiBOB solid polymer electrolyte system can be evaluated from electrochemical impedance spectroscopy.

Figure 4.10 shows the impedance plot and their corresponding fitted point for PVA–LiBOB solid polymer electrolyte system at room temperature. A0 membrane is not considered in this fitting exercise because it does not have a charge carrier. A0 is free of salt.

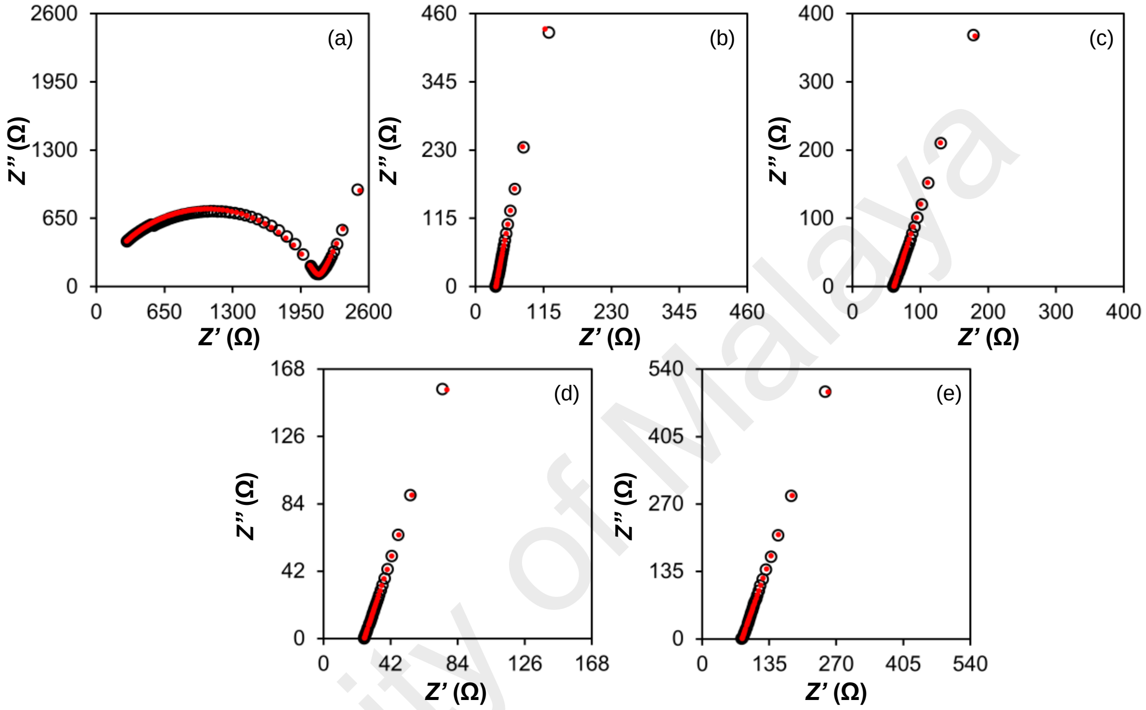

Figure 4.10: Nyquist plot (o) and their corresponding fitted point (●) for (a) A1, (b) A2, (c) A3, (d) A4 and (e) A5 solid polymer electrolyte at room temperature.

The impedance plot consisted of a depressed semicircle and a tilted spike was fitted using equations (3.17) and (3.18). The Nyquist plot that consisted of only tilted spike was fitted using equations (3.19) and (3.20). The value of R (bulk resistance of the electrolyte), p_1 (the fraction of a right angle between the diameter of the depressed semicircle and Z'' axis) and p_2 (the fraction of a right angle between the inclined spike and the Z' axis) were determined by the concept shown in Figure 3.10. The parameters k_1 (inverse of bulk geometrical capacitance) and k_2 (inverse of electrical double layer capacitance) were determined by trial and error until the fitted points quite accurately approximate the Nyquist plot at the corresponding frequencies. All the fitted points are observed to fit the plot. Table 4.4 lists the values of d, R, k_1, p_1, k_2 and p_2 for PVA–LiBOB solid polymer electrolyte system obtained in Figure 4.10.

Table 4.4: Values of d, R, k_1, p_1, k_2 and p_2 for PVA–LiBOB solid polymer electrolyte system. The Nyquist plot of which is shown in Figure 4.10.

Electrolyte	***d* (cm)**	***R* (Ω)**	p_1	k_1 **(F^{-1})**	p_2	k_2 **(F^{-1})**
A1	0.0117	2120.0	0.775	109000000	0.740	70000
A2	0.0019	34.5	–	–	0.880	69700
A3	0.0092	61.0	–	–	0.800	38450
A4	0.0227	25.5	–	–	0.795	15800
A5	0.0300	80.0	–	–	0.785	47800

Based on equations (3.24), (3.26) and (3.28), the diffusion coefficient (*D*), mobility (μ) and number density or concentration (*n*) of mobile ions for PVA–LiBOB electrolytes can be calculated if the values of k_2, τ_2 and ε_r are known. From the fitting of Nyquist plot in Figure 4.10, the value of k_2 can be obtained. The value of τ_2 can be taken at the frequency corresponding to a minimum in *Z"* i.e. at $Z'' \rightarrow 0$ ($\tau_2 = 1/\omega_2 = 1/2\pi f$, see Figure 3.10). The value of dielectric constant, ε_r for each sample can be deduced by plotting dielectric constant, ε' versus frequency, *f*. The impedance data obtained from experimental were substituted in equation (3.29) and graph of log ε' versus log *f* was plotted as shown in Figure 4.11. The value of ε_r can only be taken for the A1 electrolyte since for other electrolytes the plot of log ε' versus log *f* does not show constant values at high frequencies. Table 4.5 lists the values of τ_2 and ε_r for PVA–LiBOB electrolytes at ambient temperature.

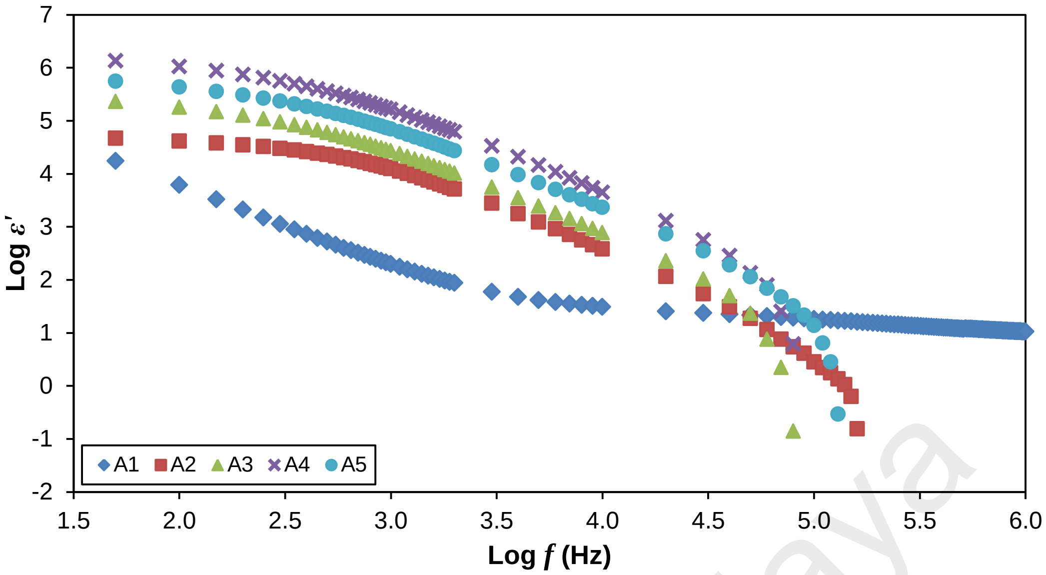

Figure 4.11: Plot of real part of complex permittivity, ε' as function of frequency for PVA–LiBOB solid polymer electrolyte system at room temperature.

Table 4.5: Values of τ_2 and ε_r for PVA–LiBOB solid polymer electrolyte system.

Electrolyte	τ_2 **(s)**	ε_r
A1	5.89×10^{-5}	10.57
A2	9.82×10^{-7}	–
A3	1.99×10^{-6}	–
A4	2.04×10^{-6}	–
A5	1.21×10^{-6}	–

From Figure 4.11, it can be seen that the dielectric constant for all electrolytes is high at low frequency. The dielectric constant of A1 electrolyte is observed to decrease as the frequency increases and is almost constant between 100 kHz and 1 MHz. The dielectric constant of A2 to A5 electrolytes is observed to decrease as frequency increased. The value of ε_r was taken in the high frequency range at which ε' is constant. Thus, only A1 electrolyte can give the value of ε_r from the impedance data.

In equations (3.24), (3.26) and (3.28), the values of ε_r is important to calculate the diffusion coefficient (*D*), mobility (μ) and number density (*n*) of charge carriers of

PVA–LiBOB solid polymer electrolyte system. From Figure 4.11, the value of ε_r for A2 to A5 electrolytes cannot be obtained because it does not show the constant value at high frequency. Thus, equations (3.24), (3.26) and (3.28) should be modified so that it is independent of ε_r. Based on Bandara & Mellander (2011), the angular frequency, ω_2 corresponding to minimum in *Z''* is given as below:

$$\omega_2 = \frac{1}{RC}\sqrt{\frac{2C}{C_e}} \tag{4.7}$$

Here, *C* is the bulk geometrical capacitance and C_e is the electrical double layer (EDL) capacitance. Rearranging equation (4.7), we get:

$$C = \frac{2}{\omega_2^{\,2} R^2 C_e} \tag{4.8}$$

Since EDL capacitance, C_e is equivalent to capacitance, k_2^{-1}, equation (4.8), can be written as:

$$C = \frac{2k_2}{\omega_2^{\,2} R^2} \tag{4.9}$$

By substituting equation (3.8) into equation (4.9), we get:

$$\frac{\varepsilon_r \varepsilon_o A}{d} = \frac{2k_2}{\omega_2^{\,2} R^2} \tag{4.10}$$

From equation (3.24), the diffusion coefficient, *D* is given by:

$$D = \left(k_2 \varepsilon_r \varepsilon_o A\right)^2 \omega_2 \tag{4.11}$$

Substituting equation (4.10) into equation (4.11), we get:

$$D = \left(\frac{2k_2{}^2 d}{\omega_2{}^2 R^2} \right)^2 \omega_2 \tag{4.12}$$

Hence, the diffusion coefficient of charge carriers, *D* for electrolyte with only tilted spike Nyquist plot can be obtained using the equation below:

$$D = \frac{4k_2{}^4 d^2}{R^4 \omega_2{}^3} \tag{4.13}$$

This equation is not dependent on the value of ε_r but the equation depends on the value of ω_2 and ω_2 can be obtained from the Nyquist plot. Table 4.6 lists the values of room temperature diffusion coefficient (*D*) of charge carriers for PVA–LiBOB electrolytes. The diffusion coefficient for A1 electrolyte was calculated using equation (4.11) and equation (4.13) was used to calculate diffusion coefficient for A2 to A5 electrolytes.

Table 4.6: Diffusion coefficient of charge carriers (*D*) for PVA–LiBOB solid polymer electrolyte at room temperature.

Electrolyte	***D* (10^{-10} cm^2 s^{-1})**
A1	7.184
A2	2.281
A3	4.208
A4	25.808
A5	8.043

Comparing the values of diffusion coefficient, *D* obtained in Tables 4.6 and Table 4.1, only A1 electrolyte gives quite similar values. The other electrolytes, A2 to A5 electrolytes do not give closer value as obtained in Table 4.1. This shows that equation (4.11) developed by (Arof *et al.*, 2014a) is valid to determine the transport properties of electrolyte A1 which have a Nyquist plot consisting of depressed semicircle and tilted spike. For the case where Nyquist plot consisted only a tilted spike, equation (4.13) can be use but further modifications should be done in order to obtain the closer transport properties values as tabulated in Table 4.1.

To obtain the value of diffusion coefficient of charge carriers for electrolyte with impedance plot consisting only of a tilted spike, the following procedure was done. The diffusion coefficient obtained by fitting method is assigned as D_o [equation (4.13)] and diffusion coefficient obtained by FTIR was assigned as D_{FTIR} [equation (4.3)]. A graph of $Ln\left(\frac{D_{FTIR}}{D_o}\right)$ against $Ln(D_o)$ for A2 to A5 electrolytes at room temperature was plotted in Figure 4.12 and their corresponding values were listed in Table 4.7.

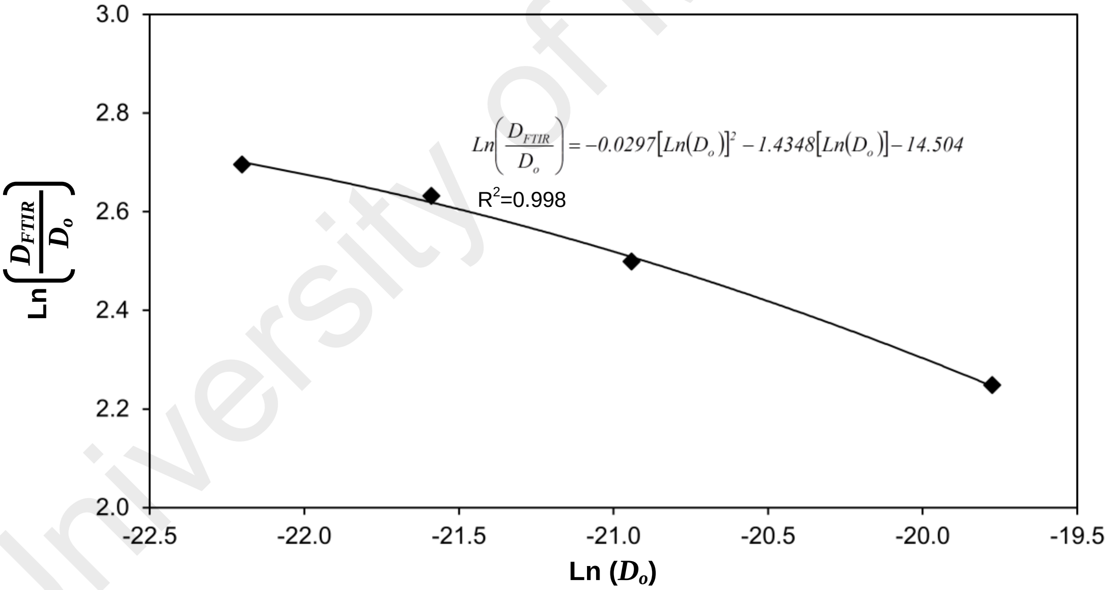

Figure 4.12: Plot of $Ln\left(\frac{D_{FTIR}}{D_o}\right)$ against $Ln(D_o)$ at room temperature.

Table 4.7: Values of $Ln\left(\frac{D_{FTIR}}{D_o}\right)$ and $Ln(D_o)$ for electrolyte A2 to A5 obtained at room temperature.

Electrolyte	$\boldsymbol{Ln\left(\frac{D_{FTIR}}{D_o}\right)}$	$\boldsymbol{Ln(D_o)}$
A2	2.695	-22.201
A3	2.632	-21.589
A4	2.248	-19.775
A5	2.498	-20.941

From Figure 4.12, it can be seen that all points can relate to each other in quadratic form:

$$Ln\left(\frac{D_{FTIR}}{D_o}\right) = -0.0297[Ln(D_o)]^2 - 1.4348[Ln(D_o)] - 14.504 \tag{4.14}$$

Hence,

$$D_{FTIR} = D_o \, exp\{-0.0297[Ln(D_o)]^2 - 1.4348[Ln(D_o)] - 14.504\} \tag{4.15}$$

It can be seen that the value of diffusion coefficient for electrolyte obtained by FTIR can be calculated by substituting the value of D_o in equation (4.15). D_o can be calculated using equation (4.13) and all parameters in equation (4.13) can be determined from fitting of tilted spike in the Nyquist plot. This implies that equation (4.15) can be used to determine the *D* for the charge carriers of the electrolyte by fitting the tilted spike in the Nyquist plot, which closer to the values of *D* obtained by FTIR. Hence, the equation below was developed to calculate the values of diffusion coefficient (*D*), mobility (μ) and number density (*n*) of mobile ions of the electrolyte from fitting of tilted spike Nyquist plot.

$$D = D_o \, exp\{-0.0297[Ln(D_o)]^2 - 1.4348[Ln(D_o)] - 14.504\} \tag{4.16}$$

$$\mu = \frac{eD_o \, exp\left\{-0.0297\left[Ln\left(D_o\right)\right]^2 - 1.4348\left[Ln\left(D_o\right)\right] - 14.504\right\}}{k_b T} \tag{4.17}$$

$$n = \frac{\sigma k_b T}{e^2 D_o \, exp\left\{-0.0297\left[Ln\left(D_o\right)\right]^2 - 1.4348\left[Ln\left(D_o\right)\right] - 14.504\right\}} \tag{4.18}$$

where

$$D_o = \frac{4k_2{}^4 d^2}{R^4 \omega_2{}^3} \tag{4.19}$$

Using the equations (4.16), (4.17) and (4.18) above, D, μ and n at room temperature for A2 to A5 electrolytes were calculated and tabulated in Table 4.8. Figures 4.13, 4.14 and 4.15 show the graphs of D, μ and n of charge carriers obtained by fitting and FTIR methods for PVA–LiBOB solid polymer electrolyte system. The fits are in good agreement.

Table 4.8: Values of D, μ and n for PVA–LiBOB solid polymer electrolyte system at room temperature obtained by fitting method.

Electrolyte	***D*** (×10^{-9} cm^2 s^{-1})	***μ*** (×10^{-7} cm^2 V^{-1} s^{-1})	***n*** (×10^{20} cm^{-3})
A1	0.718*	0.280*	3.920*
A2	3.433	1.337	8.186
A3	5.833	2.271	13.194
A4	24.609	9.582	18.459
A5	9.975	3.884	19.184

*From A–N method

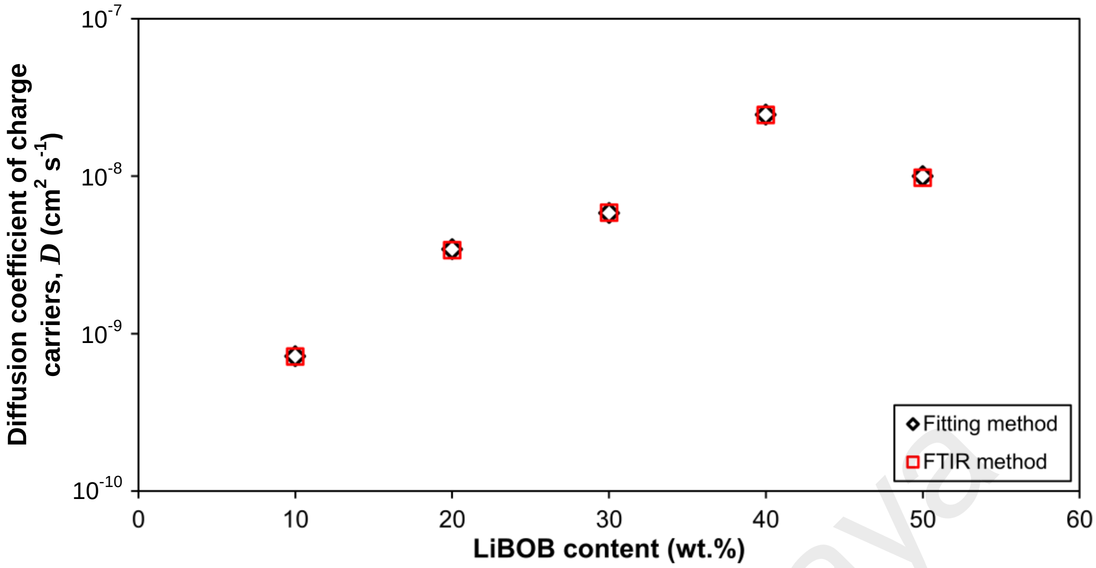

Figure 4.13: Diffusion coefficient of charge carriers, *D* against LiBOB concentration obtained from fitting and FTIR methods for PVA–LiBOB solid polymer electrolyte system.

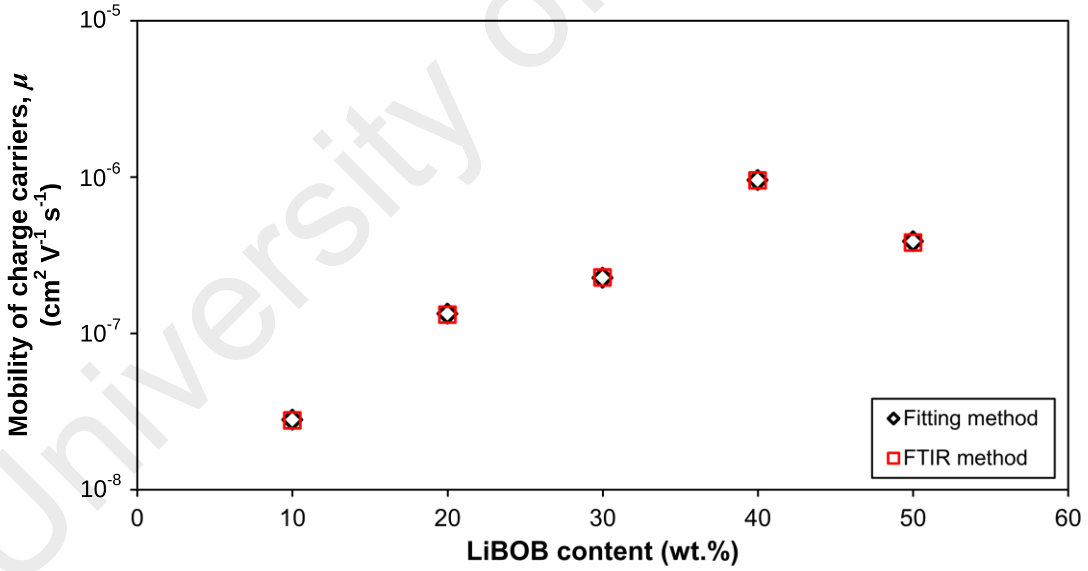

Figure 4.14: Mobility of charge carriers, μ against LiBOB concentration obtained from the fitting and FTIR methods for PVA–LiBOB solid polymer electrolyte system.

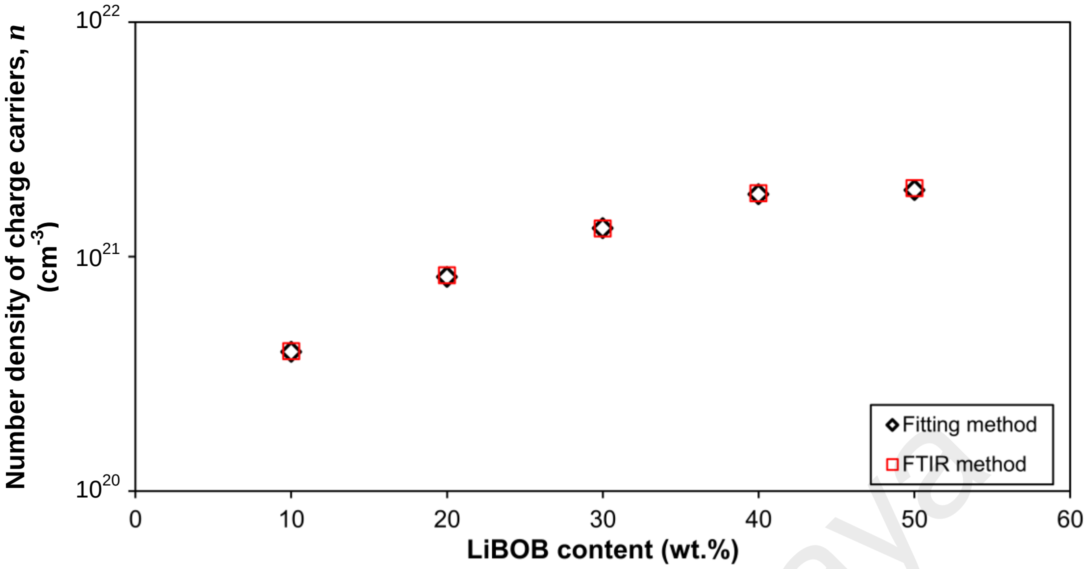

Figure 4.15: Number density of charge carrier, *n* against LiBOB concentration obtained from fitting and FTIR methods for PVA–LiBOB solid polymer electrolyte system.

4.3.3. Transport Properties of Charge Carriers of PVA–LiBOB Solid Polymer Electrolyte at Elevated Temperatures

Figure 4.16 shows the impedance plot and their corresponding fitted point for A1 electrolyte at different temperatures. All Nyquist plots for A1 electrolyte at different temperature consists of depressed semicircle and tilted spike. It is observed that the plot of real permittivity, ε' against frequency are almost constant at higher frequencies as depict in Figure 4.17. Thus, the dielectric constant, ε_r values can be obtained at 1 MHz. Table 4.9 lists all parameters obtained in Figures 4.16 and Figure 4.17.

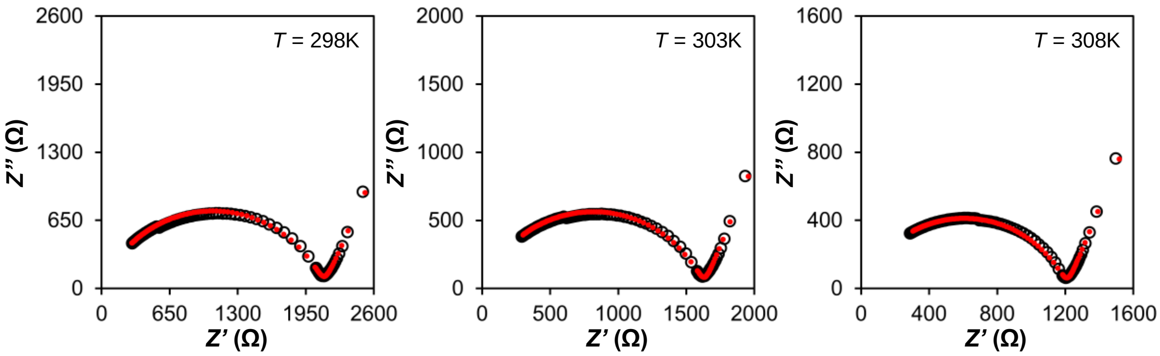

Figure 4.16, continued…

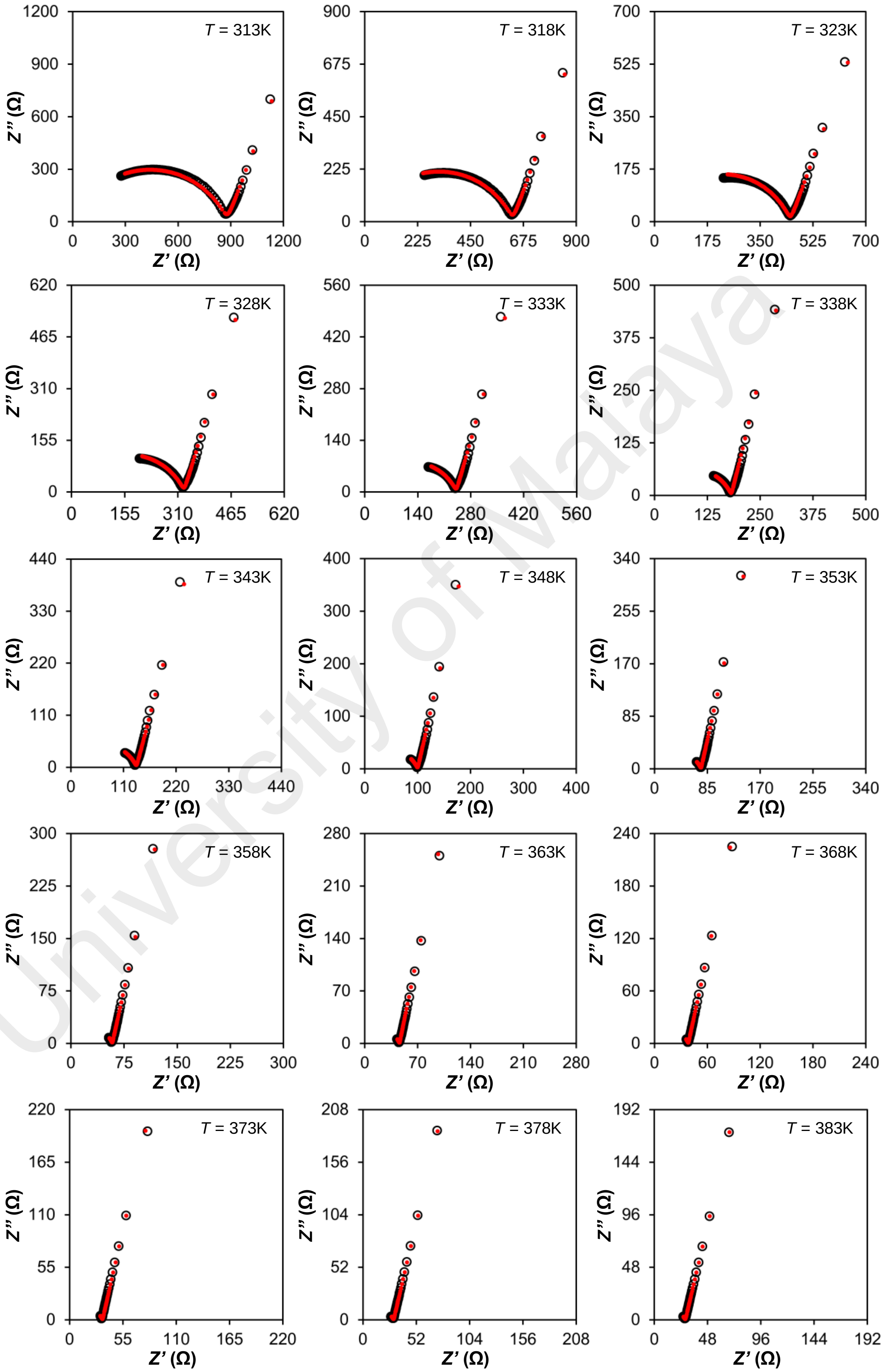

Figure 4.16, continued…

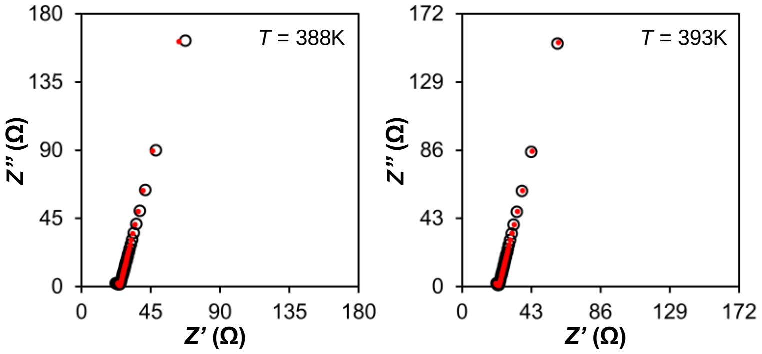

Figure 4.16: Nyquist plot (o) and their corresponding fitted point (●) for A1 electrolyte at different temperatures.

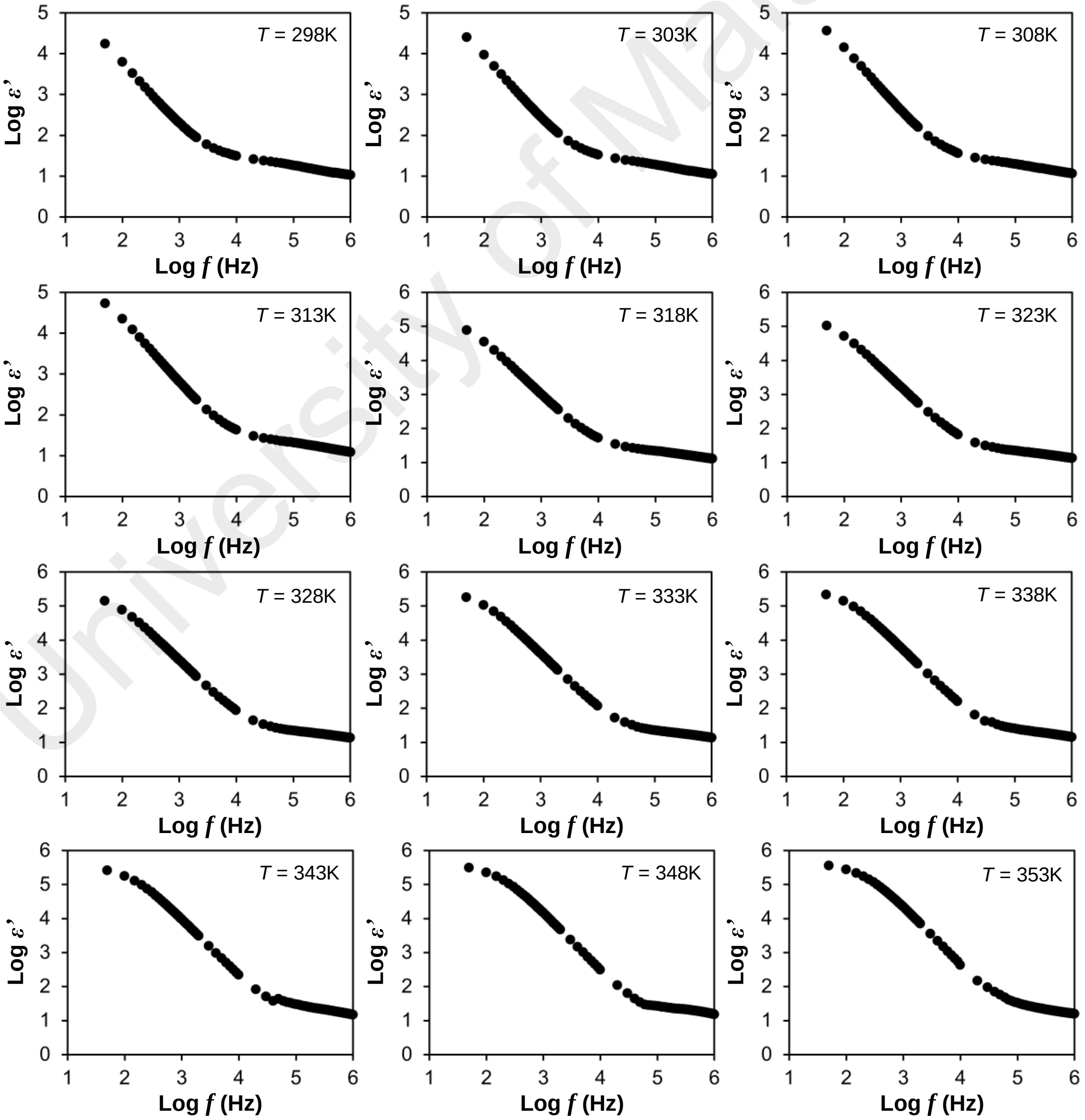

Figure 4.17, continued…

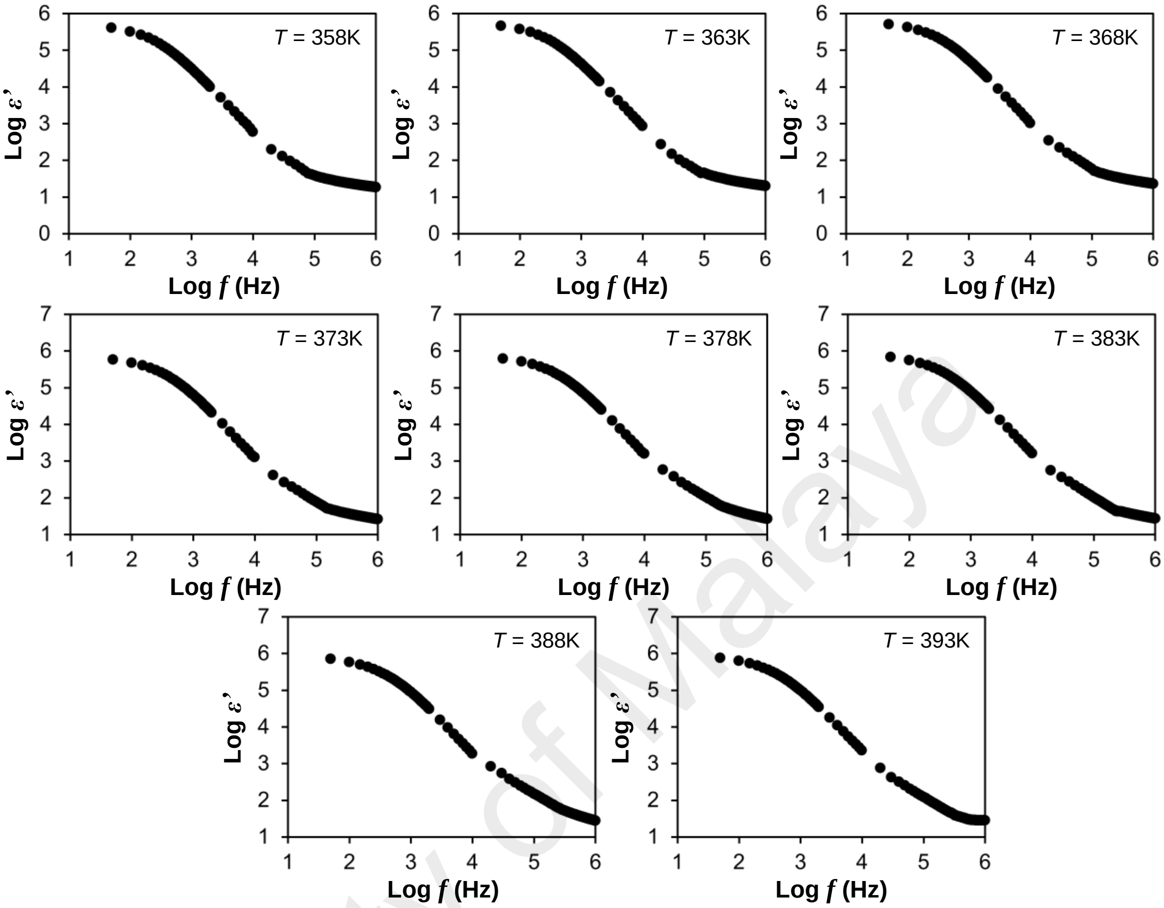

Figure 4.17: Dielectric constant, *ε'* versus frequency plot for A1 electrolyte at different temperatures.

Table 4.9: Values of *R*, $p_1, p_2, k_1, k_2, \omega_2$ and ε_r for A1 electrolyte obtained from fitting of Nyquist plot at different temperatures.

Temperature, *T* (K)	***R* (Ω)**	p_1	k_1 (F^{-1})	p_2	k_2 (F^{-1})	ω_2 (s^{-1})	ε_r
298	2120.0	0.775	109000000	0.740	70000	16965	10.568
303	1630.0	0.770	100000000	0.760	70000	20106	11.013
308	1210.0	0.761	85000000	0.755	63000	30159	11.511
313	880.0	0.755	75000000	0.775	63200	37071	12.119
318	630.0	0.761	70000000	0.785	61000	49009	12.737
323	450.0	0.780	100000000	0.780	50000	94248	13.220
328	328.0	0.761	70000000	0.820	60000	86708	13.476
333	242.0	0.750	60000000	0.830	57700	125664	13.595
338	182.0	0.761	70000000	0.850	60000	142628	14.158
343	137.0	0.761	60000000	0.840	50000	251327	14.665

Table 4.9, continued…

348	100.0	0.761	60000000	0.860	50000	320442	15.109
353	75.0	0.756	55000000	0.863	45500	477522	15.688
358	58.5	0.775	70000000	0.865	41000	534071	18.479
363	46.0	0.775	60000000	0.873	39000	615752	20.019
368	38.5	0.770	45000000	0.867	33500	735133	22.915
373	34.0	0.750	30000000	0.860	28500	892212	25.856
378	30.0	0.720	18000000	0.856	26300	1130973	26.511
383	28.0	0.709	15000000	0.855	24000	1413717	26.860
388	25.0	0.700	13000000	0.852	22300	1727876	27.719
393	23.0	0.550	1000000	0.850	21000	2073451	28.006

From the parameter values obtained and listed in Table 4.9, D, μ and n for A1 electrolyte at different temperatures were calculated using equations (3.24), (3.26) and (3.28). The calculated values are listed in Table 4.10. Figures 4.18, 4.19 and 4.20 show the plot of D, μ and n at different temperatures, respectively.

Table 4.10: Values of D, μ and n for A1 electrolyte at different temperatures.

T (K)	**D ($\times 10^{-9}$ cm^{2} s^{-1})**	**μ ($\times 10^{-7}$ cm^{2} V^{-1} s^{-1})**	**n ($\times 10^{20}$ cm^{-3})**
298	0.718	0.280	3.920
303	0.925	0.354	4.028
308	1.227	0.462	4.156
313	1.683	0.624	4.235
318	2.289	0.835	4.418
323	3.186	1.145	4.513
328	4.386	1.552	4.568
333	5.983	2.085	4.608
338	7.963	2.734	4.673
343	10.455	3.537	4.798

T (K)	**D ($\times 10^{-9}$ cm^{2} s^{-1})**	**μ ($\times 10^{-7}$ cm^{2} V^{-1} s^{-1})**	**n ($\times 10^{20}$ cm^{-3})**
348	14.150	4.718	4.927
353	18.824	6.188	5.009
358	23.720	7.688	5.169
363	29.042	9.283	5.444
368	33.520	10.569	5.713
373	37.486	11.661	5.864
378	42.541	13.059	5.934
383	45.457	13.771	6.029
388	51.082	15.276	6.087
393	55.493	16.384	6.169

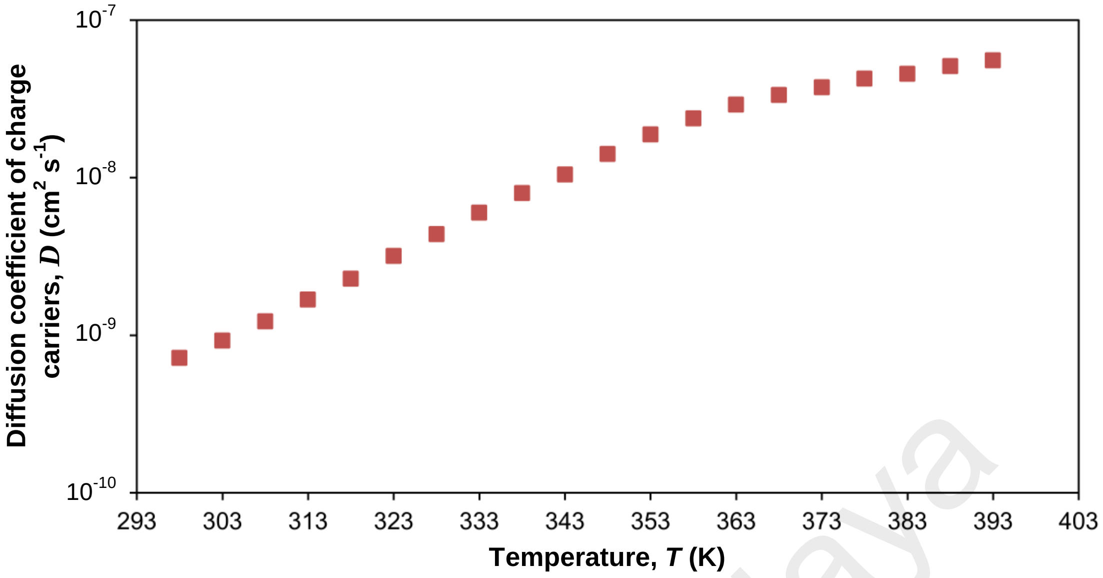

Figure 4.18: Diffusion coefficient of charge carriers, *D* for A1 electrolyte at different temperatures.

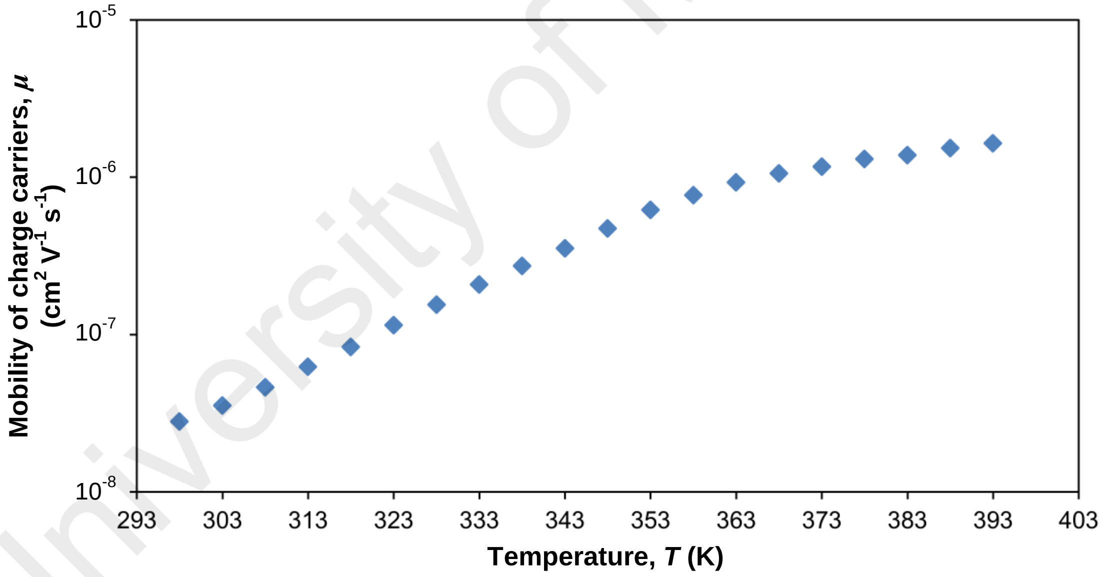

Figure 4.19: Mobility of charge carriers, μ for A1 electrolyte at different temperatures.

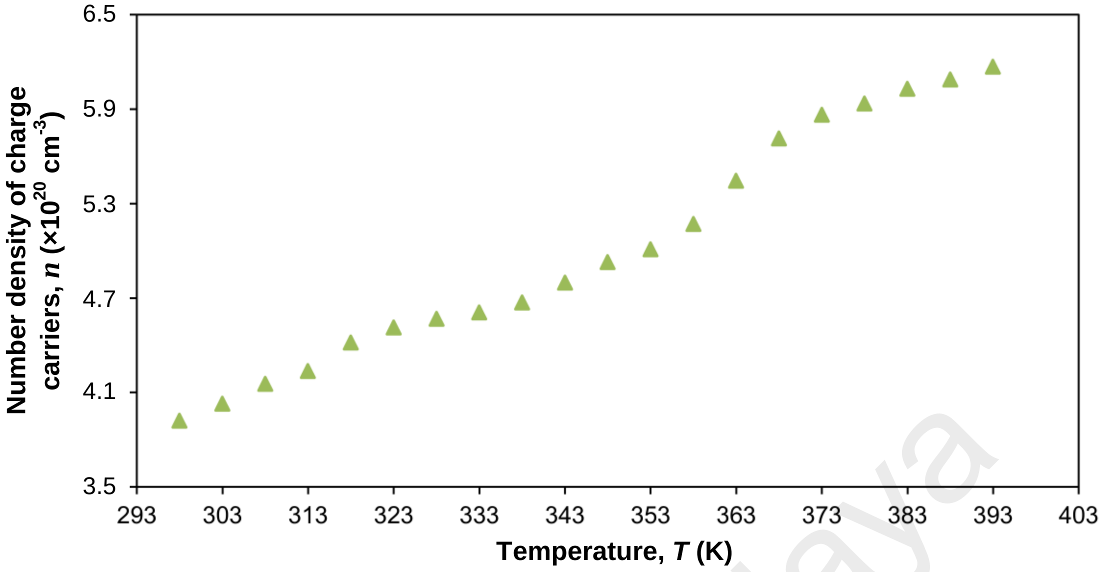

Figure 4.20: Number density of charge carriers, *n* for A1 electrolyte at different temperatures.

From Figures 4.18, 4.19 and 4.20, it can be seen that *D*, μ and *n* for A1 electrolyte increase with increasing temperature. It is observed that *D*, μ and *n* plots show similar trends. This infers that the ionic motion also obeys the Nernst–Einstein relation.

Figure 4.21 shows the Nyquist plots and their corresponding fitted point for A2 electrolyte at different temperatures. All Nyquist plot for A2 electrolyte at different temperature consists only of a tilted spike. Table 4.11 lists all fitted parameters obtained in Figure 4.21.

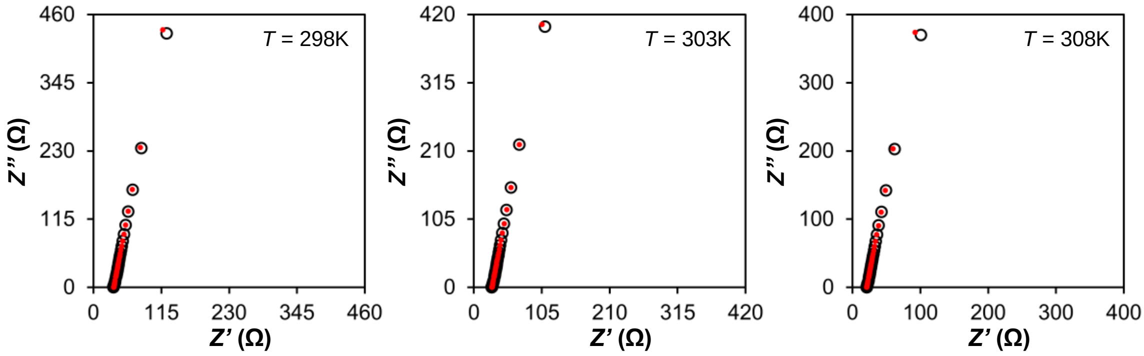

Figure 4.21, continued…

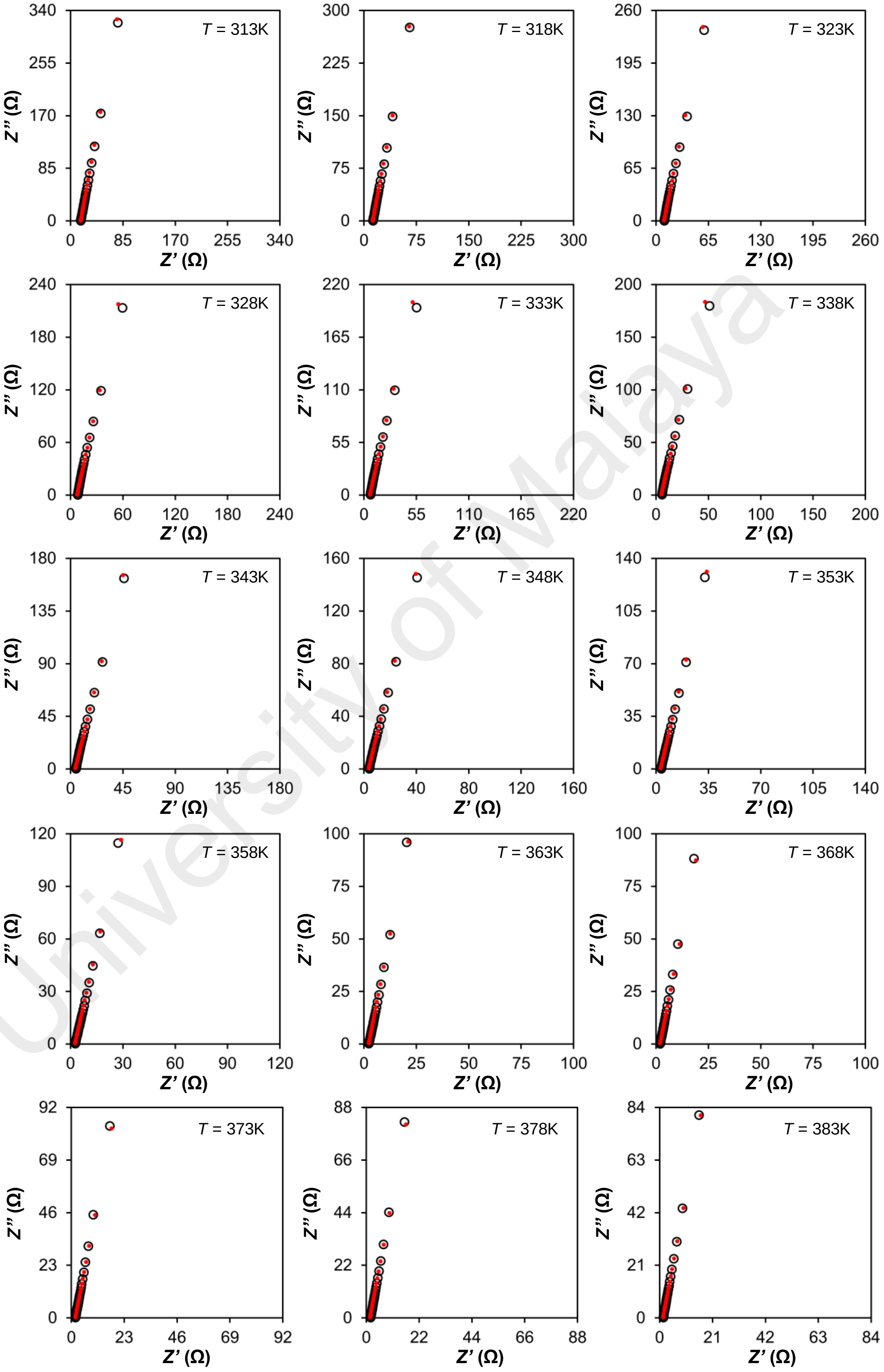

Figure 4.21, continued…

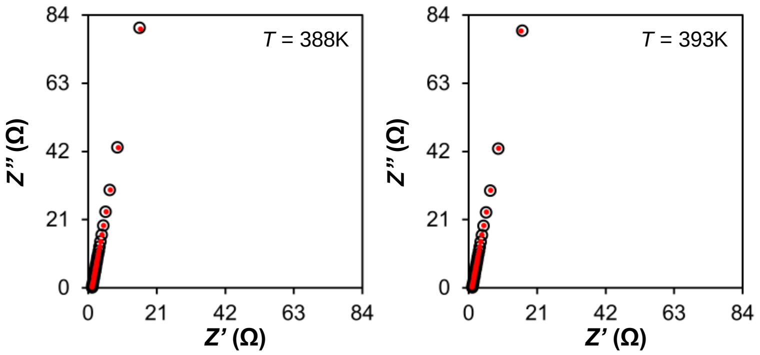

Figure 4.21: Nyquist plot (o) and their corresponding fitted point (●) for A2 electrolyte at corresponding temperatures.

Table 4.11: R, p_2, k_2 and ω_2 values for A2 electrolyte obtained from fitting of Nyquist plot at different temperatures.

T (K)	R (Ω)	p_2	k_2 (F^{-1})	ω_2 (s^{-1})
298	34.50	0.880	69700	1017876
303	28.00	0.880	65000	904245
308	21.00	0.880	60000	766077
313	16.50	0.886	54000	625967
318	12.50	0.883	45000	512814
323	9.80	0.873	37000	389148
328	7.50	0.864	32000	314868
333	6.10	0.860	29000	289837
338	5.00	0.857	26000	277469
343	4.00	0.845	22000	263748
348	3.50	0.848	20000	250181
353	3.00	0.853	18200	238249
358	2.50	0.858	16600	224078
363	2.20	0.877	15200	205365
368	1.90	0.877	13800	185563
373	1.70	0.880	13300	176276
378	1.50	0.883	13200	174316
383	1.34	0.883	13200	170936
388	1.20	0.883	13000	167974
393	1.00	0.880	12700	166606

From the parameter values listed in Table 4.11, D, μ and n for A2 electrolyte at different temperatures were calculated using equations (4.16), (4.17) and (4.18), respectively. The calculated values are listed in Table 4.12. Figures 4.22, 4.23 and 4.24 show the plot of diffusion coefficient, mobility and number density of mobile ions at different temperatures, respectively.

Table 4.12: D, μ and n values for A2 electrolyte at different temperatures.

T (K)	D ($\times 10^{-7}$ cm^2 s^{-1})	μ ($\times 10^{-6}$ cm^2 V^{-1} s^{-1})	n ($\times 10^{20}$ cm^{-3})
298	0.034	0.134	8.186
303	0.075	0.287	4.699
308	0.214	0.806	2.229
313	0.488	1.808	1.265
318	0.925	3.376	0.895
323	1.695	6.088	0.633
328	3.078	10.888	0.462
333	4.260	14.842	0.417
338	5.289	18.157	0.416
343	6.187	20.930	0.451
348	6.999	23.336	0.462
353	8.090	26.592	0.473
358	9.779	31.694	0.476
363	11.183	35.746	0.480
368	12.953	40.843	0.486
373	14.587	45.378	0.489
378	16.420	50.404	0.499
383	18.227	55.220	0.510
388	19.676	58.841	0.535
393	21.643	63.899	0.591

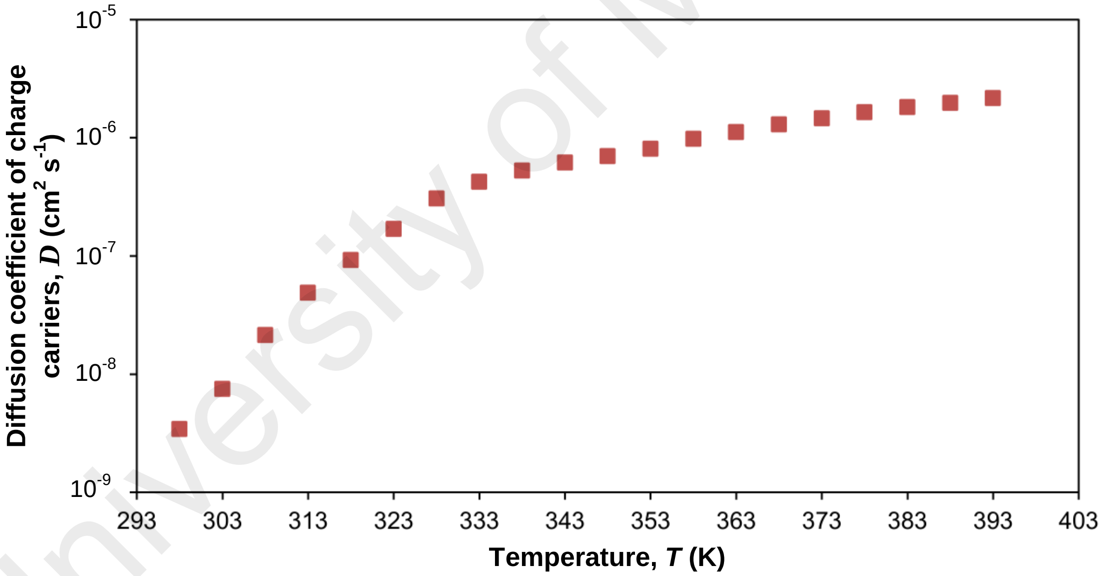

Figure 4.22: Diffusion coefficient of charge carriers, D for A2 electrolyte at different temperatures.

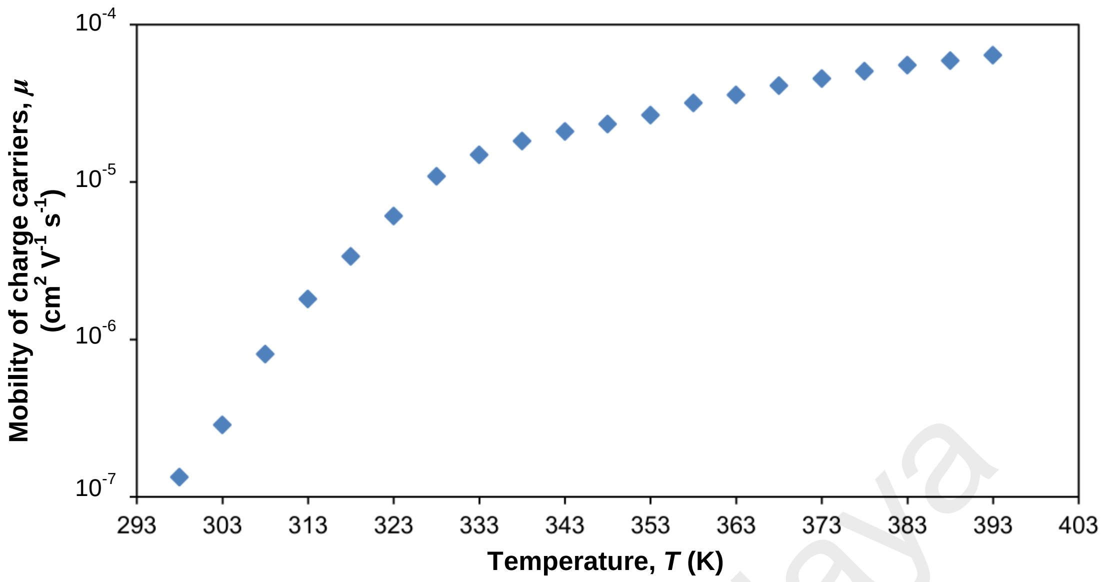

Figure 4.23: Mobility of charge carriers, μ for A2 electrolyte at different temperatures.

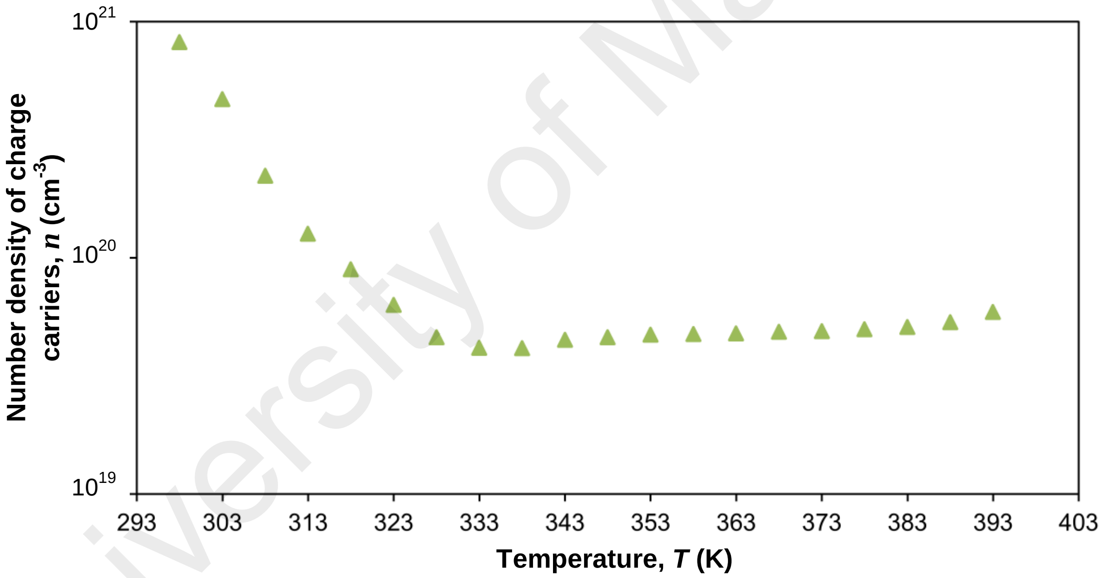

Figure 4.24: Number density of charge carriers, *n* for A2 electrolyte at different temperatures.

From Figures 4.22 and 4.23, the diffusion coefficient and mobility of the free ions for A2 electrolyte are observed to be temperature assisted. The increase in mobility and diffusion coefficient with temperature also showed that the Nernst–Einstein relation is obeyed. The number density of charge carriers for A2 electrolyte is observed to decrease an increasing temperature from 298 K to 338 K, and again increased slowly beyond 338 K as listed and shown in Table 4.12 and Figure 4.24, respectively.

Figure 4.25 shows the impedance plot and their corresponding fitted point for A3 electrolyte at different temperatures. All Nyquist plot for A3 electrolyte at different temperatures consists of tilted spike. Table 4.13 lists all fitted parameters obtained in Figure 4.25.

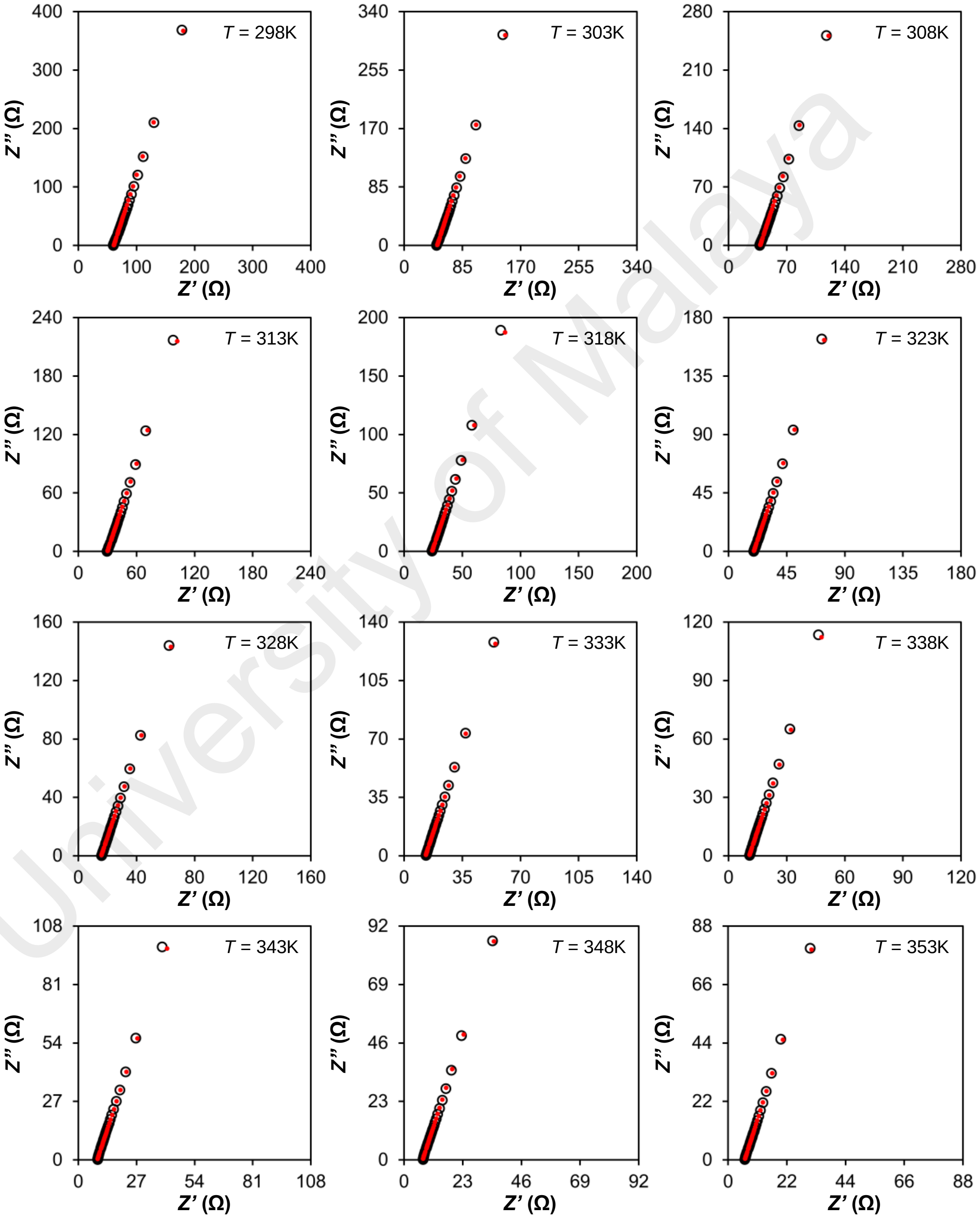

Figure 4.25, continued…

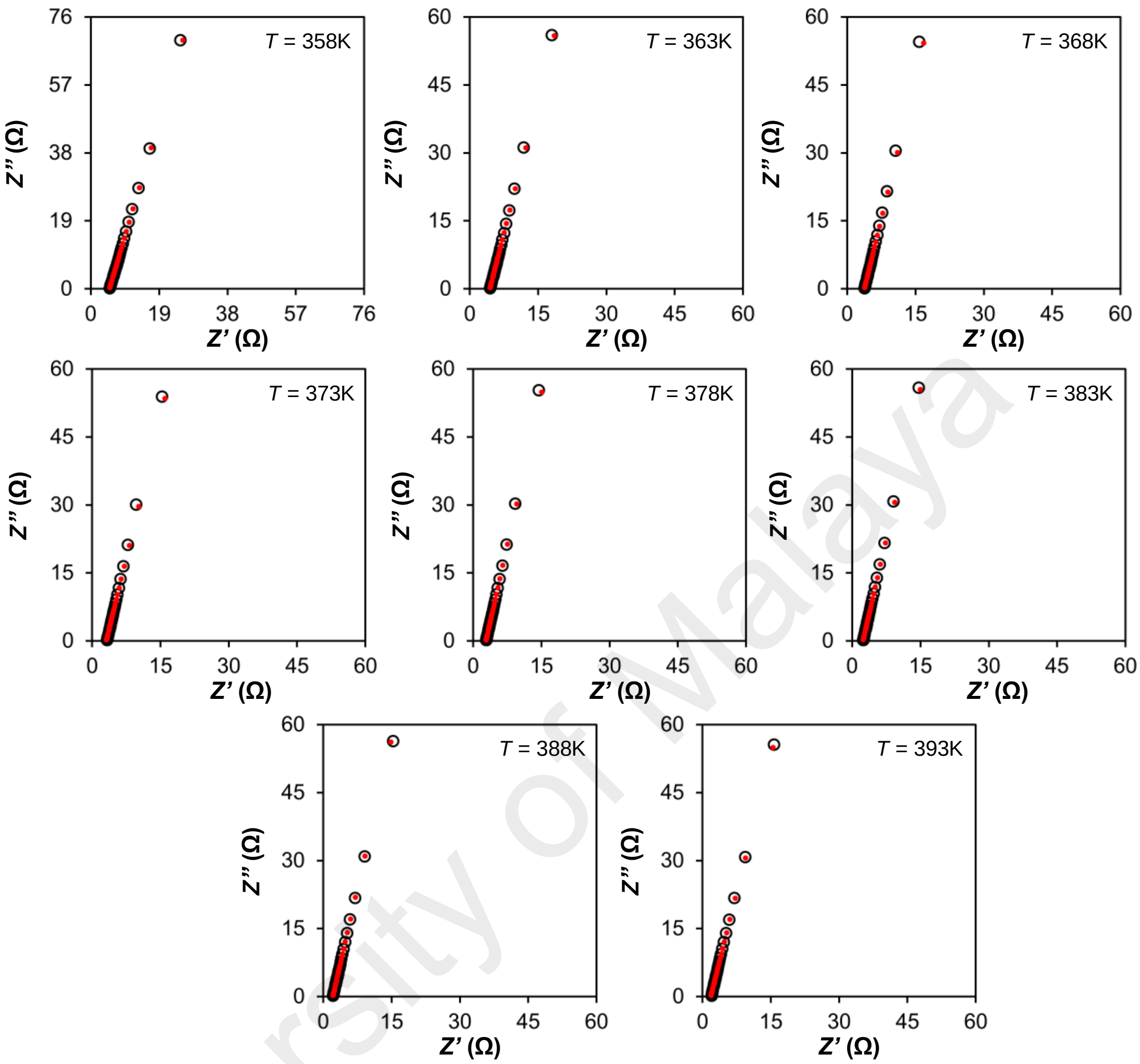

Figure 4.25: Nyquist plot (o) and their corresponding fitted point (●) for A3 electrolyte at different temperatures.

Table 4.13: Values of R, p_2, k_2 and ω_2 for A3 electrolyte obtained from fitting of Nyquist plot at different temperatures.

T (K)	R (Ω)	p_2	k_2 (F^{-1})	ω_2 (s^{-1})
298	61.00	0.800	38450	502655
303	48.00	0.800	32000	456437
308	38.00	0.798	26000	403517
313	30.00	0.795	22000	366672
318	24.00	0.794	19000	339643
323	19.50	0.794	16500	316446
328	15.80	0.794	14500	296419
333	12.90	0.796	13000	269202
338	10.70	0.796	11500	245210
343	8.80	0.796	10000	225327

Table 4.13, continued...

348	7.30	0.800	9000	211468	373	3.10	0.850	7300	157448
353	6.20	0.805	8500	201446	378	2.80	0.860	7900	156149
358	5.20	0.818	8000	183390	383	2.40	0.858	7900	157150
363	4.40	0.842	7300	169309	388	2.10	0.858	8000	157156
368	3.80	0.850	7400	161158	393	1.80	0.845	7300	154784

From the parameter values listed in Table 4.13, D, μ and n for A3 electrolyte at different temperatures was calculated by using equations (4.16), (4.17) and (4.18), respectively. The calculated values are listed in Table 4.14. Figures 4.26, 4.27 and 4.28 show the plot of diffusion coefficient, mobility and number density of free ions at different temperatures, respectively.

Table 4.14: Values of D, μ and n for A3 electrolyte at different temperatures.

T (K)	D ($\times 10^{-7}$ cm^2 s^{-1})	μ ($\times 10^{-6}$ cm^2 V^{-1} s^{-1})	n ($\times 10^{20}$ cm^{-3})	T (K)	D ($\times 10^{-7}$ cm^2 s^{-1})	μ ($\times 10^{-6}$ cm^2 V^{-1} s^{-1})	n ($\times 10^{20}$ cm^{-3})
298	0.058	0.227	13.194	348	2.239	7.466	3.354
303	0.089	0.343	11.118	353	3.007	9.884	2.983
308	0.131	0.493	9.760	358	4.289	13.900	2.529
313	0.202	0.750	8.124	363	5.442	17.396	2.388
318	0.301	1.097	6.942	368	7.463	23.531	2.044
323	0.422	1.517	6.180	373	9.997	31.097	1.896
328	0.602	2.128	5.436	378	12.561	38.559	1.693
333	0.923	3.214	4.408	383	14.720	44.594	1.708
338	1.280	4.393	3.889	388	16.840	50.360	1.729
343	1.686	5.704	3.642	393	17.889	52.816	1.923

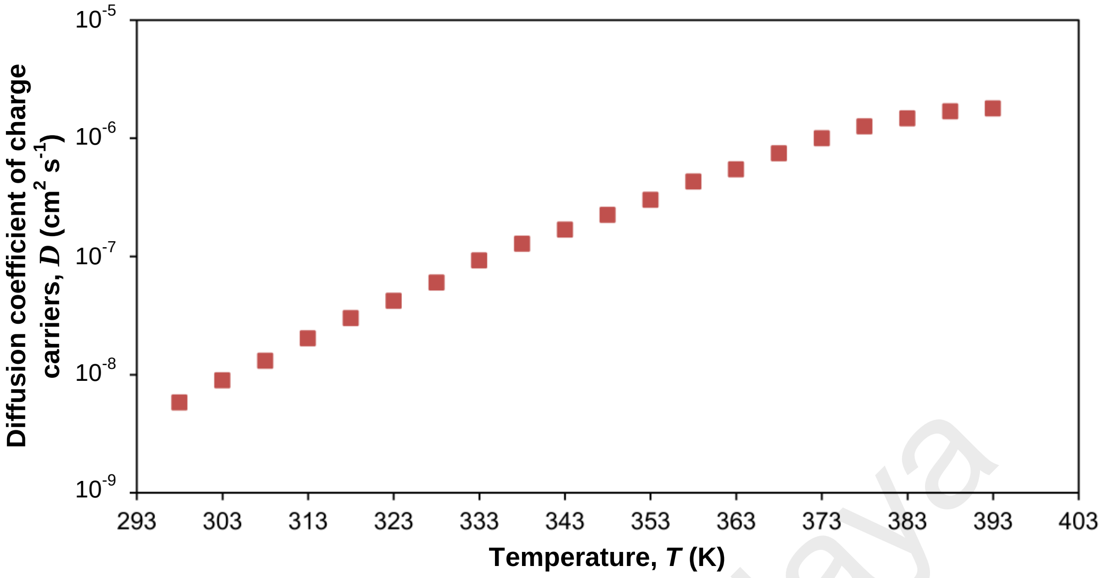

Figure 4.26: Diffusion coefficient of charge carriers, *D* for A3 electrolyte at different temperatures.

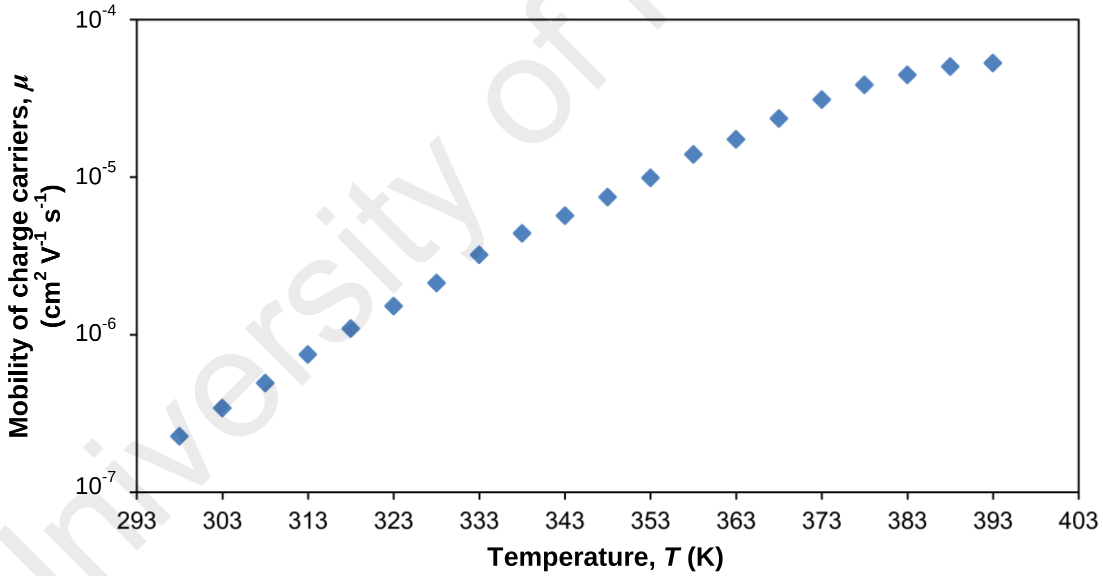

Figure 4.27: Mobility of charge carriers, μ for A3 electrolyte at different temperatures.

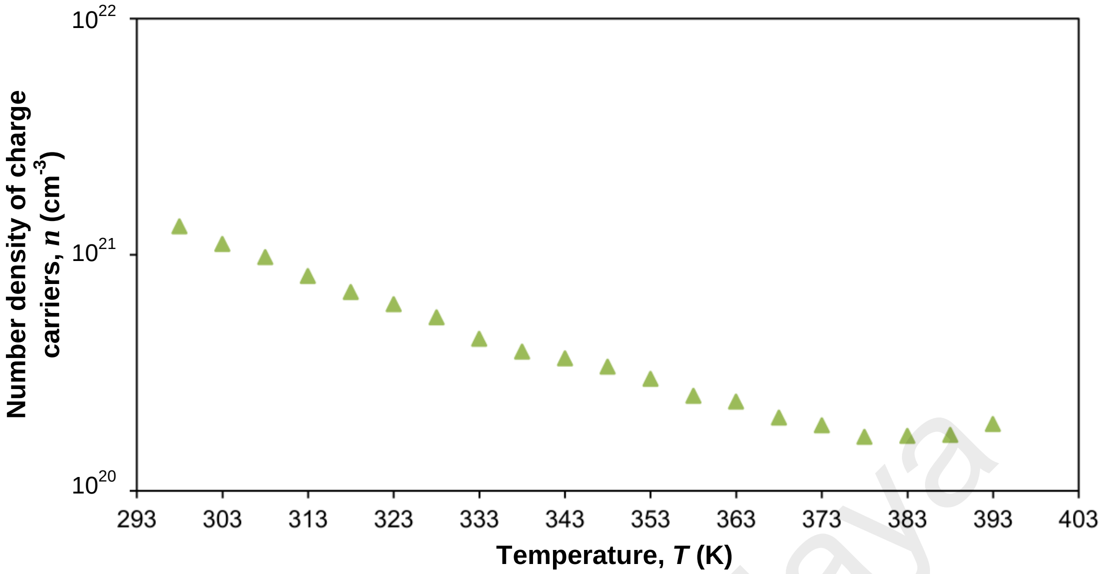

Figure 4.28: Number density of charge carriers, *n* for A3 electrolyte at different temperatures.

From Figures 4.26 and 4.27, the diffusion coefficient and mobility of charge carriers for A3 electrolyte are observed to increase with increasing temperature. The number density of charge carriers for A3 electrolyte is observed to decrease from 298 K to 378 K, and again increased beyond 378 K as listed and shown in Table 4.14 and Figure 4.28, respectively.

Figure 4.29 shows the Nyquist plot and their corresponding fitted point for A4 electrolyte at different temperatures. All Nyquist plots for A4 electrolyte at different temperatures consists of a tilted spike. Table 4.15 lists all fitted parameters obtained in Figure 4.29.

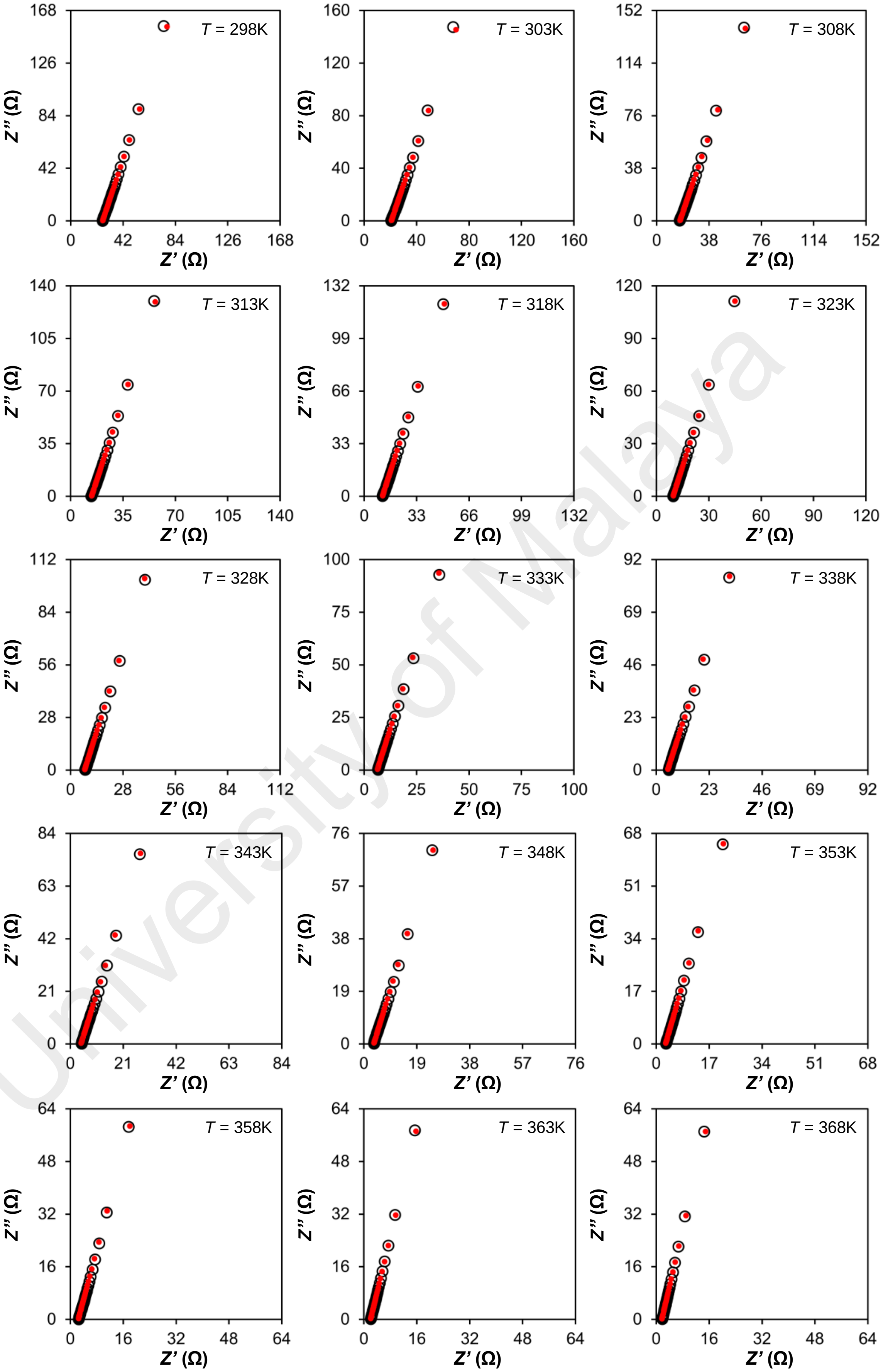
T = 298K
Z'' (Ω)
Z' (Ω)
0
42
84
126
168
T = 303K
0
40
80
120
160
T = 308K
0
38
76
114
152
T = 313K
0
35
70
105
140
T = 318K
0
33
66
99
132
T = 323K
0
30
60
90
120
T = 328K
0
28
56
84
112
T = 333K
0
25
50
75
100
T = 338K
0
23
46
69
92
T = 343K
0
21
42
63
84
T = 348K
0
19
38
57
76
T = 353K
0
17
34
51
68
T = 358K
0
16
32
48
64
T = 363K
T = 368K

Figure 4.29, continued…

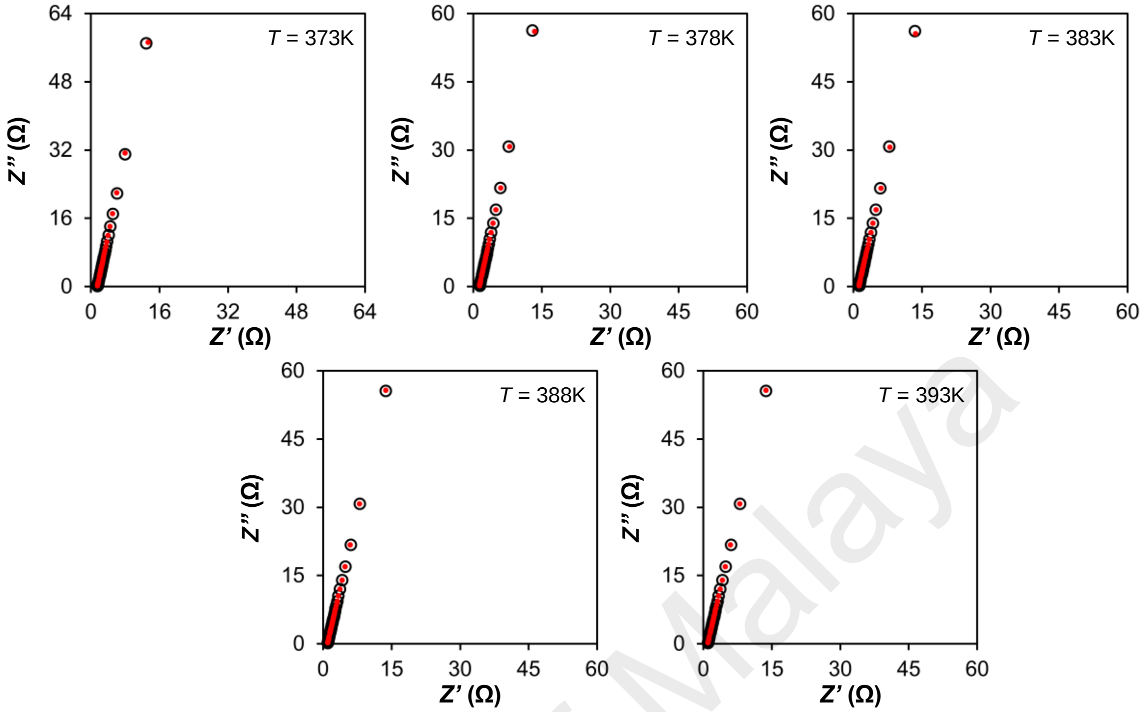

Figure 4.29: Nyquist plot (o) and their corresponding fitted point (●) for A4 electrolyte at different temperatures.

Table 4.15: Values of R, p_2, k_2 and ω_2 for A4 electrolyte obtained from fitting of Nyquist plot at varied temperatures.

T (K)	R (Ω)	p_2	k_2 (F^{-1})	ω_2 (s^{-1})
298	25.50	0.795	15800	490088
303	20.60	0.792	14600	434308
308	16.80	0.790	13800	401714
313	14.00	0.798	13400	366672
318	11.40	0.801	12700	339643
323	9.50	0.804	11900	316446
328	7.50	0.806	11000	296066
333	6.20	0.806	10100	270183
338	5.00	0.804	9050	245210
343	4.20	0.808	8300	225327
348	3.50	0.812	7800	211468
353	3.00	0.822	7600	201446
358	2.40	0.835	7400	183390
363	2.00	0.850	7800	169681
368	1.70	0.855	8000	167645
373	1.50	0.870	8700	157607
378	1.32	0.865	8300	156462
383	1.15	0.860	8000	157150
388	1.05	0.853	7700	157057
393	0.95	0.857	7900	154784

From the parameter values listed in Table 4.15, *D*, μ and *n* for A4 electrolyte at different temperatures was calculated by using equations (4.16), (4.17) and (4.18), respectively. The calculated values are listed in Table 4.16. Figures 4.30, 4.31 and 4.32 show the plot of diffusion coefficient, mobility and number density of mobile species that contribute to conductivity at different temperatures, respectively.

Table 4.16: *D*, μ and *n* values for A4 electrolyte at different temperatures.

T (K)	*D* ($\times 10^{-7}$ cm^2 s^{-1})	μ ($\times 10^{-6}$ cm^2 V^{-1} s^{-1})	*n* ($\times 10^{20}$ cm^{-3})	*T* (K)	*D* ($\times 10^{-7}$ cm^2 s^{-1})	μ ($\times 10^{-6}$ cm^2 V^{-1} s^{-1})	*n* ($\times 10^{20}$ cm^{-3})
298	0.246	0.958	18.459	348	12.394	41.327	3.118
303	0.468	1.791	12.228	353	14.770	48.551	3.097
308	0.807	3.040	8.832	358	18.584	60.232	3.120
313	1.386	5.138	6.270	363	22.121	70.711	3.189
318	2.215	8.081	4.896	368	23.753	74.894	3.543
323	3.145	11.299	4.202	373	24.658	76.706	3.920
328	4.647	16.440	3.658	378	24.624	75.588	4.521
333	6.241	21.748	3.345	383	24.377	73.852	5.311
338	8.199	28.145	3.205	388	24.151	72.224	5.948
343	10.094	34.147	3.145	393	23.291	68.767	6.904

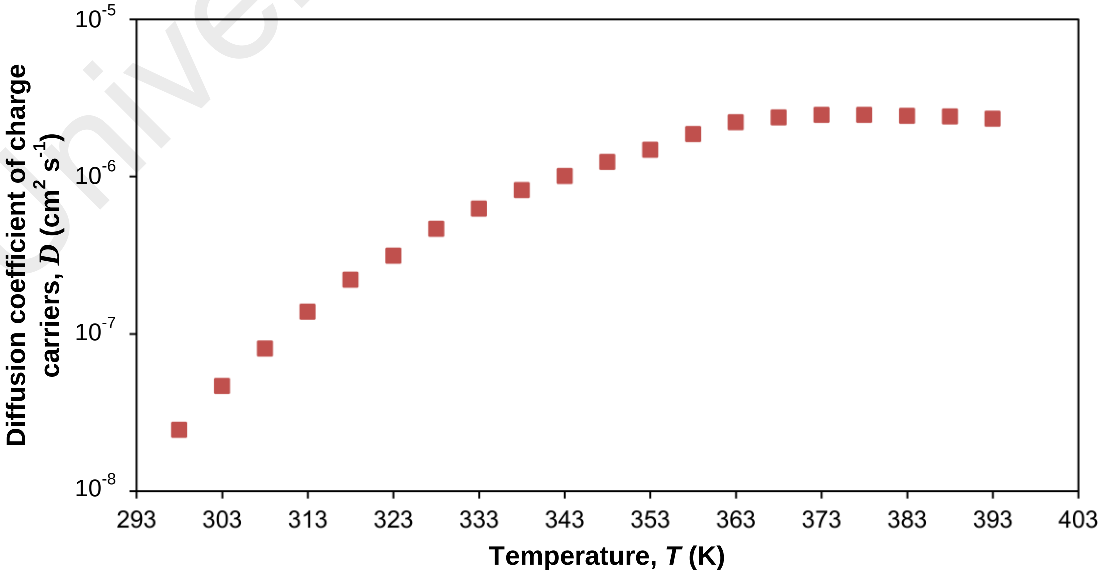

Figure 4.30: Diffusion coefficient of charge carriers, *D* for A4 electrolyte at different temperatures.

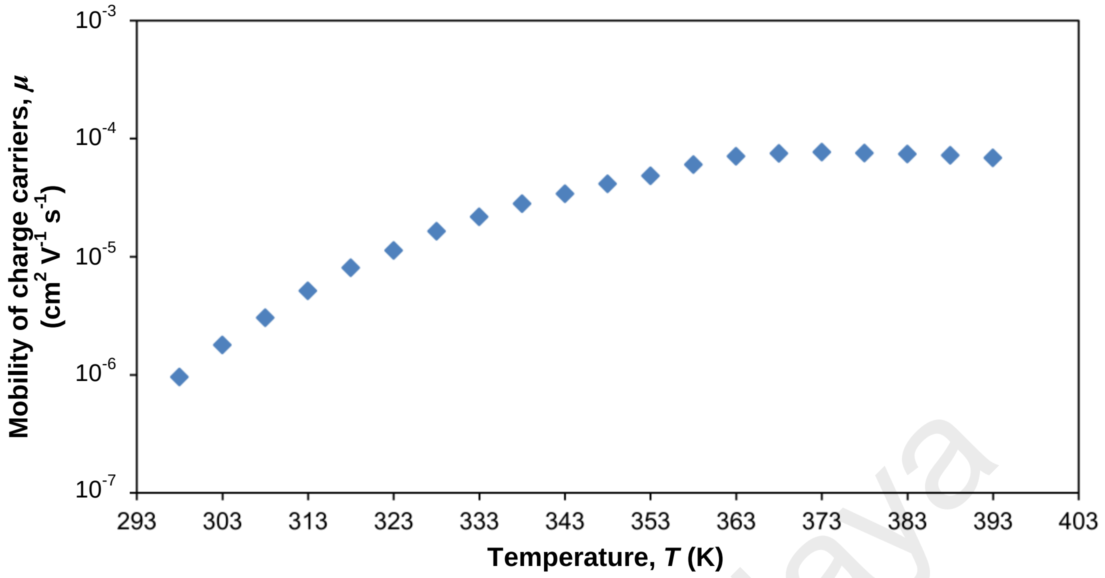

Figure 4.31: Mobility of charge carriers, μ for A4 electrolyte at different temperatures.

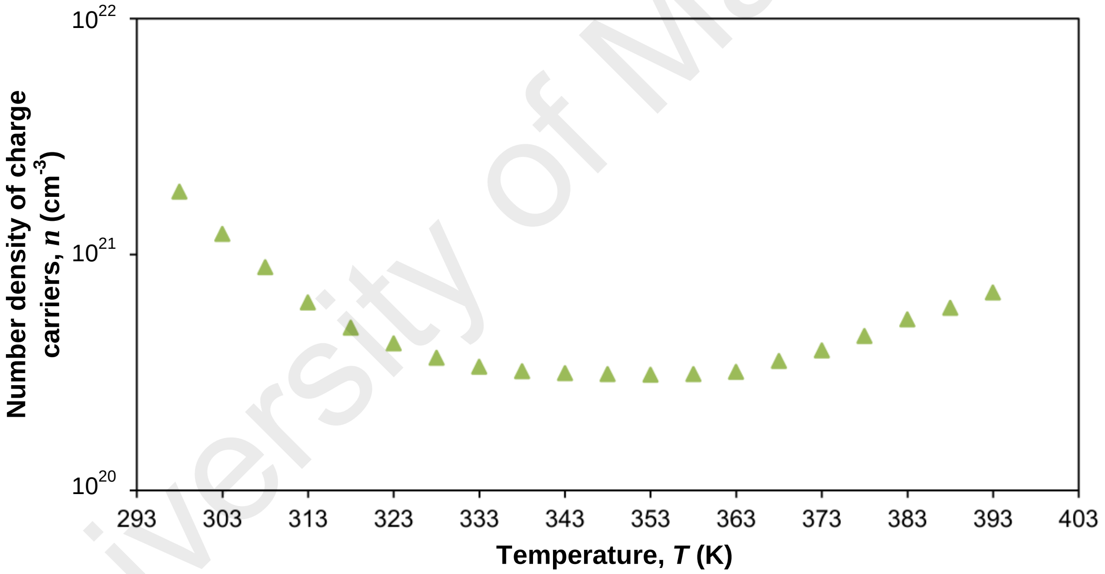

Figure 4.32: Number density of free ions, n for A4 electrolyte at different temperatures.

From Figures 4.30 and 4.31, it can be observed that the D and μ of free charge carriers for A4 electrolyte increased with temperature until 373 K. Beyond 373 K, the D and μ of free charge carriers for A4 electrolyte decreased with increasing temperature. The concentration of charge carriers that contribute to conductivity for A4 electrolyte decreased when temperature was raised from 298 K to 353 K, and again increased beyond 353 K as listed and shown in Table 4.16 and Figure 4.32, respectively.

Figure 4.33 shows the Nyquist plot and their corresponding fitted point for A5 electrolyte at different temperatures. All Nyquist plots for A5 electrolyte at different temperatures consists of only a tilted spike. Table 4.17 listed all fitted parameters obtained in Figure 4.33.

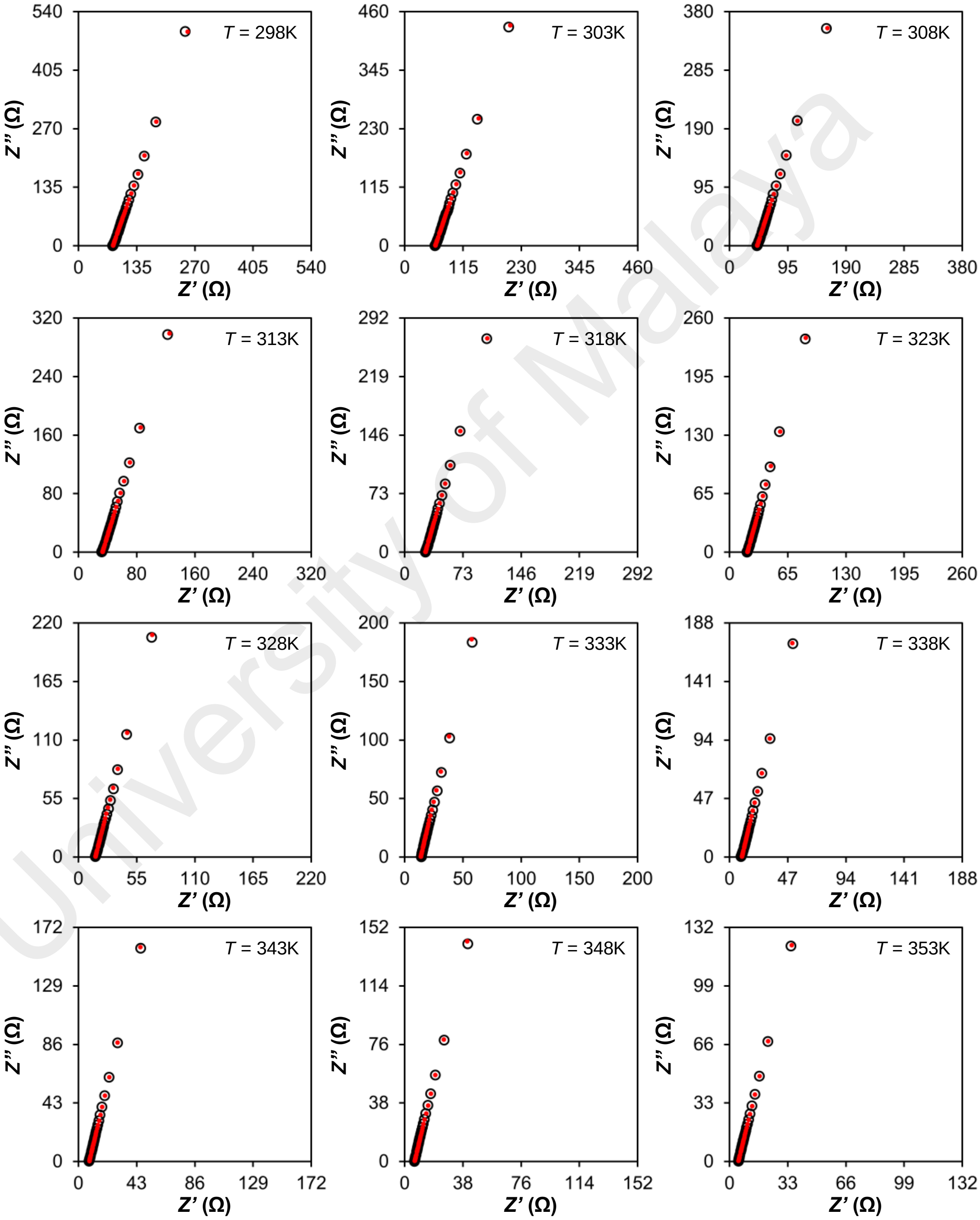

Figure 4.33, continued…

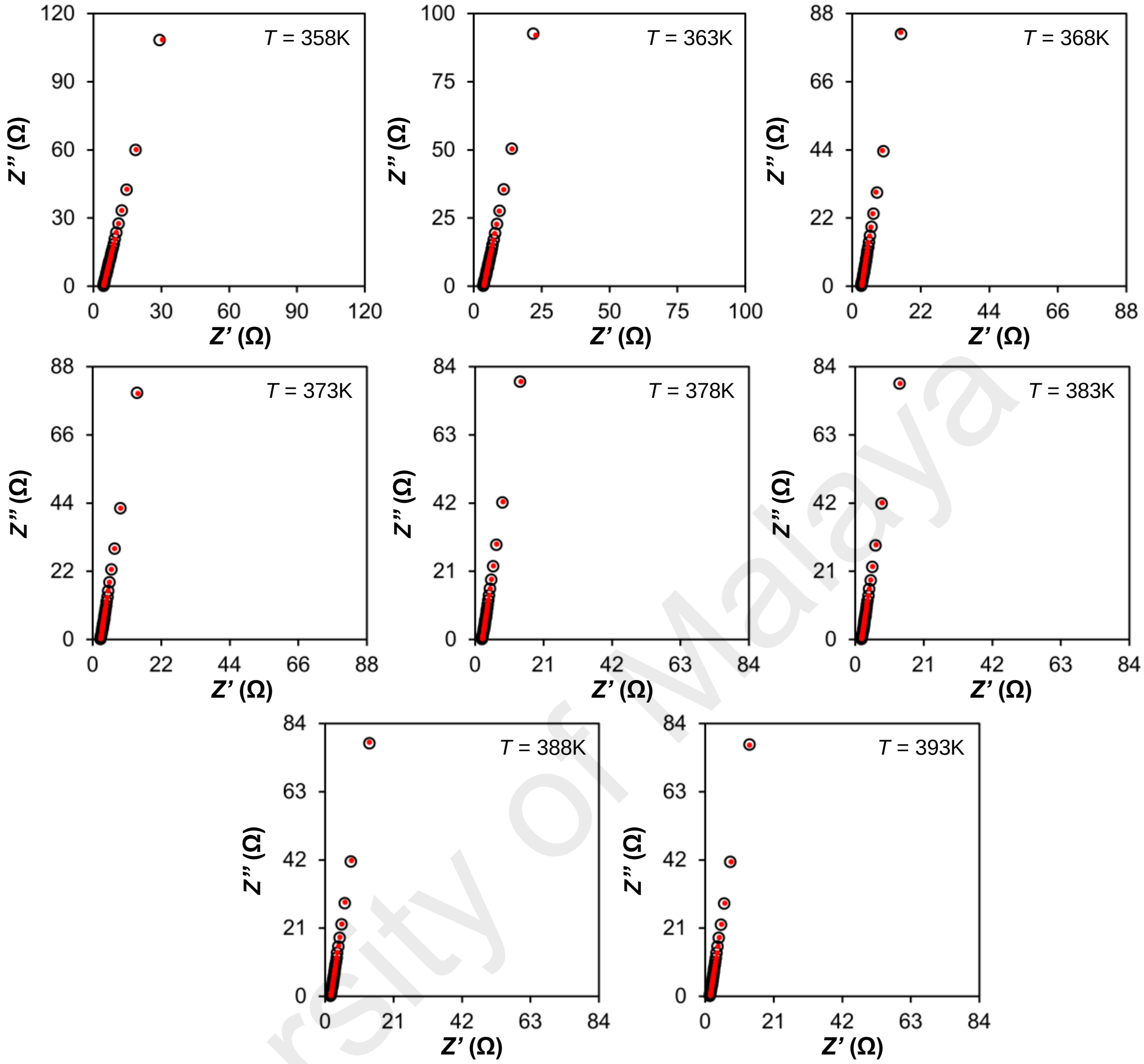

Figure 4.33: Nyquist plot (o) and their corresponding fitted point (●) for A5 electrolyte at different temperatures.

Table 4.17: R, p_2, k_2 and ω_2 values for A5 electrolyte obtained from fitting of Nyquist plot at different temperatures.

T (K)	R (Ω)	p_2	k_2 (F^{-1})	ω_2 (s^{-1})
298	80.00	0.785	47800	829380
303	60.00	0.790	43000	761496
308	45.00	0.800	37000	683658
313	33.00	0.810	33000	656479
318	26.00	0.820	31000	625153
323	20.00	0.830	29200	573545
328	16.00	0.840	27000	465726
333	13.80	0.853	25800	386494
338	10.00	0.852	23700	341706
343	8.00	0.850	21500	299218

Table 4.17, continued...

348	6.50	0.850	19500	261331	373	2.60	0.905	14600	163027
353	5.00	0.845	16200	230005	378	2.30	0.906	14700	162328
358	4.50	0.850	14800	218064	383	2.00	0.905	14500	157871
363	3.70	0.870	14000	199923	388	1.80	0.905	14400	156487
368	3.10	0.904	15000	183136	393	1.60	0.902	14000	156351

From the parameter values listed in Table 4.17, D, μ and n for A5 electrolyte at different temperatures were calculated using equations (4.16), (4.17) and (4.18), respectively. The calculated values are listed in Table 4.18. Figures 4.34, 4.35 and 4.36 show the plots of diffusion coefficient, mobility and number density of free ions at different temperatures, respectively.

Table 4.18: Values of D, μ and n for A5 electrolyte at different temperatures.

T (K)	D ($\times 10^{-7}$ cm^{2} s^{-1})	μ ($\times 10^{-6}$ cm^{2} V^{-1} s^{-1})	n ($\times 10^{20}$ cm^{-3})	T (K)	D ($\times 10^{-7}$ cm^{2} s^{-1})	μ ($\times 10^{-6}$ cm^{2} V^{-1} s^{-1})	n ($\times 10^{20}$ cm^{-3})
298	0.100	0.388	19.183	348	16.418	54.742	1.675
303	0.215	0.823	12.077	353	18.843	61.937	1.925
308	0.404	1.524	8.693	358	19.570	63.430	2.088
313	0.743	2.754	6.560	363	21.981	70.261	2.293
318	1.258	4.591	4.994	368	24.286	76.575	2.511
323	2.296	8.248	3.613	373	24.630	76.620	2.992
328	4.169	14.746	2.526	378	24.256	74.456	3.481
333	6.329	22.052	1.959	383	23.386	70.850	4.207
338	10.211	35.052	1.701	388	22.499	67.284	4.922
343	13.344	45.140	1.651	393	21.582	63.721	5.847

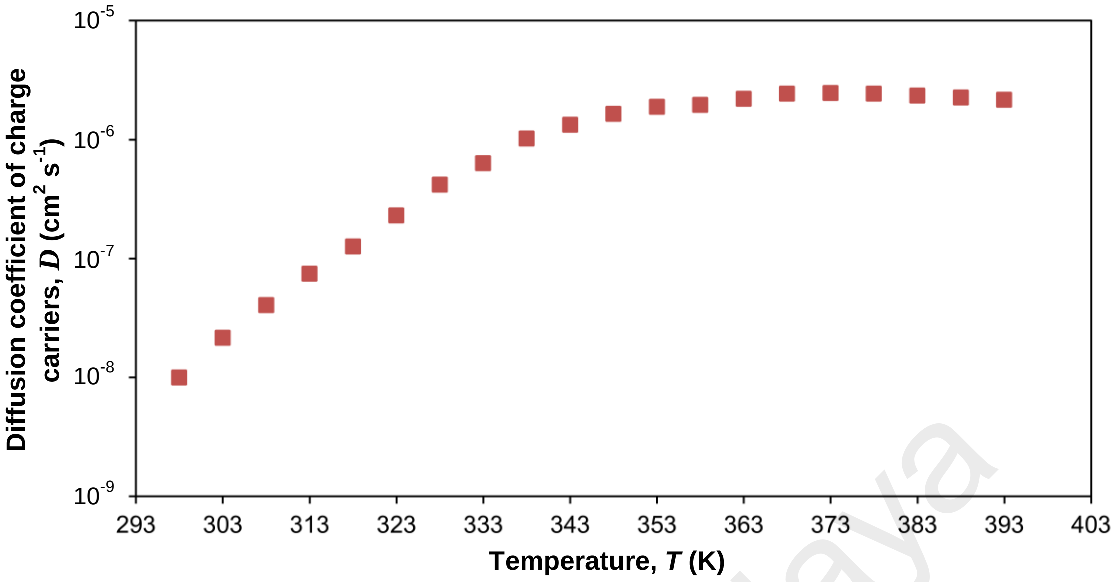

Figure 4.34: Diffusion coefficient of charge carriers, *D* for A5 electrolyte at different temperatures.

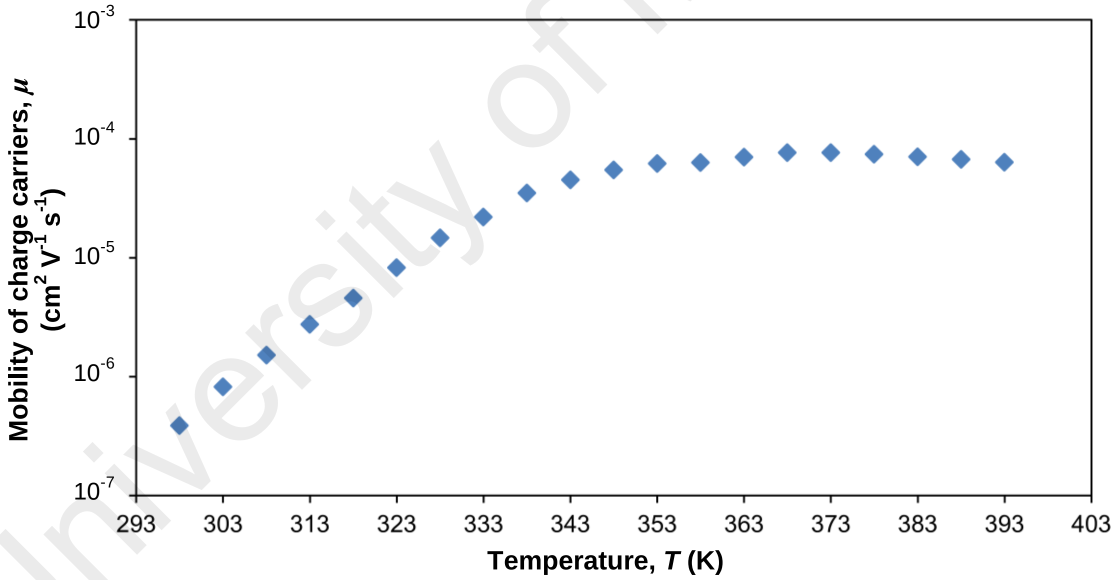

Figure 4.35: Mobility of charge carriers, μ for A5 electrolyte at different temperatures.

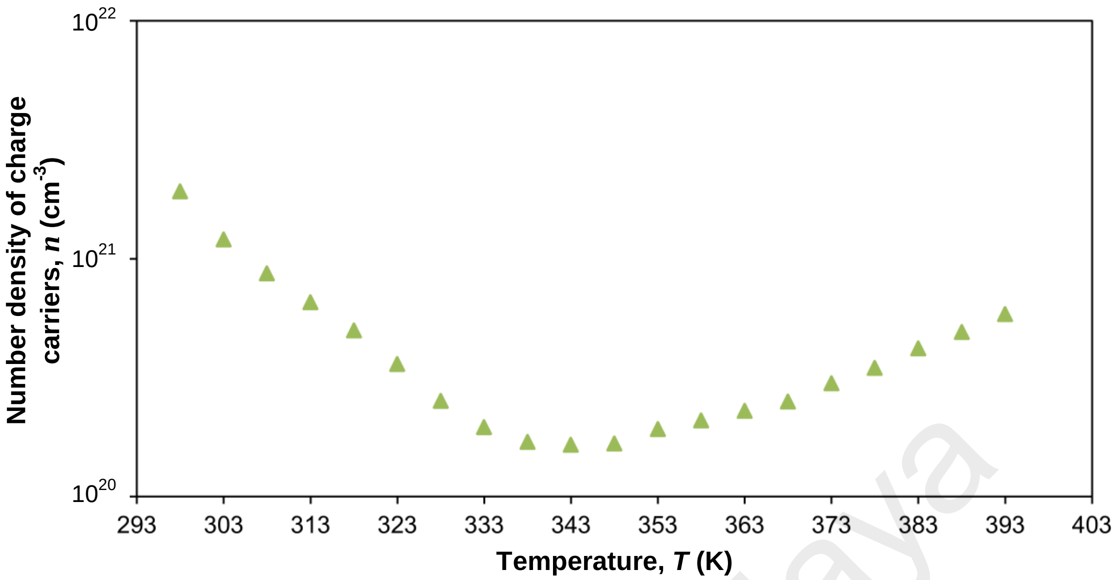

Figure 4.36: Number density of mobile ions, *n* for A5 electrolyte at different temperatures.

From Figures 4.34 and 4.35, the diffusion coefficient and mobility of free ions for A5 electrolyte are observed to increase with increasing temperature until a maximum at 373 K. Beyond the 373 K, the diffusion coefficient and mobility of charge carriers for A5 electrolyte is observed to decrease with temperature. The number density of charge carriers for A5 electrolyte decreased on raising temperature from 298 K to 343 K, and again increase beyond 343 K as listed and shown in Table 4.16 and Figure 4.32, respectively.

4.4. Summary

FTIR has proven interaction between the PVA and LiBOB. The shift of OH band at 3322 cm^{-1} to higher wavenumber proved that Li^{+} has formed an electrostatic bond with the hydroxyls oxygen atom. Deconvolution of the FTIR band between 1840 and 1760 cm^{-1} revealed the percentage of free ions and contact ions. Free ions increased in percentage until at 40 wt.% LiBOB concentration. The conductivity is also maximum at this LiBOB concentration. Beyond 40 wt.% LiBOB concentration, the percentage of free ions decreased. The diffusion coefficient, mobility and number density of free ions for all electrolytes in this system have been determined using FTIR method. In EIS studies, the increase of salt concentration in PVA host increased the room temperature conductivity of the electrolyte until a maximum of 2.83×10^{-4} S cm^{-1} at 40 wt.% LiBOB salt concentration (A4 electrolyte). Beyond 40 wt.% LiBOB salt concentration, the conductivity is observed to decrease. Conductivity–temperature dependence shows the conductivity of PVA–LiBOB solid polymer electrolyte increased with temperature. In this work, the improvement of equation developed by (Arof *et al*., 2014a) to determine the transport properties of polymer electrolyte has been done. Based on the new equations developed in this work, transport properties of charge carriers for PVA–LiBOB solid polymer electrolyte system have been calculated. At room temperature, the increase in LiBOB salt concentration up to 40 wt.% increased the diffusion coefficient, mobility and number density of mobile ions in the electrolyte. Beyond 40 wt.% LiBOB salt concentration, the concentration of free ions is observed to increase while diffusion coefficient and mobility of free ions have decreased. In different temperature range, the diffusion coefficient, mobility and concentration of free ions for each electrolyte is observed to increase/decrease with increasing temperature. As one of the objectives in this work is to utilize the electrolyte in the dye sensitized solar cells (DSSCs), iodide salt has to be added to the composition to form a I^-/I_3^- redox couple for the DSSC to function. Also to produce I_3^-, iodine (I_2) is needed to interact with an iodide (I^-) ion. Hence a second salt must be added and the polymer electrolyte be in the form of a gel for better performance of the DSSC.

CHAPTER 5 : RESULTS FOR PVA–LiBOB–TBAI–I_2–DMF GEL POLYMER ELECTROLYTE SYSTEM

5.1. Introduction

In this chapter, the high room temperature conducting electrolyte in PVA–LiBOB solid polymer electrolyte system (system 1) will be upgraded and used in a dye sensitized solar cell (DSSC). The solid polymer electrolyte with composition 60 wt.% PVA–40 wt.% LiBOB (A4 electrolyte) exhibits the highest room temperature conductivity of 2.83×10^{-4} S cm^{-1} in System 1. This solid polymer electrolyte composition was added with 2.0 g dimethylfromamide (DMF) to form a gel polymer electrolyte. The amount of 2.0 g DMF added was enough to jellify the electrolyte. This is because if more DMF was added, the electrolyte will become more liquid–like. DMF acted as a solvent and plasticizer in this PVA based gel polymer electrolyte. The second salt which was added is tetrabutylammonium iodide (TBAI). The total salt composition was maintained at 0.3333 g but the ratio between LiBOB and TBAI was varied. The purpose of TBAI in this work is to provide the I^- anions for introducing I^- conductivity and to generate the redox couple in the DSSCs with iodine (I_2) that will also be added in the electrolyte. I^- will react with I_2 to form the triiodide and lead to the I^-/I_3^- redox couple. FTIR spectroscopy and EIS measurements were performed to characterize the gel polymer electrolytes. FTIR will discuss the complexation between the polymer, salt and plasticizer. Besides that, the vibrational band corresponding to LiBOB free ions was deconvoluted to determine the percentage of free Li^+ cations in the electrolyte. EIS will discuss the variation of ionic conductivity for PVA–LiBOB–TBAI–I_2–DMF gel polymer electrolyte system at room and elevated temperatures. In addition, transport properties of charge carriers of each electrolyte at room and elevated temperatures were also studied. All electrolytes prepared in this second system were used as a medium in DSSCs and will be discussed more in Chapter 7.

5.2. Fourier Transform Infrared (FTIR) Spectroscopy

FTIR was performed to study the complexation between polymer, salt and plasticizer. Figure 5.1(a) and (b) show the infrared spectrum in transmittance mode for PVA, DMF, LiBOB salt, TBAI salt and PVA–LiBOB–TBAI–I_2–DMF complexes in the wavenumber region from 3800 to 3000 cm^{-1} and 1900 to 800 cm^{-1}.

In PVA infrared spectrum, the vibrational band at 3322 cm^{-1} is assigned to OH band (Buraidah & Arof, 2011). The vibrational frequency at 1089 cm^{-1} in DMF infrared spectrum is assigned to CH_3 rocking mode (Jacob & Arof, 2000). In LiBOB salt infrared spectrum, the vibrational band at 1803, 1158 and 972 wavenumbers are assigned to C=O out–of–phase valence vibration, O–B–O symmetric valence and O–B–O asymmetric valence of LiBOB, respectively (Holomb *et al.*, 2006). Based on the author's knowledge, only a few researchers have reported the FTIR for TBAI salt. The vibrational band at 1030 cm^{-1} has also not been reported yet by any researcher. Thus, in this work, the band at 1030 wavenumber was assigned as one of TBAI characteristics.

Addition of LiBOB and/or TBAI salts into PVA–DMF gel polymer is observed to show all the vibration modes of PVA, DMF, LiBOB and TBAI. In the spectra of PVA–LiBOB–TBAI–I_2–DMF complexes, the vibrational band at 3432, 3456, 3430, 3444, 3426, 3448, 3433 and 3443 wavenumbers correspond to the hydroxyl group of PVA. The band at 1805 and 1806 wavenumbers are assigned to C=O out–of–phase valence vibration of LiBOB. The vibrational frequencies at 1090 cm^{-1} is assigned to

CH_3 rocking mode of DMF. The band at 1023 wavenumber is assigned to TBAI characteristics.

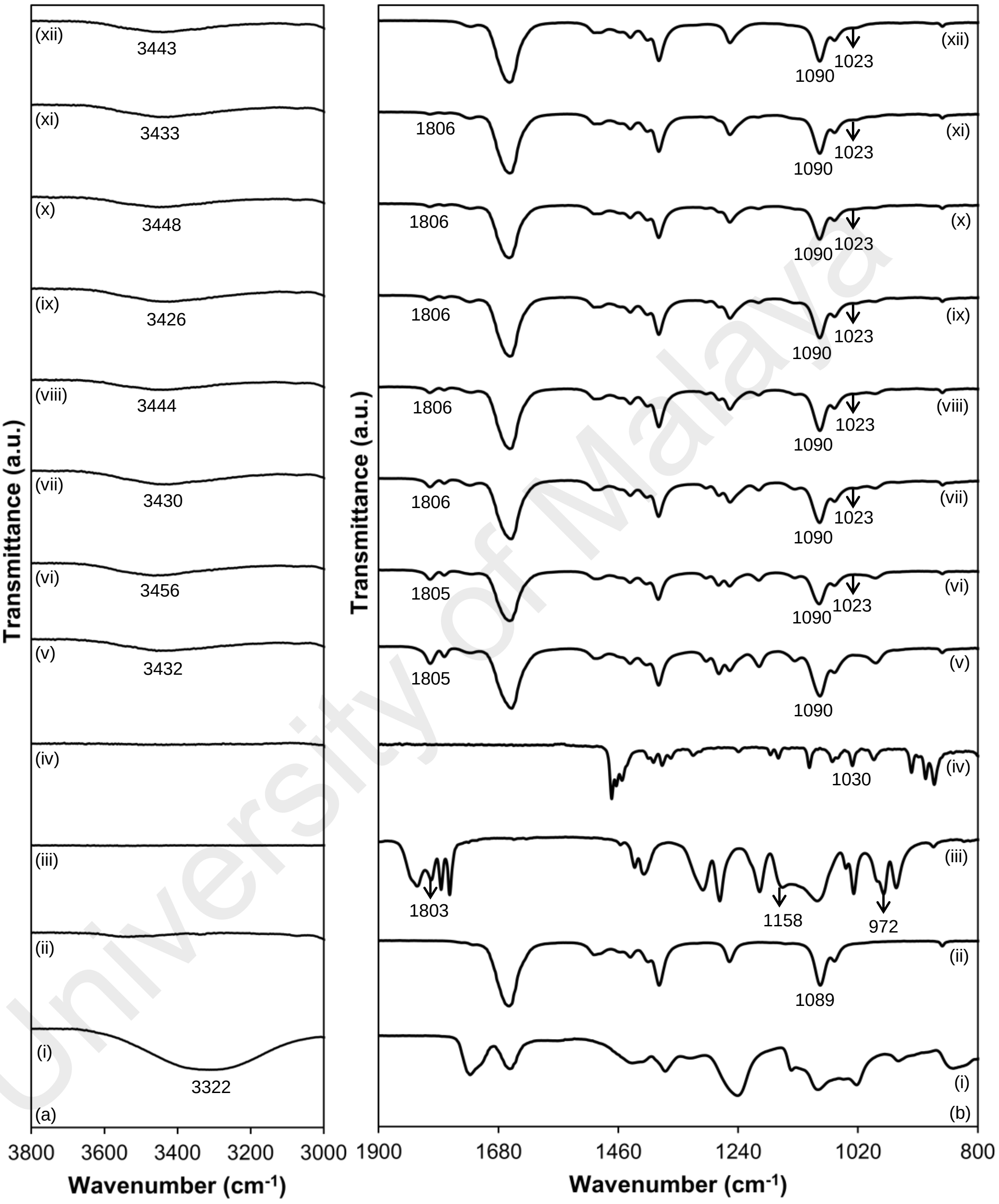

Figure 5.1: FTIR spectra of (i) PVA, (ii) DMF, (iii) LiBOB salt, (iv) TBAI salt, (v) B0, (vi) B1, (vii) B2, (viii) B3, (ix) B4, (x) B5, (xi) B6 and (xii) B7 electrolyte between (a) 3800 and 3000, and (b) 1900 and 800 wavenumber.

In system 1, as discussed in section 4.2, the vibrational band corresponding to OH group of PVA is of concern due to the interaction between the cation of salt and the oxygen atom of hydroxyl group. As can be seen in Figure 5.1(a), the vibrational band of OH group for pure PVA is observed to shift to higher wavenumber when LiBOB and/or TBAI salts were added. These indicate that the complexation between cation of both salts and oxygen atom of hydroxyl group has occurred.

Figure 5.2 shows the FTIR spectrum in absorbance mode for PVA–LiBOB–TBAI–I_2–DMF gel polymer electrolyte in the wavenumber region between 1170 and 1120, 1020 and 960, and 1035 and 1010. In Figure 5.2(a)(i) and 5.2(b)(i) referring to B0 electrolyte (consisting of 100 wt.% LiBOB–0 wt.% TBAI), two vibrational peaks at 1136 and 988 wavenumbers are observed, which correspond to O–B–O symmetric valence and O–B–O asymmetric valence of LiBOB salt, respectively.

Reducing the amount of LiBOB salt by 25 wt.% and replacing with 25 wt.% TBAI salt revealed a very small hump at 1023 cm^{-1} as shown in Figure 5.2(c)(ii). The intensity of the peaks corresponding to LiBOB characteristics at 1136 and 988 wavenumber is observed to slightly decrease. Reducing the ratio of LiBOB salt gradually up to 10 wt.% and replacing slowly with TBAI salt up to 90 wt.% shows the decreasing in intensity of peaks due to LiBOB at 1136 and 988 wavenumber. The peak intensity corresponding to TBAI at 1023 cm^{-1} is observed to increase with increasing amount of TBAI salts in the gel polymer electrolyte. In Figure 5.2(a)(viii) and 5.2(b)(viii), the vibrational peaks due to LiBOB salts do not exist anymore. Only vibrational peak corresponding to TBAI characteristics is observed [Figure 5.2(c)(viii)]. This is because the ratio between LiBOB and TBAI is now 0 wt.%:100 wt.%. Thus only TBAI characteristic was observed.

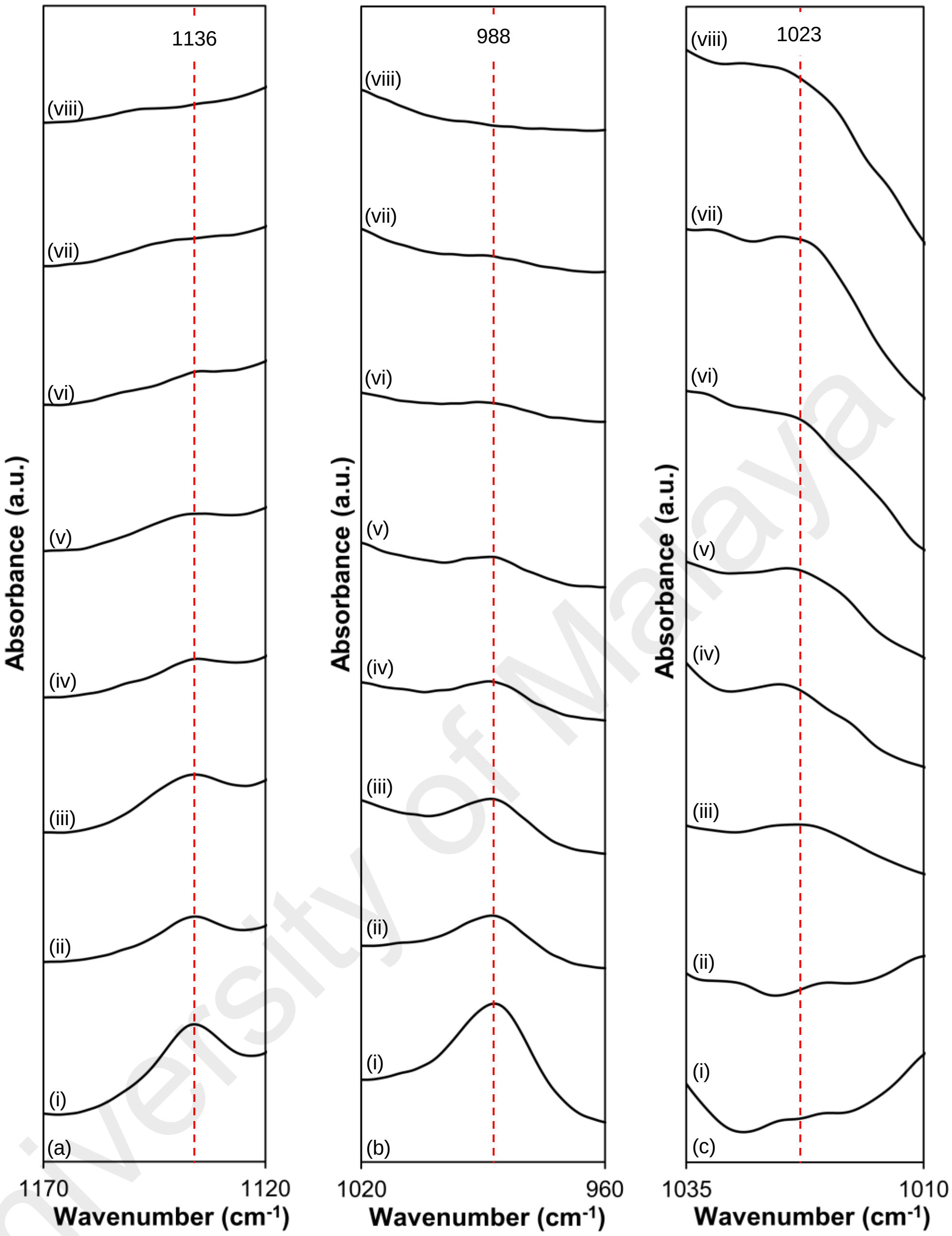

Figure 5.2: FTIR spectra between (a) 1170 and 1120 cm^{-1}, (b) 1020 and 960 cm^{-1} and (c) 1035 and 1010 cm^{-1} for (i) B0, (ii) B1, (iii) B2, (iv) B3, (v) B4, (vi) B5, (vii) B6 and (viii) B7 electrolyte.

As discussed in FTIR section in Chapter 4, the infrared spectrum of electrolyte prepared might be overlapped with the hydroxyl group of water due to hydrophilic properties of PVA. Therefore, the infrared spectrum of hydroxyl region for electrolyte prepared in this system 2 (PVA–LiBOB–TBAI–I_2–DMF gel polymer electrolyte system) were deconvoluted to confirm that there is no water contamination in the electrolyte prepared.

The FTIR deconvolution for PVA–LiBOB–TBAI–I_2–DMF gel polymer electrolyte system between 3700 and 3100 wavenumber is shown in Figure 5.3. In Figure 5.3, it can be seen that the FTIR for all gel polymer electrolytes revealed only one deconvoluted peak, which refer to hydroxyl group of PVA. Based on this observation, it is confirmed that the gel electrolytes prepared in this second system are also not contaminated and free from water.

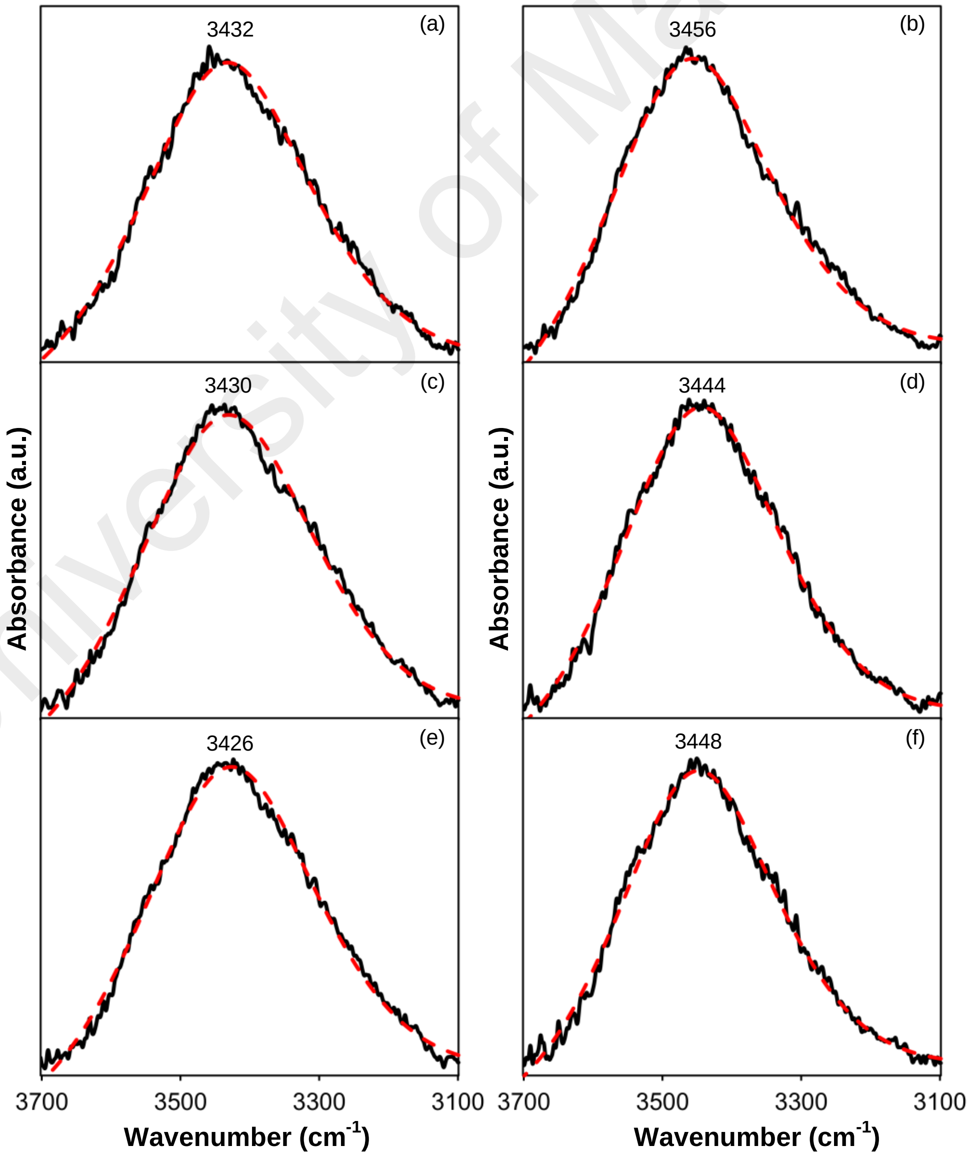

Figure 5.3, continued…

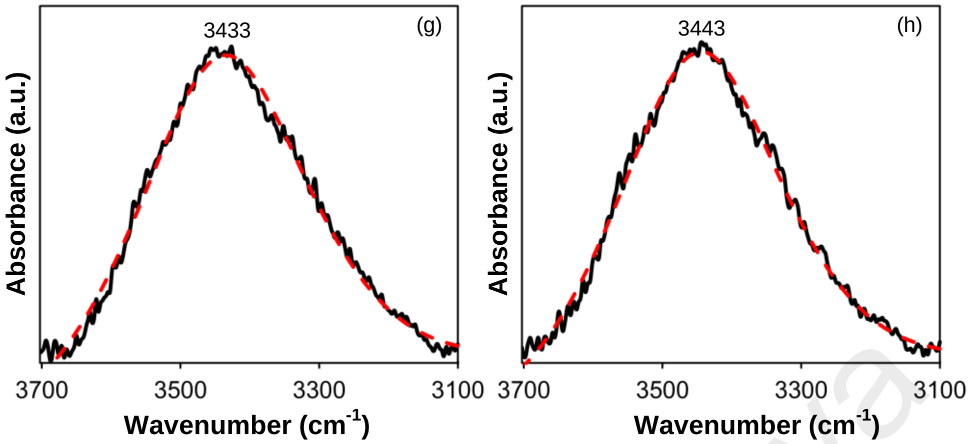

Figure 5.3: FTIR deconvolution for (a) B0, (b) B1, (c) B2, (d) B3, (e) B4, (f) B5, (g) B6 and (h) B7 electrolyte between 3700 and 3000 cm^{-1}. Line (—) due to original spectrum and line (---) due to fitted spectrum.

From FTIR spectroscopy, the percentage of free ions and ion pairs can be illustrated and quantified by deconvoluting the appropriate band (Kufian *et al*., 2012; Sim *et al*., 2012). Figure 5.4 shows the deconvolution of spectral bands for PVA–LiBOB–TBAI–I_2–DMF gel polymer electrolytes with different amounts of LiBOB salt. The FTIR spectra were deconvoluted between 1850 and 1760 cm^{-1} due to the position of free ions and ion pairs of LiBOB salt. Holomb *et al*. (2006) reported that the band of free BOB^{-} anions is observed at 1804 wavenumbers and the band for ion pairs can be observed at 1812, 1817 and 1828 cm^{-1}. In Figure 5.4, the band of free ions is observed at 1805 cm^{-1} and the bands at 1812 and 1826 cm^{-1} are attributed to ion pairs of LiBOB salt. The band at 1778 cm^{-1} is assigned to C=O out–of–phase valence vibrations of LiBOB (Holomb *et al*., 2006). The percentage of free ions and ion pairs in the electrolyte were calculated using the equation (3.1) and (3.2) and listed in Table 5.1.

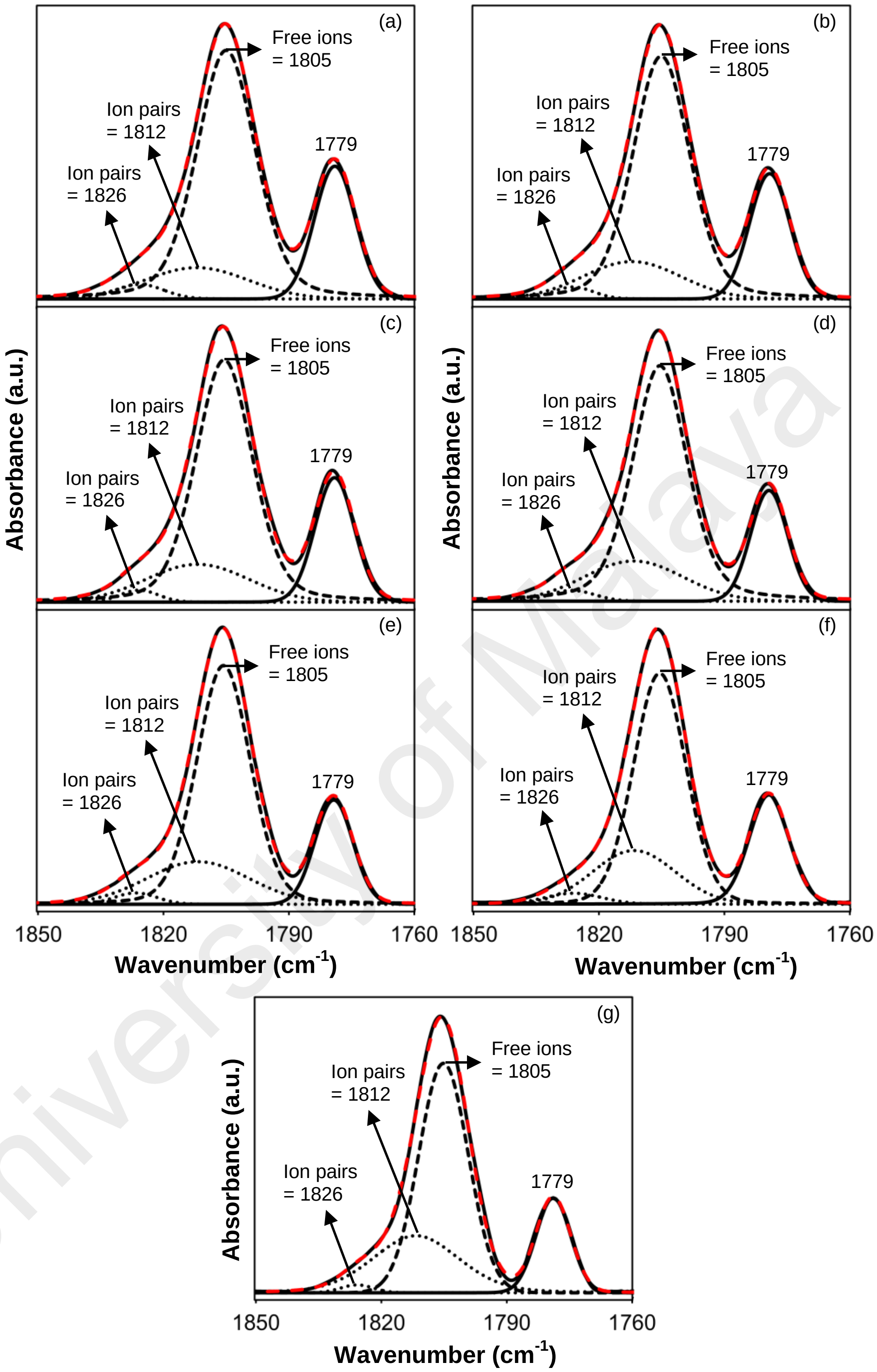

Figure 5.4:. FTIR deconvolution of (a) B0, (b) B1, (c) B2, (d) B3, (e) B4, (f) B5 and (g) B6 electrolytes. Area under line (---) due to free ions and line (·····) due to ion pairs. Line (—) refer to original spectrum and line (---) refer to fitted spectrum.

Table 5.1: Area percentage of free ions and ion pairs of PVA–LiBOB–TBAI–I_2–DMF gel polymer electrolyte system.

Electrolyte	Free ions (%)	Ion pairs (%)
B0	79.49	20.51
B1	77.74	22.26
B2	76.70	23.30
B3	75.32	24.68
B4	73.09	26.91
B5	70.86	29.14
B6	68.54	31.46

It was observed in Table 5.1 that as the amount of LiBOB salt in the electrolyte decreased, the percentage of free ions decreased. Based on literature review carried out by the author, there is no report about the position of free iodide ions that can be obtained from FTIR and ab initio studies. Thus, in this work the percentage of free iodide ion dissociated from TBAI salt cannot be determined and the decreased observed in the FTIR band deconvolution is only that of BOB^{-} anions.

So far, the calculation of D, μ and n for PVA–LiBOB–TBAI–I_2–DMF gel polymer electrolyte system, the percentage of free ions in electrolyte is required in equation (4.1), (4.2) and (4.3). As discussed above, the number of free ions obtained is only that from LiBOB salt and not from TBAI. There are also no reports about the position of free iodide ion that can be obtained from FTIR and ab initio studies. Therefore, the percentage of free iodide ion dissociated from TBAI salt cannot be determined from FTIR spectroscopy. Without the information of TBAI free ions, the values of transport properties of charge carriers for electrolyte consisting TBAI salt cannot be estimated. Hence, only gel polymer electrolyte consisting of 100 wt.% LiBOB salt (B0 electrolyte) can be used to calculate the values of transport properties of charge carriers using FTIR method. The values of V_{Total}, free ion percentage (%), n, μ and D of B0 electrolyte from FTIR studies at room temperature are listed in Table 5.2.

Table 5.2: Values of V_{Total}, free ion percentage (%), n, μ and D of B0 electrolyte from FTIR method at room temperature (298 K).

V_{Total} (cm^3)	Free ion percentage (%)	n ($\times 10^{20}$ cm^{-3})	μ ($\times 10^{-5}$ cm^2 V^{-1} s^{-1})	D ($\times 10^{-6}$ cm^2 s^{-1})
2.96	79.49	5.570	8.188	2.103

5.3. Electrochemical Impedance Spectroscopy (EIS)

5.3.1. Ionic Conductivity of PVA–LiBOB–TBAI–I_2–DMF Gel Polymer Electrolyte

The electrical properties of PVA–LiBOB–TBAI–I_2–DMF gel polymer electrolyte have been studied by electrochemical impedance spectroscopy. Figure 5.5 shows the Nyquist plots for PVA–LiBOB–TBAI–I_2–DMF gel polymer electrolyte system at room temperature. It is observed that the Nyquist plot for all electrolytes in this second system consists of only a tilted spike. From the Nyquist plot obtained in Figure 5.5, the value of bulk resistance, R_b have been obtained from the interception of tilted spike with the real impedance, *Z'* axis. The value of R_b obtained in Figure 5.5 was listed in Table 5.3. Using equation (3.4), the ionic conductivity value of PVA–LiBOB–TBAI–I_2–DMF gel polymer electrolyte at room temperature has been calculated. The thickness, d of each electrolyte was maintained at 0.26 cm. Figure 5.6 shows the variation of ionic conductivity for PVA–LiBOB–TBAI–I_2–DMF gel polymer electrolyte with different weight ratios of LiBOB and TBAI salts.

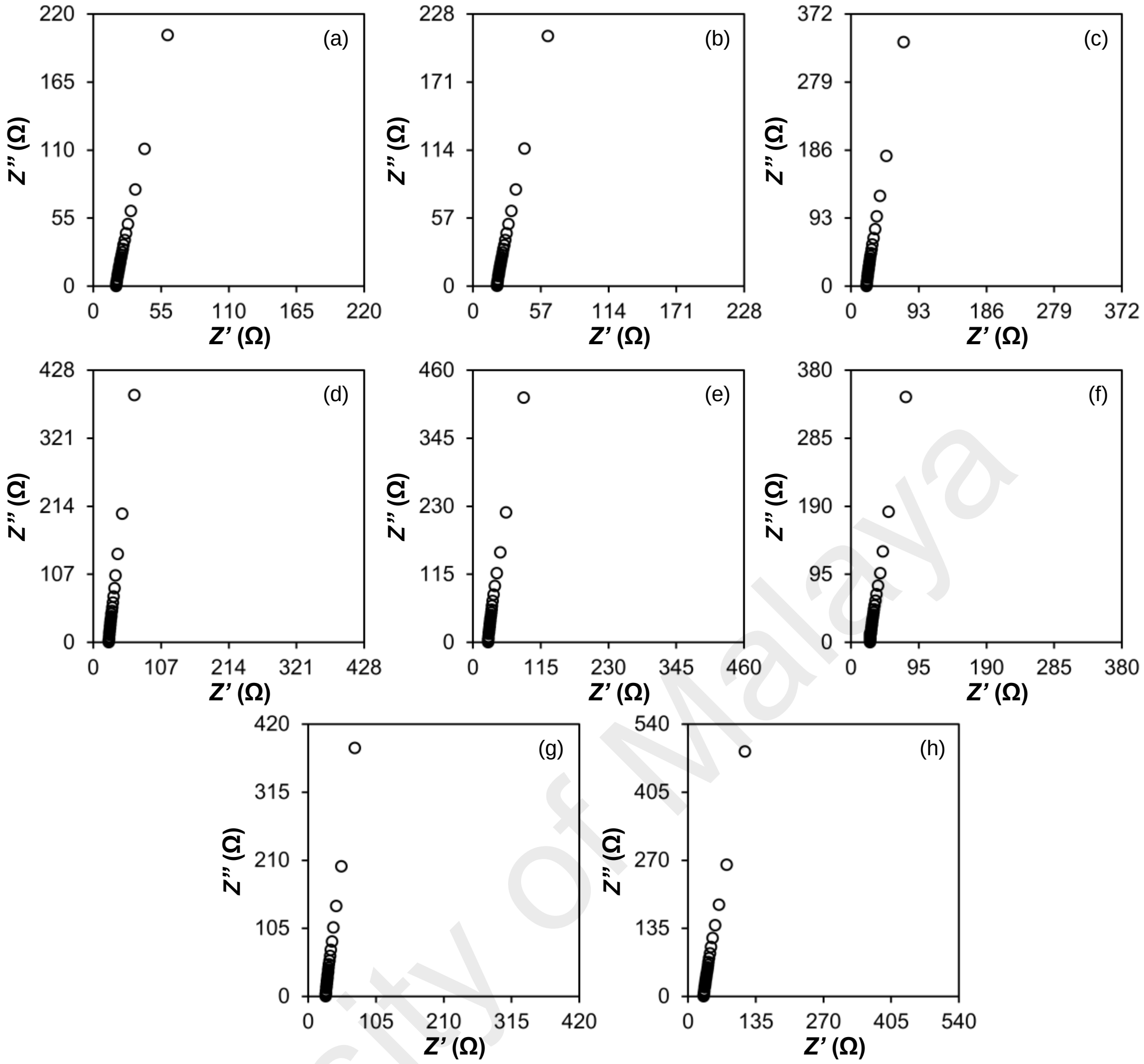

Figure 5.5: Nyquist plot of (a) B0, (b) B1, (c) B2, (d) B3, (e) B4, (f) B5, (g) B6 and (h) B7 gel polymer electrolyte at room temperature.

Table 5.3: R_b values of PVA–LiBOB–TBAI–I_2–DMF gel polymer electrolyte obtained in Figure 5.5.

Electrolyte	R_b (Ω)
B0	17.70
B1	19.50
B2	20.50
B3	23.00
B4	24.40
B5	25.20
B6	26.70
B7	29.70

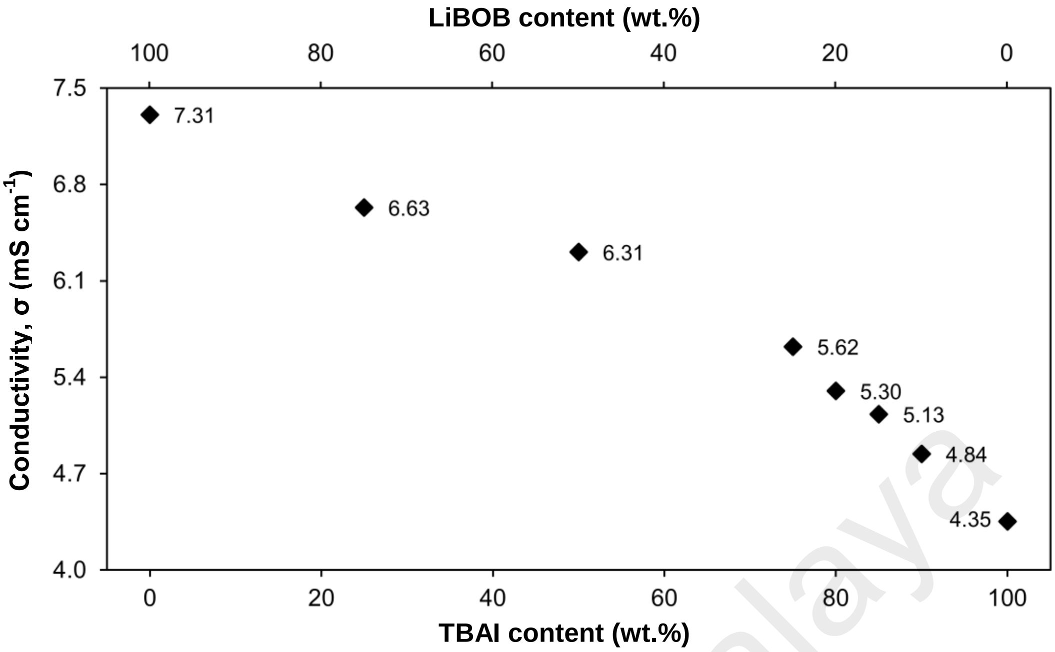

Figure 5.6: Room temperature conductivity of PVA–LiBOB–TBAI–I_2–DMF gel polymer electrolyte system.

In Figure 5.6, the conductivity of PVA based gel polymer electrolyte with 100 wt.% LiBOB (B0 electrolyte) is observed at 7.31×10^{-3} S cm^{-1}. When the amount of LiBOB salt was reduced by 25 wt.% and replaced with TBAI salt by 25 wt.% (B1 electrolyte), the ionic conductivity was observed to decrease to 6.63×10^{-3} S cm^{-1}. The conductivity was observed to decrease gradually with decreasing LiBOB salt in the electrolyte until the overall amount of the original LiBOB salt replaced with TBAI salt and gave the conductivity value of 4.35×10^{-3} S cm^{-1}.

The conductivity of PVA–LiBOB–TBAI–I_2–DMF gel polymer electrolyte was also measured at different temperatures. Figure 5.7 shows the conductivity–temperature dependence of PVA–based gel polymer electrolyte between 298 and 393 K. The conductivity of each electrolyte is seen to increase as the temperature of electrolyte increased. The conductivity–temperature dependence of this electrolyte system is observed to form a quadratic shape, which suggests that conductivity and temperature obey the VTF relationship. Figure 5.8 shows the VTF plot of conductivity–temperature dependence for PVA–LiBOB–TBAI–I_2–DMF gel polymer electrolyte. Table 5.4 listed the values of σ, T_o, E_a and regression (R^2) of PVA–LiBOB–TBAI–I_2–DMF gel electrolytes system obtained from VTF plot in Figure 5.8.

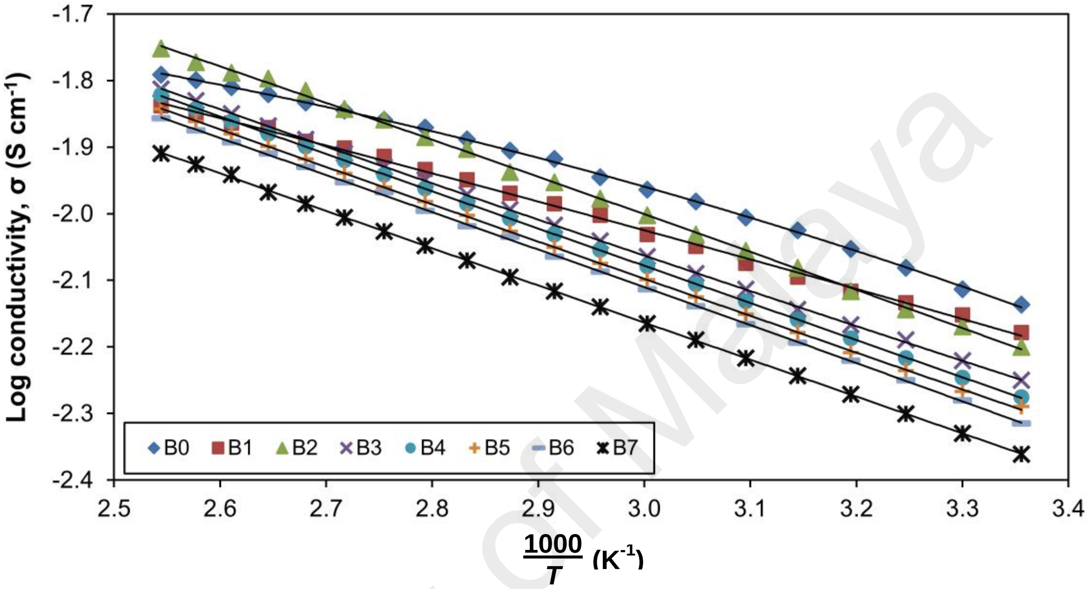

Figure 5.7: Conductivity–temperature dependence of PVA–LiBOB–TBAI–I_2–DMF gel polymer electrolyte.

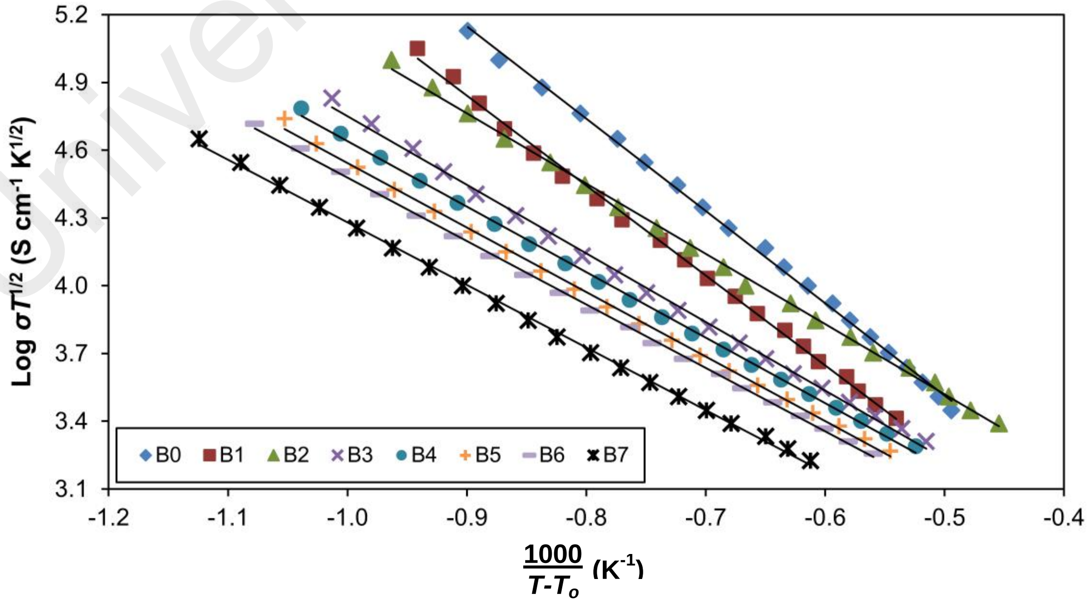

Figure 5.8: VTF plot of conductivity–temperature dependence PVA–LiBOB–TBAI–I_2–DMF gel polymer electrolyte.

Table 5.4: The σ, T_o, E_a and R^2 values of PVA–LiBOB–TBAI–I_2–DMF gel polymer electrolyte system.

Electrolyte	**σ (mS cm^{-1})**	**T_o (K)**	**E_a (meV)**	**R^2**
B0	7.31	103	48.49	0.998
B1	6.63	100	49.72	0.998
B2	6.31	98	63.71	0.999
B3	5.62	91	65.22	0.998
B4	5.30	89	68.36	0.999
B5	5.13	87	69.33	0.999
B6	4.84	86	70.64	0.999
B7	4.35	83	71.55	0.999

5.3.2. Room Temperature Transport Properties of Charge Carriers of PVA–LiBOB–TBAI–I_2–DMF Gel Polymer Electrolyte

Transport properties of charge carriers are important parameters to be known. It gives information about the variation of conductivity obtained in polymer electrolyte system. It is because the conductivity is the product of μ, n and e. Thus, by knowing the values of μ and n can shed some light on the change in conductivity obtained for the polymer electrolyte system.

Based on Figure 5.5, all Nyquist plots obtained at room temperature consisted only of a tilted spike. In section 4.3.2, we have developed the equation to determine the transport properties of free ions of the electrolyte from fitting the tilted spike impedance plot. Hence, the D, μ and n for PVA–LiBOB–TBAI–I_2–DMF gel polymer electrolyte system can be calculated using equation (4.16), (4.17) and (4.18), respectively.

Figure 5.9 shows the impedance plot and their corresponding fitted point for PVA–LiBOB–TBAI–I_2–DMF gel polymer electrolyte system at room temperature. The Nyquist or impedance plot obtained by impedance measurement was fitted using equation (3.19) and (3.20). The value of R and p_2 have been determined using the concept depicted in Figure 3.12. The parameter k_2 was determined by trial and error until the fitted points quite accurately fitted the complex impedance plot. Table 5.5 lists the values of R, k_2, p_2 and ω_2 for PVA–LiBOB–TBAI–I$_2$–DMF gel polymer electrolyte system from the fitting method or A–N method.

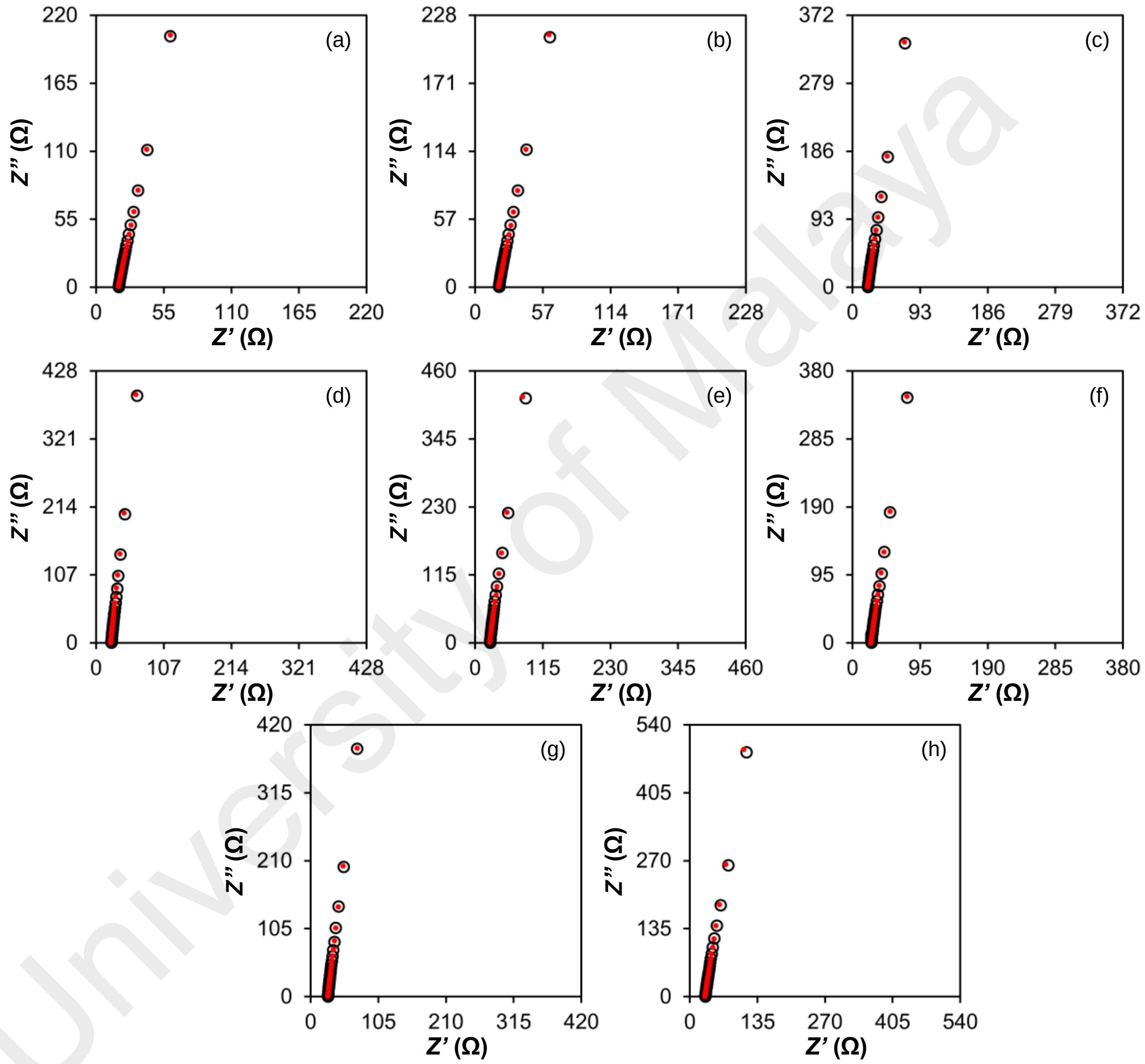

Figure 5.9: Nyquist plot (o) and their corresponding fitted point (●) for (a) B0, (b) B1, (c) B2, (d) B3, (e) B4, (f) B5, (g) B6 and (h) B7 electrolyte at room temperature.

Based on equation (4.16), (4.17) and (4.18), the value of d, R, k_2 and ω_2 should be known so that the transport properties of this gel polymer electrolyte system can be calculated. In this second electrolyte system, the thickness, d of all electrolytes was fixed at 0.26 cm since the impedance was measured with the gels placed in a coin cell of thickness 0.26 cm. The values of *R* and k_2 were obtained from fitting the Nyquist plot. The ω_2 value is the frequency value where *Z"* is a minimum i.e. at $Z'' \rightarrow 0$.

Table 5.5: Values of *R*, p_2, k_2 and ω_2 for PVA–LiBOB–TBAI–I_2–DMF gel polymer electrolyte obtained from fitting of Nyquist plot at room temperature.

Electrolyte	***R*** **(Ω)**	p_2	k_2 **(F^{-1})**	ω_2 **(s^{-1})**
B0	17.70	0.870	31000	317194
B1	19.50	0.874	32900	283789
B2	20.50	0.904	61400	532003
B3	23.00	0.935	85000	296963
B4	24.40	0.915	81000	262459
B5	25.20	0.907	64100	285528
B6	26.70	0.925	79000	342834
B7	29.70	0.900	88000	318820

From the parameter values listed in Table 5.5, *D*, μ and *n* for PVA–LiBOB–TBAI–I_2–DMF gel polymer electrolyte at room temperature were calculated using equations (4.16), (4.17) and (4.18), respectively. The calculation values are listed in Table 5.6. Figure 5.10, 5.11 and 5.12 shows the plot of *D*, μ and *n* respectively for the charge carriers in PVA–based gel polymer electrolyte containing different LiBOB:TBAI weight ratio at room temperature.

Table 5.6: Values of *D*, μ and *n* for PVA–LiBOB–TBAI–I_2–DMF gel electrolyte obtained by fitting method at room temperature.

Electrolyte	***D*** **($\times10^{-6}$ cm^2 s^{-1})**	μ **($\times10^{-5}$ cm^2 V^{-1} s^{-1})**	***n*** **($\times10^{20}$ cm^{-3})**
B0	2.159	8.407	5.424
B1	2.208	8.596	4.816
B2	2.303	8.966	4.392
B3	2.385	9.285	3.780

Table 5.6, continued...

B4	2.393	9.318	3.550
B5	2.460	9.577	3.345
B6	2.462	9.586	3.154
B7	2.467	9.604	2.830

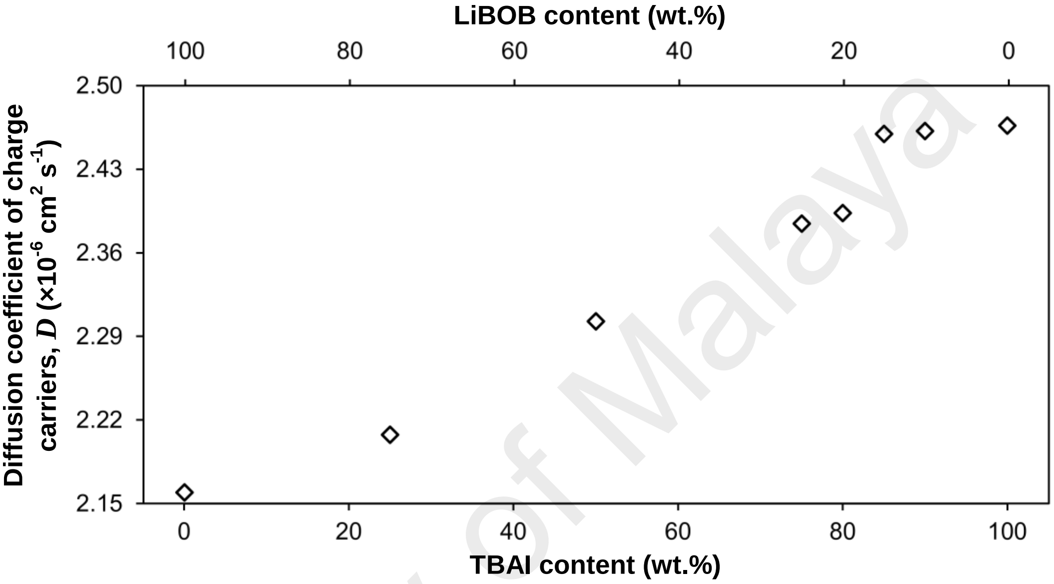

Figure 5.10: Diffusion coefficient of charge carriers, D for PVA–LiBOB–TBAI–I_2–DMF gel electrolyte at room temperature.

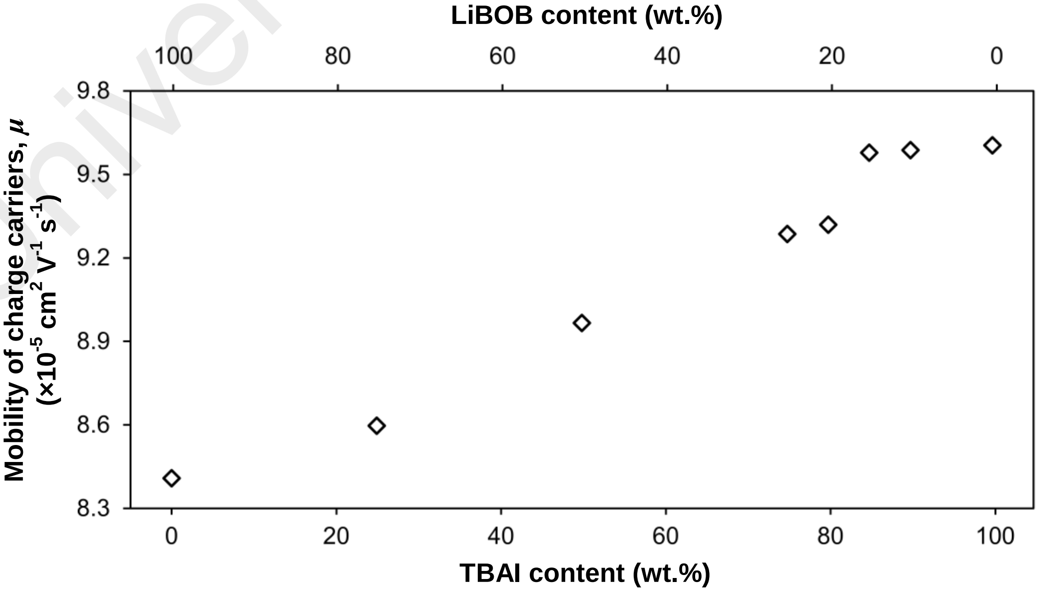

Figure 5.11: Mobility of charge carriers, μ for PVA–LiBOB–TBAI–I_2–DMF gel electrolyte at room temperature.

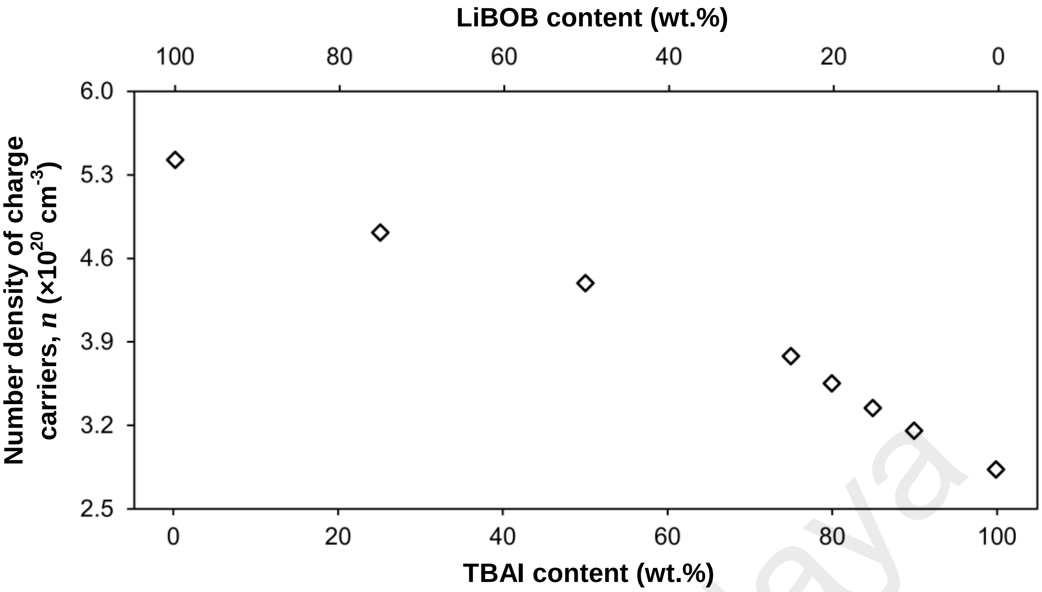

Figure 5.12: Number density of charge carriers, *n* for PVA–LiBOB–TBAI–I_2–DMF gel electrolyte at room temperature.

In this PVA–LiBOB–TBAI–I_2–DMF gel polymer electrolyte system, the weight ratio between LiBOB and TBAI salts was varied. It must be remembered that the total number density of charge carriers calculated (using impedance data and fitting) and listed in Table 5.6 is the number density of charge carriers contributed by LiBOB and TBAI salts. It is important to know the number density of charge carriers from TBAI separately. To do this, *n* as listed in Table 5.6 was subtracted from the value of *n* due to only LiBOB from FTIR analysis. Table 5.7 lists the values of number density of charge carriers for LiBOB and TBAI separately for each electrolyte. Figure 5.13(a) depicted the variation of number density of charge carriers from LiBOB and TBAI salt at different weight ratio LiBOB:TBAI at room temperature. Figure 5.13(b) shows the number density of charge carriers from TBAI only for PVA–based gel polymer electrolyte consisting of 75 to 100 wt.% TBAI salt to clarify the changes in TBAI ions exist which cannot be observed in Figure 5.13(a).

Table 5.7: Values of number density of charge carriers for LiBOB and TBAI in PVA–LiBOB–TBAI–I_2–DMF gel polymer electrolyte.

Electrolyte	n ($\times 10^{20}$ cm^{-3})	
	LiBOB	**TBAI**
B0	5.424	0
B1	3.612	1.204
B2	2.196	2.196
B3	0.945	2.835
B4	0.710	2.840
B5	0.502	2.843
B6	0.315	2.838
B7	0	2.830

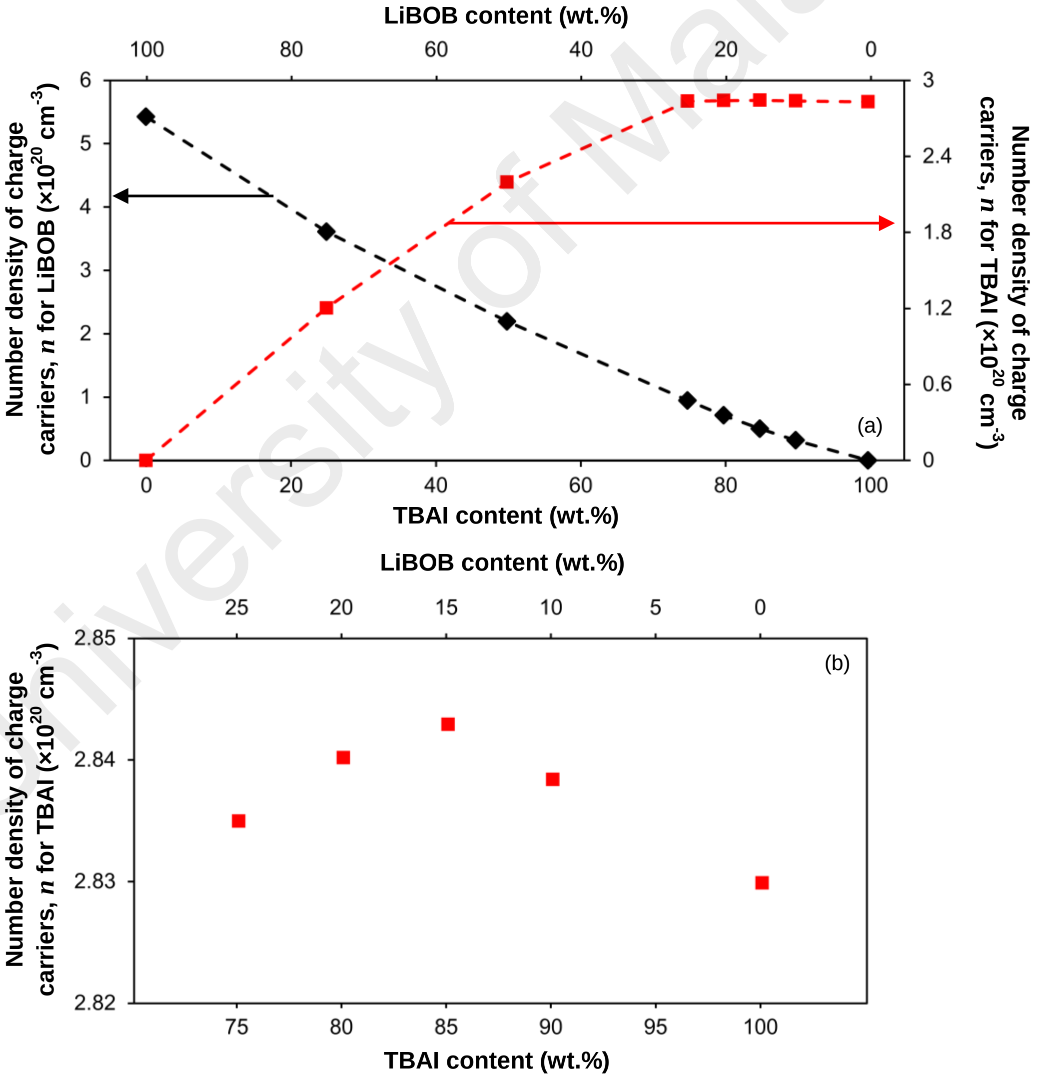

Figure 5.13: (a) Variation of number density of charge carrier for LiBOB and TBAI in PVA–LiBOB–TBAI–I_2–DMF gel polymer electrolyte at room temperature. (b) Number density of charge carrier from TBAI only in PVA–LiBOB–TBAI–I_2–DMF gel polymer electrolyte consisting of 75 to 100 wt% TBAI salt at room temperature.

In Figure 5.13(a), it can be seen that the value of *n* for LiBOB in PVA–LiBOB–TBAI–I_2–DMF gel polymer electrolyte system decreased with decreasing LiBOB content. The value of *n* for TBAI in PVA–LiBOB–TBAI–I_2–DMF gel polymer electrolyte is observed to increase gradually until it achieved a maximum of 2.84×10^{20} cm^{-3} for electrolyte containing 15 wt.% LiBOB and 85 wt.% TBAI (B5 electrolyte). Beyond this electrolyte composition, the number density of charge carrier of TBAI salt is observed to decrease as shown in Figure 5.14(b).

5.3.3. Transport Properties of Charge Carriers of PVA–LiBOB–TBAI–I_2–DMF Gel Polymer Electrolyte at Elevated Temperatures

The transport properties of charge carriers of PVA–LiBOB–TBAI–I_2–DMF gel polymer electrolyte system were studied at different temperatures. The Nyquist plots obtained by impedance measurement for all PVA–based gel polymer electrolytes prepared at different temperatures were fitted using equations (3.19) and (3.20). It is observed that all Nyquist plots obtained in this second electrolyte system consisted of only a tilted spike. Hence, equations (4.16), (4.17) and (4.18) that have been developed in Section 4.3.2. were used to calculate the transport properties of charge carriers.

Figure 5.14 displays the complex impedance plot and the fitted points for B0 electrolyte at different temperatures. The fitting parameters obtained in Figure 5.14 were listed in Table 5.8.

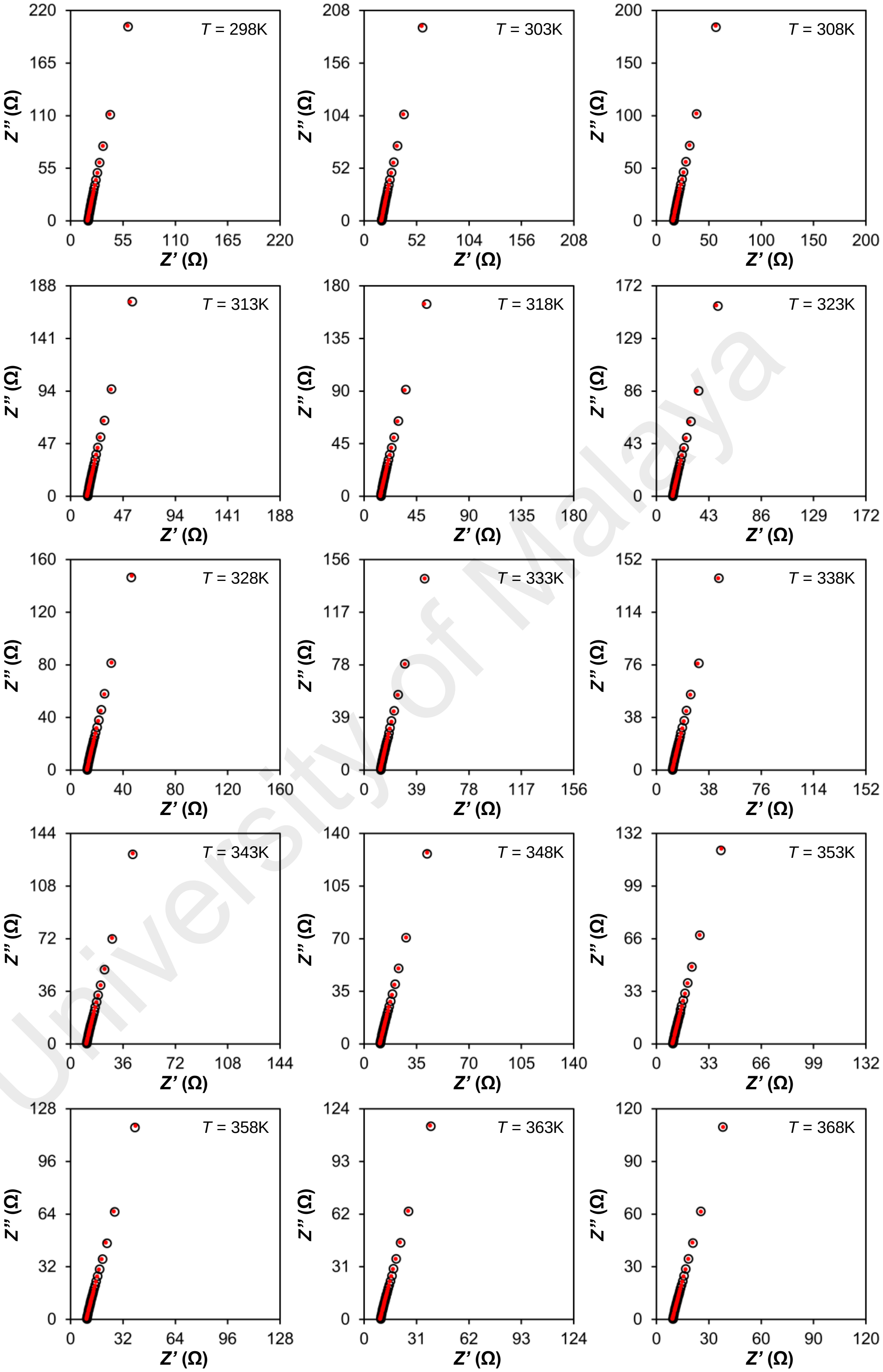
T = 298K
T = 303K
T = 308K
T = 313K
T = 318K
T = 323K
T = 328K
T = 333K
T = 338K
T = 343K
T = 348K
T = 353K
T = 358K
T = 363K
T = 368K
Z'' (Ω)
Z' (Ω)
0
55
110
165
220
52
104
156
208
50
100
150
200
47
94
141
188
45
90
135
180
43
86
129
172
40
80
120
160
39
78
117
156
38
76
114
152
36
72
108
144
35
70
105
140
33
66
99
132
32
64
96
128
31
62
93
124
30
60
90
120

Figure 5.14, continued…

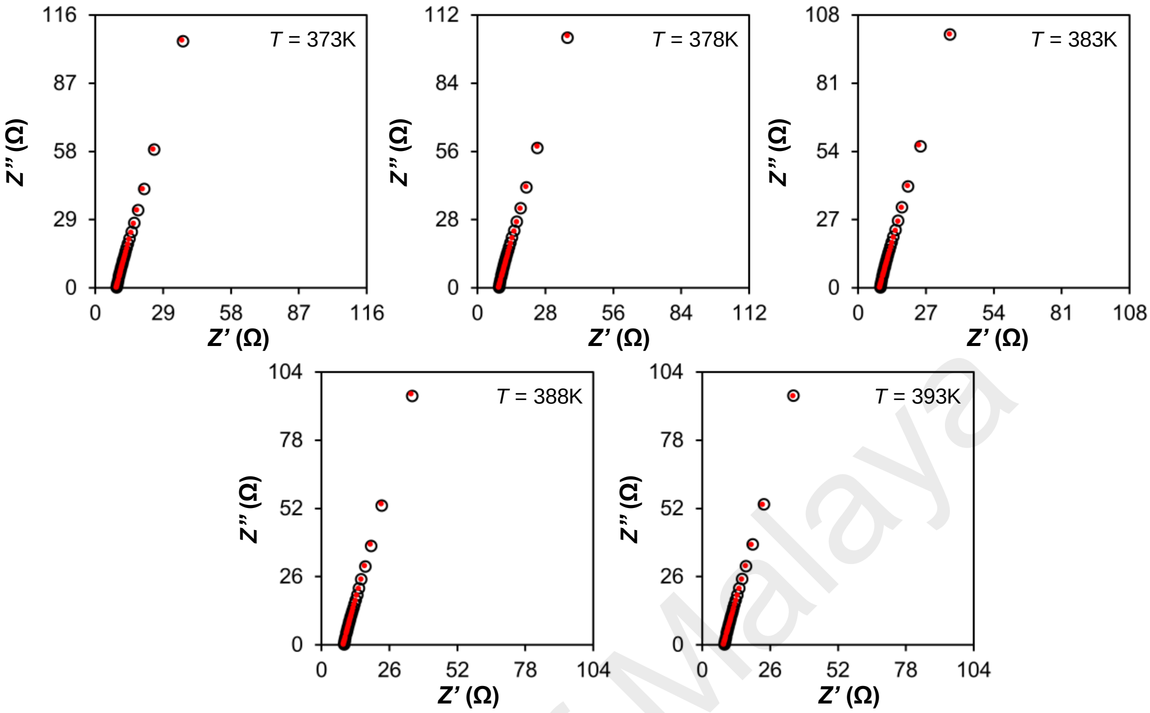

Figure 5.14: Nyquist plot (o) and their corresponding fitted point (●) for B0 electrolyte at different temperatures.

Table 5.8: Values of R, p_2, k_2 and ω_2 for B0 electrolyte obtained from fitting of Nyquist plot at different temperatures.

T (K)	R (Ω)	p_2	k_2 (F^{-1})	ω_2 (s^{-1})
298	17.70	0.870	31000	317194
303	16.80	0.870	29300	315777
308	15.60	0.862	27000	312809
313	14.60	0.860	25000	308873
318	13.70	0.856	23200	304916
323	13.10	0.856	22000	302120
328	12.40	0.855	20700	300179
333	11.90	0.854	19800	299419
338	11.40	0.850	18900	298593
343	10.70	0.847	17500	294090
348	10.40	0.845	16900	292334
353	10.00	0.843	16100	289454
358	9.60	0.841	15300	286339
363	9.35	0.838	14600	279306
368	9.05	0.835	13800	271319
373	8.80	0.834	13200	265999
378	8.55	0.830	12700	263318
383	8.35	0.828	12200	258750
388	8.15	0.831	11800	256377
393	8.00	0.826	11400	252162

From the parameter values listed in Table 5.8, diffusion coefficient (D), mobility (μ) and concentration (n) of mobile ions for B0 electrolyte at different temperatures were calculated using equations (4.16), (4.17) and (4.18), respectively. The calculated values are listed in Table 5.9. Figure 5.15 show the plots of D, μ and n at different temperatures, respectively.

Table 5.9: Values of D, μ and n for B0 electrolyte at different temperatures.

T (K)	**D ($\times 10^{-6}$ cm^2 s^{-1})**	**μ ($\times 10^{-5}$ cm^2 V^{-1} s^{-1})**	**n ($\times 10^{20}$ cm^{-3})**
298	2.158	8.265	5.813
303	2.158	8.128	6.366
308	2.156	7.994	6.916
313	2.155	7.862	7.494
318	2.153	7.735	7.966
323	2.152	7.613	8.551
328	2.150	7.493	9.053
333	2.149	7.376	9.599
338	2.146	7.261	10.390
343	2.144	7.149	10.856
348	2.142	7.041	11.464
353	2.140	6.936	12.123
358	2.138	6.834	12.633
363	2.136	6.734	13.246
368	2.134	6.638	13.818
373	2.131	6.543	14.430
378	2.128	6.446	14.997
383	2.125	6.355	15.584
388	2.121	6.263	16.111
393	2.158	8.265	5.813

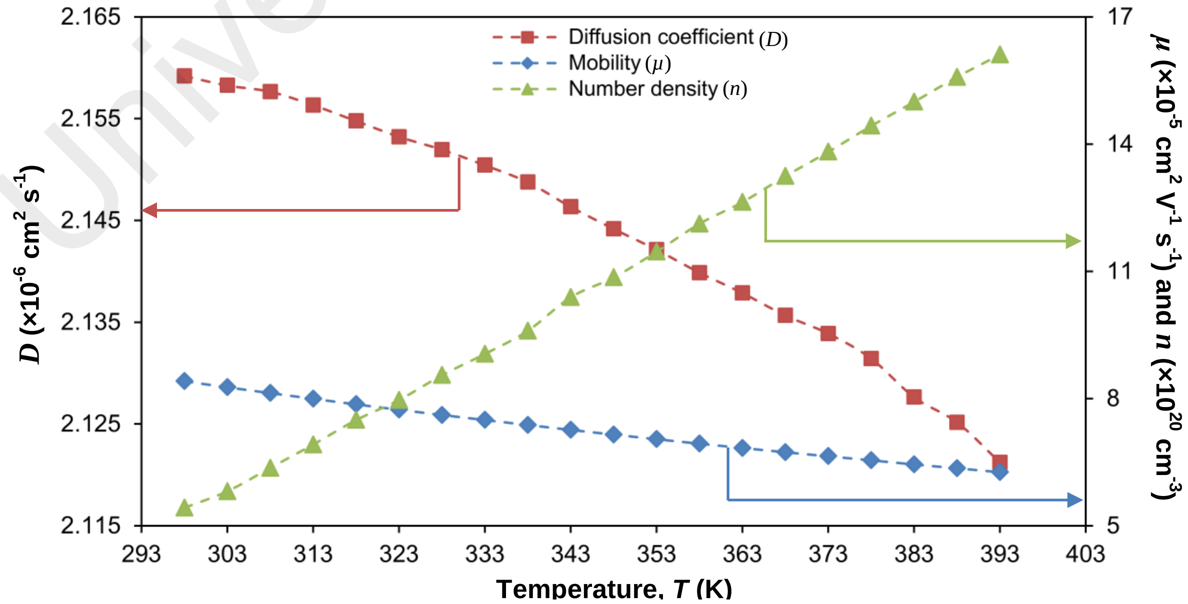

Figure 5.15: D, μ and n of mobile ions for B0 electrolyte at different temperatures.

From Figure 5.15, diffusion coefficient of mobile charged species for B0 sample is observed to decrease with increasing the temperature. The increased in temperature has caused the mobility of charge carriers for B0 electrolyte to decrease. Number density of charge carriers for B0 electrolyte is observed to increase with temperature as depicted in Figure 5.15.

Figure 5.16 display the impedance plot and their corresponding fitted points for B1 electrolyte at different temperatures. All fitted parameters obtained in Figure 5.16 are listed in Table 5.10.

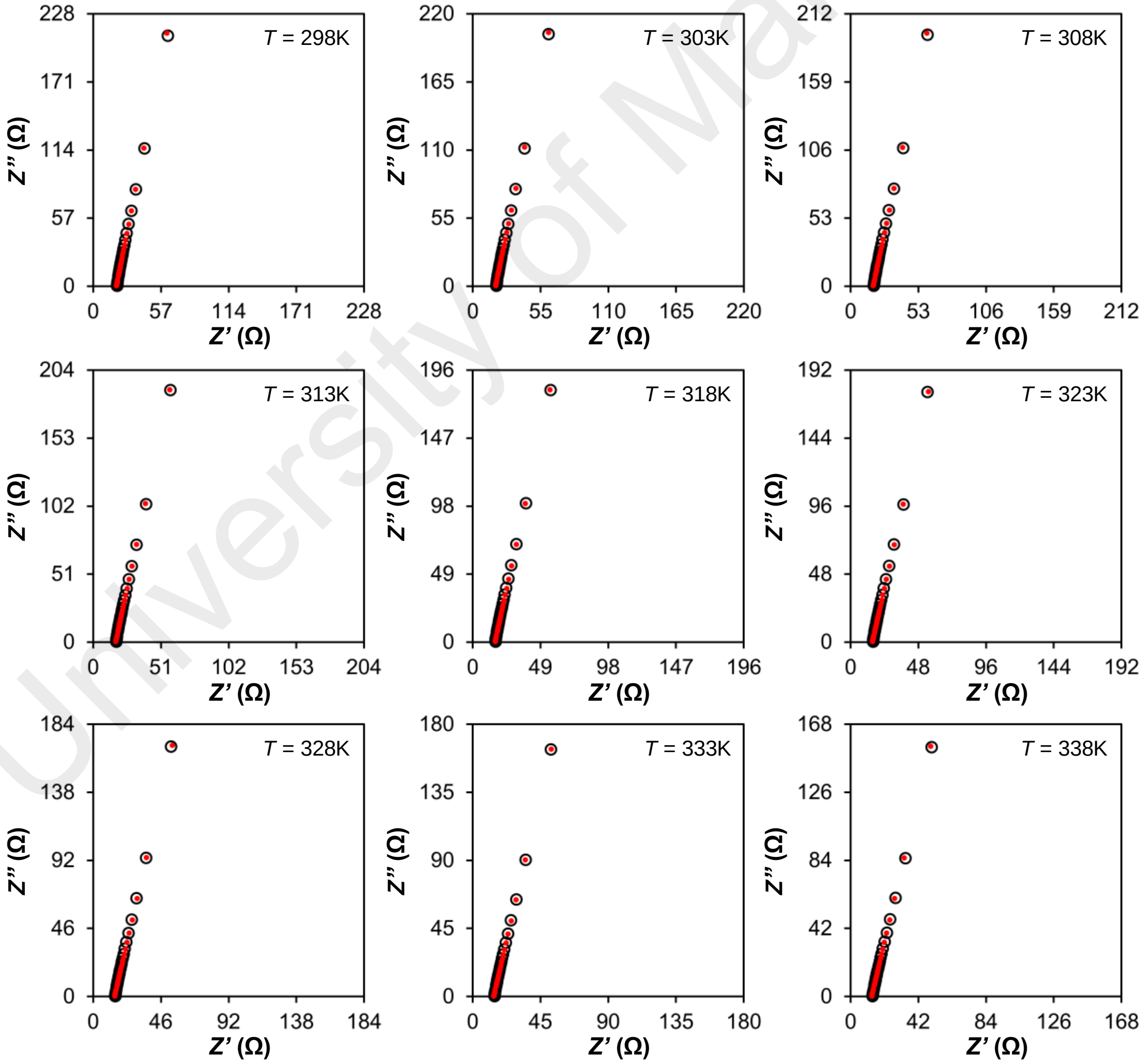

Figure 5.16, continued…

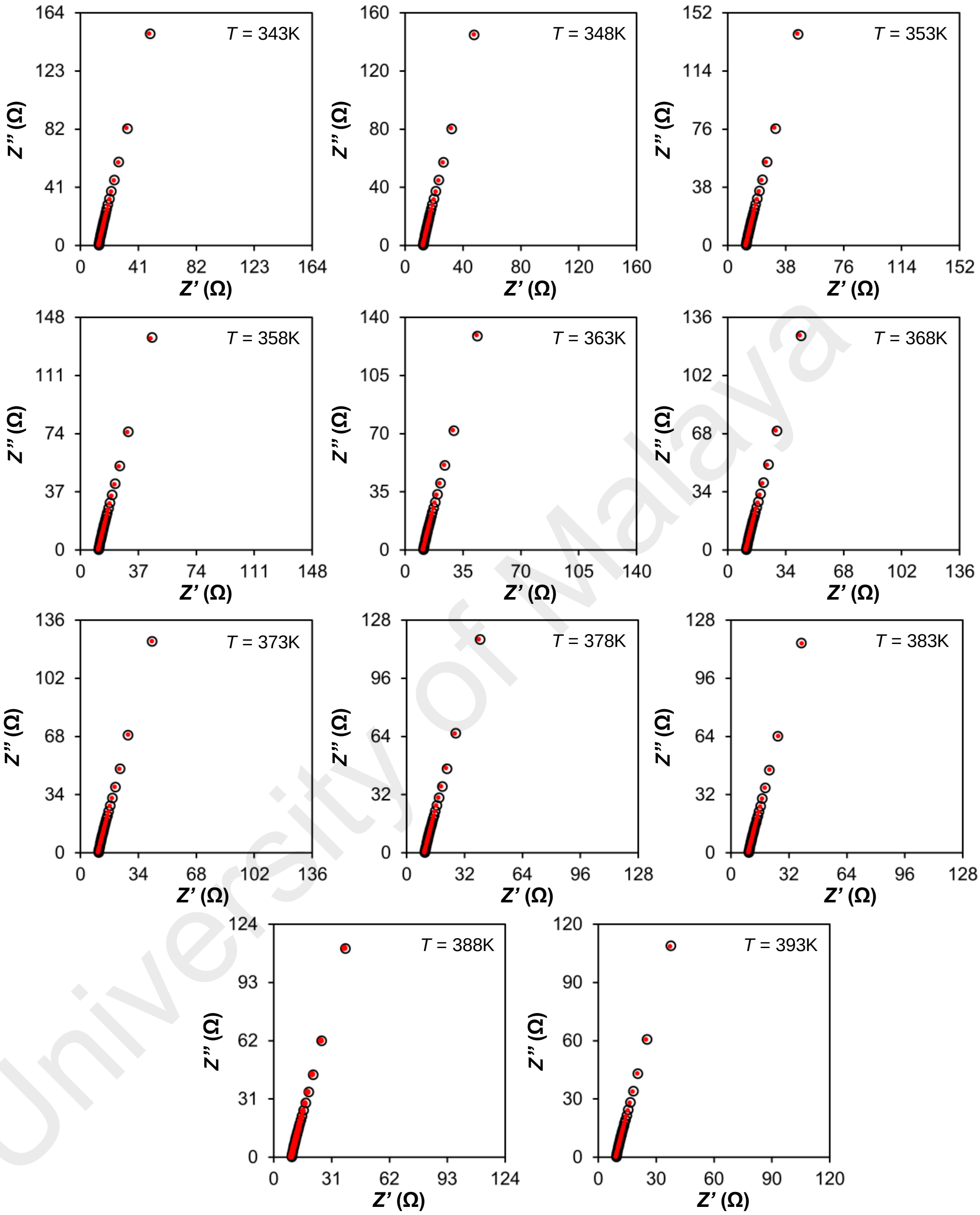

Figure 5.16: Nyquist plot (o) and their corresponding fitted point (●) for B1 electrolyte at different temperatures.

Table 5.10: *R*, p_2, k_2 and ω_2 values for B1 electrolyte obtained from fitting of Nyquist plot at varied temperatures.

T (K)	**R (Ω)**	**p_2**	**k_2 (F^{-1})**	**ω_2 (s^{-1})**	**T (K)**	**R (Ω)**	**p_2**	**k_2 (F^{-1})**	**ω_2 (s^{-1})**
298	19.50	0.874	32900	283789	348	12.05	0.848	19600	272634
303	18.35	0.868	30800	282150	353	11.50	0.847	18600	270757
308	17.60	0.866	29300	279306	358	11.10	0.845	17900	269948
313	16.90	0.865	28000	277767	363	10.60	0.843	17000	268213
318	16.10	0.863	26600	276936	368	10.30	0.842	16400	265938
323	15.35	0.859	25300	276299	373	10.07	0.840	16000	265571
328	14.47	0.855	23800	275727	378	9.60	0.840	15200	264594
333	13.90	0.854	22800	275030	383	9.45	0.840	14900	263560
338	13.00	0.852	21300	274840	388	9.20	0.840	14400	261445
343	12.50	0.850	20400	273577	393	8.90	0.838	13900	260964

From the parameter values listed in Table 5.10, *D*, *μ* and *n* of mobile ions for B1 electrolyte at different temperatures were calculated using equations (4.16), (4.17) and (4.18), respectively. The calculated values are listed in Table 5.11. Figure 5.17 show the plots of diffusion coefficient, mobility and number density of free ions at different temperatures, respectively.

Table 5.11: Values of *D*, *μ* and *n* for B1 electrolyte at different temperatures.

T (K)	**D (×10^{-6} cm^2 s^{-1})**	**μ (×10^{-5} cm^2 V^{-1} s^{-1})**	**n (×10^{20} cm^{-3})**	**T (K)**	**D (×10^{-6} cm^2 s^{-1})**	**μ (×10^{-5} cm^2 V^{-1} s^{-1})**	**n (×10^{20} cm^{-3})**
298	2.208	8.596	4.816	348	2.201	7.339	9.128
303	2.207	8.451	5.205	353	2.200	7.233	9.704
308	2.206	8.311	5.518	358	2.200	7.130	10.200
313	2.205	8.176	5.842	363	2.199	7.029	10.833
318	2.205	8.045	6.232	368	2.198	6.931	11.307
323	2.204	7.918	6.641	373	2.197	6.835	11.728
328	2.204	7.796	7.156	378	2.196	6.742	12.471
333	2.203	7.676	7.566	383	2.195	6.650	12.845
338	2.202	7.560	8.213	388	2.194	6.560	13.374
343	2.202	7.448	8.670	393	2.193	6.475	14.008

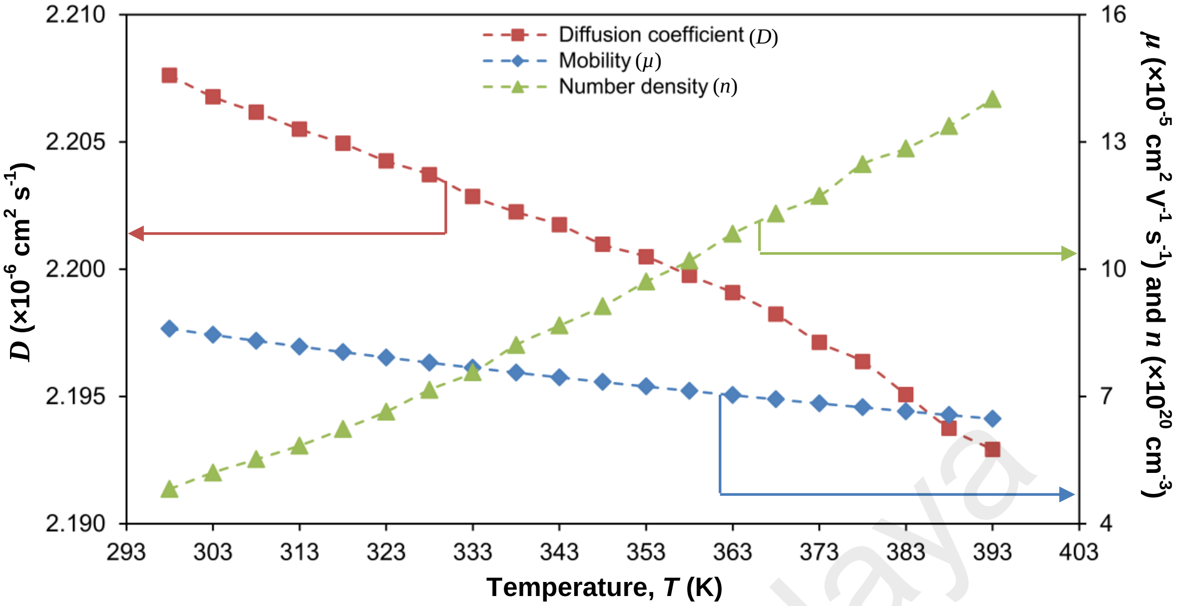

Figure 5.17: Diffusion coefficient, mobility and number density of free ions at different temperatures for B1 ion conducting membrane at different temperatures.

From Figure 5.17, the increase in temperature has decreased the diffusion coefficient of free ions for B1 electrolyte. The mobility of charge carriers for B1 electrolyte is observed to decrease with increasing temperature. Number density of charge carriers for B1 ion conducting membrane is observed to increase with temperature as depicted in Figure 5.17.

Figure 5.18 displayed the impedance plot and their corresponding fitted points for B2 membrane at different temperatures. The fitting parameters obtained in Figure 5.18 were listed in Table 5.12.

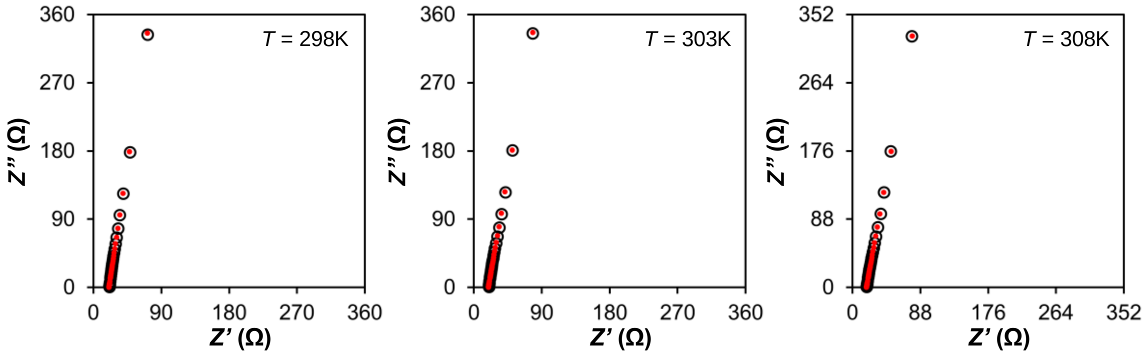

Figure 5.18, continued…

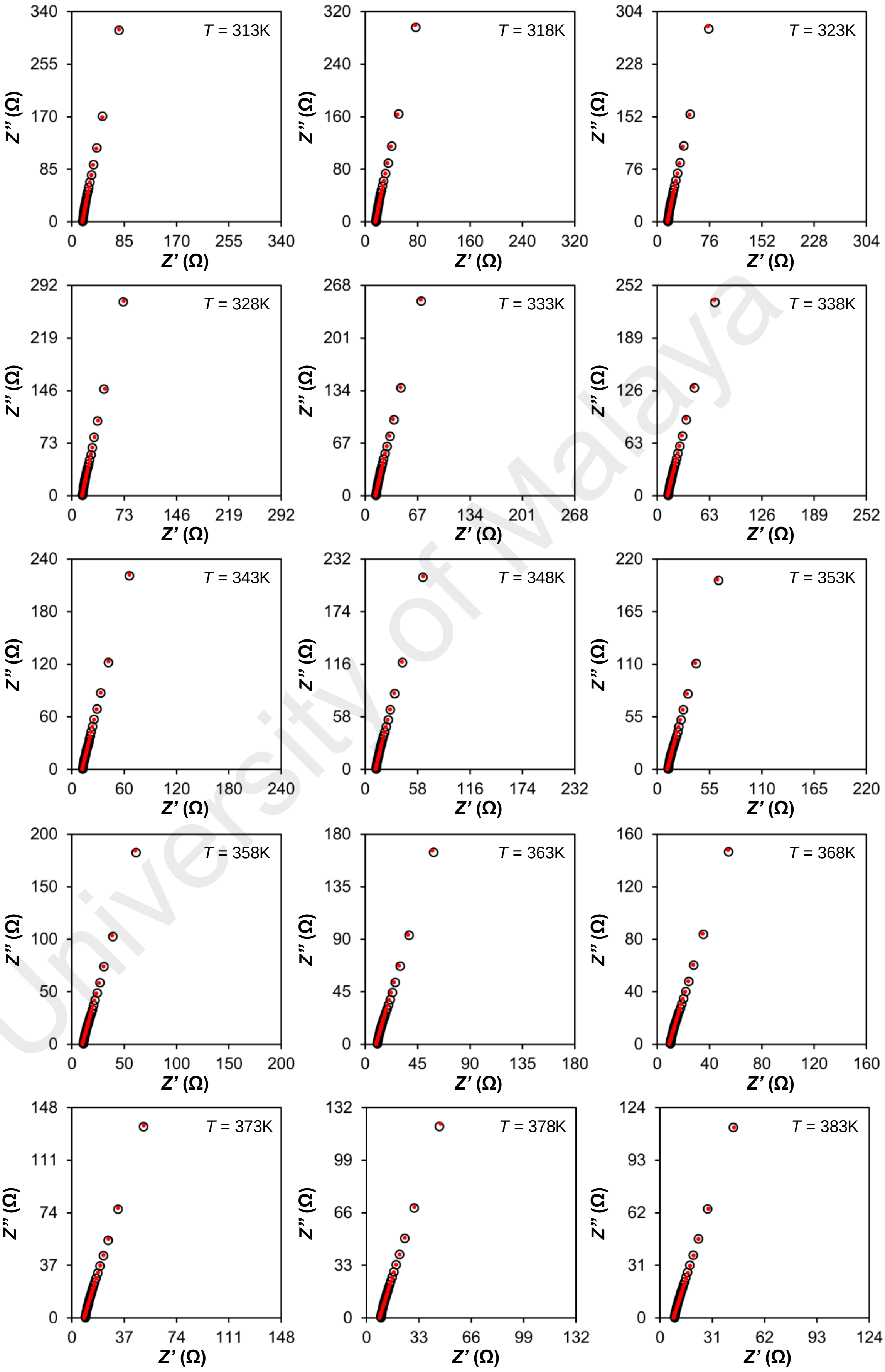

Figure 5.18, continued…

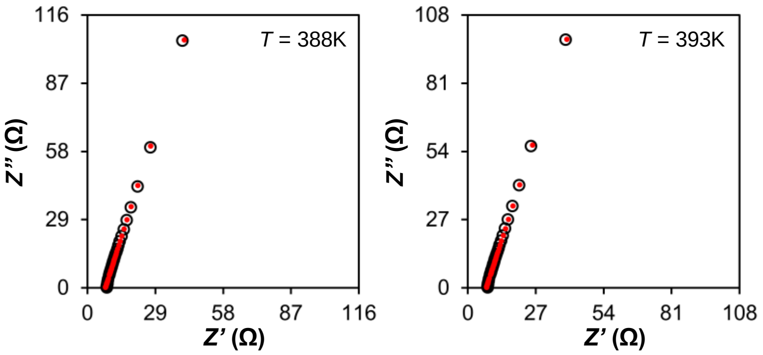

Figure 5.18: Nyquist plot (o) and their corresponding fitted point (●) for B2 electrolyte at different temperatures.

Table 5.12: The values of R, p_2, k_2 and ω_2 for B2 electrolyte obtained from fitting of Nyquist plot at different temperatures.

T (K)	**R (Ω)**	**p_2**	**k_2 (F^{-1})**	**ω_2 (s^{-1})**	**T (K)**	**R (Ω)**	**p_2**	**k_2 (F^{-1})**	**ω_2 (s^{-1})**
298	20.50	0.904	61400	532003	348	11.20	0.845	28300	474985
303	19.10	0.890	57000	531594	353	10.34	0.835	25000	460023
308	18.00	0.885	53500	530982	358	9.92	0.830	22600	433291
313	16.90	0.880	50000	529273	363	9.34	0.820	19300	389655
318	15.60	0.872	46000	528056	368	9.00	0.812	16500	338205
323	14.70	0.870	43000	525025	373	8.45	0.808	14800	322760
328	13.90	0.865	40000	523215	378	8.10	0.805	13100	295447
333	13.00	0.855	35000	486497	383	7.94	0.803	11950	272132
338	12.28	0.850	32000	477837	388	7.66	0.803	11200	268398
343	11.60	0.848	30000	477068	393	7.30	0.800	10300	262410

From the parameter values listed in Table 5.12, D, μ and n of mobile ions for B2 electrolyte at different temperatures were calculated using equations (4.16), (4.17) and (4.18), respectively. The calculated values are listed in Table 5.13. Figure 5.19 show the plots of diffusion coefficient, mobility and concentration of free ions at different temperatures, respectively.

Table 5.13: D, μ and n values for B2 electrolyte at different temperatures.

T (K)	**D ($\times10^{-6}$ cm^2 s^{-1})**	**μ ($\times10^{-5}$ cm^2 V^{-1} s^{-1})**	**n ($\times10^{20}$ cm^{-3})**
298	2.303	8.966	4.392
303	2.300	8.808	4.798
308	2.297	8.655	5.181
313	2.295	8.510	5.613
318	2.294	8.371	6.181
323	2.291	8.230	6.672
328	2.279	8.062	7.203
333	2.268	7.903	7.856
338	2.251	7.726	8.508
343	2.245	7.593	9.165
348	2.225	7.419	9.714
353	2.205	7.248	10.770
358	2.190	7.098	11.463
363	2.171	6.940	12.453
368	2.157	6.800	13.190
373	2.145	6.672	14.317
378	2.130	6.538	15.242
383	2.118	6.418	15.841
388	2.097	6.271	16.804
393	2.075	6.126	18.049

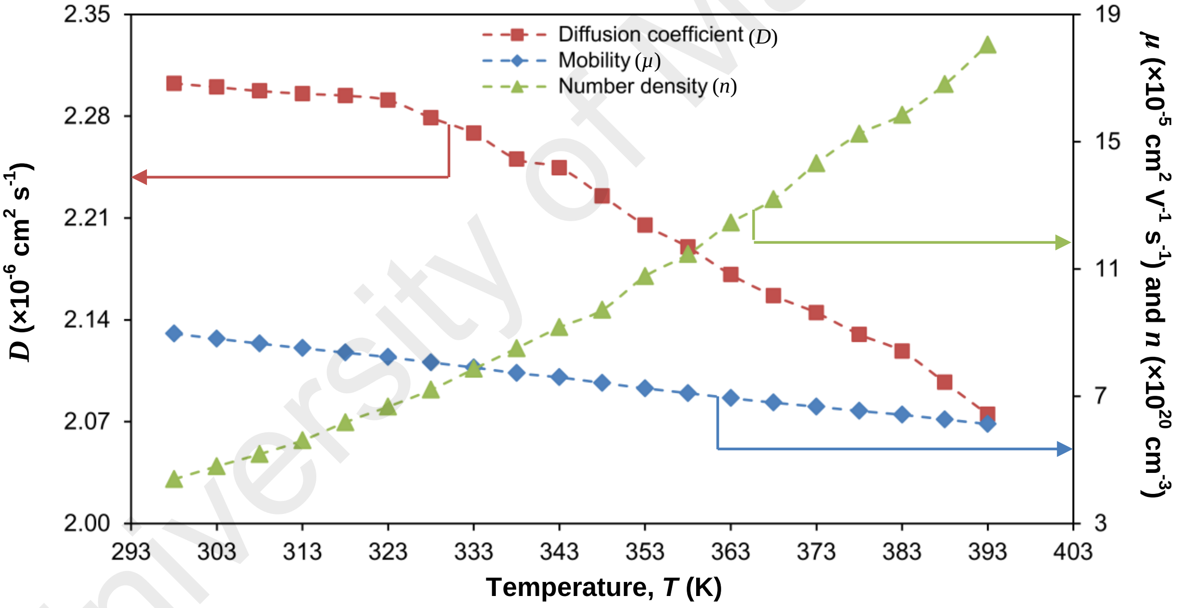

Figure 5.19: D, μ and n of mobile ions at different temperatures for B2 electrolyte.

Diffusion coefficient of free ions for B2 electrolyte has decreased with increasing temperature as shown in Figure 5.19. The increased in temperature has caused the mobility of charge carriers for B2 electrolyte to decrease. Number density of free ions for B2 membrane is observed to increase with temperature as depicted in Figure 5.19.

Figure 5.20 displays the complex impedance plot and their corresponding fitted points for B3 electrolyte at different temperatures. The fitting parameters obtained in Figure 5.20 are listed in Table 5.14.

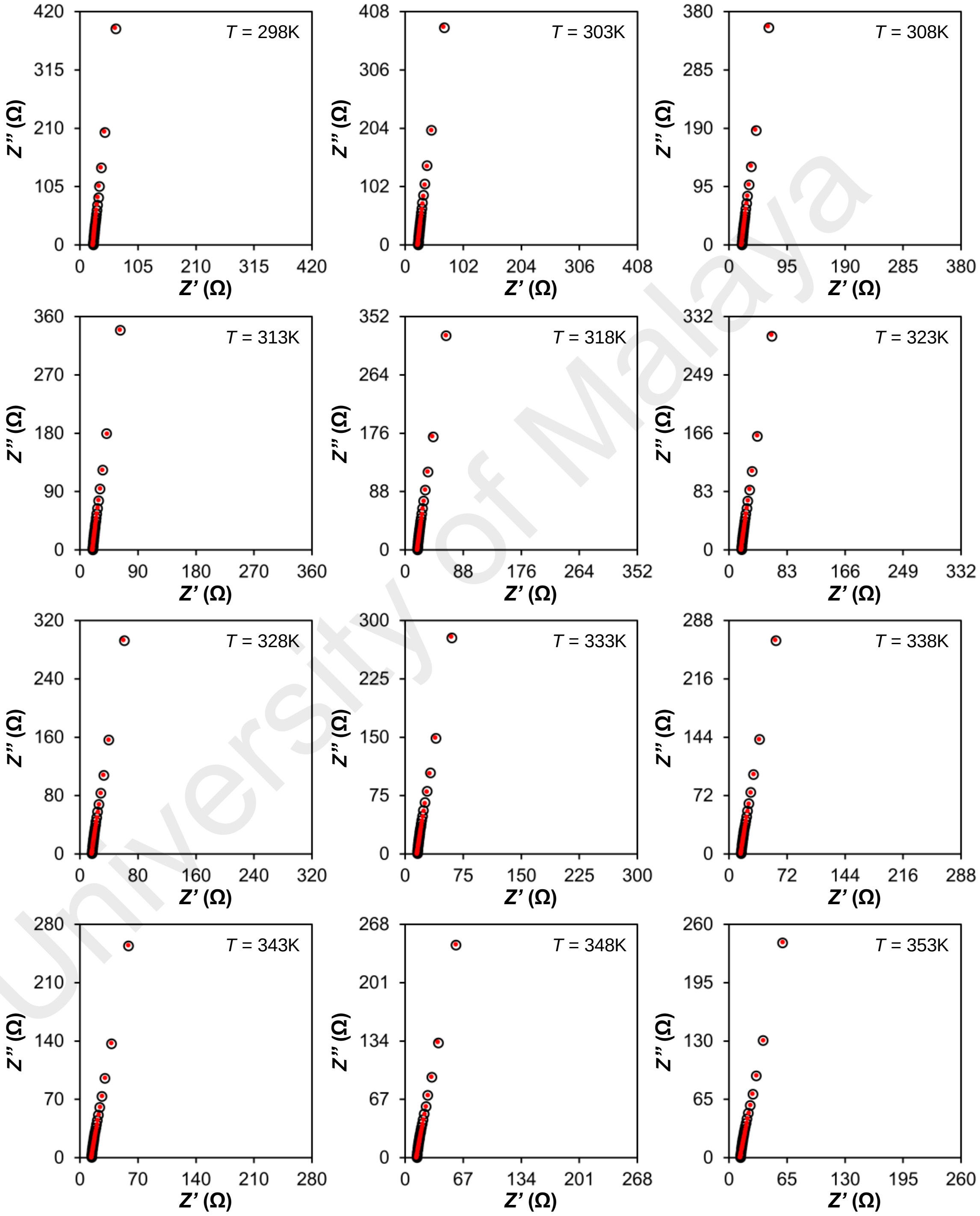

Figure 5.20, continued…

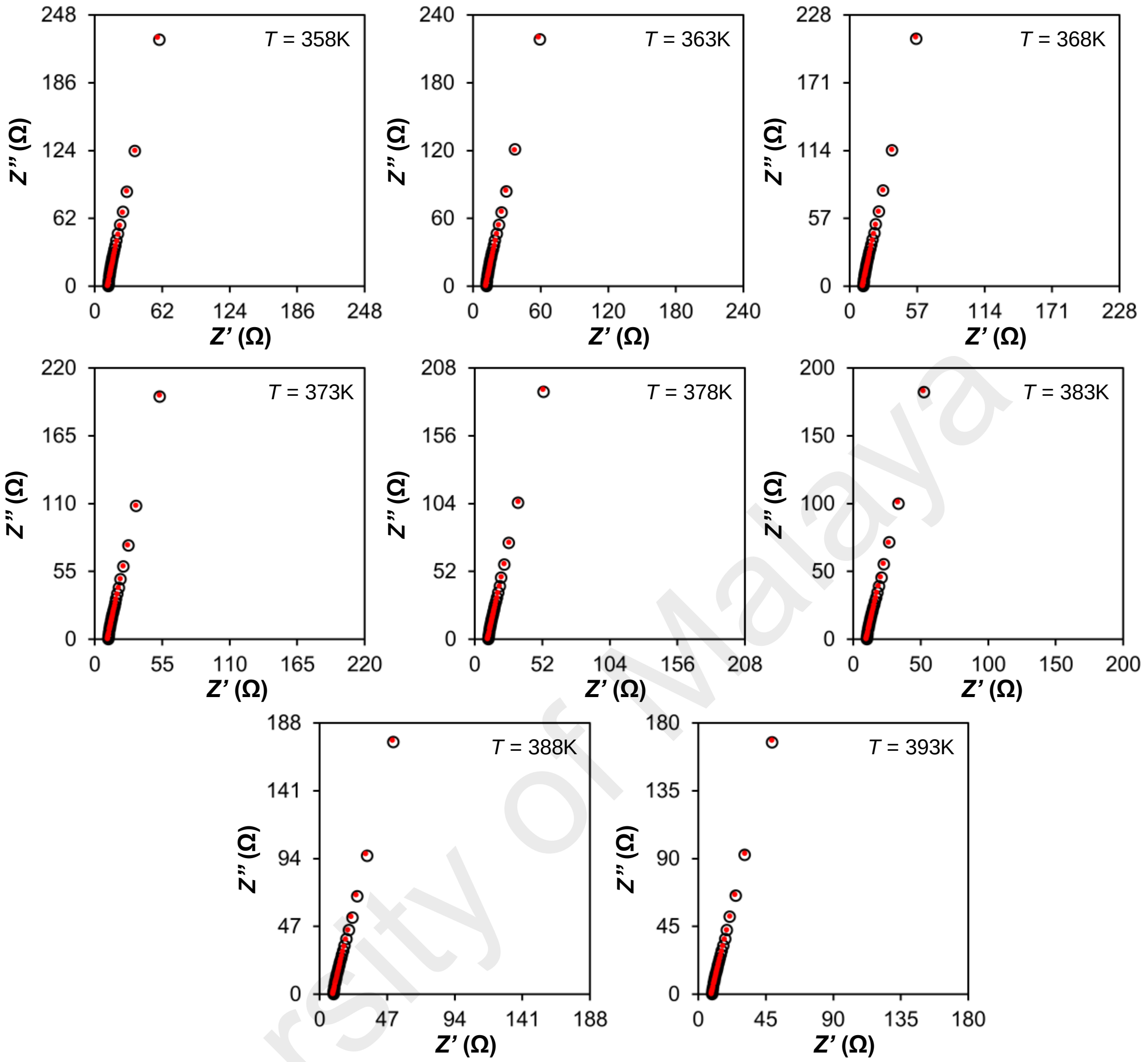

Figure 5.20: Nyquist plot (o) and their corresponding fitted point (•) for B3 electrolyte at different temperatures.

Table 5.14: R, p_2, k_2 and ω_2 values for B3 electrolyte obtained from fitting of Nyquist plot at different temperatures.

T **(K)**	***R*** **(Ω)**	p_2	k_2 (F^{-1})	ω_2 (s^{-1})
298	23.00	0.935	85000	296963
303	21.50	0.925	78500	292065
308	20.00	0.923	72500	289188
313	19.00	0.920	68000	284106
318	18.00	0.915	63000	275664
323	16.80	0.910	58000	270508
328	15.90	0.905	54000	264533
333	15.00	0.900	50000	257858
338	14.20	0.897	46500	251640
343	13.45	0.889	43000	243545

Table 5.14, continued…

348	12.75	0.883	40000	237290
353	12.10	0.875	37500	233228
358	11.50	0.873	35200	229129
363	11.00	0.867	33000	222782
368	10.50	0.855	31000	217811
373	10.00	0.865	29300	215268
378	9.55	0.830	27600	210999
383	9.15	0.855	25700	202712
388	8.75	0.852	24300	199379
393	8.40	0.850	23000	195245

From the parameter values listed in Table 5.14, diffusion coefficient (*D*), mobility (μ) and number density (*n*) of mobile charged species for B3 electrolyte at different temperatures were calculated by using equations (4.16), (4.17) and (4.18), respectively. The calculated values are listed in Table 5.15. Figures 5.21 show the plots of diffusion coefficient, mobility and number density of free ions at different temperatures, respectively.

Table 5.15: *D*, μ and *n* values for B3 electrolyte at different temperatures.

T **(K)**	***D*** **($\times 10^{-6}$ cm^2 s^{-1})**	***μ*** **($\times 10^{-5}$ cm^2 V^{-1} s^{-1})**	***n*** **($\times 10^{20}$ cm^{-3})**
298	2.385	9.285	3.780
303	2.384	9.131	4.112
308	2.384	8.982	4.494
313	2.384	8.837	4.807
318	2.384	8.698	5.156
323	2.383	8.562	5.612
328	2.383	8.431	6.022
333	2.383	8.303	6.481
338	2.383	8.179	6.950
343	2.382	8.059	7.447
348	2.382	7.942	7.972
353	2.381	7.828	8.522
358	2.381	7.717	9.096
363	2.380	7.608	9.645
368	2.380	7.503	10.246
373	2.379	7.400	10.908
378	2.378	7.300	11.579
383	2.377	7.202	12.250
388	2.376	7.107	12.981
393	2.375	7.013	13.701

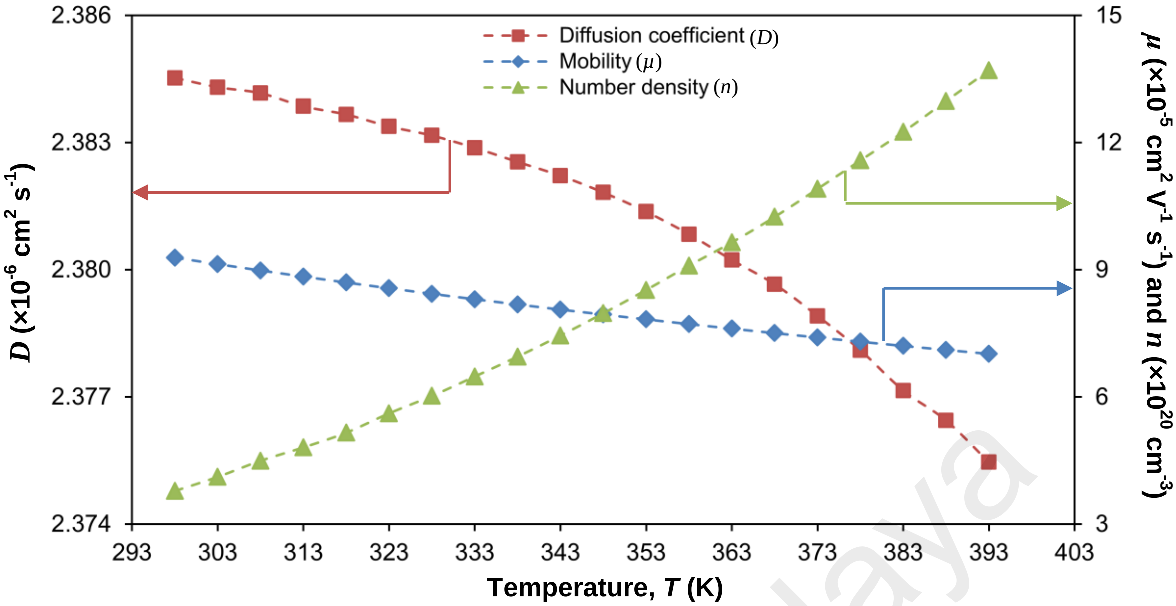

Figure 5.21: Diffusion coefficient, mobility and number density of charge carriers for B3 electrolyte at different temperatures.

From Figure 5.21, the increase in temperature has decreased the diffusion coefficient and mobility of free ions for B3 electrolyte. Number density of free ions for B3 electrolyte is observed to increase with temperature as depicted in Figure 5.21.

Figure 5.22 presents the complex impedance plot and their corresponding fitted points for B4 electrolyte at different temperatures. The fitting parameters obtained in Figure 5.22 are listed in Table 5.16.

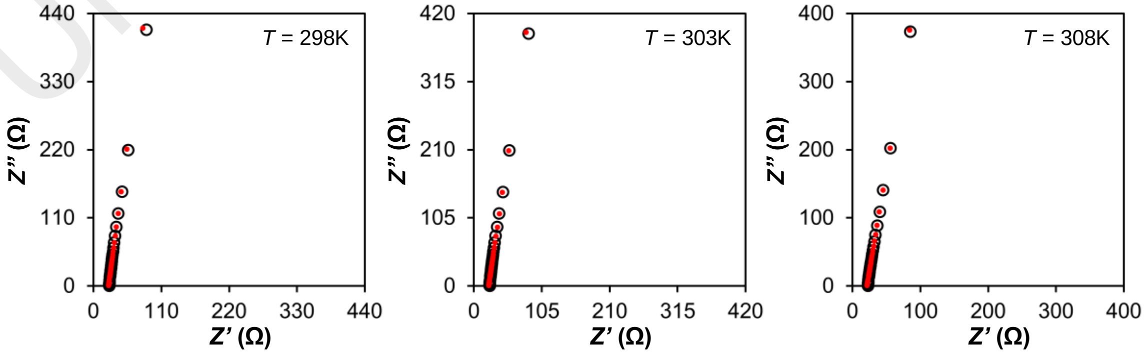

Figure 5.22, continued…

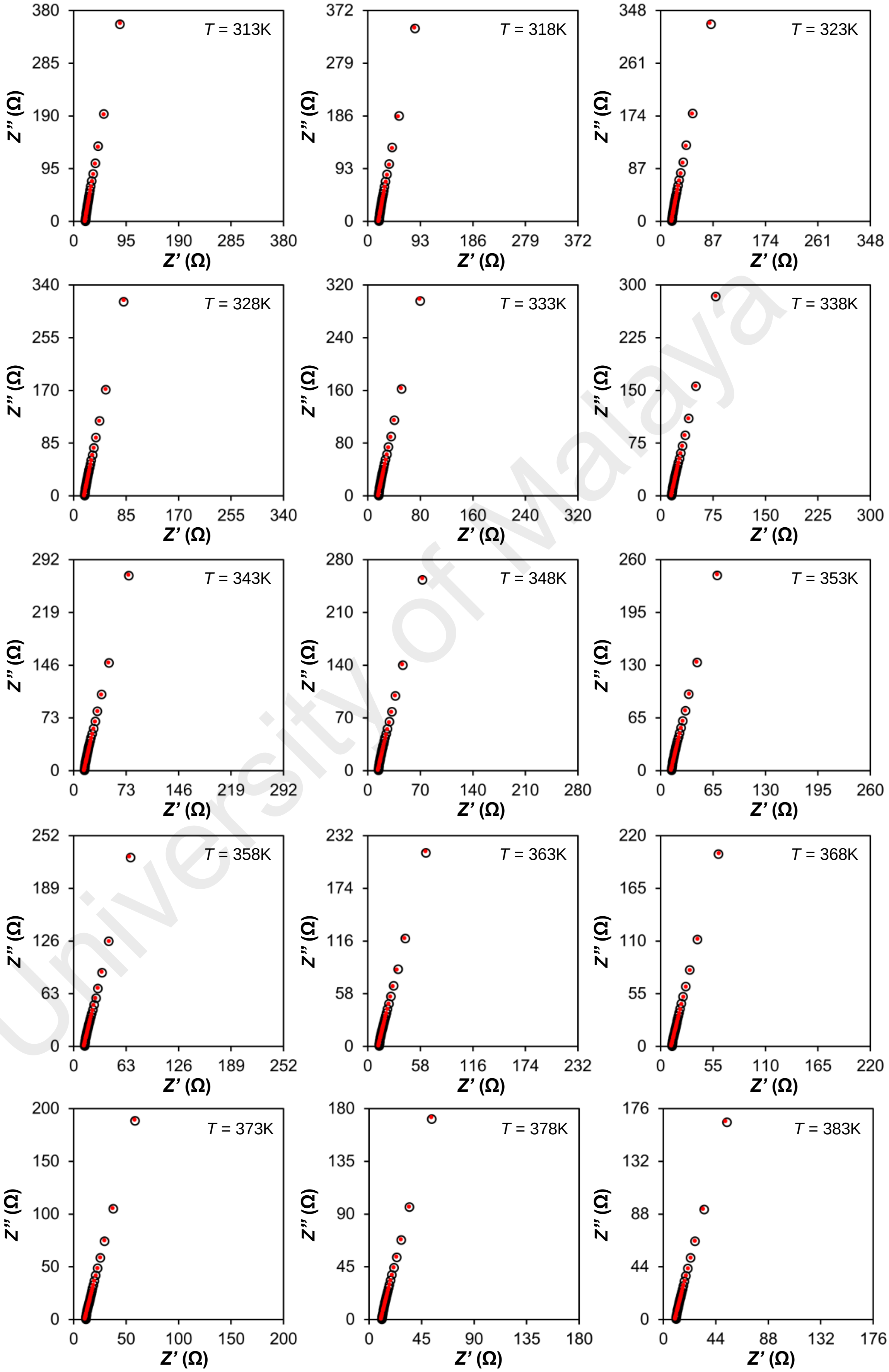

Figure 5.22, continued…

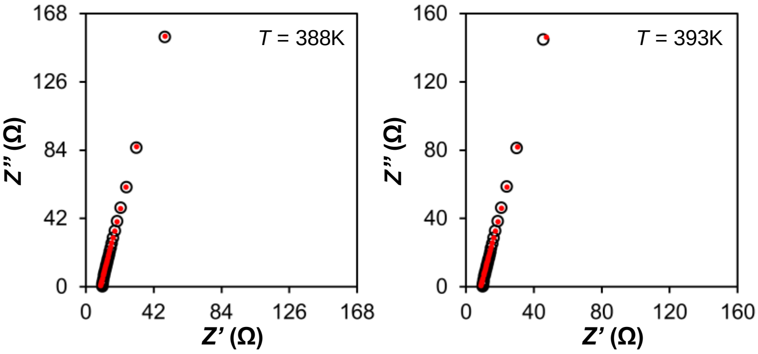

Figure 5.22: Nyquist plot (o) and their corresponding fitted point (●) for B4 electrolyte at different temperatures.

Table 5.16: Values of R, p_2, k_2 and ω_2 for B4 electrolyte obtained from fitting of Nyquist plot at different temperatures.

T (K)	R (Ω)	p_2	k_2 (F^{-1})	ω_2 (s^{-1})
298	24.40	0.915	81000	262459
303	22.80	0.907	72800	249104
308	21.30	0.894	65100	234898
313	19.90	0.888	59900	230028
318	18.65	0.883	55800	228024
323	17.50	0.878	52000	225829
328	16.50	0.872	48500	222423
333	15.50	0.867	44700	216611
338	14.65	0.860	41000	207912
343	13.90	0.857	38400	204164
348	13.15	0.855	35800	199839
353	12.50	0.852	33400	194617
358	11.85	0.850	31000	188877
363	11.30	0.848	29000	183857
368	10.75	0.845	26800	176596
373	10.25	0.843	24900	170286
378	9.80	0.843	22700	159470
383	9.40	0.840	21400	155518
388	9.00	0.838	19700	147292
393	8.57	0.835	18400	143179

From the parameter values listed in Table 5.16, transport properties of ionic conducting species for B4 electrolyte at different temperatures were calculated by using equations (4.16), (4.17) and (4.18), respectively. The calculated values are listed in Table 5.17. Figures 5.23 show the plots of diffusion coefficient, mobility and number density of free ions at different temperatures, respectively.

Table 5.17: D, μ and n values for B4 electrolyte at different temperatures.

T (K)	**D ($\times 10^{-6}$ cm^2 s^{-1})**	**μ ($\times 10^{-5}$ cm^2 V^{-1} s^{-1})**	**n ($\times 10^{20}$ cm^{-3})**	**T (K)**	**D ($\times 10^{-6}$ cm^2 s^{-1})**	**μ ($\times 10^{-5}$ cm^2 V^{-1} s^{-1})**	**n ($\times 10^{20}$ cm^{-3})**
298	2.393	9.318	3.550	348	2.390	7.968	7.704
303	2.393	9.164	3.863	353	2.389	7.853	8.224
308	2.393	9.015	4.204	358	2.388	7.740	8.800
313	2.393	8.870	4.573	363	2.388	7.632	9.360
318	2.392	8.729	4.958	368	2.387	7.526	9.977
323	2.392	8.593	5.368	373	2.386	7.422	10.610
328	2.392	8.461	5.782	378	2.385	7.321	11.250
333	2.391	8.332	6.250	383	2.384	7.223	11.889
338	2.391	8.208	6.713	388	2.383	7.127	12.584
343	2.390	8.087	7.181	393	2.382	7.033	13.393

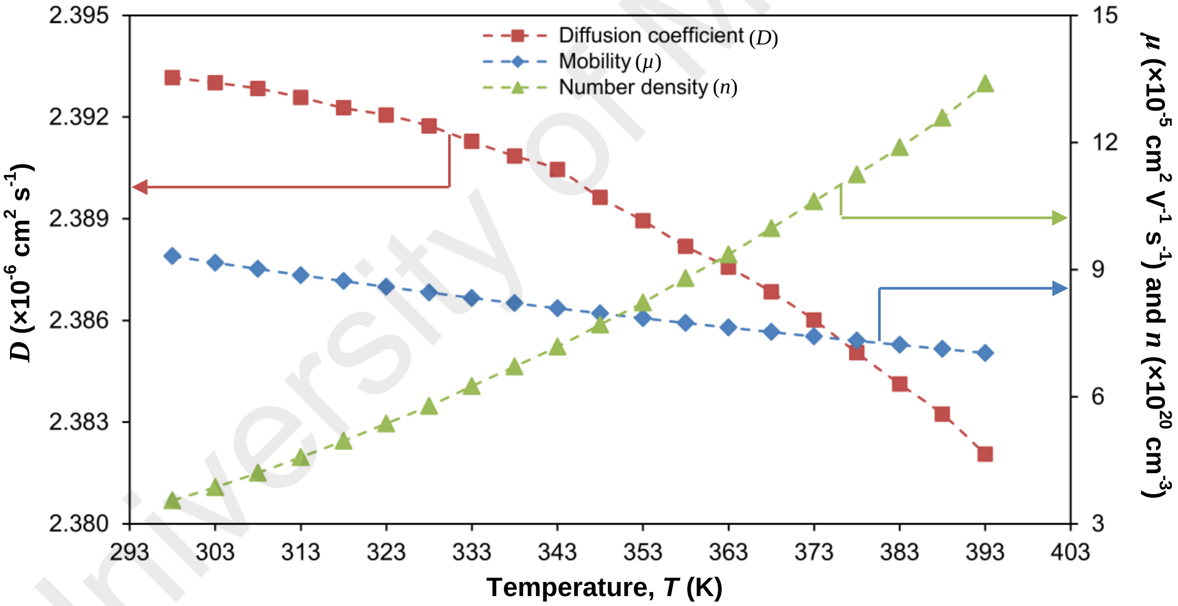

Figure 5.23: Diffusion coefficient, mobility and number density of charge carriers for B4 electrolyte at different temperatures.

From Figure 5.23, diffusion coefficient and mobility of mobile ions for B4 electrolyte has decreased with increasing temperature. Number density of mobile ions for B4 electrolyte is observed to increase with temperature as depicted in Figure 5.23.

Figure 5.24 presents the impedance plot and their corresponding fitted points for B5 electrolyte at different temperatures. All fitted parameters obtained in Figure 5.24 are listed in Table 5.18.

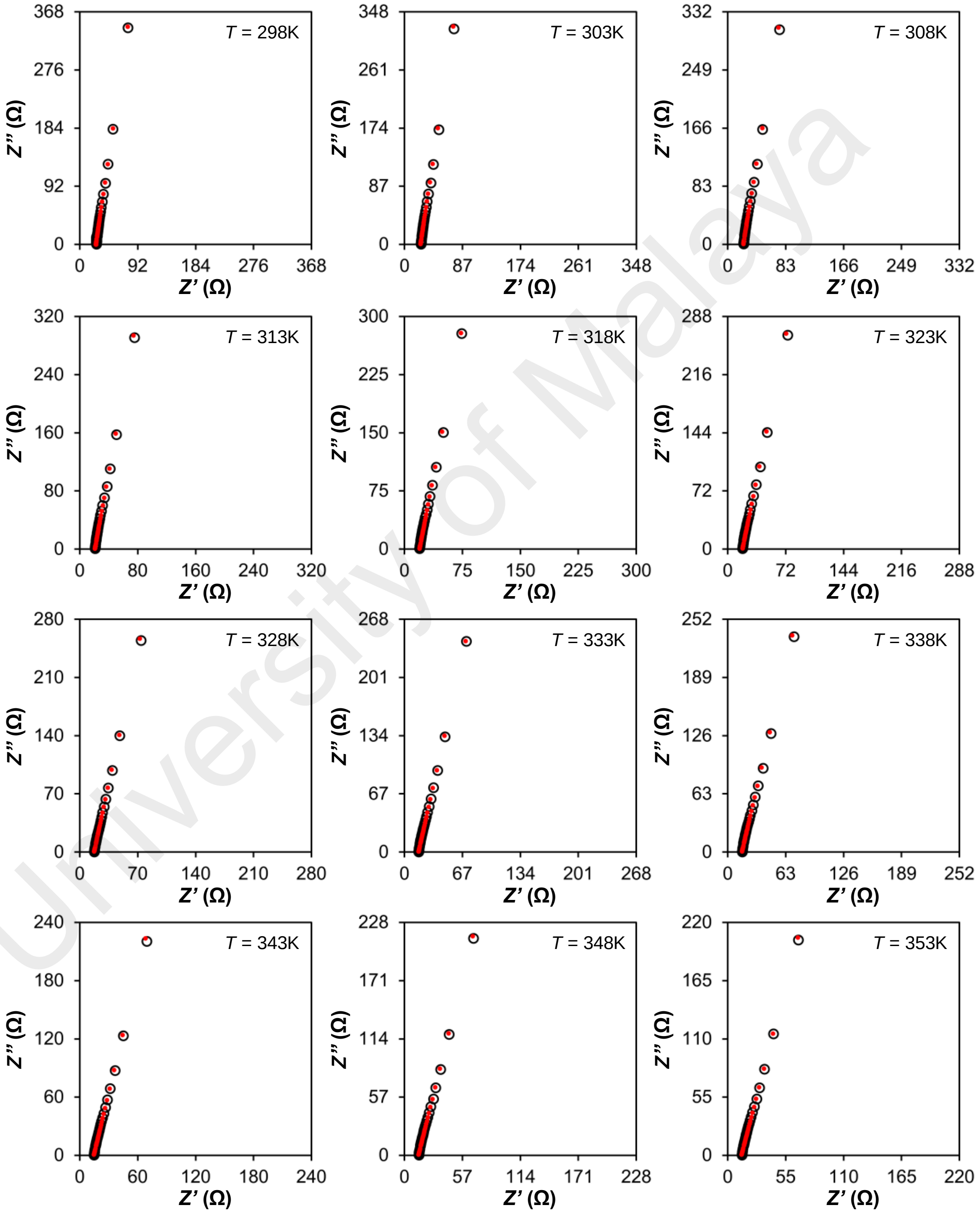

Figure 5.24, continued…

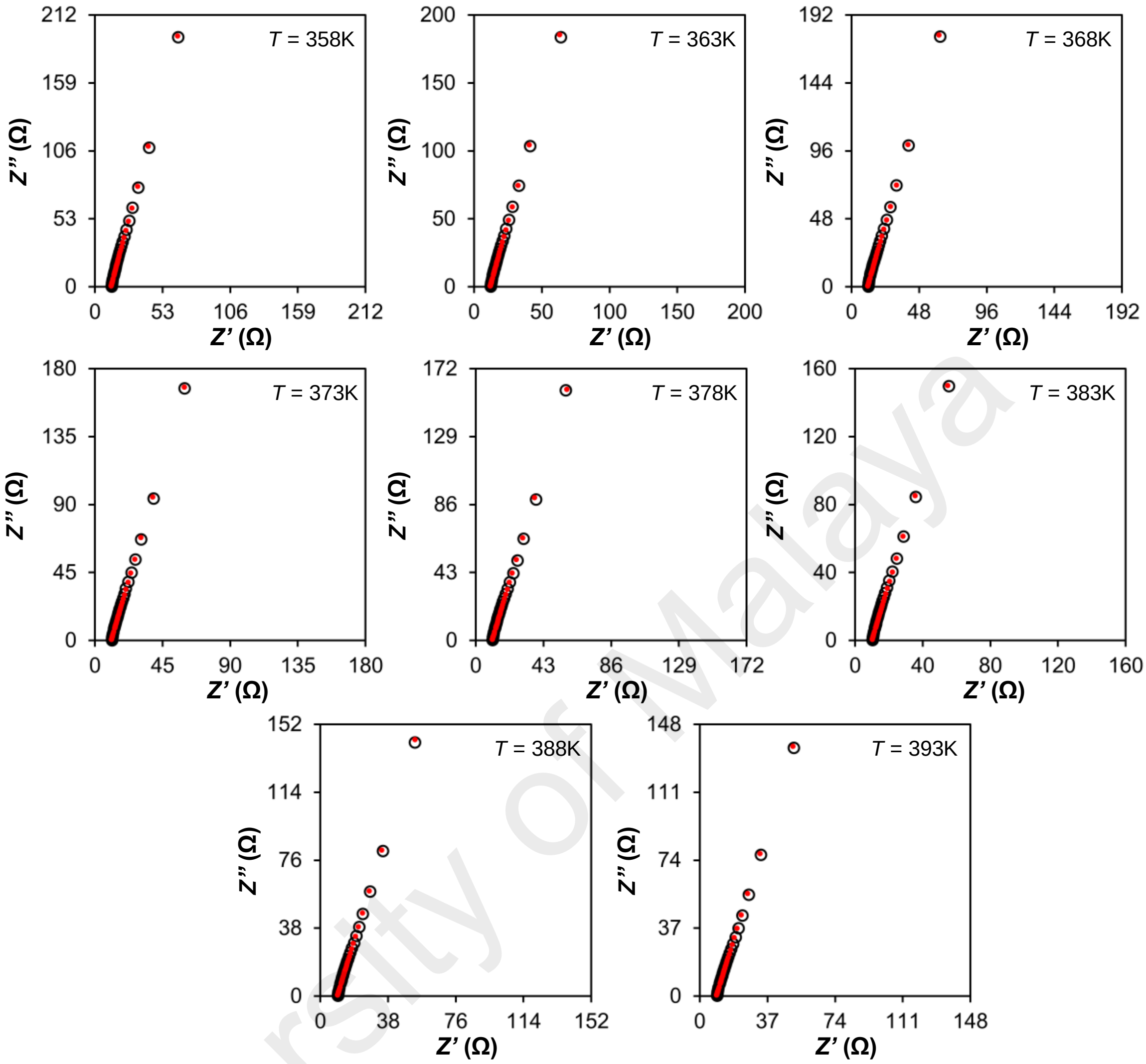

Figure 5.24: Nyquist plot (o) and their corresponding fitted point (●) for B5 electrolyte at different temperatures.

Table 5.18: R, p_2, k_2 and ω_2 values for B5 electrolyte obtained from fitting of Nyquist plot at different temperatures.

T (K)	R (Ω)	p_2	k_2 (F^{-1})	ω_2 (s^{-1})
298	25.20	0.907	64100	285528
303	23.90	0.905	60000	285517
308	22.25	0.896	54500	284443
313	20.90	0.886	48700	274357
318	19.50	0.879	44500	271733
323	18.30	0.872	41000	269875
328	17.25	0.865	38000	268874
333	16.25	0.860	35000	266044
338	15.35	0.854	32700	264605
343	14.52	0.850	30500	263735

Table 5.18, continued…

348	13.75	0.845	28500	262644	373	10.70	0.820	19500	238973
353	13.00	0.838	26300	256946	378	10.25	0.815	18000	232870
358	12.40	0.834	24500	252239	383	9.81	0.815	17000	230553
363	11.80	0.828	22500	245623	388	9.40	0.812	16000	225817
368	11.25	0.823	21000	242726	393	9.00	0.810	15000	222225

From the parameter values listed in Table 5.18, *D*, *μ* and *n* of charge carriers for B5 electrolyte at different temperatures were calculated using equations (4.16), (4.17) and (4.18), respectively. The calculated values are listed in Table 5.19. Figure 5.25 show the plots of diffusion coefficient, mobility and number density of free ions at different temperatures, respectively.

Table 5.19: Values of *D*, *μ* and *n* for B5 electrolyte at different temperatures.

T **(K)**	***D*** **($\times 10^{-6}$ cm^2 s^{-1})**	***μ*** **($\times 10^{-5}$ cm^2 V^{-1} s^{-1})**	***n*** **($\times 10^{20}$ cm^{-3})**	***T*** **(K)**	***D*** **($\times 10^{-6}$ cm^2 s^{-1})**	***μ*** **($\times 10^{-5}$ cm^2 V^{-1} s^{-1})**	***n*** **($\times 10^{20}$ cm^{-3})**
298	2.460	9.577	3.345	348	2.411	8.039	7.303
303	2.457	9.409	3.589	353	2.407	7.912	7.848
308	2.452	9.237	3.927	358	2.402	7.784	8.363
313	2.445	9.065	4.260	363	2.393	7.649	8.943
318	2.441	8.906	4.648	368	2.386	7.522	9.538
323	2.436	8.751	5.040	373	2.378	7.398	10.197
328	2.431	8.598	5.442	378	2.367	7.265	10.839
333	2.424	8.448	5.880	383	2.363	7.159	11.494
338	2.421	8.312	6.326	388	2.361	7.062	12.160
343	2.416	8.173	6.802	393	2.355	6.953	12.898

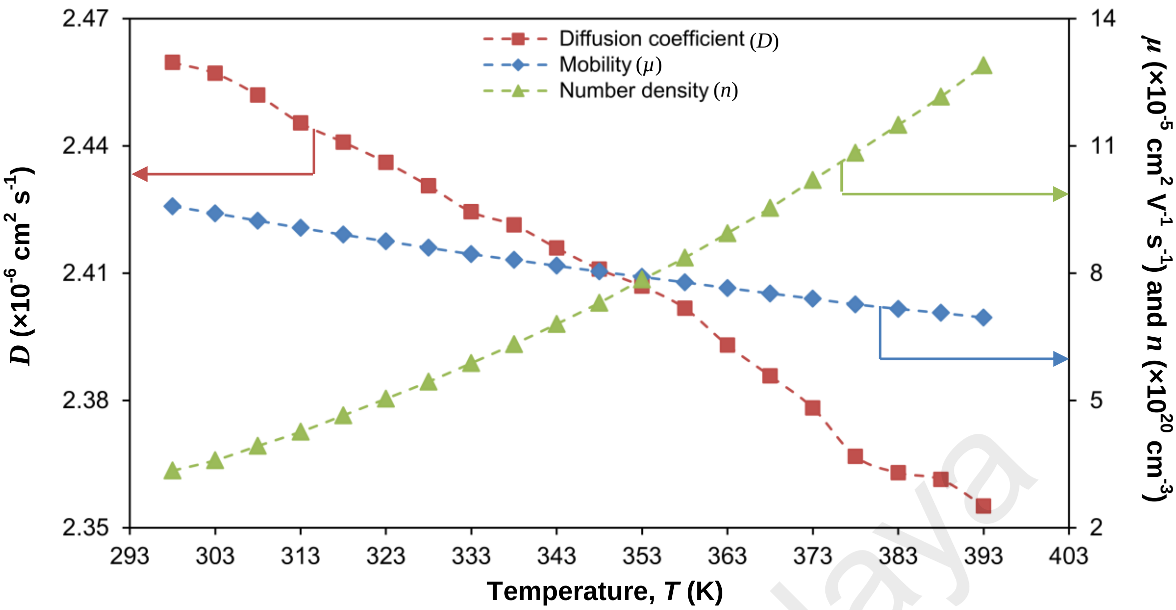

Figure 5.25: *D*, *μ* and *n* of free ions for B5 electrolyte at different temperatures.

From Figure 5.25 the increase in temperature has decreased the diffusion coefficient and mobility of charge carriers for B5 electrolyte, respectively. Concentration of mobile ions for B5 electrolyte is observed to increase with temperature as depicted in Figure 5.25.

Figure 5.26 displays the complex impedance plot and their corresponding fitted points for B6 electrolyte at different temperatures. The fitting parameters obtained in Figure 5.26 are listed in Table 5.20.

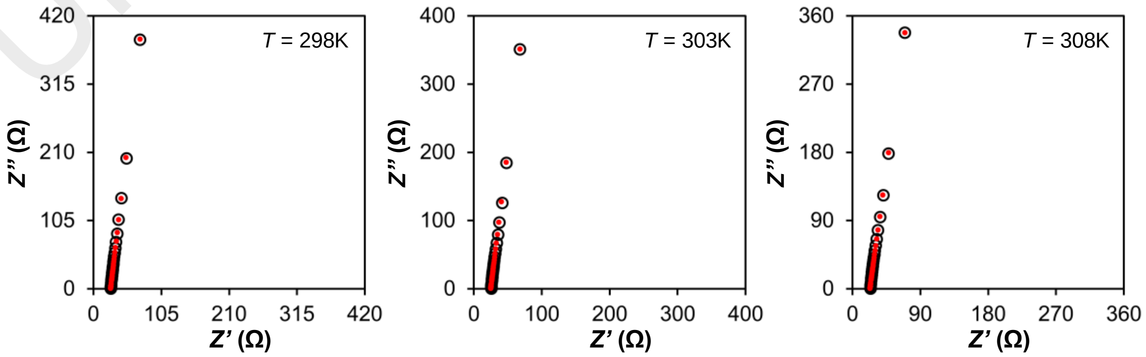

Figure 5.26, continued…

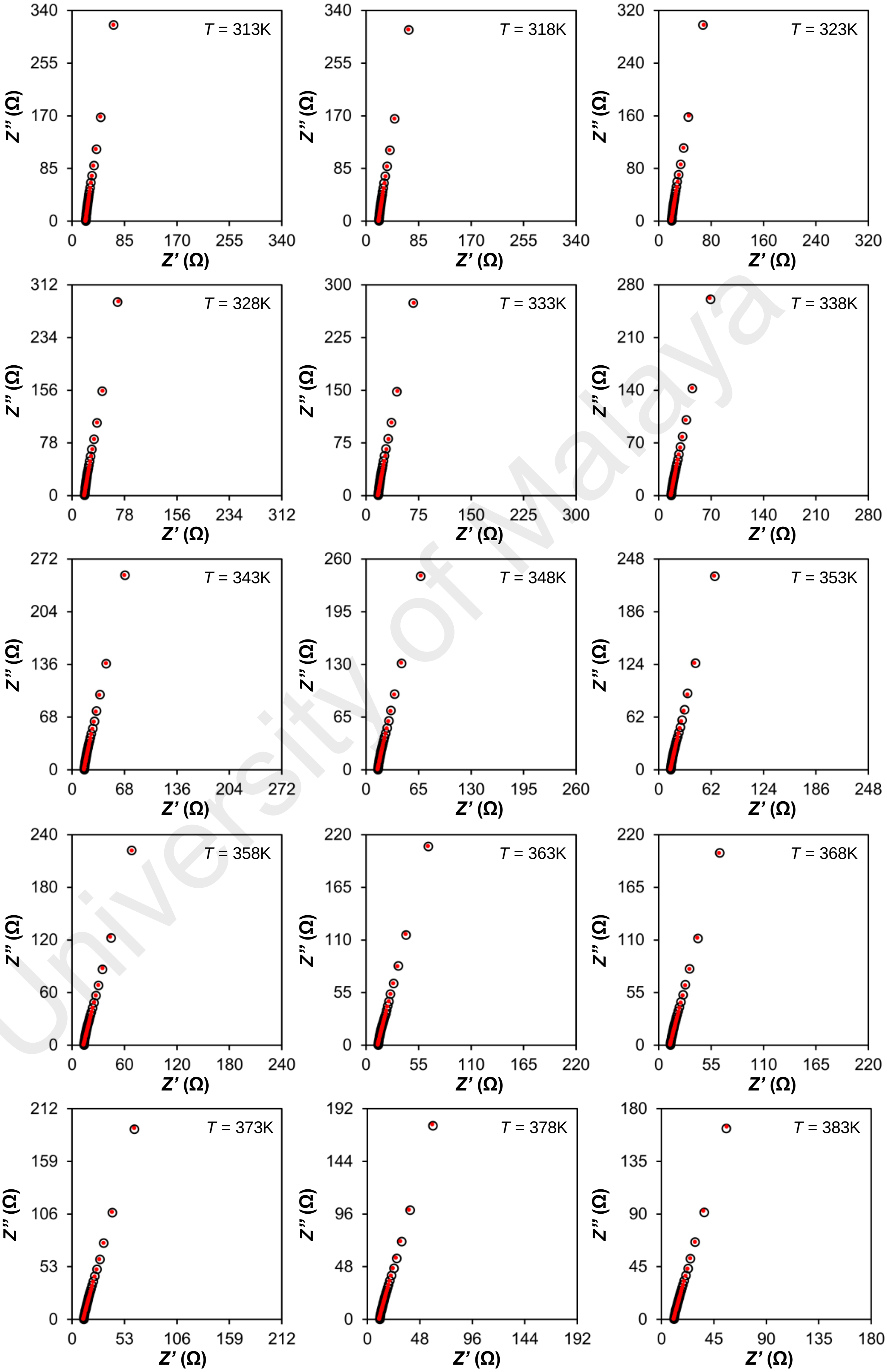

Figure 5.26, continued…

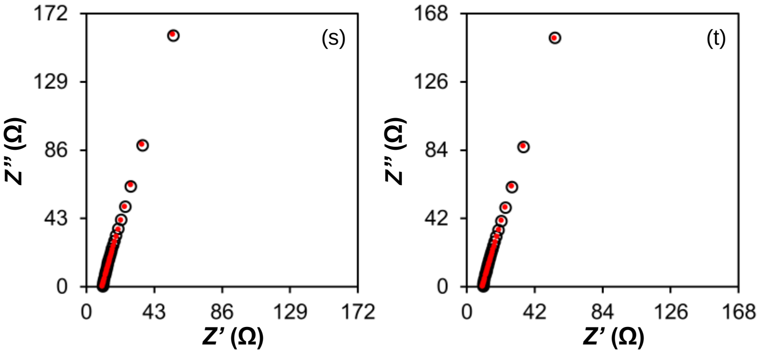

Figure 5.26: Nyquist plot (o) and their corresponding fitted point (●) for B6 electrolyte at different temperatures.

Table 5.20: Values of R, p_2, k_2 and ω_2 for B6 electrolyte obtained from fitting of Nyquist plot at different temperatures.

T (K)	R (Ω)	p_2	k_2 (F^{-1})	ω_2 (s^{-1})	T (K)	R (Ω)	p_2	k_2 (F^{-1})	ω_2 (s^{-1})
298	26.70	0.925	79000	342834	348	14.00	0.860	34500	299125
303	24.65	0.922	71000	340103	353	13.50	0.858	32500	291134
308	23.00	0.913	65000	339457	358	12.80	0.845	29500	278200
313	21.50	0.910	60000	338221	363	12.00	0.842	27200	275057
318	20.20	0.902	56000	337846	368	11.60	0.840	26000	272652
323	18.95	0.895	52000	333630	373	11.00	0.833	24000	266095
328	17.80	0.889	48500	331181	378	10.50	0.830	21800	250826
333	16.80	0.882	44500	320962	383	10.10	0.828	20000	237532
338	15.80	0.875	41000	312655	388	9.70	0.825	19000	235682
343	15.00	0.869	38000	306883	393	9.30	0.820	17800	229291

From the parameter values listed in Table 5.20, diffusion coefficient (D), mobility (μ) and concentration or number density (n) of free ions for B6 electrolyte at different temperatures were calculated by using equations (4.16), (4.17) and (4.18), respectively. The calculated values are listed in Table 5.21. Figure 5.27 show the plots of D, μ and n of free ions at different temperatures, respectively.

Table 5.21: Values of D, μ and n for B6 electrolyte at different temperatures.

T (K)	D ($\times 10^{-6}$ cm^2 s^{-1})	μ ($\times 10^{-5}$ cm^2 V^{-1} s^{-1})	n ($\times 10^{20}$ cm^{-3})
298	2.462	9.586	3.154
303	2.458	9.414	3.478
308	2.455	9.247	3.795
313	2.452	9.090	4.130
318	2.451	8.942	4.469
323	2.450	8.802	4.839
328	2.450	8.667	5.233
333	2.449	8.532	5.632
338	2.448	8.405	6.079
343	2.445	8.272	6.506
348	2.443	8.144	7.080
353	2.441	8.025	7.451
358	2.438	7.902	7.980
363	2.435	7.784	8.642
368	2.433	7.672	9.070
373	2.430	7.559	9.708
378	2.428	7.452	10.316
383	2.425	7.346	10.879
388	2.423	7.245	11.486
393	2.421	7.149	12.140

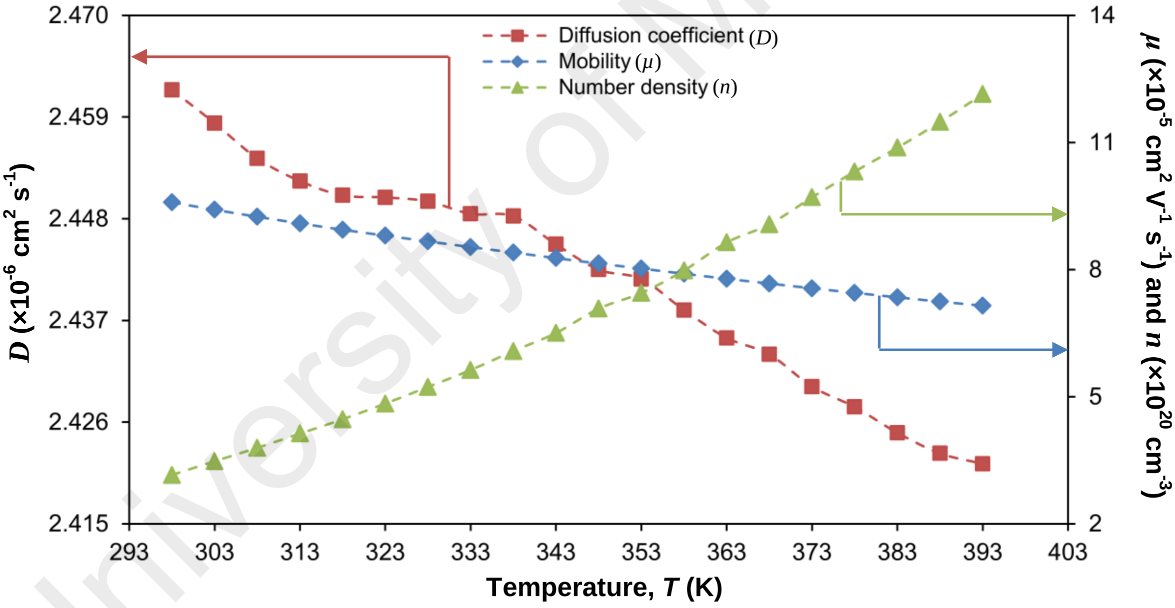

Figure 5.27: Diffusion coefficient, mobility and number density of free ions for B6 electrolyte at different temperatures.

From Figure 5.27, diffusion coefficient and mobility of charge carriers for B6 electrolyte has decrease with increasing temperature. Number density of charge carriers for B6 electrolyte is observed to increase with temperature as depicted in Figure 5.27.

Figure 5.28 displays the Nyquist or complex impedance plot and their corresponding fitted points for B7 electrolyte at different temperatures. All fitted parameters obtained in Figure 5.28 are listed in Table 5.22.

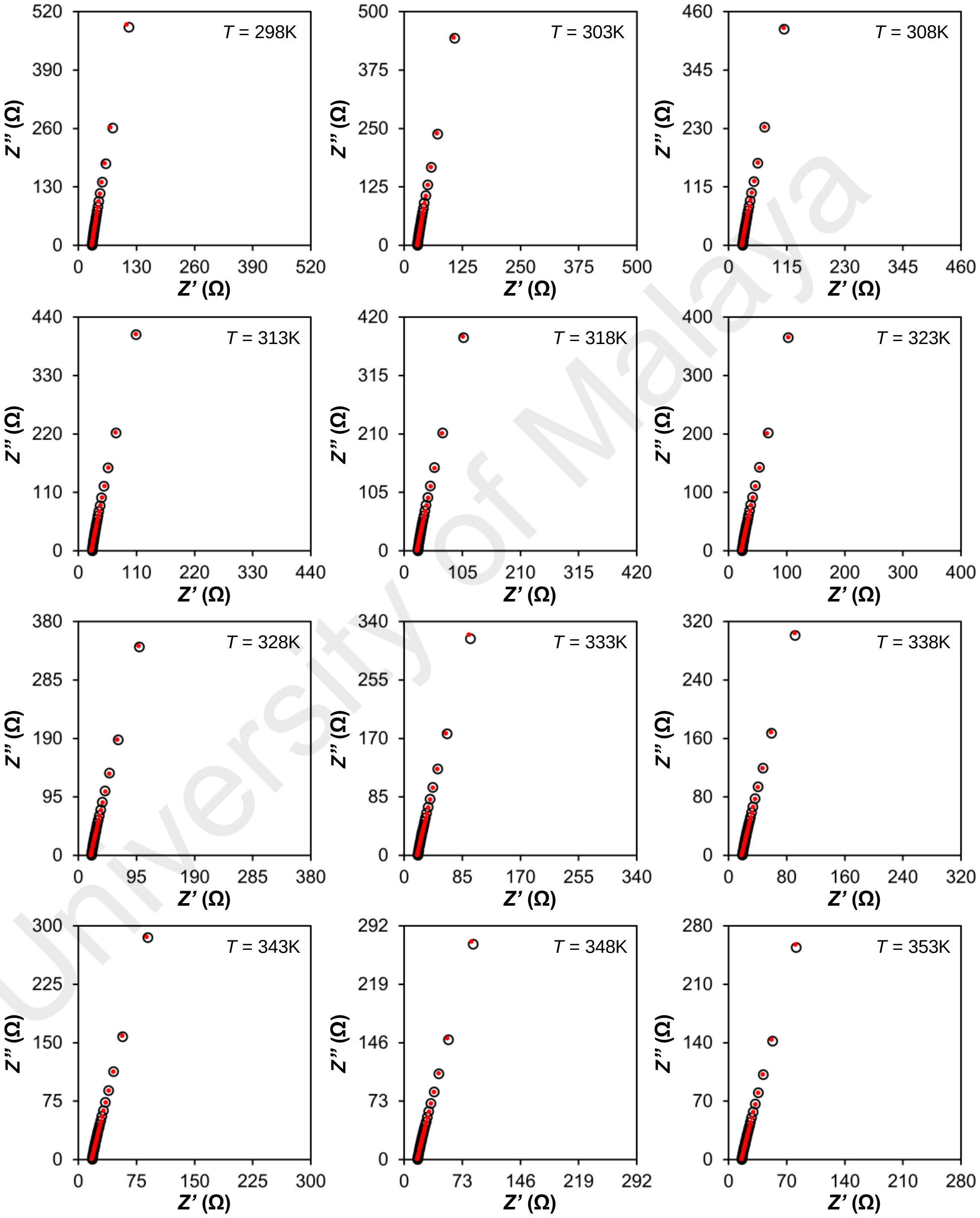

Figure 5.28, continued…

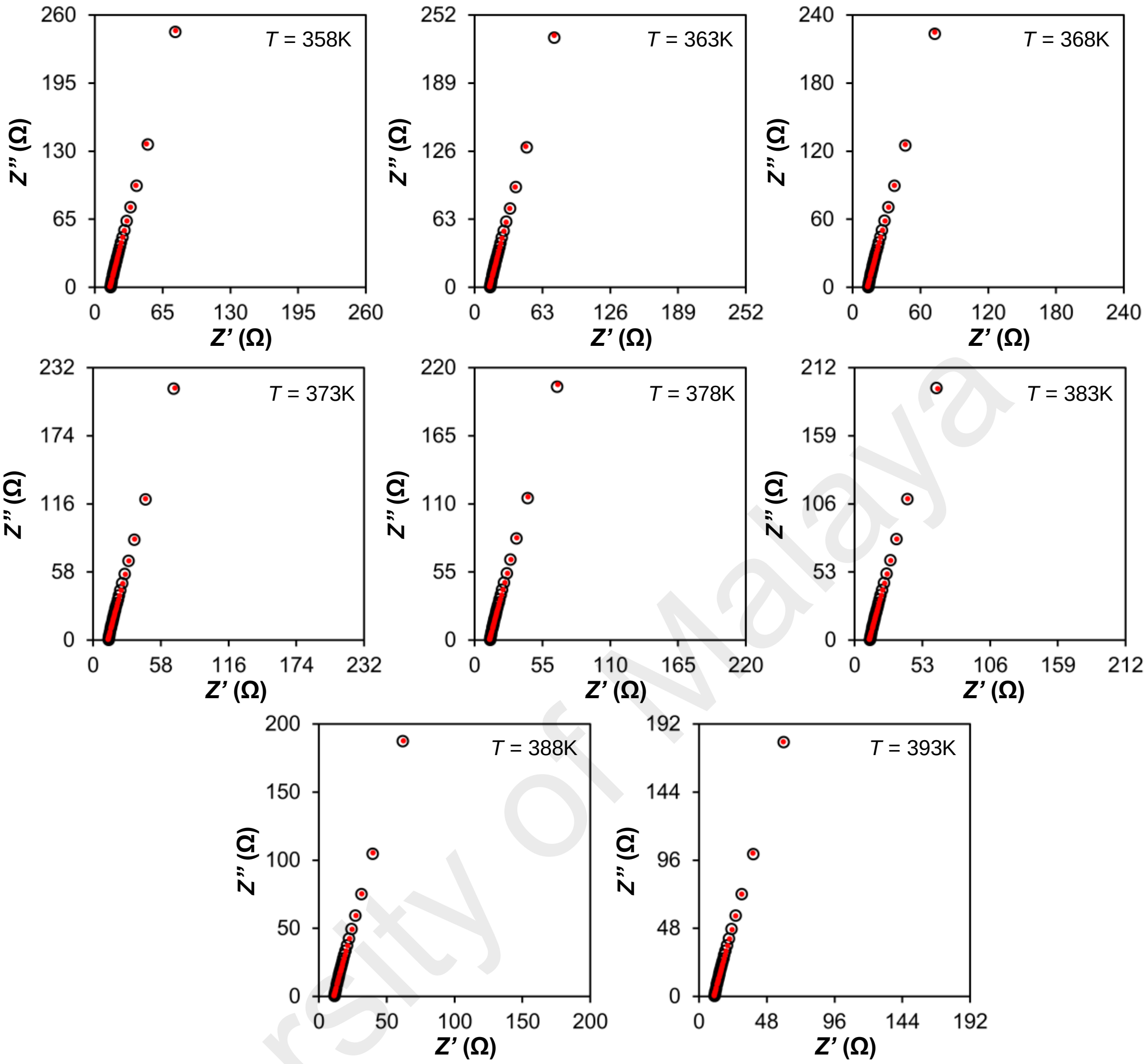

Figure 5.28: Nyquist plot (o) and their corresponding fitted point (●) for B7 electrolyte at different temperatures.

Table 5.22: R, p_2, k_2 and ω_2 values for B7 electrolyte obtained from fitting of Nyquist plot at different temperatures.

T (K)	R (Ω)	p_2	k_2 (F^{-1})	ω_2 (s^{-1})
298	29.70	0.900	88000	318820
303	27.65	0.889	75000	313775
308	25.85	0.878	68000	310546
313	24.15	0.870	62000	309312
318	22.65	0.865	57000	308123
323	21.30	0.861	53000	306845
328	20.00	0.856	48000	297147
333	18.90	0.853	44500	294638
338	17.85	0.850	41500	292586
343	16.90	0.845	38000	283434

Table 5.22, continued…

348	16.10	0.844	36000	283003
353	15.20	0.842	33700	282146
358	14.45	0.840	31700	281178
363	13.75	0.839	30000	280712
368	13.10	0.835	28300	279000
373	12.50	0.834	26900	278166
378	12.00	0.833	25700	277688
383	11.30	0.830	24000	276493
388	10.90	0.830	23000	276012
393	10.50	0.830	22000	275727

From the parameter values listed in Table 5.22, diffusion coefficient (*D*), mobility (μ) and number density or concentration (*n*) of free ions for B7 electrolyte at different temperatures were calculated using equations (4.16), (4.17) and (4.18), respectively. The calculation values are listed in Table 5.23. Figures 5.29 show the plots of *D*, μ and *n* of free mobile ions at different temperatures, respectively.

Table 5.23: *D*, μ and *n* values for B7 electrolyte at different temperatures.

***T* (K)**	***D* ($\times10^{-6}$ cm^2 s^{-1})**	**μ ($\times10^{-5}$ cm^2 V^{-1} s^{-1})**	***n* ($\times10^{20}$ cm^{-3})**
298	2.467	9.604	2.830
303	2.458	9.414	3.101
308	2.453	9.242	3.379
313	2.448	9.073	3.684
318	2.442	8.911	3.999
323	2.439	8.763	4.325
328	2.435	8.613	4.686
333	2.430	8.466	5.045
338	2.427	8.330	5.428
343	2.422	8.195	5.828
348	2.420	8.070	6.212
353	2.418	7.947	6.683
358	2.414	7.823	7.141
363	2.412	7.709	7.616
368	2.409	7.595	8.113
373	2.408	7.491	8.620
378	2.406	7.386	9.107
383	2.404	7.282	9.810
388	2.401	7.180	10.315
393	2.397	7.078	10.861

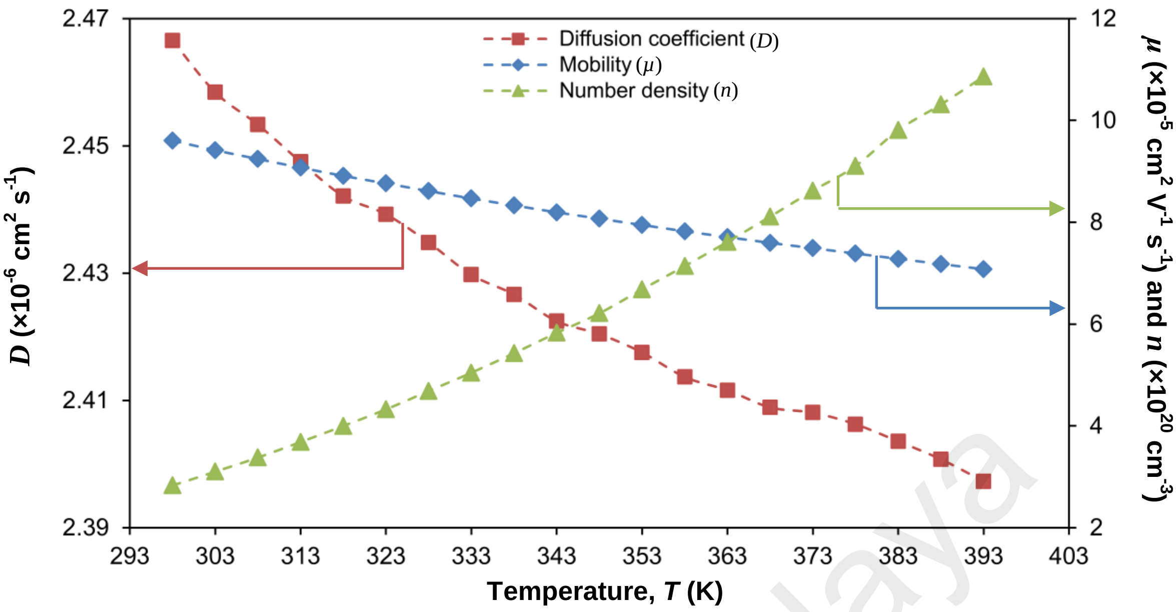

Figure 5.29: *D*, *μ* and *n* of free mobile ions for B7 electrolyte at different temperatures.

From Figure 5.29, the increase in temperature has decreased the *D* and *μ* of free mobile ions for B7 electrolyte, respectively. *n* of charge carriers for B7 electrolyte is observed to increase with temperature as depicted in Figure 5.29.

5.4. Summary

PVA–LiBOB–TBAI–I$_2$–DMF gel polymer electrolyte was characterized by fourier transform infrared (FTIR) spectroscopy and electrical impedance spectroscopy (EIS). In FTIR section, the complexation between polymer, salts and plasticizer were observed from the presence of band corresponding to all features of PVA, LiBOB, TBAI and DMF in PVA–LiBOB–TBAI–I$_2$–DMF gel polymer electrolyte IR spectrum. The shifting of OH band of PVA from 3322 cm^{-1} to high wavenumber after adding LiBOB and/or TBAI salts proved that the cation of the salt has interacted with oxygen atom of hydroxyl group. The deconvolution of hydroxyl group shows that there is no water contamination in PVA–based gel polymer electrolyte prepared. Since there is

LiBOB salt in the electrolyte, the FTIR band between 1850 and 1760 wavenumbers has been devonvoluted to determine the percentage of free Li^+. The decrease in amount of LiBOB from 100 wt.% (B0 electrolyte) to 10 wt.% (B6 electrolyte) is observed to decrease the percentage of Li^+ free ions in the electrolyte. From the literature review, there are no reports about FTIR band corresponding to free TBAI salt. Hence, the percentage of free ions obtained by FTIR for TBAI salt cannot be deduced in this study. In this work, the free ions from TBAI were obtained by subtracting the number density of free BOB^- or Li^+ ions obtained from FTIR studies from the number density of free ions from both LiBOB and TBAI as obtained from EIS. In EIS section, the highest room temperature conductivity of 7.31×10^{-3} S cm^{-1} is obtained by B0 electrolyte (electrolyte with 100 wt.% LiBOB:0 wt.% TBAI composition). The conductivity is observed to decrease with reducing LiBOB salt. The amount of LiBOB salt reduced was replaced with TBAI salt. The conductivity for B7 electrolyte (electrolyte with 0 wt.% LiBOB:100 wt.% TBAI composition) is 4.35×10^{-3} S cm^{-1}. The conductivity–temperature dependence shows the conductivity of PVA–LiBOB–TBAI–I_2–DMF gel polymer electrolyte increase with increasing temperature. The transport properties of charge carriers for PVA–LiBOB–TBAI–I_2–DMF gel polymer electrolyte system have been calculated at room and at elevated temperatures. The entire electrolytes prepared in this second system were used as a medium for charge transfer in dye sensitized solar cells (DSSC). The performance of DSSC will be discussed in Chapter 7.

CHAPTER 6 : RESULTS FOR PVA–LiBOB–TBAI–BMII–I_2–DMF GEL POLYMER ELECTROLYTE SYSTEM

6.1. Introduction

In this chapter, 1–butyl–3–methylimidazolium iodide (BMII) ionic liquid (IL) was added into B5 electrolyte i.e. PVA–LiBOB–TBAI–I_2–DMF gel polymer electrolyte system (system 2). B5 electrolyte was chosen due to the high solar conversion efficiency obtained from the DSSC compared to the other DSSCs employing other gel polymer electrolytes. The electrolyte prepared in this third system was characterized using FTIR spectroscopy and EIS. FTIR will discuss the complexation between PVA, LiBOB, TBAI, BMII and plasticizer. Since this electrolyte system contains LiBOB salt, the FTIR band corresponding to free ion of LiBOB salt will also be deconvoluted. The results obtained will be used to calculate the percentage of free ions of LiBOB in each electrolyte prepared. In EIS section, the conductivity of PVA–LiBOB–TBAI–BMII–I_2–DMF gel polymer electrolytes was measured at room and elevated temperatures. Based on the method proposed in Chapter 4, the transport properties of charge carriers of each electrolyte at room and varied temperatures were determined from fitting the tilted spike in the complex impedance plot. All electrolytes prepared in this third system were used as a medium for redox process in DSSC to obtain the highest solar conversion efficiency. The performance of DSSC will be discussed in Chapter 7.

6.2. Fourier Transform Infrared (FTIR) Spectroscopy

The complexation between polymer, salts, ionic liquid and plasticizer were studied by analyzing the FTIR spectrum of electrolytes prepared. Figures 6.1(a) and (b) show the infrared spectrum in transmittance mode for PVA, DMF, LiBOB salt, TBAI salt, BMII ionic liquid and PVA–LiBOB–TBAI–BMII–I_2–DMF complexes in the wavenumber region from 3800 to 3000 cm^{-1} and 1900 to 800 cm^{-1}.

In PVA infrared spectrum, the band at 3322 cm^{-1} is assigned to OH band (Buraidah & Arof, 2011). The vibrational frequency at 1089 cm^{-1} in DMF infrared spectrum is assigned to CH_3 rocking mode (Jacob & Arof, 2000). In LiBOB salt infrared spectrum, the vibrational band at 1803, 1158 and 972 wavenumbers are assigned to C=O out–of–phase valence, O–B–O symmetric valence and O–B–O asymmetric valence of LiBOB, respectively (Holomb et al., 2006). The band at 1030 wavenumber was assigned to TBAI characteristics. The vibrational frequency at 3467 and 1165 wavenumbers in BMII ionic liquid infrared spectrum are assigned to H_2O group (Rajkumar & Ranga Rao, 2008) and imidazole H–C–C (Buraidah et al., 2010) of BMII ionic liquid.

Addition of BMII into C0 gel polymer electrolyte still showed all the vibration modes of PVA, DMF, LiBOB, TBAI and BMII. In PVA–LiBOB–TBAI–BMII–I_2–DMF complexes infrared spectrum, the vibrational band shown at 3448, 3446, 3446, 3452, 3451 and 3437 wavenumbers correspond to the hydroxyl group of PVA. The band at 1806 wavenumbers is assigned to C=O out–of–phase valence vibrations of LiBOB. The vibrational frequencies at 1090 cm^{-1} is assigned to CH_3 rocking mode of DMF. The band at 1023 wavenumber is assigned to TBAI and the band at 1170 wavenumber is assigned to imidazole H–C–C of BMII ionic liquid.

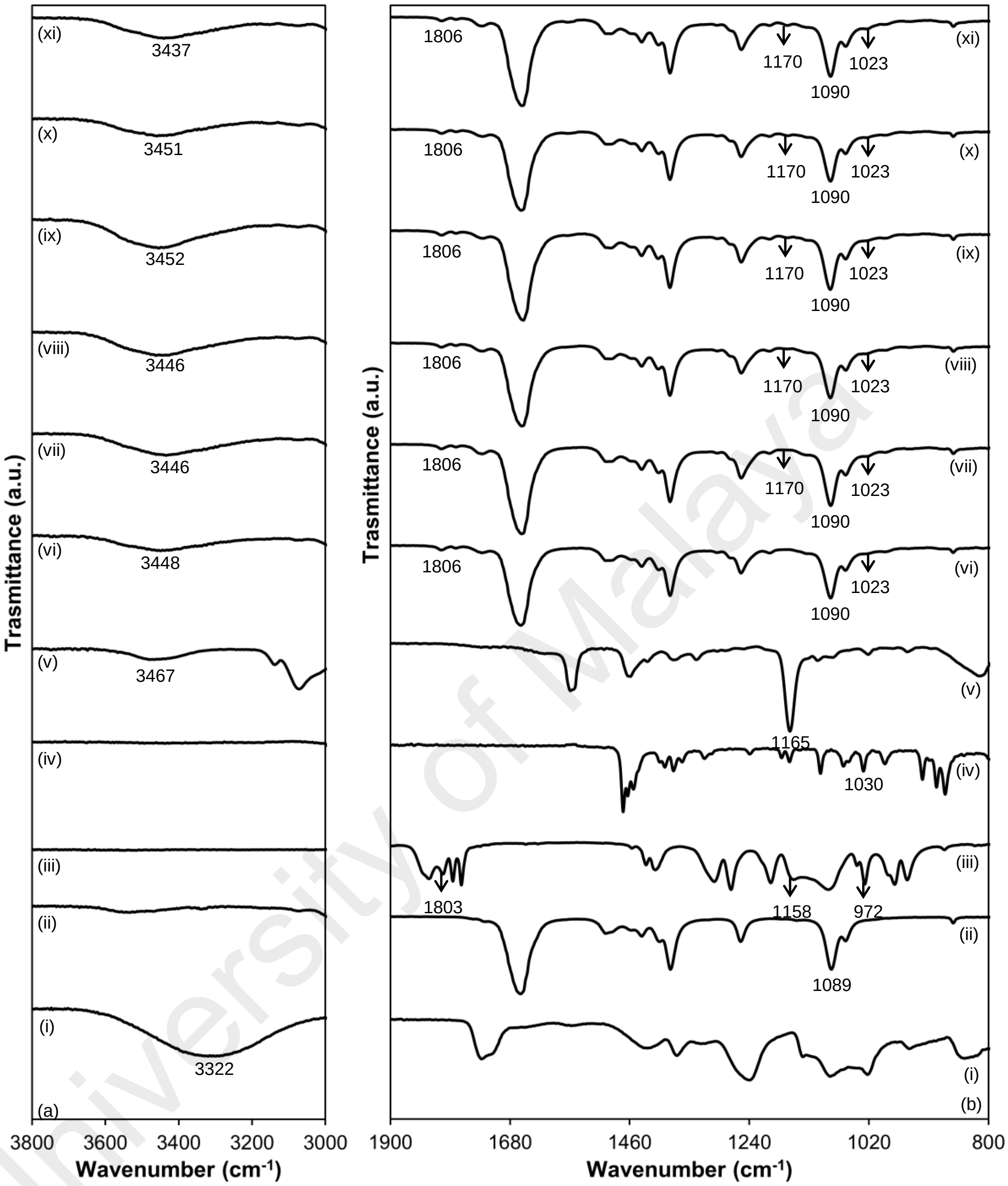

Figure 6.1: FTIR spectra of (i) PVA, (ii) DMF, (iii) LiBOB salt, (iv) TBAI salt, (v) BMII ionic liquid, (vi) C0, (vii) C1, (viii) C2, (ix) C3, (x) C4 and (xi) C5 electrolyte between (a) 2000 and 800, and (b) 3800 and 2800 wavenumbers.

In Chapter 4 and Chapter 5, the vibrational band corresponding to OH group of PVA is of concern due to the expected interaction between the cation from salt and the oxygen atom of hydroxyl group. The shifting of the OH band can be observed from 3322 cm^{-1} in pure PVA to higher wavenumber in the complexes. Thus, in this third electrolyte system, the infrared spectrum corresponding to hydroxyl group of PVA will be analyzed. In Figure 6.1(a), it can be seen that the OH band of PVA was shifted to higher wavenumber as BMII was added. The shifted of hydroxyl group of PVA which originally at 3322 cm^{-1} proved the interaction between polymer and BMII has occurred.

Figure 6.2 shows the FTIR spectrum in absorbance mode for PVA–LiBOB–TBAI–BMII–I_2–DMF gel polymer electrolyte between 1220 and 1120 wavenumber. It can be seen that the addition of 1 wt.% BMII ionic liquid into C0 electrolyte revealed a very small hump at 1170 cm^{-1} which assigned to imidazole H–C–C of BMII (Buraidah *et al.*, 2010). Increasing the amount of BMII ionic liquid in C0 electrolyte, it is observed that this band increased in intensity at 1170 wavenumbers. This implies that BMII ionic liquid has complexes with PVA–LiBOB–TBAI–I_2–DMF gel polymer electrolyte. The present of feature of PVA, LiBOB, TBAI, BMII and DMF in this third electrolyte system further strengthen the occurrence of complexation.

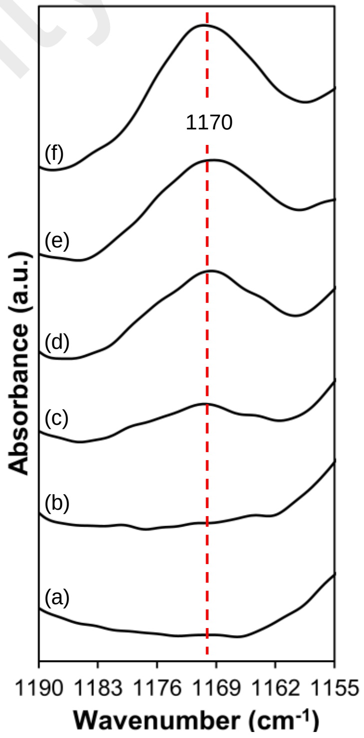

Figure 6.2: FTIR spectra between 1220 and 1120 wavenumber for (a) C0, (b) C1, (c) C2, (d) C3, (e) C4 and (f) C5 electrolyte.

Figure 6.3 shows the FTIR deconvolution of hydroxyl band of PVA between 3700 and 3150 wavenumber. It can be observed that there is only one deconvoluted peak is revealed which corresponding to OH group of PVA. As mention in Chapter 4, PVA is hydrophilic polymer that tends to interact with OH group of water. Since there is no other deconvoluted peak is observed in Figure 6.3, thus this implied that PVA–LiBOB–TBAI–BMII–DMF gel electrolyte is free from water contamination.

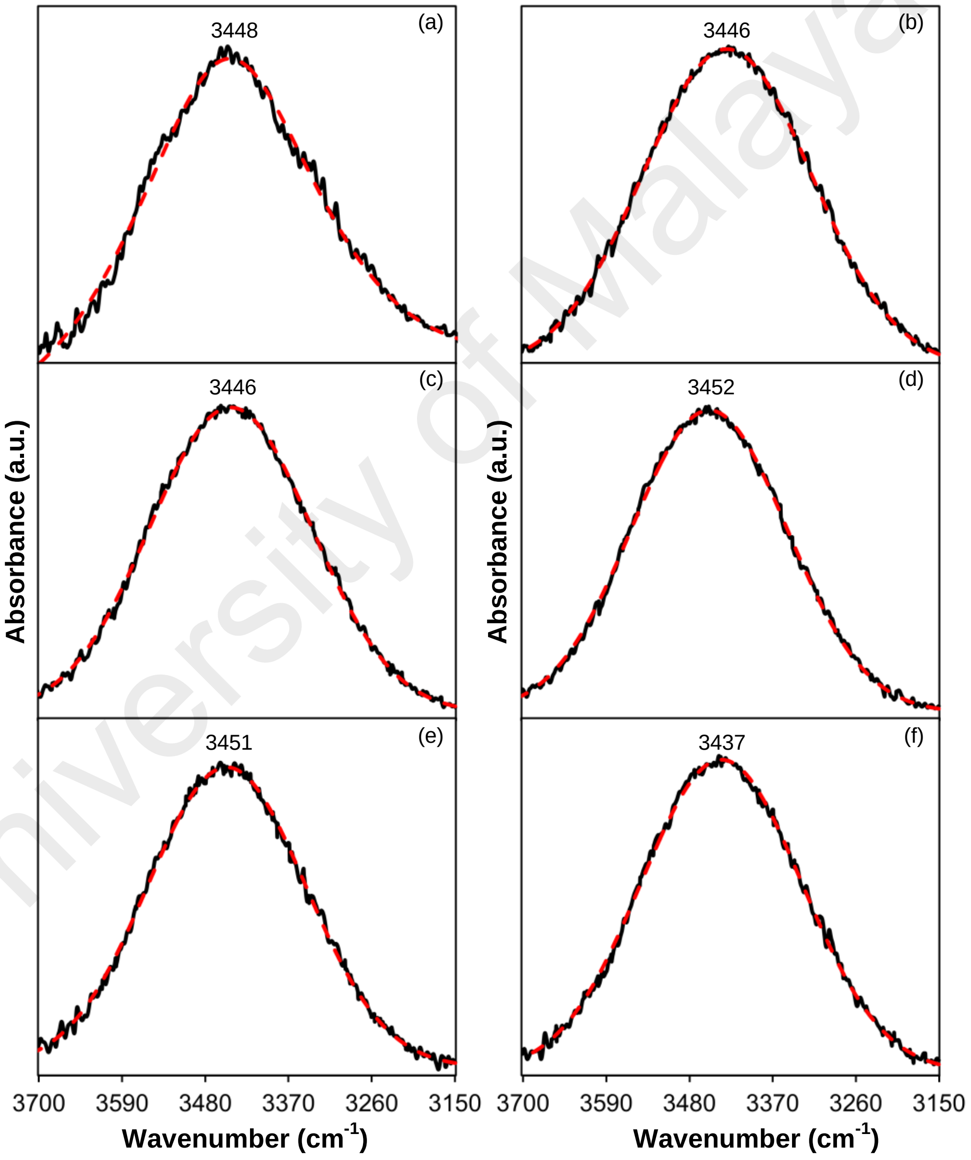

Figure 6.3: FTIR deconvolution of band between 3700 and 3150 wavenumber for (a) C0, (b) C1, (c) C2, (d) C3, (e) C4 and (f) B5 electrolytes. Line (—) due to original spectrum, line (---) due to fitted spectrum.

Figure 6.4 shows the FTIR deconvolution for PVA–LiBOB–TBAI–BMII–I_2–DMF gel polymer electrolyte system in the wavenumber region between 1850 and 1760 cm^{-1}. This is the region that refers to free ions and ion pairs of LiBOB. The deconvoluted band at 1804 cm^{-1} is assigned to free ions of LiBOB salt while the band at 1812 and 1826 cm^{-1} are assigned to ion pairs. The band at 1778 cm^{-1} is assigned to C=O out–of–phase valence vibrations of LiBOB (Holomb *et al.*, 2006). The area percentage of ionic species of gel polymer electrolyte in this third system is shown in Figure 6.5.

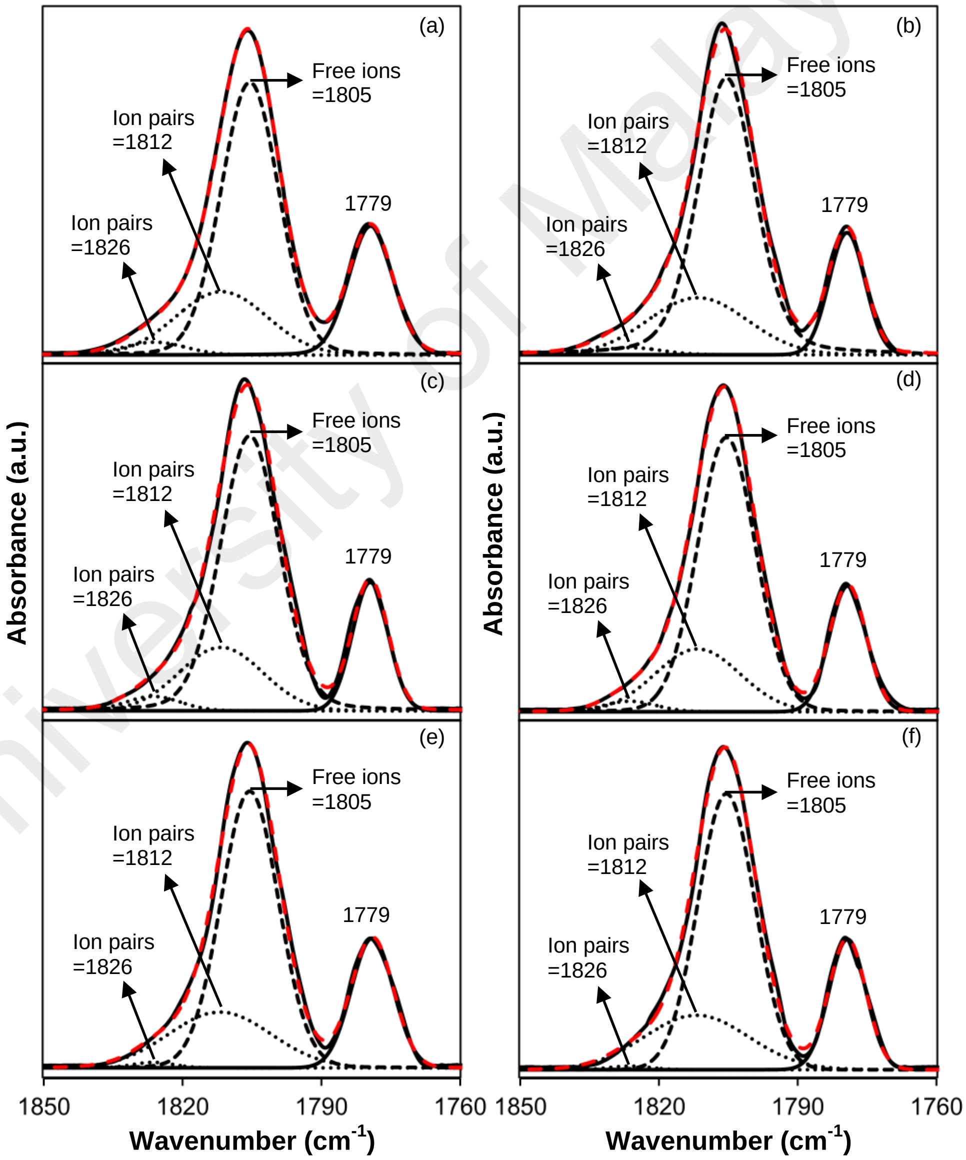

Figure 6.4: FTIR deconvolution of (a) C0, (b) C1, (c) C2, (d) C3, (e) C4 and (f) C5 electrolyte. Area under line (---) due to free ions and line (·····) due to ion pairs. Line (—) refer to original spectrum and line (---) refer to fitted spectrum.

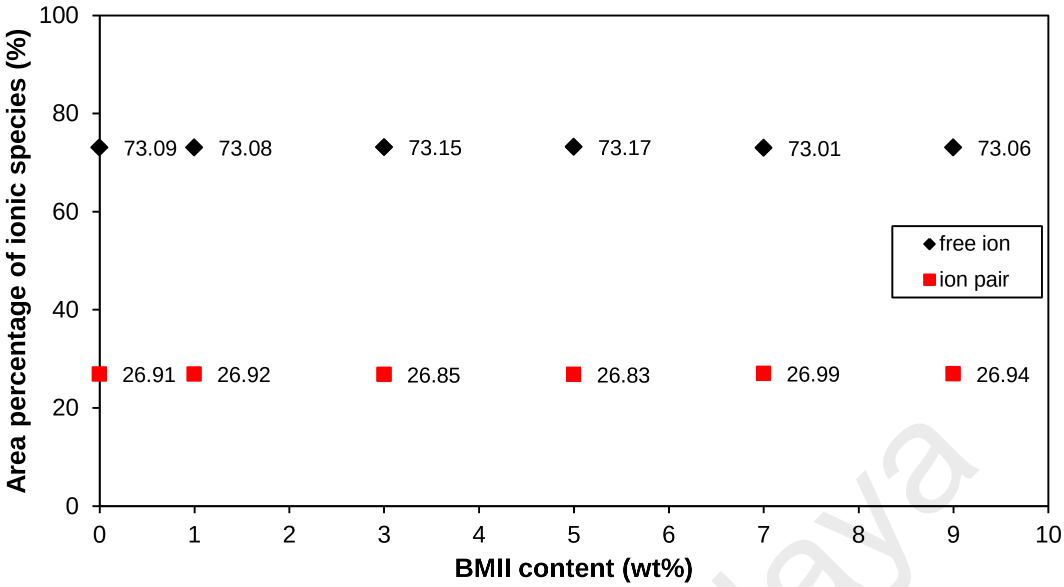

Figure 6.5: Area percentage of free ions and ion pairs of PVA–LiBOB–TBAI–BMII–I_2–DMF gel electrolytes system.

From Figure 6.5, it is observed that the percentage of free ions (Li$^+$ and BOB$^-$) and ion pairs (Li$^+$BOB$^-$Li$^+$, Li$^+$BOB$^-$) without and with BMII ionic liquid are almost the same. From the literature reviews, there is no report for free ions of TBAI and BMII ionic liquid so the FTIR band could not be deconvoluted for the respective ions. There is also no work done ab initio on these materials.

6.3. Electrochemical Impedance Spectroscopy (EIS)

6.3.1. Ionic Conductivity of PVA–LiBOB–TBAI–BMII–I_2–DMF Gel Polymer Electrolyte

Electrochemical impedance spectroscopy was carried out to study the electrical properties of PVA–LiBOB–TBAI–BMII–I_2–DMF gel polymer electrolyte. Figure 6.6 shows the Nyquist plots for PVA–LiBOB–TBAI–BMII–I_2–DMF gel polymer electrolyte system at room temperature. In Figure 6.6, the Nyquist plots for all electrolytes are observed to consists of only a tilted spike. The intercept of tilted spike with the real impedance, *Z'* axis gives the value of bulk resistance, R_b of the electrolyte. The values of R_b obtained in Figure 6.6 were listed in Table 6.1. Based on these values, the ionic conductivity of PVA–LiBOB–TBAI–BMII–I_2–DMF gel polymer electrolyte system at room temperature was calculated using equation (3.4). The thickness, *d* of each electrolyte was maintained at 0.26 cm. Figure 6.7 depicted the variation of ionic conductivity of PVA–LiBOB–TBAI–BMII–I_2–DMF gel polymer electrolyte system at room temperature.

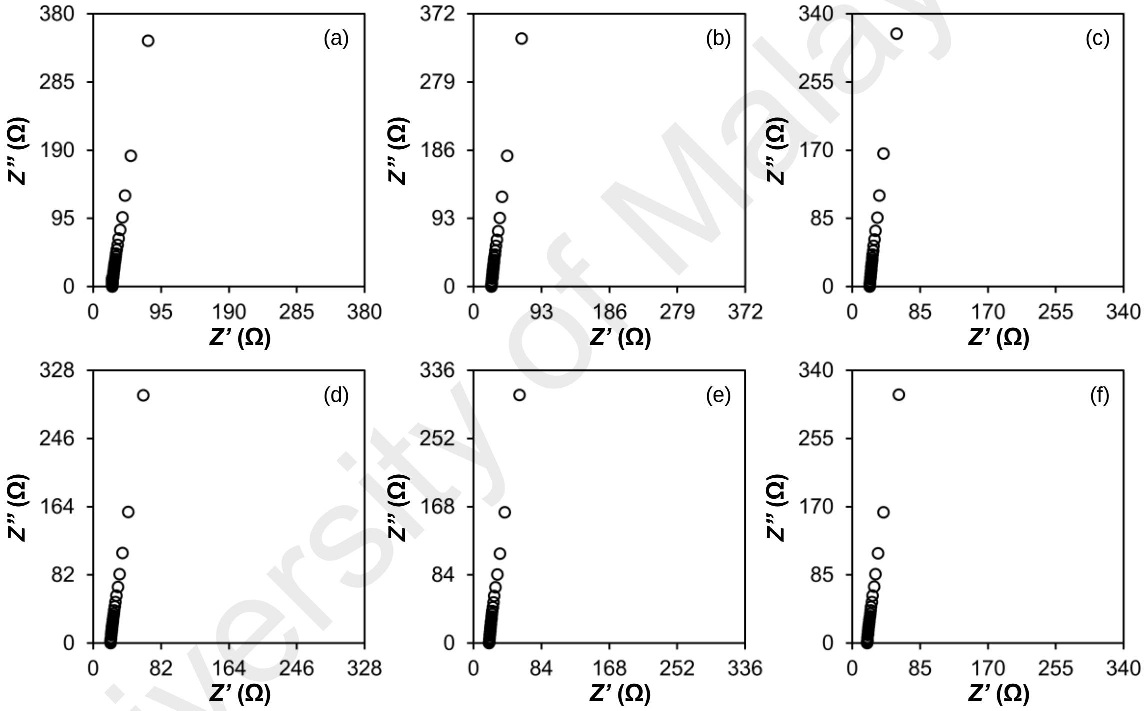

Figure 6.6: Nyquist plot of (a) C0, (b) C1, (c) C2, (d) C3, (e) C4 and (f) C5 gel polymer electrolyte at room temperature.

Table 6.1: R_b values of PVA–LiBOB–TBAI–BMII–I_2–DMF gel polymer electrolyte obtained in Figure 6.6.

Electrolyte	R_b **(Ω)**
C0	25.20
C1	23.80
C2	21.00
C3	20.00
C4	18.70
C5	17.20

Based on Figure 6.7, the ionic conductivity of gel polymer electrolyte without BMII ionic liquid (C0 electrolyte) is found to be 5.13×10^{-3} S cm^{-1}. As 1 wt.% BMII ionic liquid is added into C0 electrolyte, the conductivity increased to 5.43×10^{-3} S cm^{-1} (C1 electrolyte). A gradual increase in conductivity was observed when the amount of BMII ionic liquid was increased up to 9 wt.%.

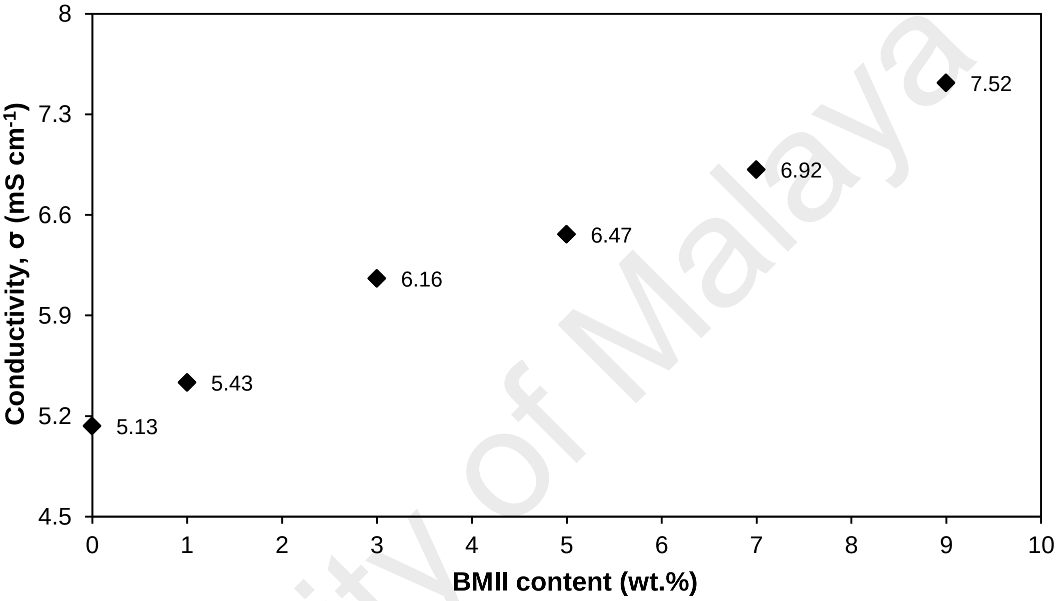

Figure 6.7: Room temperature conductivity of PVA–LiBOB–TBAI–BMII–I_2–DMF gel polymer electrolyte system.

The conductivity of PVA–LiBOB–TBAI–BMII–I_2–DMF gel polymer electrolyte system was studied at different temperatures range. Figure 6.8 shows the conductivity–temperature dependence of PVA–LiBOB–TBAI–I_2–DMF gel polymer electrolyte with different BMII ionic liquid contents between 298 and 393 K. The conductivity of each electrolyte is observed to increase with increasing temperature. The conductivity–temperature dependence of each electrolyte in this third system is observed to form a quadratic shape, which suggests that conductivity and temperature obey the VTF relationship. Figure 6.9 shows the VTF plot of conductivity–temperature dependence for PVA–LiBOB–TBAI–I_2–DMF gel polymer electrolyte. The values of room temperature conductivity (σ), T_o, E_a and regression (R^2) of PVA–LiBOB–TBAI–BMII–I_2–DMF gel polymer electrolyte system from VTF plot in Figure 6.9 were also listed in Table 6.2.

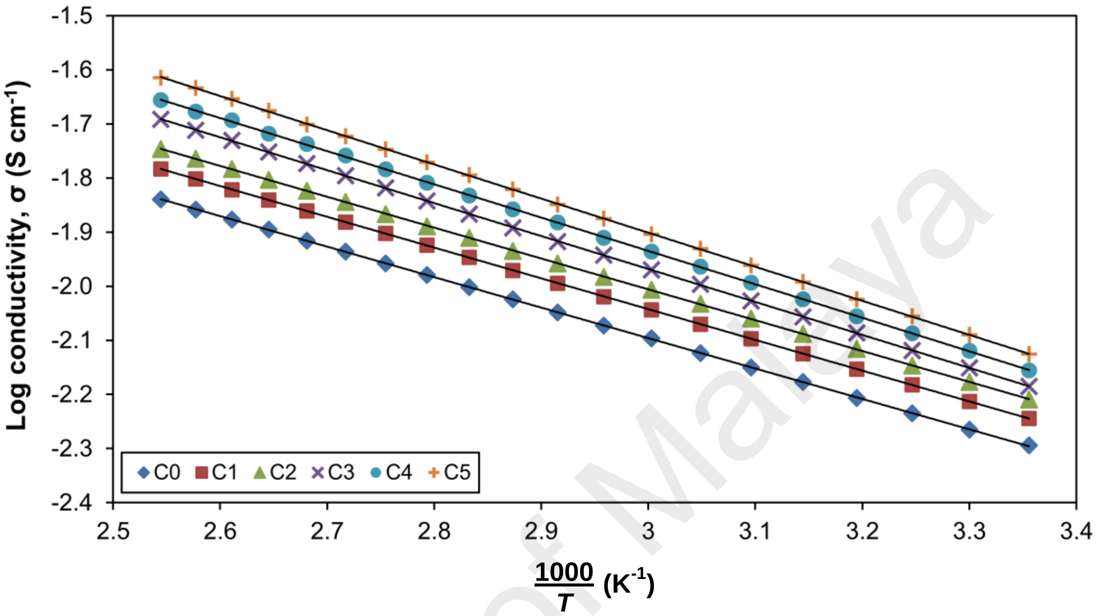

Figure 6.8: Conductivity–temperature dependence of PVA–LiBOB–TBAI–BMII–I_2–DMF gel polymer electrolyte system.

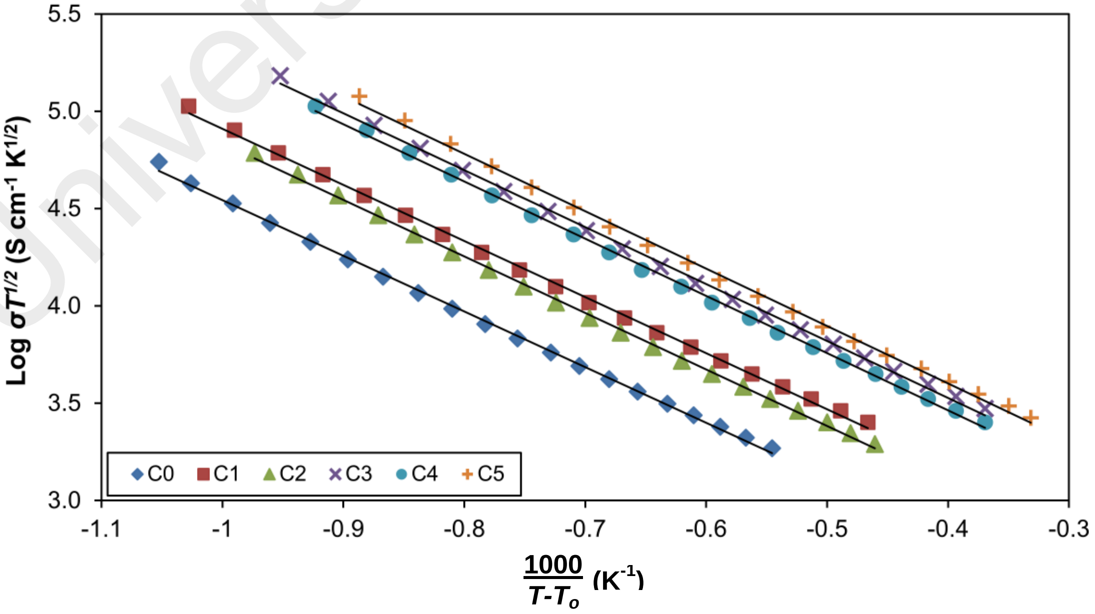

Figure 6.9: VTF plot of conductivity–temperature dependence PVA–LiBOB–TBAI–BMII–I_2–DMF gel polymer electrolyte.

Table 6.2: The σ, T_o, E_a and R^2 values of PVA–LiBOB–TBAI–I_2–DMF gel polymer electrolyte system.

Electrolyte	**σ (mS cm^{-1})**	**T_o (K)**	**E_a (meV)**	**R^2**
C0	5.13	87	69.33	0.999
C1	5.43	99	68.83	0.999
C2	6.16	372	68.30	0.999
C3	6.47	105	67.78	0.999
C4	6.92	99	67.46	0.999
C5	7.52	101	67.21	0.999

6.3.2. Room Temperature Transport Properties of Charge Carriers of PVA–LiBOB–TBAI–BMII–I_2–DMF Gel Polymer Electrolyte

Diffusion coefficient (*D*), mobility (μ) and number density (*n*) of charge carriers are three parameters that influence the conductivity of an electrolyte. It is because conductivity is the product of ion mobility (μ), number density of charge carriers (*n*) and elementary charge (*e*). The variation of conductivity obtained in one electrolyte system should be attributed with the variation of these three parameters. Thus, it is important to determine the values of diffusion coefficient (*D*), mobility (μ) and number density (*n*) of charge carriers in one electrolyte system.

Figure 6.10 shows the Nyquist plot and their corresponding fitted points for PVA–LiBOB–TBAI–BMII–I_2–DMF gel polymer electrolyte system at room temperature. The Nyquist plot obtained by impedance measurement was fitted using equations (3.19) and (3.20). The value of *R* and p_2 were determined by the concept shown in Figure 3.12. The parameters k_2 were determined by trial and error until the fitted points fit the Nyquist plot at the corresponding frequencies. All the fitted points are observed to fit the plot. Table 6.3 lists the values of *R*, k_2, p_2 and ω_2 for PVA–

LiBOB–TBAI–BMII–I_2–DMF gel polymer electrolyte system obtained using the fitting method.

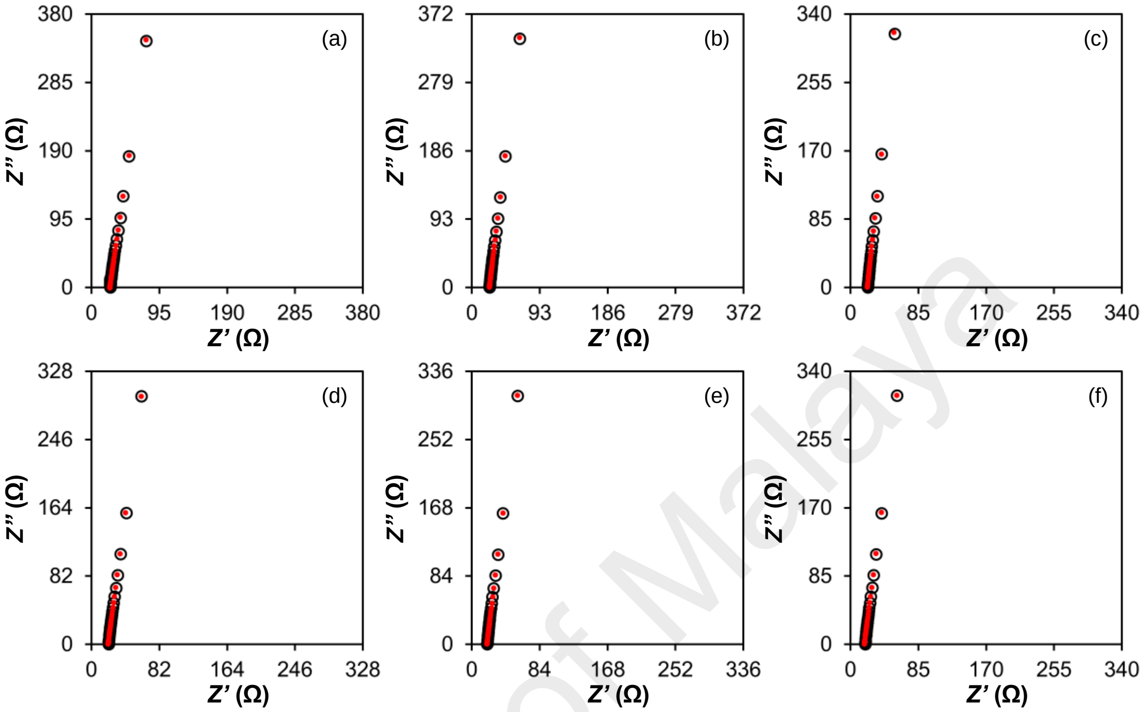

Figure 6.10: Nyquist plot (o) and their corresponding fitted point (●) for (a) C0, (b) C1, (c) C2, (d) C3, (e) C4 and (f) C5 electrolyte at room temperature.

Table 6.3: Values of R, p_2, k_2 and ω_2 for PVA–LiBOB–TBAI–BMII–I_2–DMF gel polymer electrolyte obtained from fitting of Nyquist plot at room temperature.

Electrolyte	R **(Ω)**	p_2	k_2 **(F^{-1})**	ω_2 **(s^{-1})**
C0	25.20	0.907	64100	285528
C1	23.80	0.923	69200	272458
C2	21.00	0.933	68200	308760
C3	20.00	0.915	58000	261657
C4	18.70	0.925	62000	309856
C5	17.20	0.917	61000	332990

In order to calculate the value of diffusion coefficient (D), mobility (μ) and number density (n) of charge carriers of PVA–LiBOB–TBAI–BMII–I_2–DMF gel polymer electrolyte, the value of d, R, k_2 and ω_2 should be known so equations (4.16), (4.17) and (4.18) can be used easily. In this third electrolyte system, the thickness, d of all electrolytes was fixed at 0.26 cm. The value of R and k_2 was obtained from fitting the Nyquist plot in Figure 6.10. The value of ω_2 was taken at the frequency corresponding to a minimum in imaginary parts of the impedance, Z'' i.e. at $Z'' \rightarrow 0$.

From the parameter values listed in Table 6.3, diffusion coefficient (D), mobility (μ) and number density (n) of charge carriers for PVA–LiBOB–TBAI–BMII–I_2–DMF gel polymer electrolyte at room temperature was calculated by using equations (4.16), (4.17) and (4.18), respectively. The calculated values are listed in Table 6.4. Figures 6.11 and 6.12 show the plots of diffusion coefficient, mobility and number density of charge carriers, respectively for PVA–LiBOB–TBAI–I_2–DMF gel polymer electrolyte containing different BMII ionic liquid weight ratios at room temperature.

Table 6.4: Values of D, μ and n for PVA–LiBOB–TBAI–BMII–I_2–DMF gel electrolyte at room temperature obtained by fitting method.

Electrolyte	**D ($\times 10^{-6}$ cm^2 s^{-1})**	**μ ($\times 10^{-5}$ cm^2 V^{-1} s^{-1})**	**n ($\times 10^{20}$ cm^{-3})**
C0	2.460	9.577	3.345
C1	2.457	9.566	3.545
C2	2.453	9.551	4.025
C3	2.450	9.539	4.231
C4	2.448	9.532	4.529
C5	2.444	9.515	4.932

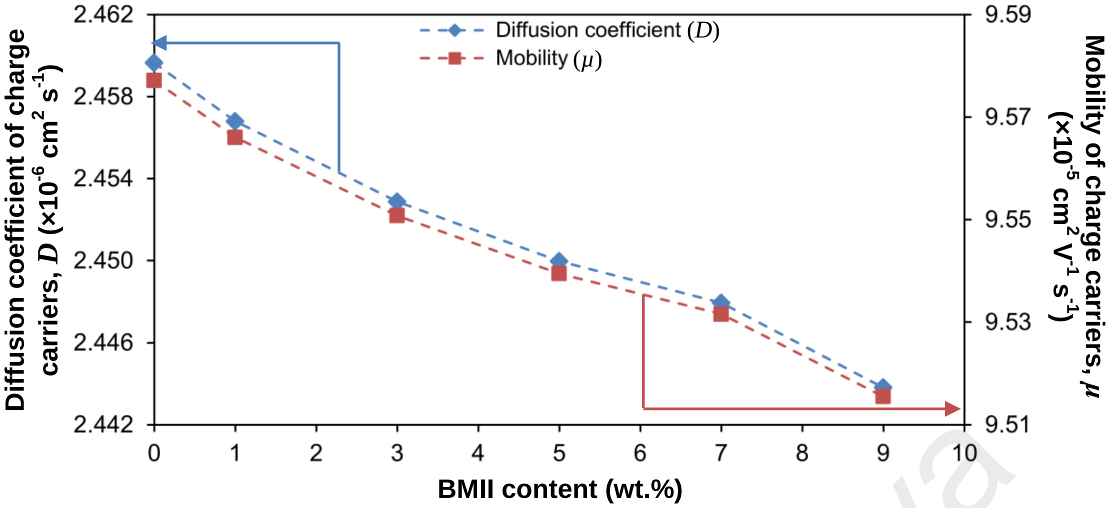

Figure 6.11: Diffusion coefficient (D) and mobility (μ) of charge carriers for PVA–LiBOB–TBAI–BMII–I_2–DMF gel electrolyte at room temperature.

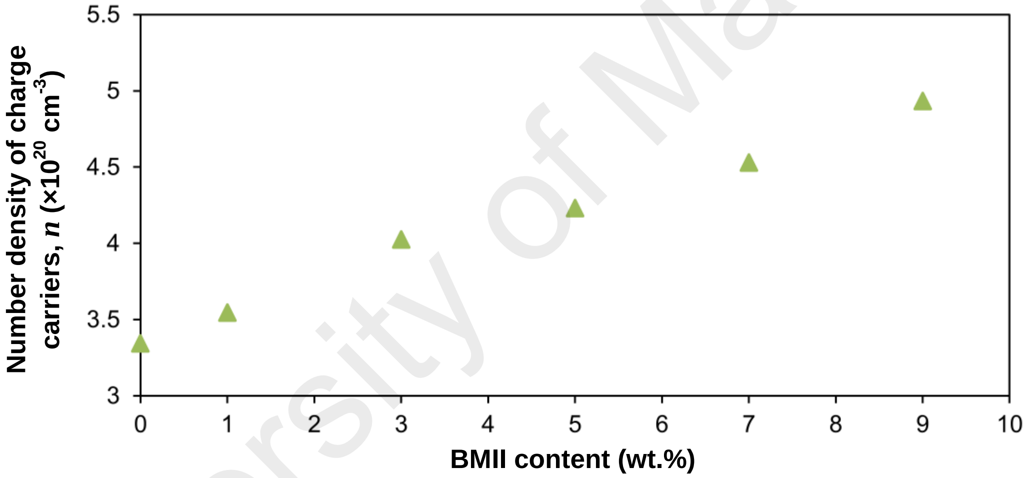

Figure 6.12: Number density of charge carriers, n of PVA–LiBOB–TBAI–BMII–I_2–DMF gel electrolyte at room temperature.

In Figure 6.11, the diffusion coefficient of charge carriers for PVA–LiBOB–TBAI–BMII–I_2–DMF gel electrolyte at room temperature is seen to decrease with increasing BMII ionic liquid content in the electrolyte up to 9 wt.%. The mobility of charge carriers for PVA–LiBOB–TBAI–BMII–I_2–DMF gel electrolyte at room temperature is observed to follow the same trend as diffusion coefficient, shown in Figure 6.11. The number density of charge carriers of this third electrolyte system at room temperature is observed to increase with increasing BMII ionic liquid content (Figure 6.12).

Based on the number density of charge carriers estimated for C0 electrolyte (B5 electrolyte) in Table 5.7, the number density of charge carriers of each LiBOB salt, TBAI salt and BMII ionic liquid was calculated. The values of number density of charge carriers of each component were estimated and listed in Table 6.5. The estimation calculation was done according to the constant percentage of free LiBOB ions obtained in Figure 6.5. The total *n* (dissociation ions of LiBOB, TBAI and BMII) obtained from fitting method in Table 6.4 was deducted with total *n* of C0 electrolyte (B5 electrolyte) obtained in Table 5.7.

Table 6.5: Value of number density of charge carriers for LiBOB salt, TBAI salt and BMII ionic liquid in PVA–LiBOB–TBAI–BMII–I_2–DMF gel electrolyte.

Electrolyte	***n*** **($\times 10^{20}$ cm^{-3})**		
	LiBOB	**TBAI**	**BMII**
C0	0.502	2.843	0
C1	0.502	2.843	0.201
C2	0.502	2.843	0.680
C3	0.502	2.843	0.886
C4	0.502	2.843	1.184
C5	0.502	2.843	1.587

From Table 6.5, it can be seen that the value of *n* for LiBOB and TBAI is constant. The value of *n* for BMII ionic liquid in observed to increase with increasing amounts of BMII ionic liquid in PVA–LiBOB–TBAI–BMII–I_2–DMF gel polymer electrolyte.

6.3.3. Transport Properties of Charge Carriers of PVA–LiBOB–TBAI–BMII–I_2–DMF Gel Polymer Electrolyte at Elevated Temperatures

The transport properties of charge carriers of PVA–LiBOB–TBAI–BMII–I_2–DMF gel electrolyte system were studied at different temperatures. The Nyquist plots obtained by impedance measurement for all electrolytes prepared at different temperatures were fitted using equations (3.19) and (3.20). It is observed that all Nyquist plots obtained in this third electrolyte system consists of only a tilted spike. Hence, equations (4.16), (4.17) and (4.18) that have been developed in Section 4.3.2, were used to calculat the transport properties of charge carriers. Figure 6.13 shows the Nyquist plot and their corresponding fitted points for C1 electrolyte at different temperatures. Table 6.6 lists all fitted parameters obtained in Figure 6.13.

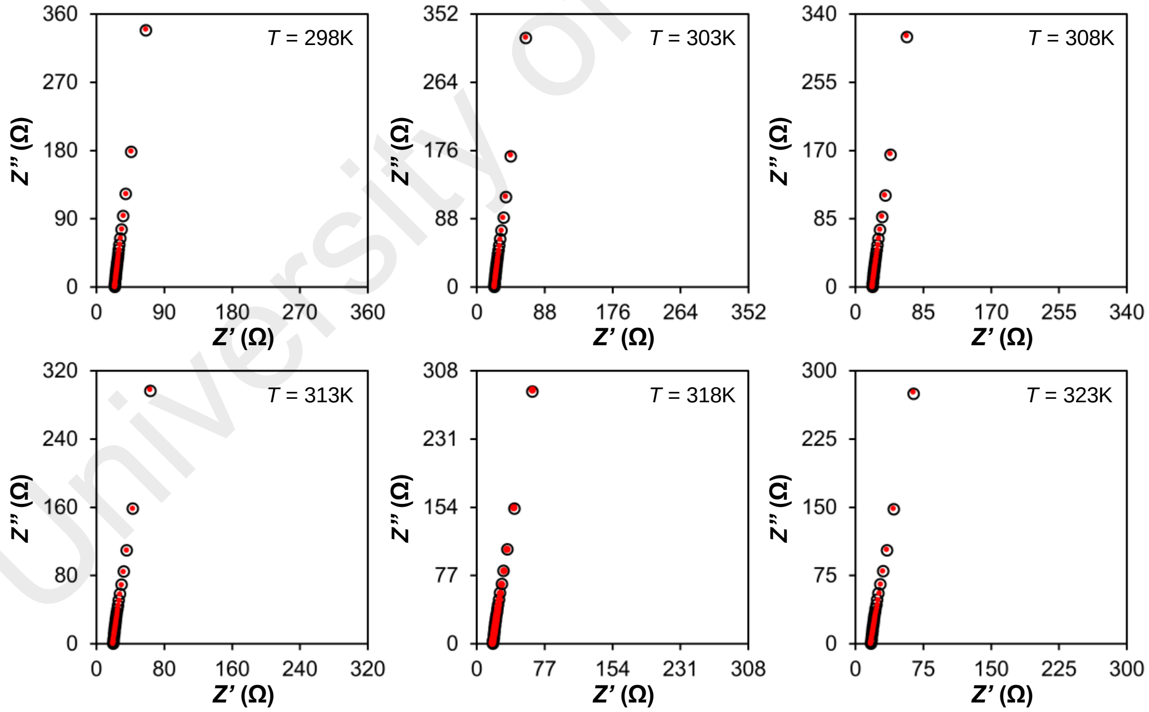

Figure 6.13, continued…

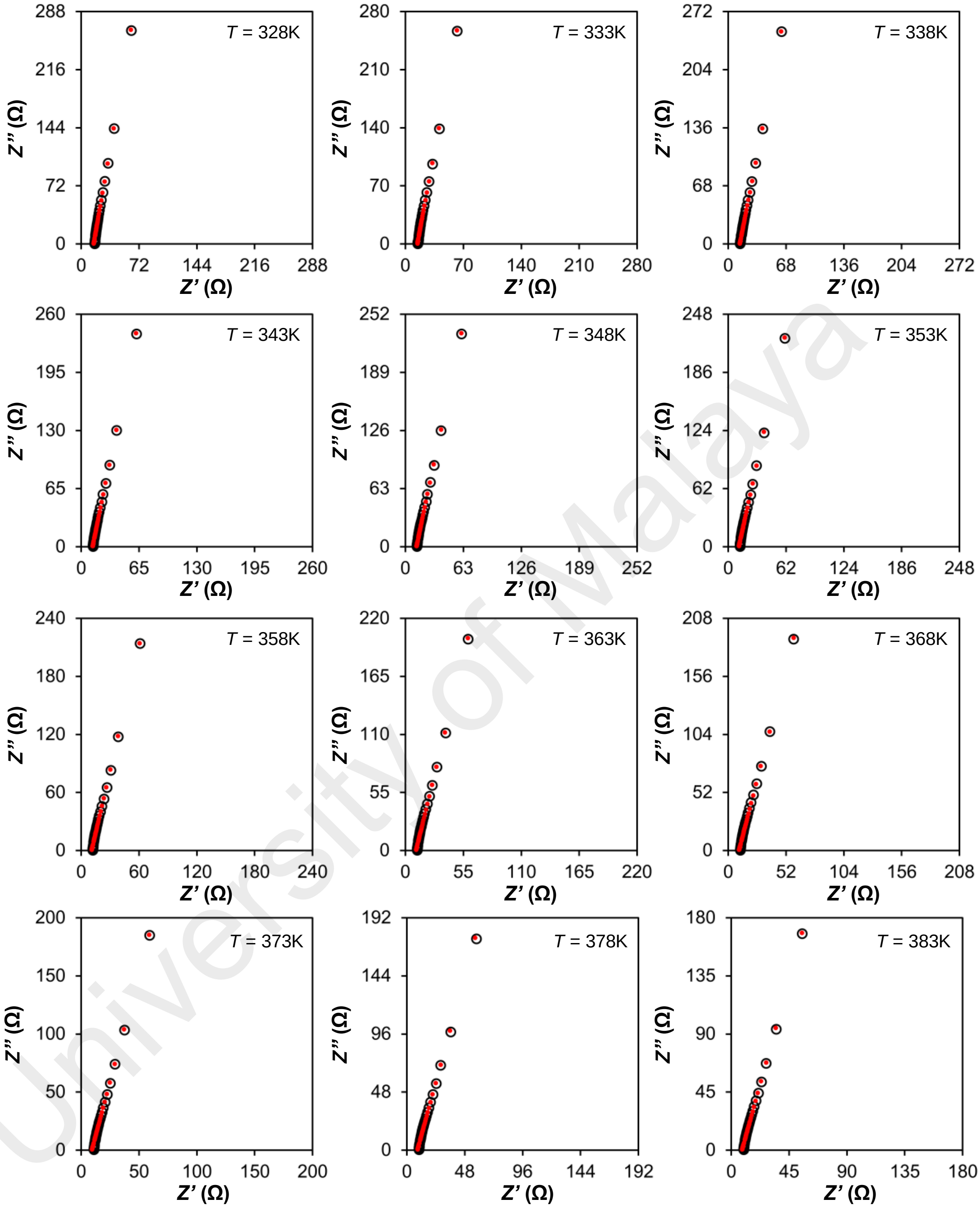

Figure 6.13, continued…

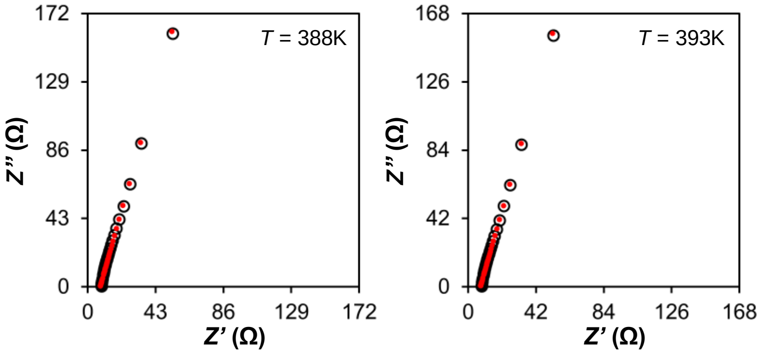

Figure 6.13: Nyquist plot (o) and their corresponding fitted point (●) for C1 electrolyte at different temperatures.

Table 6.6: *R*, p_2, k_2 and ω_2 values for C1 electrolyte obtained from fitting of Nyquist plot at different temperatures.

T **(K)**	***R*** **(Ω)**	p_2	k_2 **(F^{-1})**	ω_2 **(s^{-1})**	***T*** **(K)**	***R*** **(Ω)**	p_2	k_2 **(F^{-1})**	ω_2 **(s^{-1})**
298	23.80	0.923	69200	272458	348	12.00	0.868	34800	250395
303	22.00	0.920	64500	271471	353	11.30	0.862	32450	246639
308	20.40	0.913	60300	271391	358	10.70	0.855	30000	238121
313	18.90	0.907	55500	265878	363	10.10	0.847	27000	221041
318	17.60	0.900	51300	260983	368	9.60	0.839	24500	206156
323	16.40	0.893	47700	257917	373	9.11	0.834	23200	204282
328	15.40	0.890	45000	257175	378	8.65	0.830	21500	196999
333	14.40	0.883	42000	256133	383	8.25	0.828	20400	194940
338	13.50	0.877	39300	253722	388	7.85	0.825	19200	190856
343	12.70	0.872	36700	250715	393	7.50	0.822	18300	189917

From the parameter values listed in Table 6.6, diffusion coefficient (*D*), mobility (μ) and number density (*n*) of charge carriers for C1 electrolyte at different temperatures were calculated using equations (4.16), (4.17) and (4.18), respectively. The calculated values are listed in Table 6.7. Figures 6.14 show the plots of diffusion coefficient, mobility and number density of charge carriers at different temperatures, respectively.

Table 6.7: Values of D, μ and n for C1 electrolyte at different temperature.

T (K)	D ($\times 10^{-6}$ cm^2 s^{-1})	μ ($\times 10^{-5}$ cm^2 V^{-1} s^{-1})	n ($\times 10^{20}$ cm^{-3})	T (K)	D ($\times 10^{-6}$ cm^2 s^{-1})	μ ($\times 10^{-5}$ cm^2 V^{-1} s^{-1})	n ($\times 10^{20}$ cm^{-3})
298	2.457	9.566	3.545	348	2.440	8.134	8.270
303	2.454	9.399	3.904	353	2.439	8.017	8.910
308	2.452	9.238	4.283	358	2.438	7.902	9.546
313	2.450	9.082	4.703	363	2.435	7.784	10.268
318	2.448	8.932	5.135	368	2.433	7.671	10.961
323	2.446	8.787	5.602	373	2.431	7.562	11.717
328	2.444	8.645	6.063	378	2.430	7.458	12.512
333	2.443	8.514	6.584	383	2.429	7.358	13.298
338	2.442	8.382	7.133	388	2.427	7.257	14.170
343	2.441	8.258	7.697	393	2.426	7.163	15.026

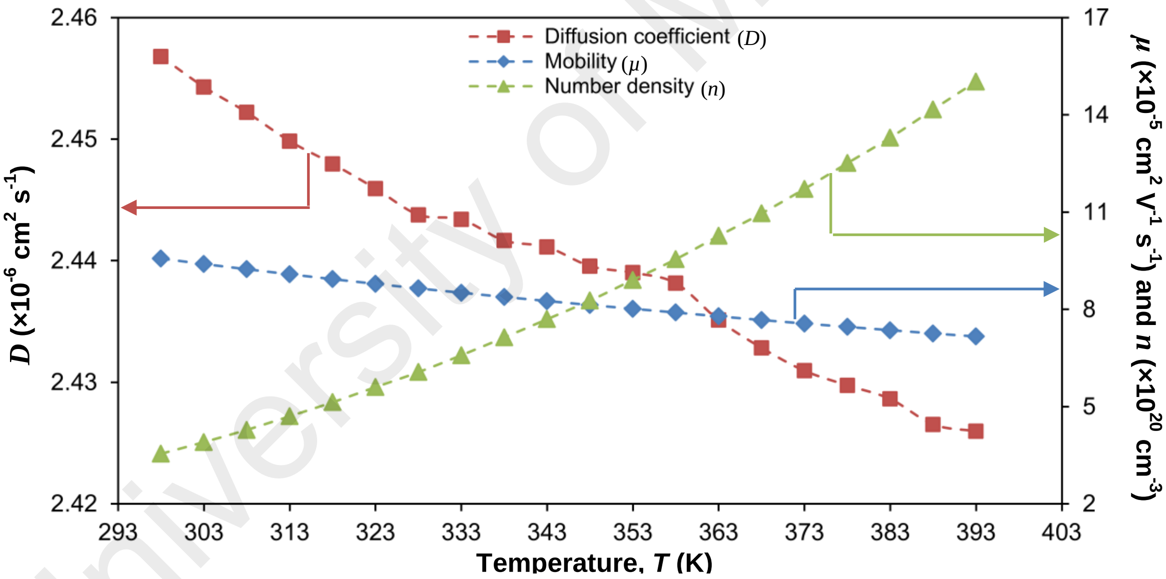

Figure 6.14: Diffusion coefficient, mobility and number density of charge carriers for C1 electrolyte at different temperatures.

From Figure 6.14, D and μ of C1 electrolyte is observed to decrease as the temperature increase from 298 K to 393 K. n of free mobile ions for C1 electrolyte is observed to increase with temperature as shown in Figure 6.14.

Figure 6.15 shows the Nyquist plot and their corresponding fitted points for C2 electrolyte at different temperatures. All fitted parameters obtained in Figure 6.15 were listed in Table 6.8.

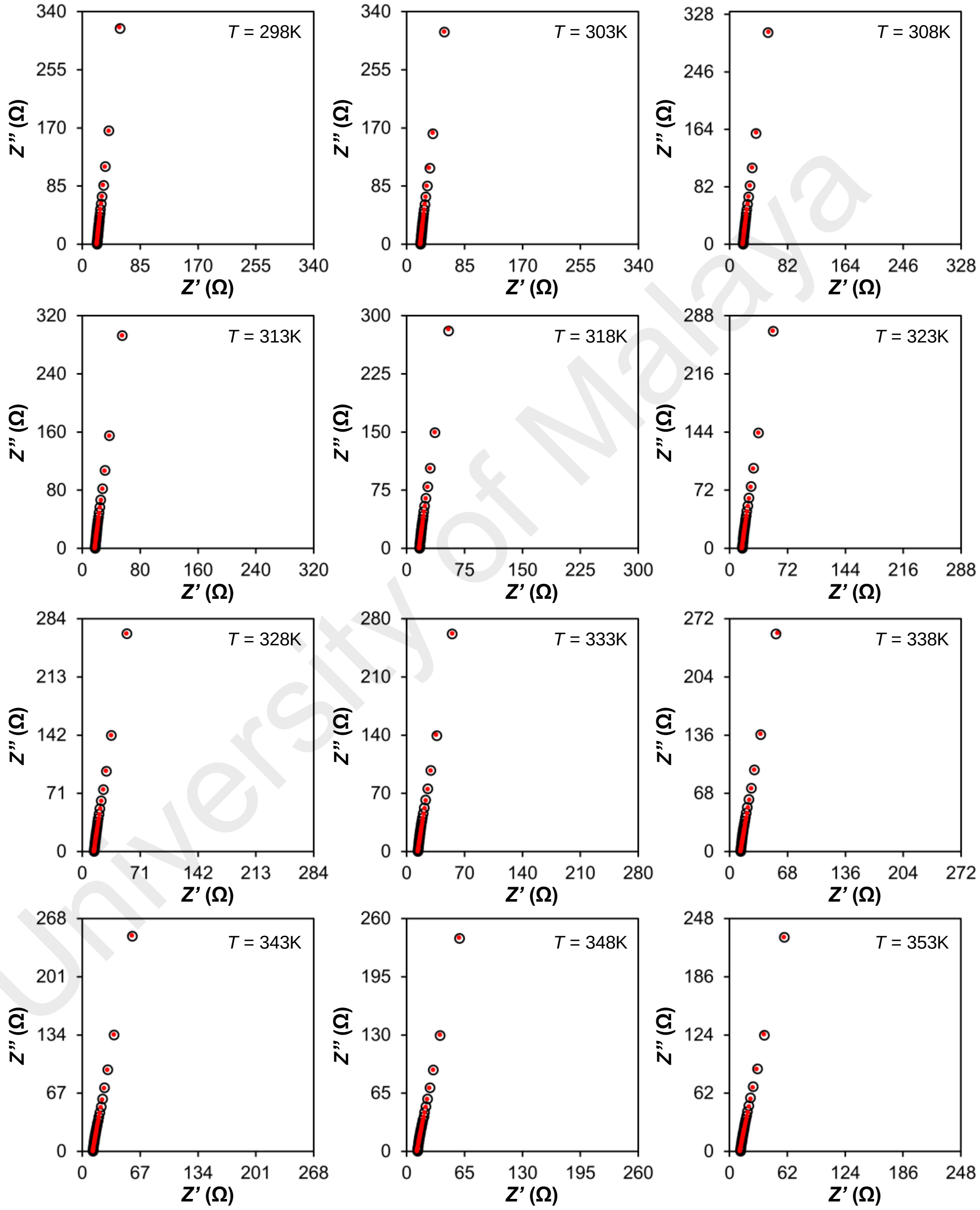

Figure 6.15, continued…

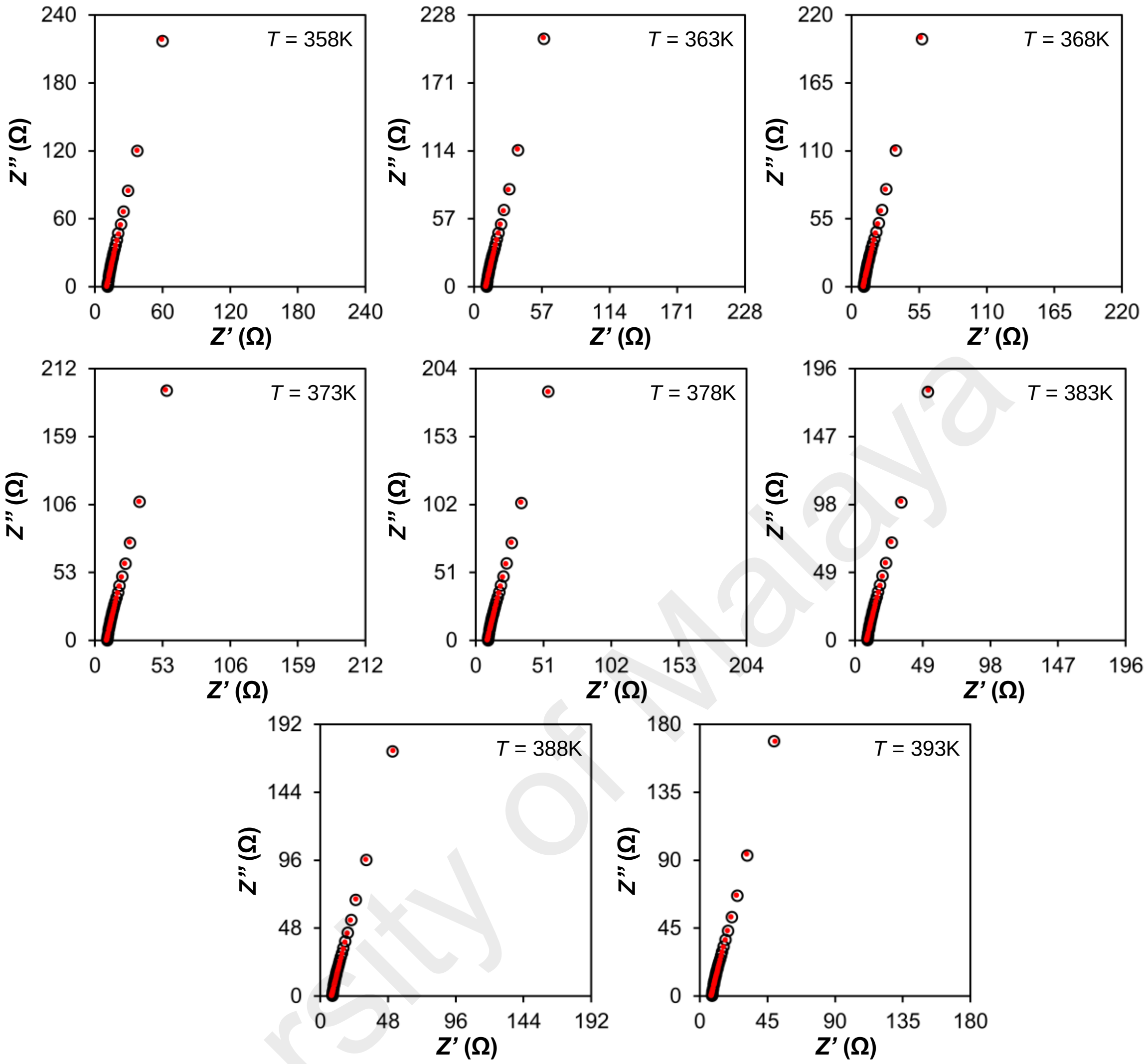

Figure 6.15: Nyquist plot (o) and their corresponding fitted point (●) for C2 electrolyte at different temperatures.

Table 6.8: Values of R, p_2, k_2 and ω_2 for C2 electrolyte obtained from fitting of Nyquist plot at different temperatures.

T (K)	**R (Ω)**	**p_2**	**k_2 (F^{-1})**	**ω_2 (s^{-1})**
298	21.00	0.933	68200	308760
303	19.50	0.928	65000	308429
308	18.20	0.924	62000	306477
313	17.00	0.918	58000	303238
318	16.00	0.915	55000	302762
323	15.00	0.910	51000	294408
328	14.10	0.905	49000	292660
333	13.30	0.900	47000	294908
338	12.60	0.893	44000	286298
343	11.90	0.885	41000	279016

Table 6.8, continued…

348	11.30	0.875	37300	258378
353	10.70	0.870	34700	251391
358	10.20	0.860	31500	232467
363	9.70	0.855	29300	222872
368	9.20	0.855	28300	221679
373	8.80	0.852	27000	218001
378	8.40	0.847	25100	208905
383	8.00	0.845	24000	206978
388	7.70	0.843	22800	202031
393	7.40	0.845	22200	201349

From the parameter values listed in Table 6.8, diffusion coefficient (*D*), mobility (μ) and number density (*n*) of charge carriers for C2 electrolyte at different temperatures were calculated using equations (4.16), (4.17) and (4.18), respectively. The calculated values are listed in Table 6.9. Figures 6.16 show the plots of *D*, μ and *n* free ions at different temperatures, respectively.

Table 6.9: *D*, μ and *n* for C2 values electrolyte at different temperatures.

T **(K)**	***D*** **($\times 10^{-6}$ cm^2 s^{-1})**	***μ*** **($\times 10^{-5}$ cm^2 V^{-1} s^{-1})**	***n*** **($\times 10^{20}$ cm^{-3})**
298	2.453	9.551	4.025
303	2.445	9.364	4.421
308	2.436	9.178	4.833
313	2.432	9.017	5.266
318	2.429	8.863	5.692
323	2.425	8.710	6.178
328	2.412	8.534	6.708
333	2.407	8.386	7.237
338	2.401	8.243	7.771
343	2.398	8.112	8.362
348	2.390	7.968	8.965
353	2.388	7.849	9.611
358	2.382	7.720	10.250
363	2.376	7.595	10.956
368	2.362	7.446	11.783
373	2.355	7.325	12.523
378	2.351	7.216	13.317
383	2.343	7.098	14.215
388	2.339	6.995	14.986
393	2.327	6.871	15.875

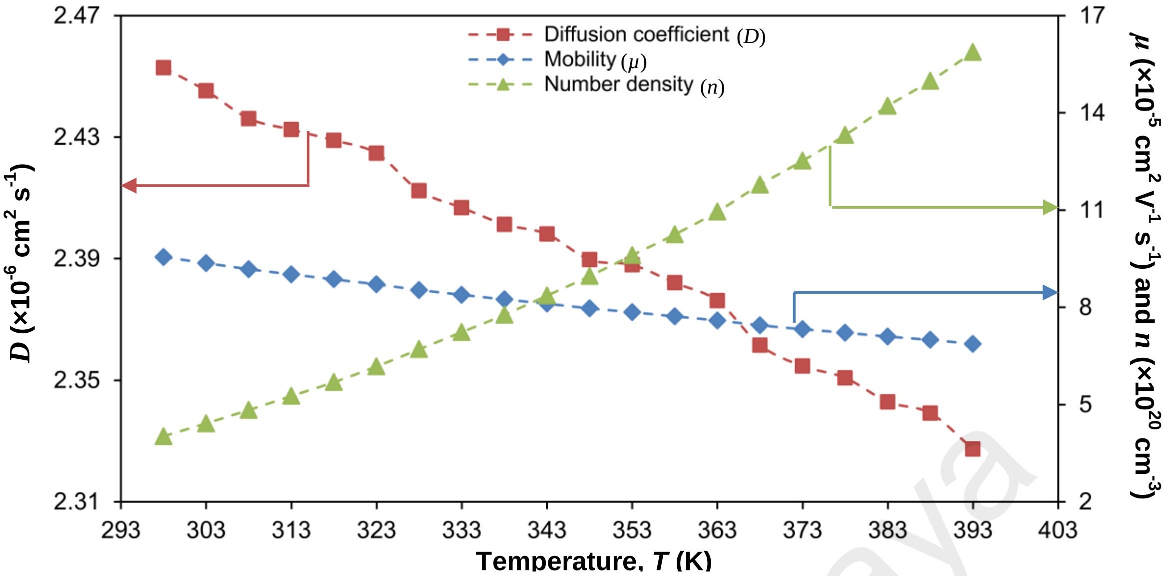

Figure 6.16: *D*, *μ* and *n* of mobile ions for C2 electrolyte at different temperatures.

From Figures 6.16, increasing temperature has increased both diffusion coefficient and mobility of charge carriers of C2 electrolyte. Number density of charge carriers for C2 electrolyte is observed to increase with temperature.

Figure 6.17 presents the Nyquist plot and the fitted points for C3 electrolyte at different temperatures. Table 6.10 listed all fitted parameters obtained in Figure 6.17.

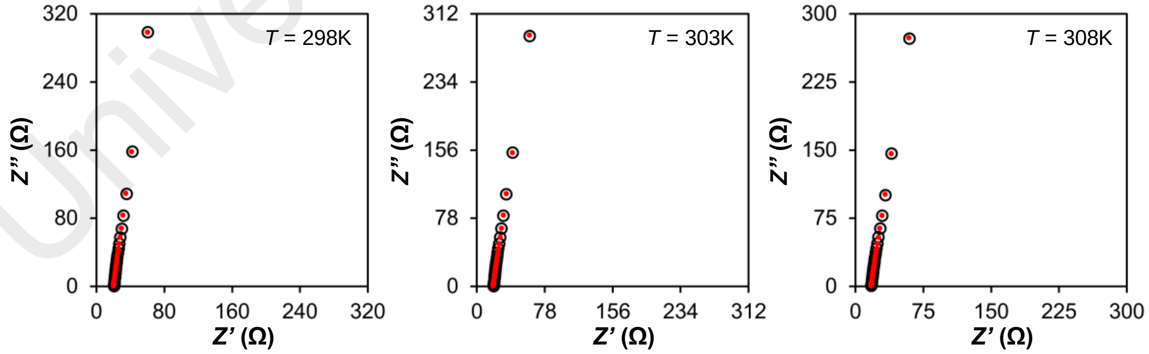

Figure 6.17, continued…

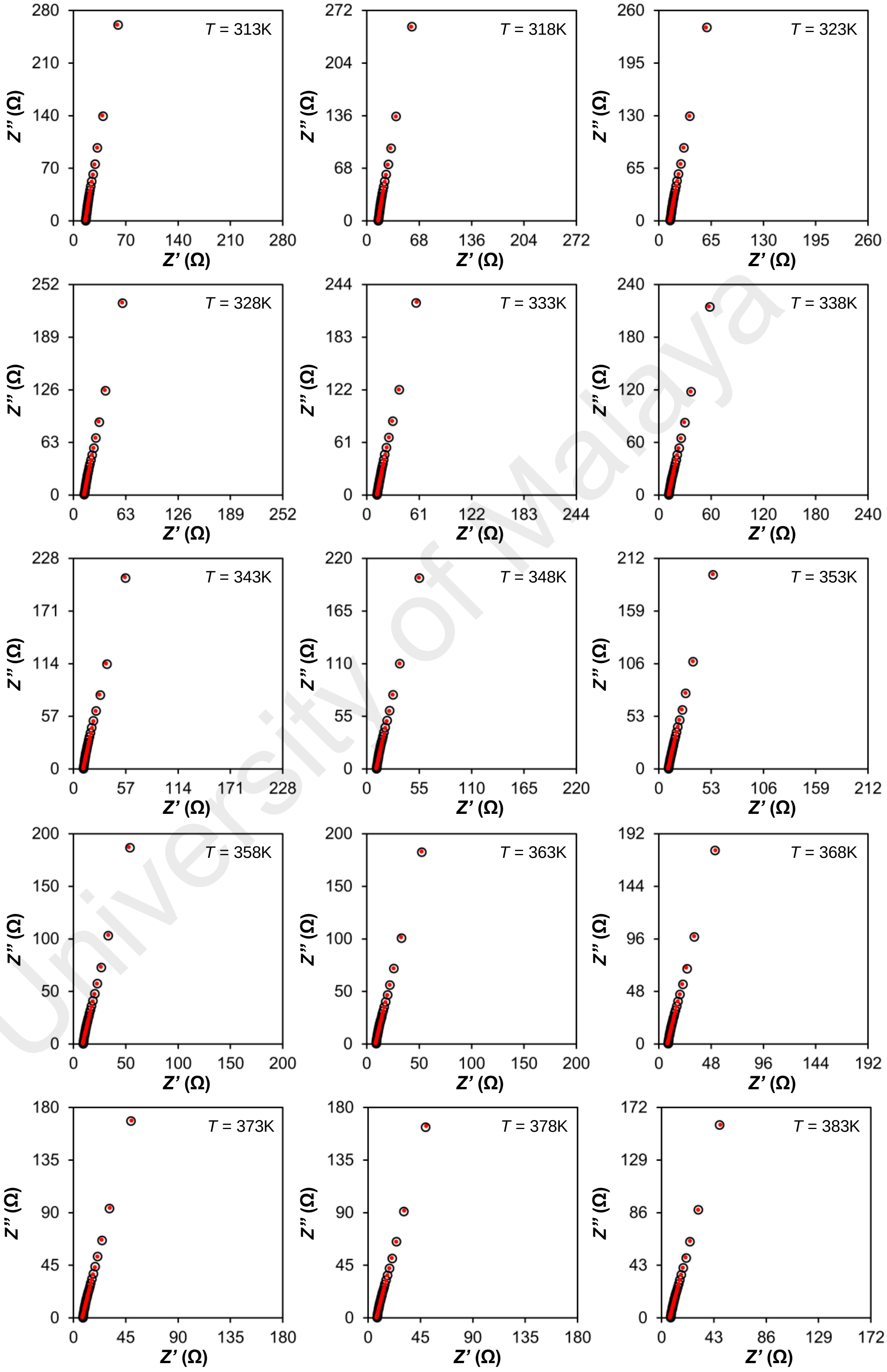

Figure 6.17, continued…

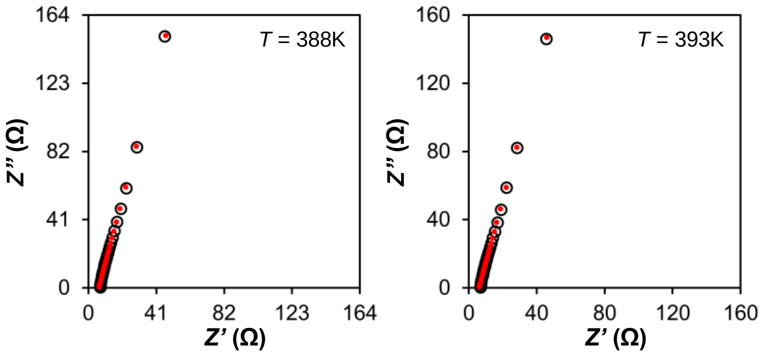

Figure 6.17: Nyquist plot (o) and their corresponding fitted points (●) for C3 electrolyte at different temperatures.

Table 6.10: Values of R, p_2, k_2 and ω_2 for C3 electrolyte obtained from fitting of Nyquist plot at different temperatures.

T (K)	R (Ω)	p_2	k_2 (F^{-1})	ω_2 (s^{-1})
298	20.00	0.915	58000	261657
303	18.40	0.908	53800	261375
308	17.00	0.903	49800	259614
313	15.70	0.897	46000	258506
318	14.60	0.892	43000	257801
323	13.60	0.882	38800	245526
328	12.60	0.875	36000	245031
333	11.80	0.870	34000	244131
338	11.10	0.865	31800	240058
343	10.40	0.863	30400	239196
348	9.80	0.860	28800	238998
353	9.20	0.855	27500	238424
358	8.70	0.853	26000	232628
363	8.20	0.850	25000	231420
368	7.75	0.845	23500	226530
373	7.35	0.843	22200	224711
378	7.00	0.838	21000	221020
383	6.60	0.836	20000	217504
388	6.30	0.834	19000	212601
393	6.00	0.832	18200	212394

From the parameter displayed listed in Table 6.10, transport properties of charge carriers for C3 electrolyte at different temperatures were calculated using equations (4.16), (4.17) and (4.18), respectively. The values that have been calculated are listed in Table 6.11. Figures 6.18 present the plots of diffusion coefficient, mobility and number density of charge carriers at different temperatures, respectively.

Table 6.11: Values of *D*, μ and *n* for C3 electrolyte at different temperatures.

T **(K)**	***D*** **($\times10^{-6}$ cm^2 s^{-1})**	***μ*** **($\times10^{-5}$ cm^2 V^{-1} s^{-1})**	***n*** **($\times10^{20}$ cm^{-3})**
298	2.450	9.539	4.231
303	2.447	9.372	4.681
308	2.445	9.212	5.154
313	2.444	9.061	5.674
318	2.442	8.910	6.205
323	2.440	8.766	6.771
328	2.439	8.628	7.425
333	2.435	8.484	8.063
338	2.432	8.350	8.709
343	2.423	8.195	9.471
348	2.420	8.069	10.208
353	2.411	7.925	11.072
358	2.401	7.783	11.921
363	2.388	7.632	12.897
368	2.381	7.509	13.872
373	2.380	7.404	14.833
378	2.377	7.295	15.807
383	2.362	7.156	17.091
388	2.354	7.038	18.204
393	2.349	6.935	19.399

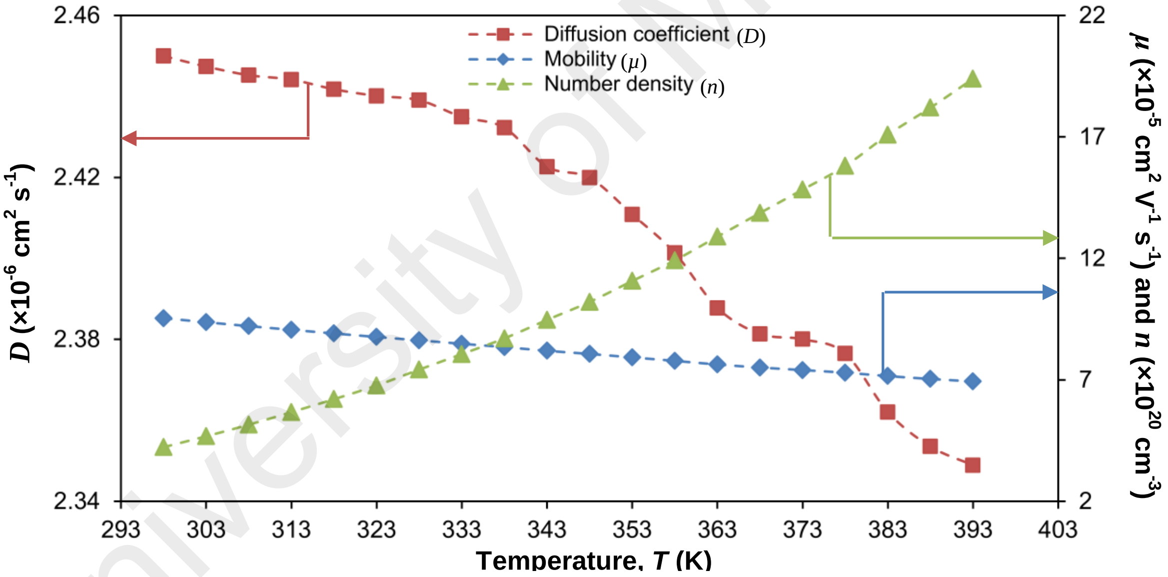

Figure 6.18: Diffusion coefficient, mobility and number density of free ions for C3 electrolyte at different temperatures.

From Figure 6.18 and, *D* and μ of C3 electrolyte is decrease with temperature increased from 298 K to 393 K. *n* for C3 electrolyte is observed to increase with temperature.

Figure 6.19 presents the Nyquist plot and the corresponding fitted points for C4 electrolyte at different temperatures. All fitted parameters obtained in Figure 6.19 were displayed in Table 6.12.

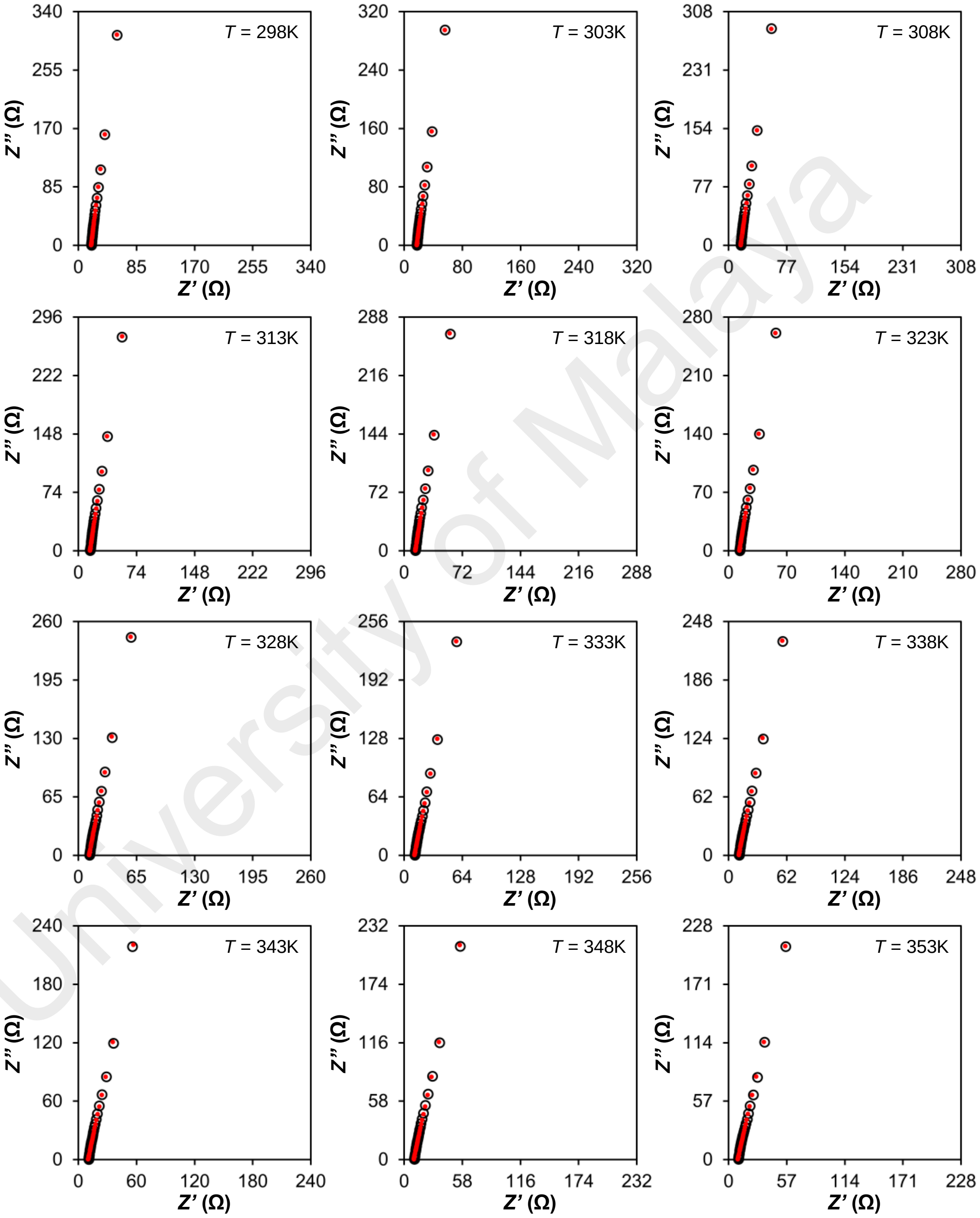

Figure 6.19, continued…

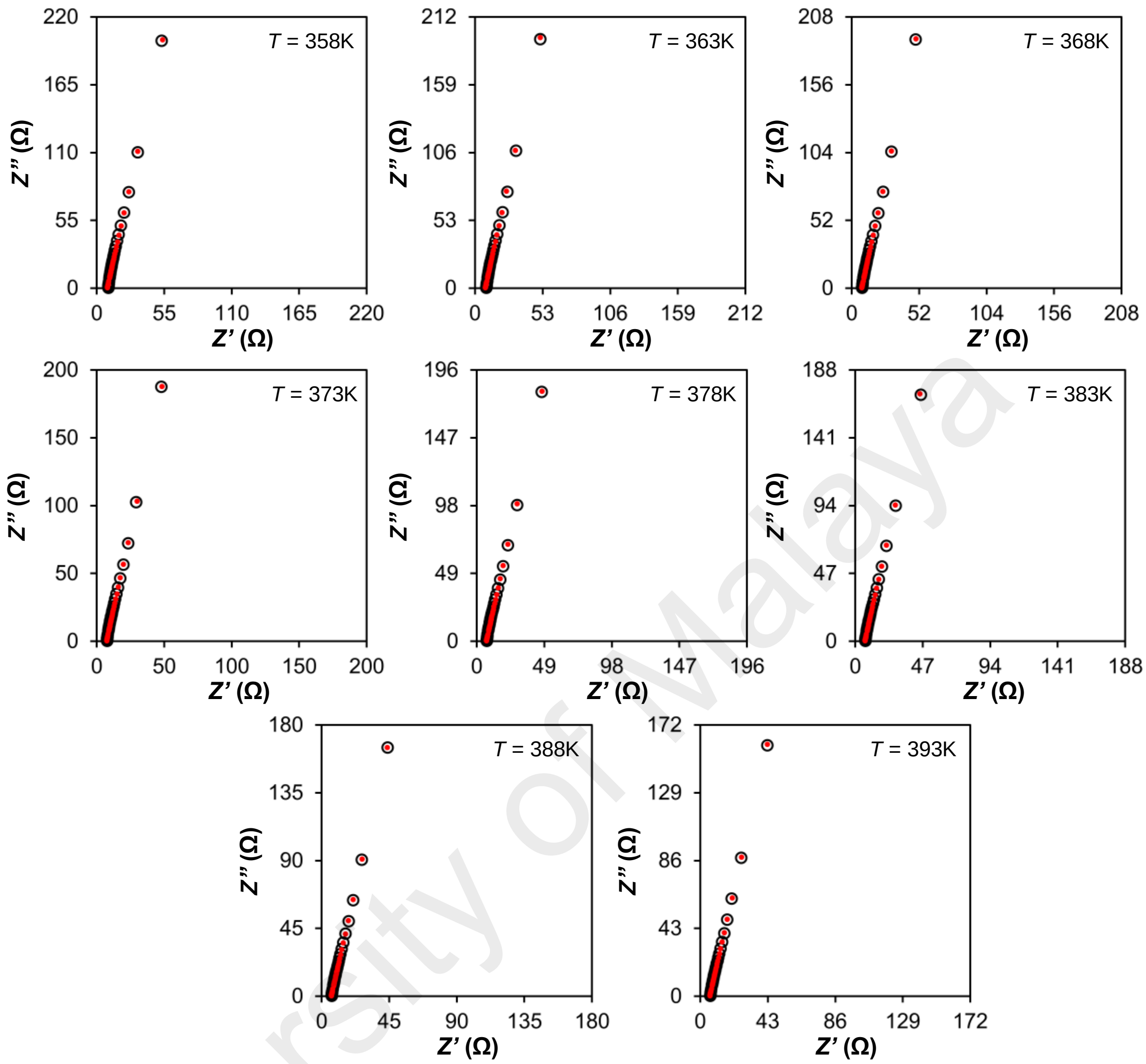

Figure 6.19: Nyquist plot (o) and their corresponding fitted points (●) for C4 electrolyte at different temperatures.

Table 6.12: Values of R, p_2, k_2 and ω_2 for C4 electrolyte obtained from fitting of Nyquist plot at different temperatures.

T (K)	R (Ω)	p_2	k_2 (F^{-1})	ω_2 (s^{-1})
298	18.70	0.925	62000	309856
303	17.10	0.917	58000	308893
308	15.90	0.910	54000	306770
313	14.80	0.905	50000	302120
318	13.80	0.900	48000	298332
323	12.90	0.895	45500	292242
328	12.00	0.880	39000	258664
333	11.30	0.877	37000	254085
338	10.70	0.872	35000	248816
343	10.00	0.867	33000	242583

Table 6.12, continued...

348	9.50	0.865	31500	240192	373	7.20	0.863	27500	233323
353	8.90	0.860	30000	238939	378	6.90	0.860	26000	227489
358	8.50	0.860	29000	237543	383	6.60	0.860	24700	223355
363	8.00	0.862	28500	236541	388	6.30	0.858	23500	219852
368	7.60	0.863	28000	236065	393	6.00	0.856	22500	218379

From the parameter values shown in Table 6.12, diffusion coefficient, mobility and concentration of charge carriers for C4 electrolyte at different temperatures were calculated using the equations mention previously. The calculation values are listed in Table 6.13. Figure 6.20 display the plots of diffusion coefficient, mobility and number density of charge carriers at different temperatures, respectively.

Table 6.13: *D*, *μ* and *n* values for C4 electrolyte at different temperatures.

T **(K)**	***D*** **($\times 10^{-6}$ cm^{2} s^{-1})**	***μ*** **($\times 10^{-5}$ cm^{2} V^{-1} s^{-1})**	***n*** **($\times 10^{20}$ cm^{-3})**	***T*** **(K)**	***D*** **($\times 10^{-6}$ cm^{2} s^{-1})**	***μ*** **($\times 10^{-5}$ cm^{2} V^{-1} s^{-1})**	***n*** **($\times 10^{20}$ cm^{-3})**
298	2.448	9.532	4.529	348	2.351	7.840	10.838
303	2.440	9.343	5.052	353	2.336	7.680	11.810
308	2.438	9.183	5.528	358	2.324	7.531	12.609
313	2.435	9.028	6.042	363	2.285	7.305	13.812
318	2.419	8.826	6.627	368	2.254	7.106	14.947
323	2.404	8.637	7.245	373	2.210	6.875	16.307
328	2.399	8.486	7.926	378	2.205	6.767	17.287
333	2.387	8.317	8.589	383	2.197	6.657	18.371
338	2.378	8.163	9.241	388	2.189	6.545	19.576
343	2.360	7.983	10.112	393	2.178	6.430	20.924

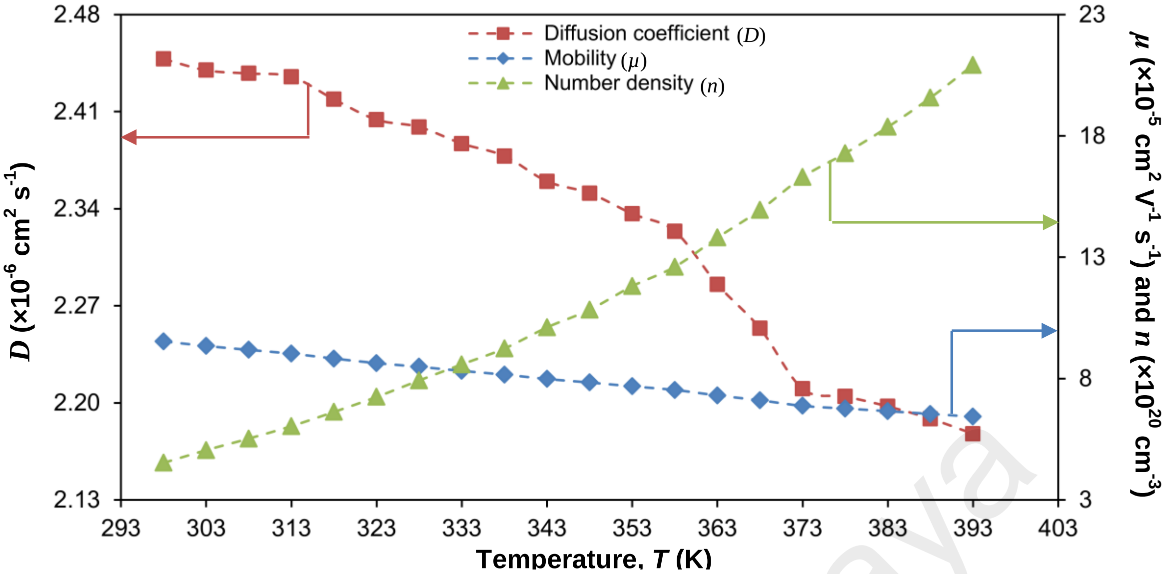

Figure 6.20: Plot of D, μ and n for C4 electrolyte at different temperatures.

The increase in temperature has increased diffusion coefficient and mobility of free ions of C4 electrolyte as shown in Figure 6.20. The number density of charge carriers for C4 electrolyte is observed to increase with temperature.

Figure 6.21 shows the Nyquist plot and their corresponding fitted point for C5 electrolyte at different temperatures. Table 6.14 lists all fitted parameters obtained in Figure 6.21.

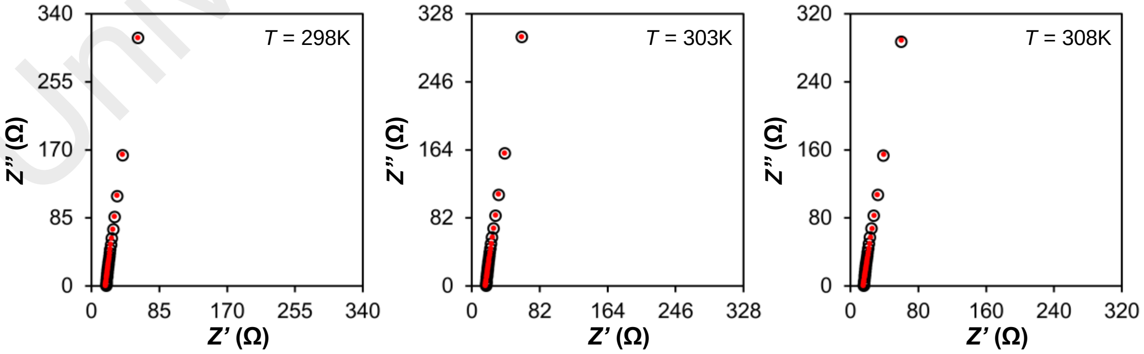

Figure 6.21, continued…

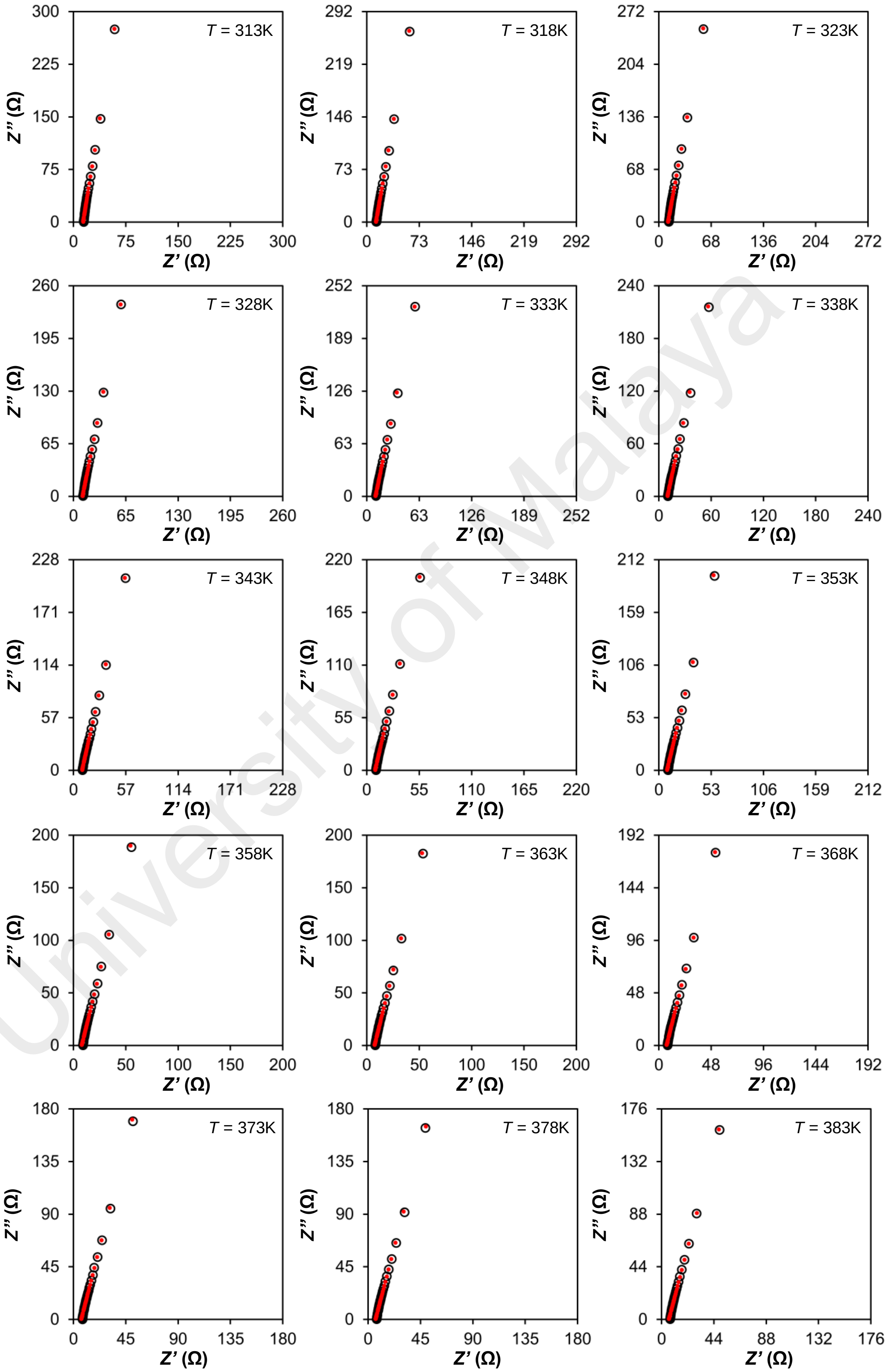

Figure 6.21, continued…

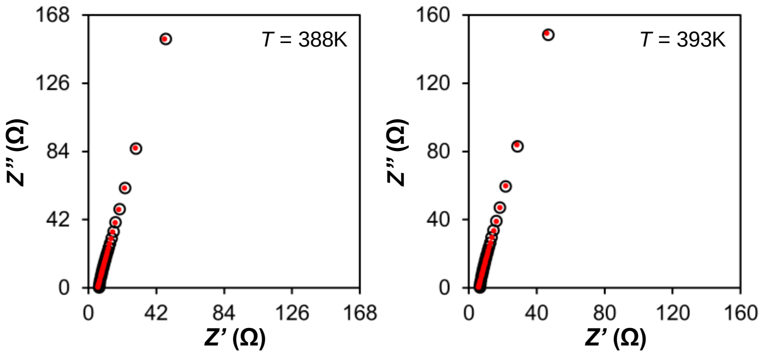

Figure 6.21: Nyquist plot (o) and their corresponding fitted points (●) for C5 electrolyte at different temperatures.

Table 6.14: R, p_2, k_2 and ω_2 values for C5 electrolyte obtained from fitting of Nyquist plot at different temperatures.

T (K)	R (Ω)	p_2	k_2 (F^{-1})	ω_2 (s^{-1})
298	17.20	0.917	61000	332990
303	15.90	0.908	56200	330567
308	14.70	0.901	52000	328222
313	13.70	0.897	48500	327293
318	12.80	0.890	45000	320454
323	11.90	0.885	41300	312526
328	11.20	0.875	37000	284756
333	10.50	0.870	34500	272200
338	9.80	0.865	32000	263189
343	9.30	0.860	30000	257045
348	8.70	0.855	28300	255459
353	8.20	0.850	26800	252631
358	7.80	0.847	25500	246846
363	7.40	0.845	24300	243738
368	7.00	0.843	23200	243384
373	6.60	0.840	22100	239386
378	6.30	0.837	21000	235396
383	6.00	0.835	20000	232285
388	5.70	0.832	19000	228857
393	5.50	0.832	18500	229172

From the parameter values listed in Table 6.14, D, μ and n of free mobile ions for C5 electrolyte at different temperatures were calculated. The calculated values are listed in Table 6.15. Figure 6.22 show the plots of D, μ and n of free mobile ions at different temperatures, respectively.

Table 6.15: Values of D, μ and n for C5 electrolyte at different temperatures.

T (K)	D ($\times10^{-6}$ cm^2 s^{-1})	μ ($\times10^{-5}$ cm^2 V^{-1} s^{-1})	n ($\times10^{20}$ cm^{-3})
298	2.444	9.515	4.932
303	2.443	9.356	5.426
308	2.441	9.196	5.971
313	2.440	9.046	6.514
318	2.437	8.892	7.092
323	2.435	8.746	7.756
328	2.426	8.583	8.397
333	2.413	8.409	9.142
338	2.403	8.251	9.983
343	2.400	8.120	10.689
348	2.393	7.980	11.627
353	2.386	7.841	12.554
358	2.375	7.696	13.446
363	2.365	7.561	14.427
368	2.358	7.436	15.507
373	2.342	7.286	16.785
378	2.336	7.172	17.866
383	2.329	7.055	19.069
388	2.320	6.938	20.411
393	2.314	6.831	21.485

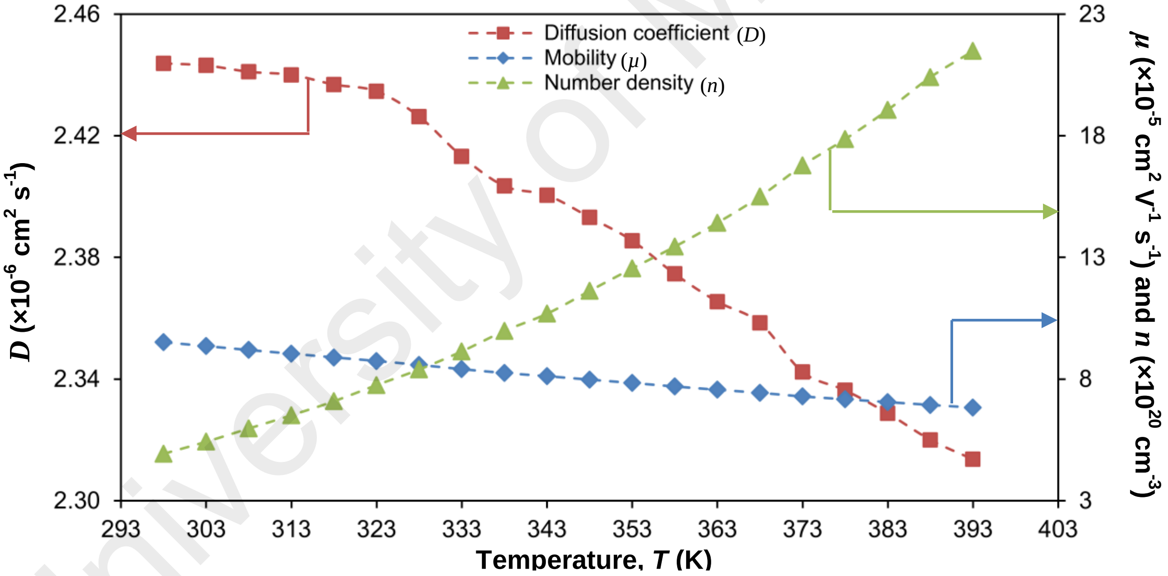

Figure 6.22: Diffusion coefficient, mobility and concentration of free ions for C5 electrolyte at different temperatures.

It is observed in Figure 6.22 that diffusion coefficient and mobility of C5 electrolyte decrease as the temperature increased. Number density of free mobile ions for C5 electrolyte is observed to increase with temperature.

6.4. Summary

The effect of BMII ionic liquid in PVA–LiBOB–TBAI–I_2–DMF gel polymer electrolyte has been studied by fourier transform infrared (FTIR) spectroscopy and electrical impedance spectroscopy (EIS). In FTIR section, the shifting of the hydroxyl group of PVA to higher wavenumbers proved that interaction between polymer and salt has occurred. The presence of bands corresponding to of PVA, LiBOB, TBAI, BMII ionic liquid and DMF in PVA–LiBOB–TBAI–BMII–I_2–DMF gel polymer electrolyte infrared spectrum implies the complexation between polymer, salts, ionic liquid and plasticizer has occurred. The FTIR deconvolution corresponding to LiBOB free ions band shows the percentage of free ions in electrolytes is almost constant. EIS shows that the addition of 1 wt.% BMII ionic liquid into C0 electrolyte (0 wt.% BMII ionic liquid) increased the ionic conductivity from 5.13×10^{-3} S cm^{-1} to 5.43×10^{-3} S cm^{-1}. With increasing amounts of BMII ionic liquid up to 9 wt.% in C0 electrolyte, the ionic conductivity was observed to increase up to 7.52×10^{-3} S cm^{-1}. The conductivity–temperature dependence showed that conductivity of PVA–LiBOB–TBAI–BMII–I_2–DMF gel polymer electrolyte increased with increasing temperature. The transport properties of charge carriers for PVA–LiBOB–TBAI–BMII–I_2–DMF gel polymer electrolyte system have been calculated at room and varied temperature. The entire electrolytes prepared in this third system were used as a medium for charge transfer in dye sensitized solar cells (DSSC). The performance of DSSC will be discussed in Chapter 7.

CHAPTER 7 : RESULTS FOR DYE SENSITIZED SOLAR CELLS

7.1. Introduction

In this chapter, all gel polymer electrolytes prepared in the second and third systems have been used as a medium for electron transfer in DSSCs. The electrolytes were sandwiched between TiO_2/dye photoanode and Pt electrode, and the photocurrent density–voltage (*J–V*) characteristics were determined. The dye used was ruthenium 535–bis–tetrabutylammonium (TBA) or also known as N719.

7.2. PVA–LiBOB–TBAI–I_2–DMF Gel Polymer Electrolyte Systems

All electrolytes prepared in system 2 were used as a medium for electron transfer in DSSCs except the B0 electrolyte. This is because B0 electrolyte does not have an iodide ion that is important for redox process in DSSC application. Figure 7.1 shows the photocurrent density–voltage (*J–V)* curves for DSSCs fabricated with PVA gel polymer electrolytes containing different compositions of LiBOB and TBAI salts. The DSSCs were illuminated under 1000 W m^{-2} or 1 sun at room temperature. The performance parameters for DSSCs obtained from the *J–V* curves are listed in Table 7.1.

From Table 7.1, it can be seen that the open circuit voltage (V_{oc}) of PVA–LiBOB–TBAI–I_2–DMF gel polymer electrolyte increased with decreasing LiBOB salt composition. The short circuit current density (J_{sc}) of the second electrolyte system is observed to increase from 8.79 mA cm^{-2} to a maximum of 13.05 mA cm^{-2} at B5 electrolyte. Beyond B5 electrolyte composition, the J_{sc} is observed to decrease to 11.04 mA cm^{-2}. The solar conversion efficiency is seen to follow the same trend as J_{sc} where the B5 electrolyte gives a maximum solar conversion efficiency of 6.11%.

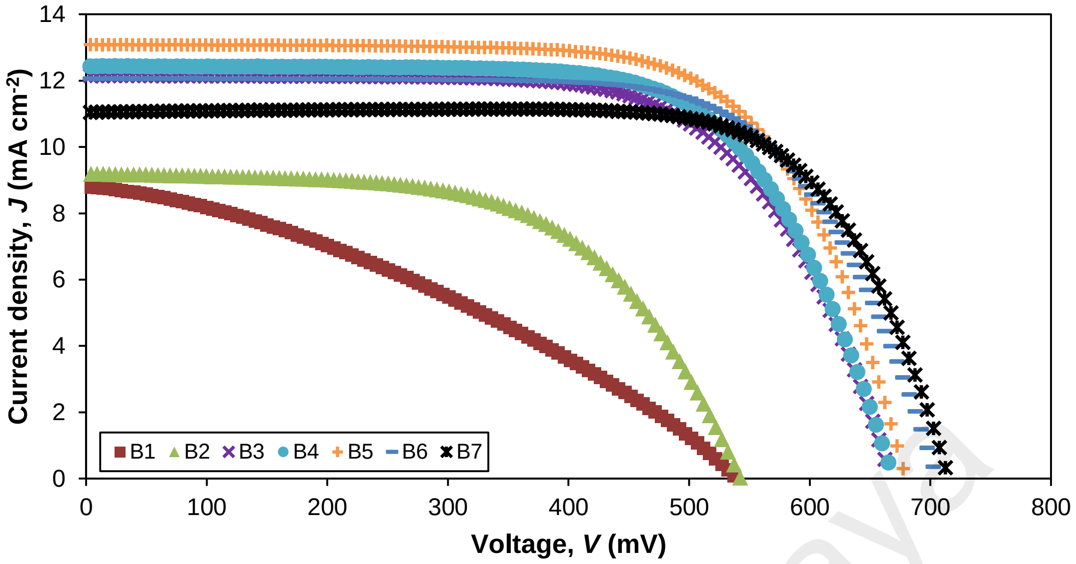

Figure 7.1: *J–V* characteristics for DSSCs fabricated with PVA–LiBOB–TBAI–I_2–DMF gel polymer electrolyte.

Table 7.1: Values of V_{oc}, J_{sc}, *FF* and η for DSSCs fabricated with PVA–LiBOB–TBAI–I_2–DMF gel polymer electrolyte.

Electrolyte	**V_{oc} (mV)**	**J_{sc} (mA cm^{-2})**	**Fill Factor, *FF* (%)**	**Efficiency, η (%)**
B1	537	8.79	34.84	1.65
B2	542	9.19	58.71	2.93
B3	657	12.15	67.19	5.36
B4	665	12.43	68.03	5.63
B5	682	13.05	68.62	6.11
B6	703	12.06	68.76	5.83
B7	713	11.04	72.10	5.67

One of the objectives of doing this work is to study the effect of LiBOB salt in DSSC performance. LiBOB salt is used in the electrolyte to provide a large number of Li^+ which can modify the surface states of the TiO_2 semiconducting layer of the photoanode and increase the rate of electron injection from dye excited–state into the conduction band of TiO_2. Usually an iodide salt is used in DSSC. Thus, in order to study the effect of LiBOB salt in DSSC, lithium iodide (LiI) and potassium iodide (KI) salts was used to replace LiBOB salt in the electrolyte. Tables 7.2 and 7.3 show the compositions of the electrolytes containing LiI and KI salts with their corresponding designations, respectively.

Table 7.2: Composition and designation of PVA–LiI–TBAI–I_2–DMF gel polymer electrolytes system.

Designation	**PVA (g)**	**LiI (g)**	**TBAI (g)**	**I_2 (g)**	**DMF (g)**	**LiI : TBAI (wt.% : wt %) composition**
L3	0.5000	0.0833	0.2500	0.0172	2.0000	25 : 75
L4	0.5000	0.0667	0.2666	0.0183	2.0000	20 : 80
L5	0.5000	0.0500	0.2833	0.0195	2.0000	15 : 85
L6	0.5000	0.0333	0.3000	0.0206	2.0000	10 : 90

Table 7.3: Composition and designation of PVA–KI–TBAI–I_2–DMF gel polymer electrolytes system.

Designation	**PVA (g)**	**KI (g)**	**TBAI (g)**	**I_2 (g)**	**DMF (g)**	**KI : TBAI (wt.% : wt %) composition**
K3	0.5000	0.0833	0.2500	0.0172	2.0000	25 : 75
K4	0.5000	0.0667	0.2666	0.0183	2.0000	20 : 80
K5	0.5000	0.0500	0.2833	0.0195	2.0000	15 : 85
K6	0.5000	0.0333	0.3000	0.0206	2.0000	10 : 90

Figure 7.2 shows the *J–V* curves for DSSCs fabricated with PVA gel polymer electrolytes containing different compositions of LiI and TBAI salts. The DSSCs were illuminated under 1000 W m^{-2} or 1 sun at room temperature. The performance parameters for DSSCs obtained from the *J–V* curves are listed in Table 7.4.

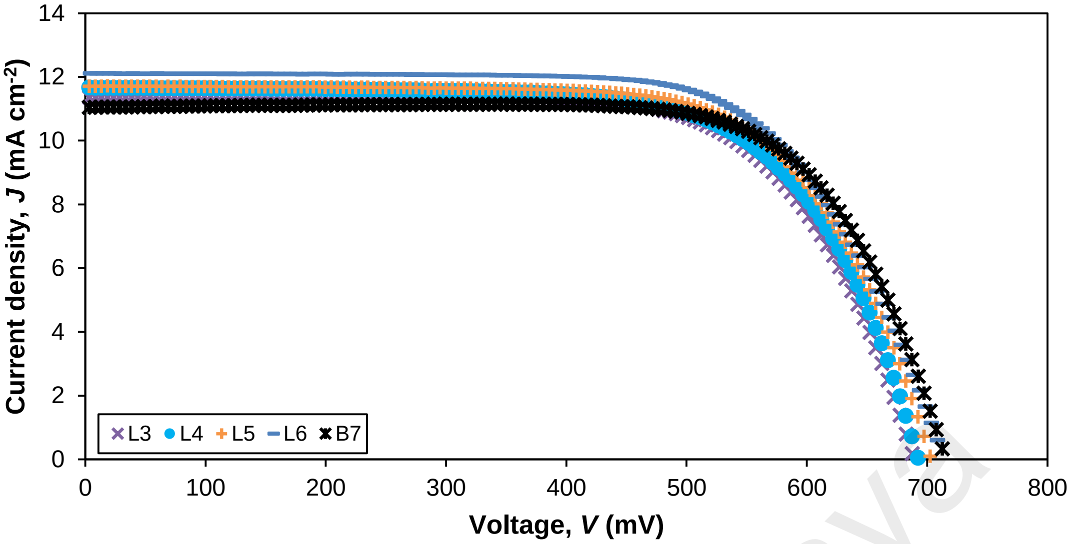

Figure 7.2: *J*–*V* characteristics for DSSCs fabricated with PVA–LiI–TBAI–I_2–DMF gel polymer electrolyte.

Table 7.4: Values of V_{oc}, J_{sc}, *FF* and *η* for DSSCs fabricated with PVA–LiI–TBAI–I_2–DMF gel polymer electrolyte.

Electrolyte	**V_{oc} (mV)**	**J_{sc} (mA cm^{-2})**	**Fill Factor, *FF* (%)**	**Efficiency, *η* (%)**	**Conductivity, *σ* (mS cm^{-1})**
L3	688	11.36	69.56	5.43	5.17
L4	692	11.66	68.36	5.52	5.05
L5	703	11.71	70.69	5.82	4.68
L6	709	12.00	69.74	5.93	4.52
B7	713	11.04	72.10	5.67	4.35

From Table 7.4, it can be seen that the V_{oc} of PVA–LiI–TBAI–I_2–DMF gel polymer electrolyte increased with decreasing LiI salt composition. The J_{sc} of DSSC is observed to increase from 11.36 mA cm^{-2} to a maximum of 12.00 mA cm^{-2} on replacing LiBOB with LiI. The *η* is seen to follow the same trend as J_{sc} where the L6 electrolyte gives a maximum solar conversion efficiency of 5.93%.

J–*V* curves for DSSCs fabricated with PVA gel polymer electrolytes containing different compositions of KI and TBAI salts is shown in Figure 7.3. The DSSCs were illuminated under 1000 W m^{-2} at room temperature. Table 7.5 listed the performance parameters for DSSCs obtained from the *J*–*V* curves.

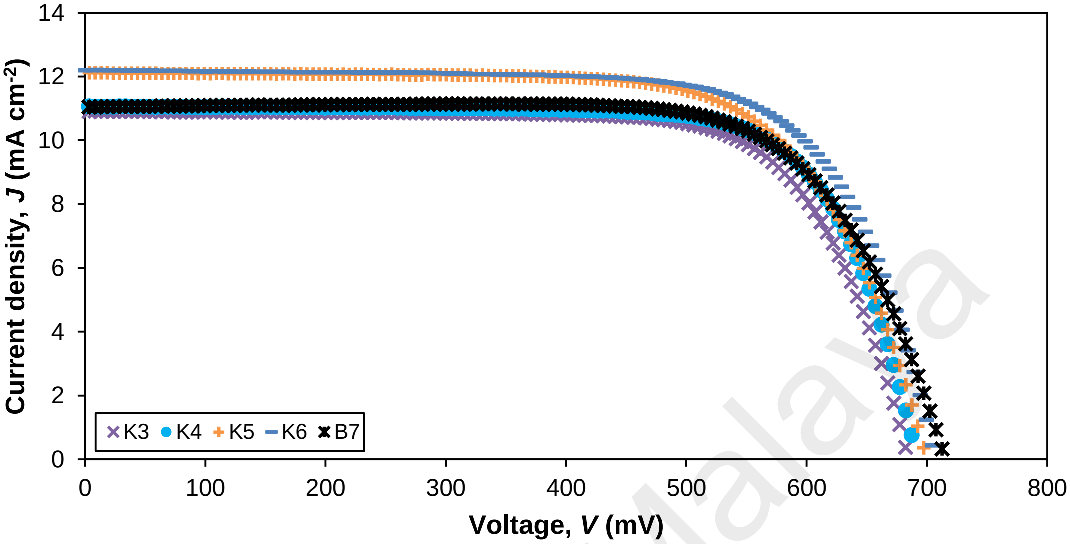

Figure 7.3: *J*–*V* characteristics for DSSCs fabricated with PVA–KI–TBAI–I_2–DMF gel polymer electrolyte.

Table 7.5: Values of V_{oc}, J_{sc}, *FF* and η for DSSCs fabricated with PVA–KI–TBAI–I_2–DMF gel polymer electrolyte.

Electrolyte	V_{oc} (mV)	J_{sc} (mA cm^{-2})	Fill Factor, *FF* (%)	Efficiency, η (%)	Conductivity, σ (mS cm^{-1})
K3	682	10.91	73.15	5.44	6.05
K4	687	11.06	74.88	5.70	5.83
K5	698	12.12	70.21	5.93	5.31
K6	705	12.20	71.81	6.17	5.15
B7	713	11.04	72.10	5.67	4.35

From Table 7.5, it can be seen that the open circuit voltage of PVA–KI–TBAI–I_2–DMF gel polymer electrolyte increased with decreasing KI salt content. The J_{sc} value is observed to increase from 10.91 mA cm^{-2} to a maximum of 12.20 mA cm^{-2} at K6 electrolyte. Beyond K6 electrolyte composition, the J_{sc} is observed to decrease to 11.04 mA cm^{-2}. The solar conversion efficiency is seen to follow the same trend as J_{sc} where the K6 electrolyte gives a maximum solar conversion efficiency of 6.17%.

Figures 7.4, 7.5 and 7.6 show the plots of V_{oc}, J_{sc} and efficiency against PVA–x–TBAI–I_2–DMF (x = LiBOB, LiI, KI) gel polymer electrolyte at different salt concentration.

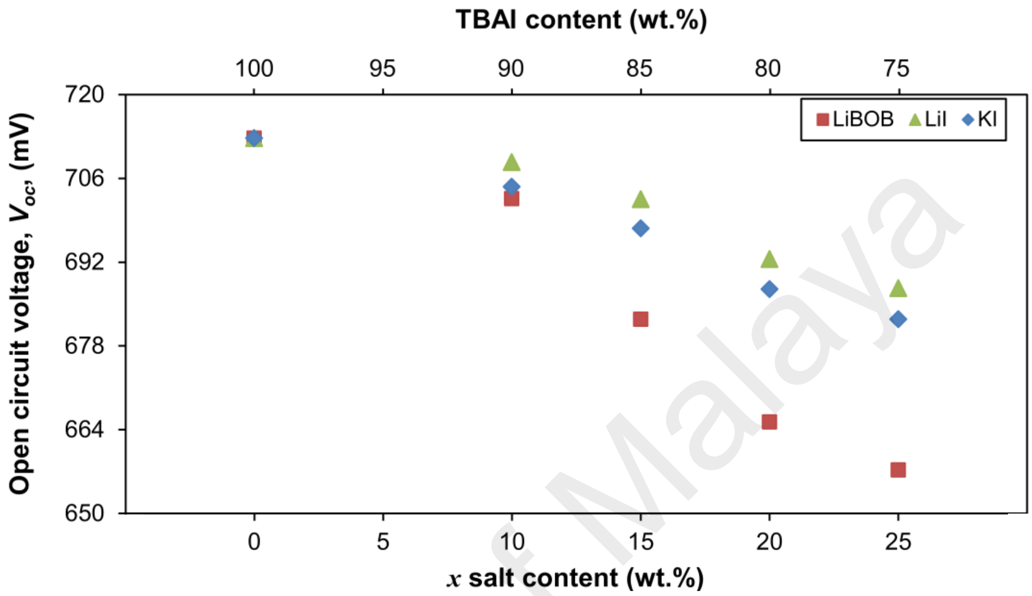

Figure 7.4: Plot of open circuit voltage, V_{oc} of PVA–x–TBAI–I_2–DMF (x = LiBOB, LiI, KI) gel polymer electrolyte at different salt concentration.

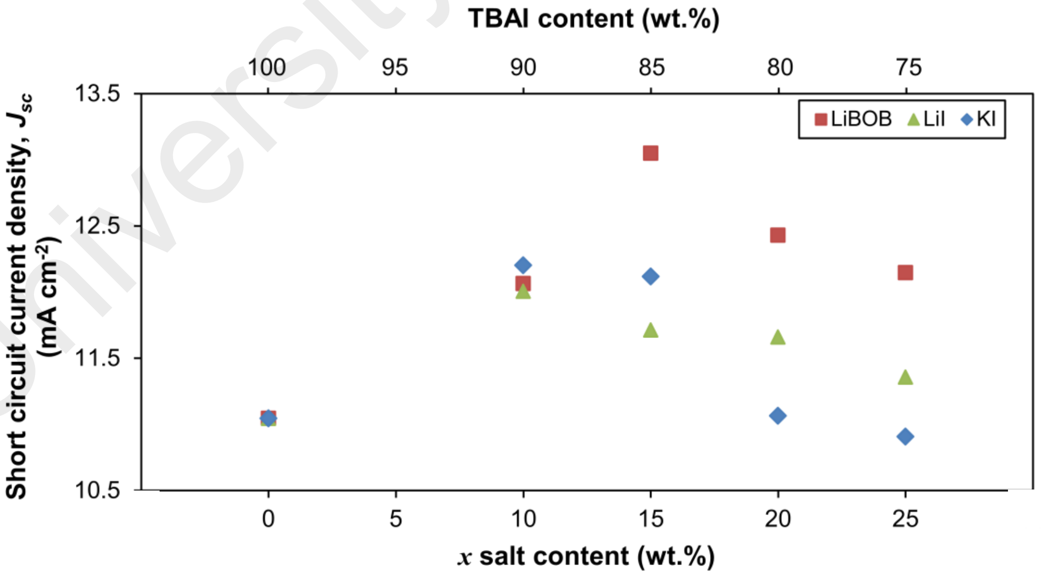

Figure 7.5: Plot of short circuit current density, J_{sc} of PVA–x–TBAI–I_2–DMF (x = LiBOB, LiI, KI) gel polymer electrolyte at different salt concentration.

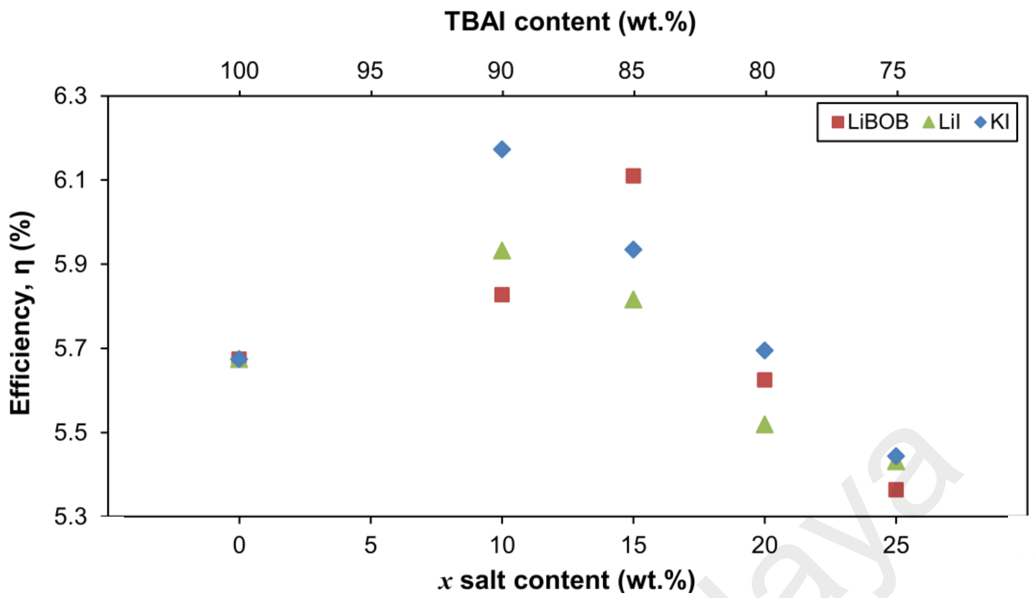

Figure 7.6: Plot of solar conversion efficiency, *η* of PVA–*x*–TBAI–I_2–DMF (*x* = LiBOB, LiI, KI) gel polymer electrolyte at different salt concentration.

7.3. PVA–LiBOB–TBAI–BMII–I_2–DMF Gel Polymer Electrolyte Systems

Figure 7.7 shows the photocurrent density–voltage (*J–V)* curves for DSSCs prepared with gel polymer electrolytes having six different compositions of BMII ionic liquid at room temperature. Table 7.6 lists the performance parameters for the DSSCs obtained from *J–V* curve analysis.

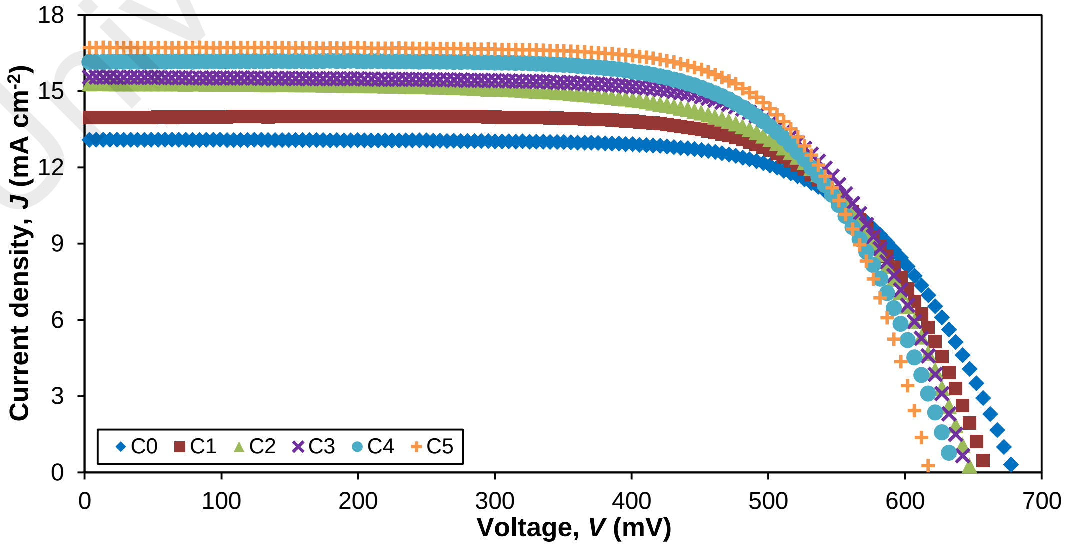

Figure 7.7: *J–V* characteristics for DSSCs fabricated with PVA–LiBOB–TBAI–BMII–I_2–DMF gel polymer electrolyte.

Table 7.6: Values of J_{sc}, V_{oc}, FF and η for DSSCs fabricated with PVA–LiBOB–TBAI–BMII–I_2–DMF gel electrolyte.

Electrolyte	**V_{oc} (mV)**	**J_{sc} (mA cm^{-2})**	**Fill Factor, FF (%)**	**Efficiency, η (%)**
C0	682	13.05	68.62	6.11
C1	657	13.95	69.30	6.35
C2	647	15.30	66.37	6.57
C3	642	15.54	69.07	6.89
C4	632	16.15	67.74	6.91
C5	617	16.71	70.58	7.28

From Table 7.6, it can be seen that the V_{oc} value for C0 electrolyte is 682 mV. As 1 wt.% of BMII ionic liquid is added into the gel polymer electrolyte (C1 electrolyte), the V_{oc} of the DSSC is observed to decrease to 657 mV. Increasing the amount of BMII ionic liquid in the electrolyte up to 9 wt.% (C5 electrolyte) is seen to decrease the V_{oc} value to 617 mV. The J_{sc} value of DSSC assembled with electrolyte in system 3 is observed to increase as the amount of BMII ionic liquid in the electrolyte increase. The solar conversion efficiency of the DSSC assembled with PVA–LiBOB–TBAI–BMII–I_2–DMF gel polymer electrolyte is observed to increase from 6.11% with C0 electrolyte to 7.28% with C5 electrolyte.

7.4. Summary

The open circuit voltage, V_{oc} for DSSC assembled with PVA–LiBOB–TBAI–I_2–DMF gel polymer electrolyte increased with decreasing LiBOB salt concentration. The short circuit current density, J_{sc} of the DSSC containing B5 electrolyte is the highest compared to the other electrolyte. The solar conversion efficiency of DSSC followed the same trend as J_{sc}. The highest solar conversion efficiency obtained in second electrolyte system is 6.11%. DSSC using second electrolyte system was compared with

DSSC using electrolyte consisting of LiI and KI salts. The V_{oc} value for DSSC assembled with PVA–LiI–TBAI–I_2–DMF and PVA–KI–TBAI–I_2–DMF gel polymer electrolyte increased with decreasing LiI and KI salt concentration, respectively. The highest J_{sc} value obtained for DSSC using electrolyte consisting of LiI is 12.00 mA cm^{-2} while DSSC using electrolyte consists of KI is 12.20 mA cm^{-2}. The highest solar conversion efficiency obtained for DSSC using electrolyte consists of LiI is 5.93% while DSSC using electrolyte consists of KI is 6.17%. For DSSC assembled with PVA–LiBOB–TBAI–BMII–I_2–DMF gel polymer electrolyte, the open circuit voltage, V_{oc} decreased with increasing BMII ionic liquid content. The short circuit current density, J_{sc} of the DSSC using electrolyte in system 3 increased with increasing BMII ionic liquid content. The solar conversion efficiency of DSSC follows the same trend as J_{sc}. The highest solar conversion efficiency obtained in third electrolyte system is 7.28%.

CHAPTER 8 : DISCUSSION

As stated in the first chapter, the primary objective of this thesis is to produce a high conducting electrolyte (10^{-3} S cm^{-1}) based on PVA and LiBOB salt. The highest conducting sample has composition 60 wt.% PVA–40 wt.% LiBOB and the room temperature conductivity was 2.83×10^{-4} S cm^{-1} in the solid form. This result is higher than that of 50 wt.% PAN–50 wt.% LiBOB (2.55×10^{-5} S cm^{-1}) (Arof *et al*., 2014b), 50 mole% PEO–1 mole% LiBOB (7×10^{-5} S cm^{-1}) (Appetecchi *et al*., 2004), 85 mole% PEO–15 mole% $LiClO_4$ (3.98×10^{-7} S cm^{-1}) (Karmakar & Ghosh, 2012), 70 mole% PEO–30 mole% $LiCF_3SO_3$ (1.63×10^{-6} S cm^{-1}) (Karan *et al*., 2008), 80 mole% PAN–20 mole% $LiClO_4$ (6.51×10^{-7} S cm^{-1}) (Yang *et al*., 1996) and 65 wt.% PMMA–35 wt.% $LiCF_3SO_3$ (9.88×10^{-5} S cm^{-1}) (Ramesh & Wong, 2009). This can be attributed to the higher dielectric constant of PVA ($\varepsilon_r = 8.1$) compared to PAN ($\varepsilon_r = 5.0$), PEO ($\varepsilon_r = 4.5$) and PMMA ($\varepsilon_r = 4.0$) (Thomas *et al*., 2012) that indicates PVA being able to solvate LiBOB and other lithium salt to a higher extent and therefore provide more ions for conduction. It may also be observed that less amount of LiBOB is required in the PVA based electrolyte compared to PAN based electrolyte.

Since only 40 wt.% LiBOB was required to achieve a high conductivity, the strategy taken to enhance conductivity is to jellify the 60 wt.% PVA–40 wt.% LiBOB electrolyte (A4 electrolyte). The conductivity in the gel form was 7.31×10^{-3} S cm^{-1} (B0 electrolyte). However, with this composition the electrolyte could not be used in the fabrication of DSSC with an iodide/triiodide redox couple, although the conductivity is already sufficiently high. Thus, an iodide salt and some iodine (I_2) crystals have to be added. Hence, the electrolyte with composition 17.53 wt.% PVA–1.75 wt.% LiBOB–9.93 wt.% TBAI–0.68 wt.% I_2–70.11 wt.% DMF (B5 electrolyte, $\sigma = 5.13\times10^{-3}$ S cm^{-1})

was obtained and used to fabricate DSSC that gave the highest efficiency of 6.11%. It is to be noted that if we do not consider the amount of I_2 and DMF added, the composition of the electrolyte is 60 wt.% PVA–6 wt.% LiBOB–34 wt.% TBAI indicating that the total amount of salt is 40 wt.%. The conductivity of the 17.53 wt.% PVA–1.75 wt.% LiBOB–9.93 wt.% TBAI–0.68 wt.% I_2–70.11 wt.% DMF electrolyte is less than that of 60 wt.% PVA–40 wt.% LiBOB gel electrolyte. This can be attributed to the lesser number of mobile ions in the former since the electrolyte has only 6 wt.% LiBOB and 34 wt.% TBAI and can be explained because TBAI has a higher lattice energy (512.6 kJ mol^{-1}) compared to that of LiBOB (496 kJ mol^{-1}). The lattice energy of TBAI was calculated based on the radius of TBA$^+$ and I^- using the software obtained from (Sydney, 2009).

As shown by (Bandara *et al*., 2011; Dissanayake *et al*., 2012; Aziz *et al*., 2013), the use of binary iodide salt can improve the efficiency of a DSSC. To further improve our LiBOB–TBAI system, BMII was added. The highest conducting system has composition 15.95 wt.% PVA–1.59 wt.% LiBOB–9.04 wt.% TBAI–9 wt.% BMII–0.62 wt.% I_2–63.8 wt.% DMF (C5 electrolyte, $\sigma = 7.52\times10^{-3}$ S cm^{-1}). The effect of BMII addition must have increase the number density of mobile ions for the conductivity to increase. The DSSC employing this electrolyte exhibited a photon to current efficiency of 7.28%. Thus we have managed to produce a DSSC with I^-/I_3^- redox couple of reasonably high efficiency. It is to be realized that the highest efficiency obtainable from a I^-/I_3^- DSSC is 12.3% using liquid electrolyte (Yella *et al*., 2011). The results obtained in the present work showed that the study on the influence of BMII in the electrolyte and DSSC has been achieved.

In the above discussion, we have mentioned that the increase in conductivity is due to increase in number density of mobile ions. This explanation has been used by

(Ericson *et al*., 2000; Bandara *et al*., 2011; Bandara & Mellander, 2011). However, the explanation given was only qualitative in nature. To quantify this, we have devised a method based on impedance spectroscopy to obtain the number density of mobile ions. For the 60 wt.% PVA–40 wt.% LiBOB gel electrolyte, the number density of mobile ions was 5.42×10^{20} cm^{-3}. For the 17.53 wt.% PVA–1.75 wt.% LiBOB–9.93 wt.% TBAI–0.68 wt.% I_2–70.11 wt.% DMF, $n = 3.35\times10^{20}$ cm^{-3} which showed a decrease as expected because the conductivity has decreased. This again implied that the possible cause was due to the lesser amount of LiBOB and the higher TBAI lattice energy. For the third system with composition 15.95 wt.% PVA–1.59 wt.% LiBOB–9.04 wt.% TBAI–9 wt.% BMII–0.62 wt.% I_2–63.8 wt.% DMF, the BMII composition has increase and we again attributed this to the large amount of number density of mobile ions (4.93×10^{20} cm^{-3}). The mixture of different salts (those differ both in cation and anion) might spontaneously cause the ion exchange reaction to take place. This reaction does not affect the conductivity of electrolyte system as well as performance of DSSC because it will form neutral ion pairs. In addition, these ion pairs are immobile and thus do not affect the properties of number density of charge carriers.

To verify these results, the number density of mobile ions was also obtained from FTIR results. For the 60 wt.% PVA–40 wt.% LiBOB gel electrolyte system, FTIR results show that the total number density of mobile ions is 5.57×10^{20} cm^{-3}, for the second system with LiBOB and TBAI salts $n = 3.34\times10^{20}$ cm^{-3} and for the LiBOB–TBAI–BMII system $n = 4.93\times10^{20}$ cm^{-3}. It is obvious that the FTIR results support the results obtained from our method. These results showed that the transport properties of charge carriers in PVA–LiBOB based gel polymer electrolytes have been achieved. It has been showed that the A–N method has been verified by FTIR spectroscopy for solid and gel polymer electrolyte systems.

Conductivity is defined as the product of *n*, μ and elementary charge. The fundamental problem inhabiting the understanding of ionic conductors is the incapability to explicitly estimate the number density of free ions, their diffusivity and mobility from the measured dc conductivity. We have partially discussed the influence of number density, but does the increase in dc conductivity attributable to only the number density, or only to the mobility or both? Does the ionic conductivity obey the Nernst–Einstein equation since this equation state that mobility and diffusion coefficient are proportional to one another?

In the highest conducting PVA–LiBOB solid electrolyte system, *n* continued to increase up to 50 wt.% LiBOB when the sample preparation was stopped. The highest room temperature conductivity was only up to 40 wt.% LiBOB. Although the number density of charge carriers was higher in the 50 wt.% LiBOB containing sample, its mobility has dropped. This is also true for the diffusion coefficient variation with LiBOB concentration. Since *D* was obtained from the Nernst–Einstein equation, it can be implied the ionic mobility also obeys the same equation. Hence conductivity is also influenced by mobility in the case of PVA–LiBOB solid electrolyte system. On converting from solid to gel electrolyte, it was found that *n* decreased while μ increased. μ followed the variation of *D* with LiBOB content. The trend showed by *n*, μ and *D* is also the same for the second and third systems where *n* continued to increase but μ and *D* showed a drop at 50 wt.% LiBOB.

Addition of LiBOB salt might increase the viscosity of the electrolyte system. Based on Stokes–Einstein equation, viscosity is inversely proportional to mobility (Swiergiel *et al.*, 2015). Thus, we can infer the viscosity of electrolyte system on the mobility trend with LiBOB concentration obtained. In PVA–LiBOB solid polymer electrolyte, the mobility of the electrolyte system increased with increasing LiBOB salt concentration up to 40 wt.%. This may infer that the rate of viscosity increase is low enabling the mobility to increase until the amount of LiBOB salt is more than 40 wt.% that the rate of viscosity increase become more dominant. This led the mobility of the electrolyte to decrease.

On comparing the 60 wt.% PVA–40 wt.% LiBOB solid and gel systems, it is realized that the number density in the gel system is less than in the solid system. The higher conductivity exhibited by the gel system can be attributed the higher mobility of the ions which is of the order 10^{-5} compared to 10^{-7} cm^2 V^{-1} s^{-1} in the solid system. These results can be explained since the gel has both the characteristics of solid and liquid electrolytes and the mobility of ions in liquid electrolytes is higher compared to that of solid electrolyte. In the second electrolyte system, mobility of 60 wt.% PVA–40 wt.% LiBOB gel electrolyte ($\mu = 8.41\times10^{-7}$ cm^2 V^{-1} s^{-1}) is lower than 17.53 wt.% PVA–1.75 wt.% LiBOB–9.93 wt.% TBAI–0.68 wt.% I_2–70.11 wt.% DMF electrolyte (μ = 9.58×10^{-7} cm^2 V^{-1} s^{-1}). This can be attributed to a large number density of mobile ions (n = 5.42 cm^{-3}) that hops from one site to another aided by segmental motion of the polymer. The similar phenomena was also observed in third electrolyte system with increasing BMII composition and the room temperature conductivity in both systems were dominantly influenced by number density of mobile ions.

Conductivity–temperature dependence shows the conductivity increase with increasing temperature. The bend in the curve of Arrhenius plot suggests that this polymer electrolyte system followed the Vogel–Tamman–Fulcher (VTF) relationship. VTF relationship suggests the mechanism of ion transport in polymer electrolyte system aided by segmental motion of polymer chain (Karan *et al*., 2008). The polymer chain undergo a compression–elongation or “worm–like” movement that brings adjacent sites closer and an ion on a particular site can easily jump or hop to the site that has come nearer to it. Pseudoactivation energy (E_a) obtained provide information on minimum energy required for ion to move from one adjacent site to another. E_a is observed to follow the same trend as ionic mobility in all three electrolyte systems which implied that both E_a and μ are related to each other. A low E_a helps implies high μ.

The changes in temperature influence the mobility and number density of charge carriers in polymer electrolyte since conductivity increase with temperature. Increasing temperature has increased the segmental motion of polymer chain leading to increase in diffusivity and mobility of charge carriers (Yin *et al.*, 2009). Walsh & Zoller (1995) observed that the volume of PVA polymer increased with increasing temperature using the confining fluid principle. The increase in temperature causes the polymer segment to vibrate and creates a small amount of space around itself leading to volume increase. The volume increase enables ion pairs to dissociate form more free ions. Increase in temperature also helps in breaking the ionic bond between cation and anion of salt and becomes free ions. In the second and third electrolyte systems, ionic mobility is seen to decrease with temperature. This phenomenon is attributed to the increase of ion number density that impedes each other, thus lowering mobility.

All gel electrolytes in second and third systems have been used as a medium for redox process in DSSCs. The objective of performing DSSC using electrolyte in second and third systems is to study the influence of LiBOB and BMII on the performance of DSSCs, respectively. Usually iodide–based salt is added to the electrolyte to provide the free cation and I^- ions for enhancing the performance of DSSCs. However, the effect of cations cannot be understood clearly due to the presence of I^- ions coming from the iodide–based salt. In this work, LiBOB salt was used in the electrolyte to provide larger number of smaller Li cations without interference from I^- ions. The I^- ions come from TBAI salt in the second system and from TBAI and BMII salts in the third system. The

Li^+ ions are expected to modify the surface states of the TiO_2 semiconducting layer of the photoanode making the surface state energy levels more positive that they shift towards the redox potential. The downshift of the energy levels increase the rate of electron injection from dye excited–state into the conduction band of TiO_2, resulting in increased short circuit current density (J_{sc}). The banding width of TiO_2 energy level can be estimated using Mott–Schottky equation (Grätzel, 2001) which we are not interested to discuss in this work.

One of the important parameters of a DSSC is the open circuit voltage (V_{oc}). V_{oc} is given by the difference between the surface state level or the quasi–Fermi energy level (E_{FL}) of TiO_2 and the redox potential of the electrolyte (Snaith, 2010). The value of V_{oc} will decrease when E_{FL} of the TiO_2 is shifted towards the positive potential i.e. towards the redox potential. The shifting of E_{FL} is influenced by the cations such as Li^+, TBA^+ and BMI^+ that come from the electrolyte (Cahen *et al*., 2000; Watson & Meyer, 2004). In the electrolyte, there are charge carriers (cations and anions). The free cations can adsorb and accumulate at the surface of TiO_2 and on the walls of its pores. This will cause the potential drop across the Helmholtz layer at the interface of TiO_2 and electrolyte to change and led to the shifting of the E_{FL} of TiO_2 towards the redox potential (Cahen *et al*., 2000). When a large number of positive charge carriers accumulate at the surface of TiO_2, the E_{FL} will be shifted more towards the redox potential, thus reducing the V_{oc} of the DSSCs. It is reported that the cation size play an important role in the DSSCs. The size of the cations affects the number of adsorption of free cations onto the TiO_2 mesopores. The cation with small size or small radii can easily adsorb onto the TiO_2 pore walls, thus a large number of these smaller cations will accumulate at the surface of the TiO_2 and the walls of its pores compared to the bigger cations (Park *et al*., 2000; Shi *et al*., 2011).

In this work, the V_{oc} value for DSSCs fabricated with electrolytes in the second system increased from 537 to 713 mV as the concentration of LiBOB decreased in the electrolytes. This is because the total amount of Li^+ and TBA^+ adsorbed and accumulated on the surface of TiO_2 and its pore walls have decreased. Li^+ has atomic radius of 0.76 Å (Bhattacharya *et al*., 2009) while TBA cation radius was 2.20 Å (Kelly *et al*., 1999). Due to smaller size of Li^+, it plays a good role to adsorb onto TiO_2 mesopores and accumulate more on the pore walls of TiO_2 compared to TBA^+. As observed in Figure 5.13, number density of charge carriers for LiBOB reduced from 3.61×10^{20} (75 wt.% LiBOB) to 0 cm^{-3} (0 wt.% LiBOB) with reducing LiBOB content while TBAI free ions increased from 1.20×10^{20} (25 wt.% TBAI) to 2.83×10^{20} cm^{-3} (100 wt.% TBAI). The total number of cations have decreased from 4.82×10^{20} (B1 electrolyte) to 2.83×10^{20} cm^{-3} (B7 electrolyte) with increasing TBAI content. This led to the upshift of TiO_2 E_{FL} away from the redox potential as shown in Figure 8.1. The potential difference between the E_{FL} and the redox potential is increased and is manifested as the increase in V_{oc} of DSSC.

As can be seen in Figure 8.1, the V_{oc} value for the DSSC fabricated with B7 electrolyte (17.51 wt.% PVA–11.67 wt.% TBAI–0.8 wt.% I_2– 70.02 wt.% DMF) is 713 mV. When the weight percentage of TBAI salt was reduced by 10 % and replaced with 10 wt.% of LiBOB salt in the electrolyte (B6 electrolyte), the value of V_{oc} is observed to decrease to 703 mV. This implies that the number of positive charge carriers that accumulated at the surface of TiO_2 and the walls of the pores for DSSC fabricated with B6 electrolyte (n_{cation} = 1.58×10^{20} cm^{-3}) is more than DSSC with B7 electrolyte (n_{cation} = 1.42×10^{20} cm^{-3}), hence the E_{FL} of TiO_2 is downshifted towards the redox potential.

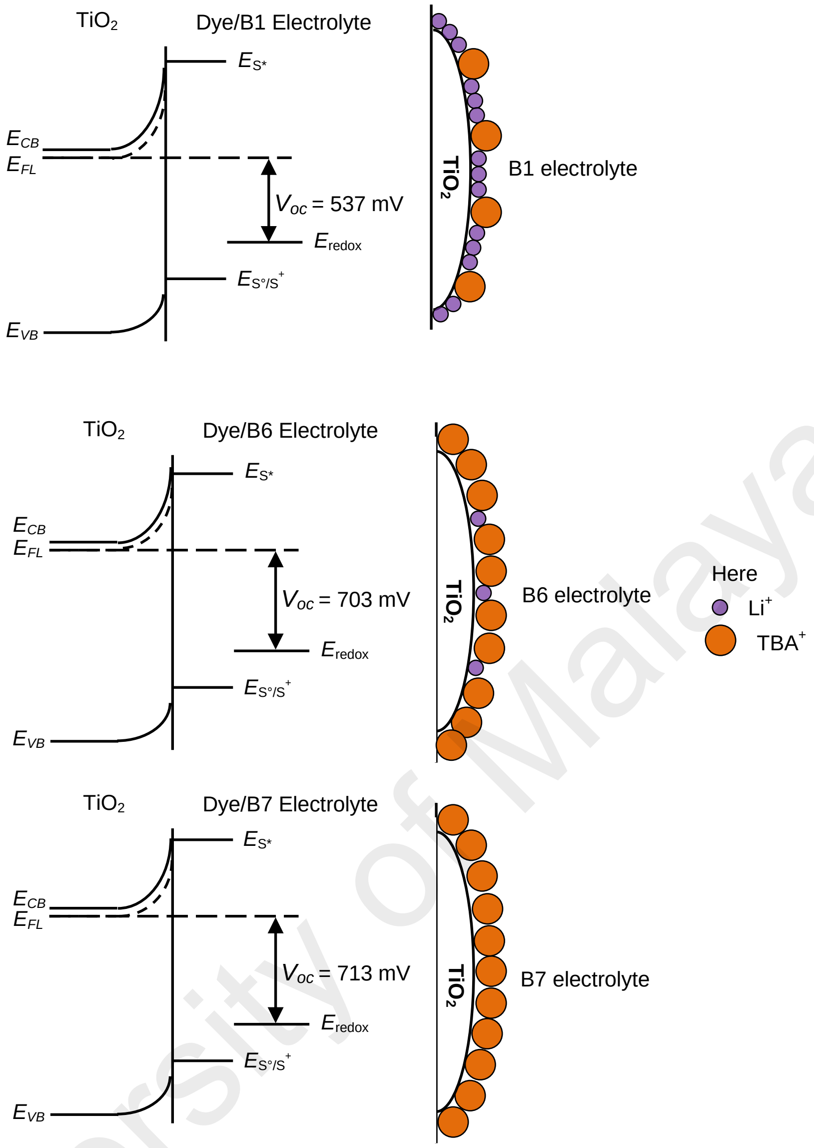

Figure 8.1: Schematic diagram shows the cations interface on TiO_2 surface in DSSC with PVA–LiBOB–TBAI–I_2–DMF gel polymer electrolytes.

As mentioned above, TBA^+ is 2.9 times larger than that of Li^+ (Kelly *et al.*, 1999). Therefore free TBA^+ ions will have difficulty to adsorb onto the TiO_2 mesopores due to competition with Li^+ ions. This is what is thought to happen in the DSSC fabricated with B7 electrolyte in which there are less cations accumulating at the walls of the TiO_2 mesopores causing the E_{FL} of TiO_2 to shift less toward the positive potential and is relatively more negative compared to the difference in potential in the DSSC with B6 electrolyte. For the DSSC fabricated with B6 electrolyte, the positive charge carriers accumulated at the surface of TiO_2 are the total number of TBA^+ and Li^+ cations. Due to the smaller size of Li^+ ions, much more Li^+ ions can adsorb onto the TiO_2 mesopores compared to TBA^+ ions. This led to an increase in the number of charge carriers adsorbed onto the TiO_2 surface and on the pore walls. With this large number of positive charge carriers accumulated on the TiO_2 surface and on the walls of its pores for DSSC with B6 electrolyte, the shifting of E_{FL} of TiO_2 towards the redox potential in DSSC is larger than in DSSC with B7 electrolyte. This resulted in a lower V_{oc} compared to that for DSSC with B6 (V_{oc} = 703 mV) and B7 electrolytes (V_{oc} = 713 mV) as shown in Figure 8.1.

From Table 7.1, the value of V_{oc} is observed to decrease from 703 to 537 mV when the concentration of LiBOB salt in the electrolyte increased from 10 wt.% (B6 electrolyte) to 75 wt.% (B1 electrolyte). This is because the number of positive charge carriers accumulated at the surface of TiO_2 increased from 1.42×10^{20} to 2.41×10^{20} cm^{-3} which is dominantly influenced by the Li^+. As can be seen from the FTIR deconvolution of LiBOB characteristics in Figure 5.4, the percentage of free Li^+ ions increased from 68.54 to 79.49 % with increasing ratio of LiBOB salt in the electrolyte. This led to more free Li^+ ions to adsorb and accumulate onto the surface of TiO_2 and its pore walls. When more charge carriers are accumulated at the TiO_2 surface, more downshifting of E_{FL} towards the redox potential, thus resulting in lower V_{oc}. The argument is in agreement with results shown in Table 7.1 where the value of V_{oc} decreased from B7 (V_{oc} = 713 mV) to B1 (V_{oc} = 537 mV) electrolyte due to the increasing number of free Li^+ accumulating on the pore walls and the surface of TiO_2.

The short circuit current density (J_{sc}) of the DSSC was influenced by the dynamics of interfacial electron transfer. This includes the electron injection yield into the conduction band of the TiO_2 semiconductor, the rate of electron transfer from counter electrode to photoelectrode and the electron recombination of the oxidized dye. The electron injection yield into the TiO_2 conduction band (CB) is related to the dye excited–state and the TiO_2 CB. According to literature (Kelly *et al*., 1999; Watson & Meyer, 2004) the distance between the dye excited–state and TiO_2 CB play an important role in electron injection dynamics. The large energy gap between the dye excited–state and TiO_2 CB increased the driving force for electron injection (Watson & Meyer, 2004). Shifting the CB of TiO_2 towards the positive potential makes the electrons more energetic when injected from the dye excited–state into the TiO_2 CB.

Kelly *et al*. (1999) reported that increasing the number of positive charge carriers at TiO_2 surface shifted the TiO_2 CB towards the positive potential, resulting in more favorable energetics for electron injection. Kelly *et al*. (1999) also reported that the quantum yield for electron injection into the TiO_2 semiconductor increased as the size of cation decreased in the order $TBA^+ > Cs^+ > K^+ > Na^+ > Li^+$. (Redmond & Fitzmaurice (1993) reported that the J_{sc} for DSSC with Li^+ accumulated at TiO_2 surface was ~3.5 times greater than with TBA^+ determined from spectroelectrochemical measurements. This indicated that the accumulation of free cations with smaller size at the TiO_2 surface shifted the TiO_2 CB towards positive potential, thus promoting electron transfer from the excited state of the dye.

From Table 7.1, it can be seen that the J_{sc} values of the DSSC with B5 electrolyte (J_{sc} = 13.05 mA cm^{-2}) is higher than that for DSSC with B7 (J_{sc} = 11.04 mA cm^{-2}) and B6 (J_{sc} = 12.06 mA cm^{-2}) electrolytes. The highest J_{sc} was influenced by the lithium cation effect accumulating on the TiO_2 surface, which is mostly influenced by the Li^+ from the LiBOB salt. This effect downshifted the CB of TiO_2 towards the positive potential. This increased the electron injection from dye excited–state to the TiO_2 CB and led to the increase in J_{sc}. Also the high iodine ion conductivity contributed by TBAI (large number density of I^- ions, $n_{iodine} = 1.42\times10^{20}$ cm^{-3}) helps the transfer of electrons from counter electrode to the photoanode. On increasing the LiBOB salt concentration from B5 to B1 electrolyte in DSSC, J_{sc} is observed to decrease from 13.05 to 8.79 mA cm^{-2}. This is not because the injection of electron has become less energetic, but the number of free iodide ions has becomes less (decreased from 1.42×10^{20} to 0.60×10^{20} cm^{-3}). On increasing the LiBOB salt in the electrolyte, the amount of TBAI salt decreased. Iodide ions are very important in DSSC because of their role as redox mediator in order to transfer electrons from the counter electrode to the ionized dye. If the number of iodide ions decreased, the rate of electron transfer becomes slower thus decreasing J_{sc} for the DSSC.

The efficiency of DSSC fabricated with B7 electrolyte (containing 100 wt.% TBAI) is 5.67% as tabulated in Table 7.1. For the DSSC with 10 wt.% of LiBOB salt in the electrolyte B6, the efficiency increased to 5.83% and continued to increase until 6.11% for DSSC fabricated with B5 electrolyte. The efficiency of the DSSCs was observed to decrease as the concentration of LiBOB salt increased beyond 15 wt.%. It is noted that the solar energy efficiency of DSSC is directly proportional to J_{sc}, V_{oc} and fill factor (FF) as stated in equation 3.31. Solar energy efficiency for DSSC with second electrolyte system is seen to follow the same trend as J_{sc}. This indicates that J_{sc} influence dominate the change in the efficiency of DSSC and the large J_{sc} obtained was influenced by the Li^+ from the LiBOB that had shifted the CB of TiO_2 by making the surface state more positive in energy that results in higher solar energy efficiency.

Generally, the electrolyte used in DSSC contains iodide salts. In this work, LiBOB salt was used instead of LiI to provide cations for attachment to the DSSC photoanode. However, to show the importance of the smaller cation such as Li^+, the use of a non–iodide lithium salt will be more convincing. LiBOB salt has the ability to dissociate into a large number of free ions. This is because LiBOB has a bigger anion thus easy for it to dissociate the lithium cation when forming the polymer electrolyte. The low lattice energy of 496 kJ mol^{-1} of LiBOB salt (Holomb *et al.*, 2006) also helps the salt to dissociate. Arof *et al.* (2014) has reported that ~72% of free ions dissociated when 50 wt.% of LiBOB salt was incorporated into 50 wt.% of PAN determined from FTIR deconvolution. In this work, we obtained ~75% of LiBOB free ions in 60 wt.% PVA–40 wt.% LiBOB solid polymer electrolyte. It is reported that lattice energy of LiI is 757 kJ mol^{-1} (Reger *et al.*, 2009). This high lattice energy makes it more difficult for LiI to dissociate compared to LiBOB. LiBOB salt has ~32% less lattice energy than LiI. This shows that for the same weight ratio of LiI and LiBOB, the latter can produce a larger number of free Li^+ cations.

In order to verify the effect of Li^+ in DSSC, lithium iodide (LiI) and potassium iodide (KI) salts were used in place of LiBOB in the electrolyte. From Figure 7.4, the V_{oc} for electrolyte consisting of LiBOB salt decreased drastically, followed by electrolyte with KI salt and the decrease in V_{oc} is lesser in electrolyte consisting of LiI salt. LiBOB salt has the lowest lattice energy of 496 kJ mol^{-1}. KI and LiI have lattice energy of 632 kJ mol $^{-1}$ and 757 kJ mol^{-1}, respectively. This implied that LiBOB is easily dissociated into free ions followed by KI and lastly LiI. To validate this argument, the number density of charge carriers for electrolyte with composition of 17.65 wt.% PVA–11.76 wt.% LiBOB–70.59 wt.% DMF, 17.65 wt.% PVA–11.76 wt.% KI–70.59 wt.% DMF and 17.65 wt.% PVA–11.76 wt.% LiI–70.59 wt.% DMF was calculated using fitting method of impedance data proposed in this work. The results were tabulated in Table 8.1.

Table 8.1: Number density of charge carriers for PVA–*x*–DMF (*x* = LiBOB, LiI, KI) gel polymer electrolyte at 298 K.

Electrolyte	***n*** **($\times 10^{20}$ cm^{-3})**
17.65 wt.% PVA–11.76 wt.% LiBOB–70.59 wt.% DMF	5.42
17.65 wt.% PVA–11.76 wt.% KI–70.59 wt.% DMF	5.22
17.65 wt.% PVA–11.76 wt.% LiI–70.59 wt.% DMF	4.99

From Table 8.1, number density of free ions was in order of LiBOB > KI > LiI. These results suggested that LiBOB salt dissociated more Li^+ compared to LiI and implied that the higher number of Li^+ ions from LiBOB played a greater role in modifying the TiO_2 surface of photoanode compared to LiI. Due to the fewer number density of free ions dissociated from LiI, less cations are adsorbed and accumulated at the surface of TiO_2 and on the walls of its pores, thus the V_{oc} of DSSC with LiI salt is observed to be higher than V_{oc} of DSSC with LiBOB electrolyte system. Based on Table 8.1, KI dissociated more free ions than LiI due to lower lattice energy possessed by KI. These results in lower V_{oc} value of DSSC with KI electrolyte than V_{oc} of DSSC with LiI electrolyte system but higher than DSSC with LiBOB electrolyte system. As more K^+ ions adsorb and accumulate at the surface of TiO_2 and on the walls of its pores, more positive shift of the E_{FL} results in lower V_{oc} compared to LiI electrolyte system.

It can be seen in Table 7.5 that J_{sc} value is the highest for DSSC fabricated with LiBOB electrolyte (B5 electrolyte, J_{sc} = 13.05 mA cm^{-2}) i.e. compared to KI (K5 electrolyte, J_{sc} = 12.12 mA cm^{-2}) and LiI (L5 electrolyte, J_{sc} = 11.71 mA cm^{-2}) electrolytes. This was attributed to the high electron injection from dye excited–state to the TiO_2 CB when the DSSC fabricated with B5 electrolyte due to the effect of Li^+ from LiBOB (small cation size and large *n*) that have downshifted CB of TiO_2 more towards positive potential compared to K^+ from KI and Li^+ from LiI. For DSSC fabricated with B6 and K6 electrolytes, the J_{sc} value is slightly higher in DSSC with K6 electrolyte (J_{sc}

= 12.20 mA cm^{-2}, V_{oc} = 705 mV) although the difference between dye excited–state and TiO_2 CB of DSSC with B6 electrolyte (J_{sc} = 12.06 mA cm^{-2}, V_{oc} = 703 mV) is slightly larger than DSSC with K6 electrolyte. This is attributed to I^- ions dissociated from KI combined with free I^- of TBAI that helped to increase the redox process, thus assisting in increasing J_{sc} of the DSSC. At this junction it can be observed that performance of a DSSC is influenced not only by the shifting of E_{FL} towards redox potential or the increase in electron injection, but also to the rate of redox process that was influenced by the number density of I^- ions in these I^-/I_3^- redox mediator DSSCs. Compared to the DSSC consisting of B6 electrolyte that only produce I^- from TBAI, the J_{sc} value is lesser than J_{sc} values for DSSC with KI electrolyte up to 10 wt.% salt content (Figure 7.5) since there are more I^- ions in KI compared to only I^- ions from TBAI in the LiBOB system. Although LiI can also provide I^- ions together with TBAI, J_{sc} from DSSC with 10 wt.% LiI is a little lower than that for LiBOB based electrolyte. It can be realized at this stage that the shifting of E_{FL} has a higher impact than the assistance of I^- ions from LiI in determining J_{sc}. The J_{sc} values for DSSC fabricated with LiBOB electrolytes system (J_{sc} = 12.06 mA cm^{-2}) is higher than J_{sc} values for DSSC fabricated with LiI electrolytes (J_{sc} = 12.00 mA cm^{-2}). J_{sc} for DSSC fabricated with KI electrolyte (J_{sc} = 12.20 mA cm^{-2}) is highest at 10 wt.% salt concentration. Above 10 wt.% salt concentration, J_{sc} is highest for LiBOB based electrolyte compared to KI and LiI based electrolyte.

In order to increase the performance of DSSC, electrolyte with high solar efficiency in second system (B5 electrolyte, η = 6.11%) was added with BMII ionic liquid to provide more iodide anions for redox process. From Table 7.6, it can be seen that the V_{oc} value decreased from 682 to 617 mV with increasing the concentration of BMII from 0 to 9 wt.% due to the downshifting of E_{FL} of TiO_2 towards the redox potential. The shift of E_{FL} was affected by the BMI$^+$ (radius size = 3.85Å) (Liu *et al.*, 2010) that accumulated at the surface of TiO_2 and the walls of its pores. As more BMI$^+$ accumulate at the TiO_2 mesopores, the more the E_{FL} was moved towards redox potential (Figure 8.2). From the FTIR deconvolution in Chapter 6, the free ion percentage of Li$^+$ in the electrolyte is observed to be almost constant in all electrolyte compositions (Figure 6.5). The number densities of free ions of LiBOB and TBAI in the third electrolyte system are also constant ($n_{LiBOB} = 0.50\times10^{20}$ cm^{-3}, $n_{TBAI} = 2.84\times10^{20}$ cm^{-3}) while n for BMII increased from 0 to 1.59×10^{20} cm^{-3} at 9 wt.% BMII concentration (Table 6.5). This deduction further strengthened the decrease of V_{oc} values from 682 to 617 mV with increasing BMII content in 17.53 wt.% PVA–1.75 wt.% LiBOB–9.93 wt.% TBAI–0.68 wt.% I_2–70.11 wt.% DMF electrolyte (C0 or B5 electrolyte). The downshift of E_{FL} towards redox potential is due to the increasing imidazolium cations dissociated from BMII on the surface of mesoporous TiO_2.

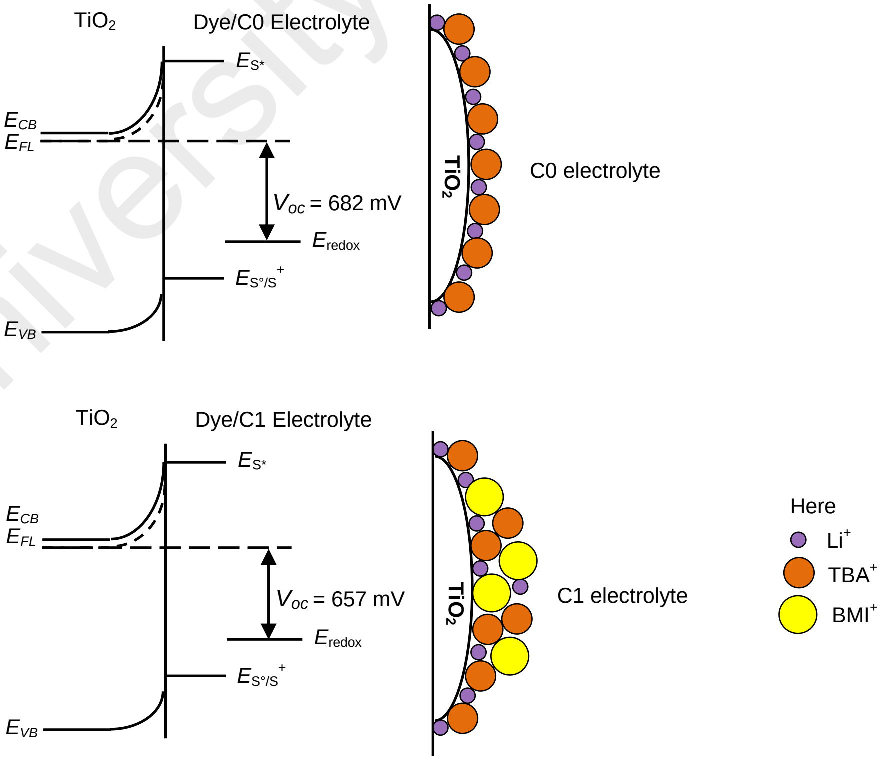

Figure 8.2, continued...

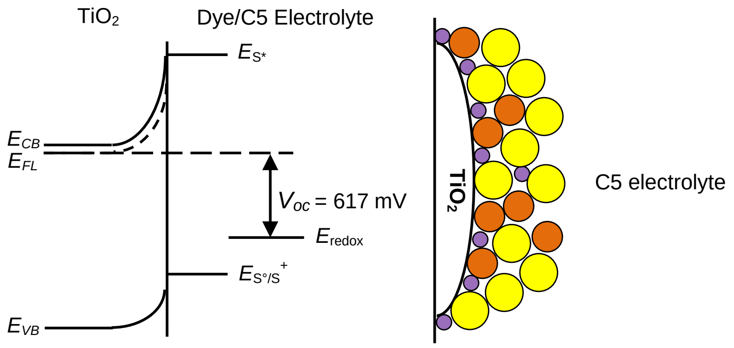

Figure 8.2: Schematic diagram shows the cations interface on TiO_2 surface in DSSC with PVA–LiBOB–TBAI–BMII–I_2–DMF gel polymer electrolyte system.

The downshift of E_{FL} toward the redox potential indirectly increased the energy difference between dye–excited state and CB of TiO_2. This caused the rate of electron injection from dye–excited state to CB of TiO_2 to increase, thus increase J_{sc}. Based on results tabulated in Table 7.6, the J_{sc} value for the cell without BMII (C0 electrolyte) was 13.05 mA cm^{-2}. As 1 wt.% of BMII ionic liquid is added into the electrolyte (C1 electrolyte), the J_{sc} value of the cell increased to 13.95 mA cm^{-2} and kept increasing up to 16.71 mA cm^{-2} for the assembled cell with electrolyte consisting 9 wt.% BMII (C5 electrolyte). BMII dissociated into free BMI$^+$ and I^-. Free I^- from BMII helped to increase the rate of redox process, thus assisting in increasing J_{sc} of the DSSC. As shown in Chapter 6, the conductivity of the PVA–LiBOB–TBAI–BMII–I_2–DMF gel polymer electrolyte system increased from 5.13 to 7.52 mS cm^{-1} with increasing amount of BMII from 0 to 9 wt.%. This means that the rate of electron transfer from counter electrode to the deionized dye was also increased due to increase in conductivity of the I^- in the redox mediator (n for BMII increase from 0 to 1.59×10^{20} cm^{-3}). Based on this work, it can be inferred that the role of BMII as second salt in third electrolyte system has increased the redox process conductivity and at the same time modified the TiO_2

surface states so that the rate of electron injection from dye–excited state to TiO_2 CB increased, resulting in high J_{sc}.

The solar conversion efficiency of the DSSC assembled with PVA–LiBOB–TBAI–BMII–I_2–DMF gel polymer electrolyte increased from 6.11% with C0 electrolyte to 7.28% with C5 electrolyte. The increase in efficiency of DSSC is due to increasing J_{sc} of the cell. This is because the efficiency is directly proportional to the J_{sc} and V_{oc}. Even though V_{oc} decreased, but the J_{sc} is increasing dominantly, thus influencing the cell performance. This can be seen in Table 8.2 where the ratio of J_{sc} to V_{oc} increased with increasing BMII ionic liquid content.

Table 8.2: The ratio of J_{sc} to V_{oc} of PVA–LiBOB–TBAI–BMII–I_2–DMF gel polymer electrolyte.

Electrolyte	**V_{oc} (mV)**	**J_{sc} (mA cm^{-2})**	**J_{sc} /V_{oc} (mS cm^{-2})**
C0	682	13.05	19.12
C1	657	13.95	21.22
C2	647	15.30	23.65
C3	642	15.54	24.21
C4	632	16.15	25.55
C5	617	16.71	27.09

CHAPTER 9 : CONCLUSIONS AND SUGGESTION FOR FURTHER WORK

PVA has been chosen as the polymer host this work due to its high dielectric constant of 8.1 indicating that it is able to solvate large amount of mobile ions. PVA–LiBOB complexes revealed room temperature conductivity (σ_{RT}) of 10^{-3} S cm^{-1}, which was in line with the main objective of this work to produce a high conducting electrolyte. The highest σ_{RT} PVA–LiBOB solid electrolyte was 2.83×10^{-4} S cm^{-1} at 40 wt.% LiBOB loading. On jellifying this electrolyte with DMF, σ_{RT} increased to 7.31×10^{-3} S cm^{-1}. As one the objectives in this work was to fabricate DSSCs using LiBOB containing electrolyte, TBAI and I_2 were added to provide the iodide/triodide redox couple and the total salt concentration was fixed but the ratio between TBAI and LiBOB was varied. The electrolyte with composition 17.53 wt.% PVA–1.75 wt.% LiBOB–9.93 wt.% TBAI–0.68 wt.% I_2–70.11 wt.% DMF (B5 electrolyte, σ_{RT} = 5.13×10^{-3} S cm^{-1}) gave the highest efficiency of 6.11%. A second iodide salt i.e. BMII was added in B5 electrolyte to enhance solar efficiency and electrolyte conductivity. The electrolyte with composition 15.95 wt.% PVA–1.59 wt.% LiBOB–9.04 wt.% TBAI–9 wt.% BMII–0.62 wt.% I_2–63.8 wt.% DMF (σ_{RT} = 7.52×10^{-3} S cm^{-1}) exhibited the highest efficiency of 7.28%.

Transport parameters of mobile ions for all electrolytes at room temperature were determined quantitatively by fitting the complex impedance plot obtained experimentally to the impedance of an appropriate equivalent circuit. The diffusion coefficient (D) and mobility (μ) of free ions in PVA–LiBOB solid electrolyte system increased with LiBOB concentration up to 40 wt.%. Beyond this salt concentration, D and μ decreased. The mobile ion number density (n) increased with LiBOB concentration up to 50 wt.%. On transforming the electrolyte from the solid to gel form D increased from 2.46×10^{-8} (solid form) to 2.16×10^{-6} cm^{2} s^{-1} (gel form) and μ from 9.58×10^{-7} to 8.41×10^{-5} cm V^{-1} s^{-1} due to solid–liquid properties of the gel, but n decreased from 1.85×10^{21} to 5.42×10^{20} cm^{-3}. Reducing LiBOB and replacing it with TBAI, but keeping the salt content to 40 wt.% in the gel electrolyte, D increased to 2.47×10^{-6} cm^{2} s^{-1} and μ to 9.60×10^{-5} cm V^{-1} s^{-1} while n decreased to 2.83×10^{20} cm^{-3}. In the BMII electrolyte system, however, D decreased from 2.46×10^{-6} to 2.44×10^{-6} cm^{2} s^{-1}, μ decreased from 9.58×10^{-5} to 9.52×10^{-5} cm V^{-1} s^{-1} and n increased from 3.35×10^{20} to 4.93×10^{-6} cm^{-3} indicated that more mobile ions as BMII added. On increasing temperature of the electrolyte environment, D and μ decreased and n increased in the second and third electrolyte systems.

As mentioned above, the highest solar conversion efficiency obtained in second and third electrolyte systems is 6.11% and 7.28%, respectively. The solar conversion efficiency of DSSC was dominantly influenced by the short circuit current density, J_{sc} of the cells where high J_{sc} revealed high solar efficiency. The increase of J_{sc} of the cell was influenced by the cations [(Li^{+} for system 2) and (BMII^{+} for system 3)] that accumulated on the surface of TiO_2 mesopores and its pores walls. Adsorption of these cations downshifted the Fermi level of the TiO_2 towards positive potential and indirectly increased the energy gap between the dye excited state and TiO_2 conduction band. Also the high concentration of iodide anion helps in transferring the electrons from counter electrode to the ionized dye at a faster rate. One of the objectives of this work was achieved where the use of non–iodide salt i.e. LiBOB had affected the performance of the DSSCs. The Li^{+} dissociated from LiBOB made the potential of the Fermi level of TiO_2 more positive and shifted the Fermi level towards the redox potential in the DSSC employing electrolyte from the second system. This effect increased the J_{sc} as well as the solar conversion efficiency. The BMII ionic liquid was observed to help increase the energy gap between the dye excited state and conduction band of TiO_2 as well as increased the conductivity of redox mediator for electron transfer from counter electrode to the ionized dye.

This research work has given some ideas to further pursue a more in–depth study. Some suggestions for further work based on these research findings are:

- maintain the composition of the PVA–LiBOB–TBAI–BMII–DMF electrolyte with I_2, but study other parameters such as transference number, linear sweep voltammetry and cyclic voltammetry to increase the literature of knowledge on this material,
- study the stability of the DSSC,
- study more on the DSSC such as (i) the IPCE and (ii) modifying DSSC electrode in order to obtain higher solar conversion efficiency by using nanowire TiO_2 photoanode prepared using electrospining method,
- using other measurement technique to determine diffusion coefficient, mobility and number density of charge carriers of electrolyte and comparing the results from the method developed in this work,
- extend the Nyquist plot fitting method developed in this work to determine transference number of electrolyte.

REFERENCES

Abdul Rahaman, M. H., Khandaker, M. U., Khan, Z. R., Kufian, M. Z., Noor, I. S. M., and Arof, A. K. (2014). Effect of gamma irradiation on poly(vinyledene difluoride)–lithium bis(oxalato)borate electrolyte. *Physical Chemistry Chemical Physics, 16*(23), 11527–11537

Ahmad, Z. (2012). Polymeric dielectric materials. In Silaghi, M. A., *Dielectric Material,* 3–26 : InTech

Albinsson, I. (1994). *Dielectric and conductivity studies of polymer electrolytes.* (Unpublished doctoral dissertation), Chalmers University of Technology, Gothenburg, Sweden

An, Y., Zuo, P., Cheng, X., Liao, L., and Yin, G. (2011). The effects of LiBOB additive for stable SEI formation of PP13TFSI–organic mixed electrolyte in lithium ion batteries. *Electrochimica Acta, 56*(13), 4841–4848

Anandan, S., Pitchumani, S., Muthuraaman, B., and Maruthamuthu, P. (2006). Heteropolyacid–impregnated PVDF as a solid polymer electrolyte for dye sensitized solar cells. *Solar Energy Materials and Solar Cells, 90*(12), 1715–1720

Appetecchi, G., Zane, D., and Scrosati, B. (2004). PEO–based electrolyte membranes based on $LiBC_4O_8$ Salt. *Journal of the Electrochemical Society, 151*(9), A1369–A1374

Armand, M., Chabagno, J., Duclot, M., Vashishta, P., Mundy, J., and Shenoy, G. (1979). Fast ion transport in solids. In *Vashishta, P., Mundy, JN and Shenoy, G. K*: North Holland, Amsterdan.

Arof, A. K., Amirudin, S., Yusof, S. Z., and Noor, I. M. (2014a). A method based on impedance spectroscopy to determine transport properties of polymer electrolytes. *Physical Chemistry Chemical Physics, 16*(5), 1856–1867

Arof, A. K., Naeem, M., Hameed, F., Jayasundara, W. J. M. J. S. R., Careem, M. A., Teo, L. P., and Buraidah, M. H. (2013). Quasi solid state dye–sensitized solar cells based on polyvinyl alcohol (PVA) electrolytes containing I^-/I_3^- redox couple. *Optical and Quantum Electronics, 46*(1), 143–154

Arof, A. K., Shuhaimi, N. E. A., Amirudin, S., Kufian, M. Z., Woo, H. J., and Careem, M. A. (2014b). Polyacrylonitrile–lithium bis(oxalato) borate polymer electrolyte for electrical double layer capacitors. *Polymers for Advanced Technologies, 25*(3), 265–272

Aziz, M. F., Buraidah, M. H., and Arof, A. K. (2013a). Dye sensitized solar cells using binary iodide–PVA gel electrolyte. *Proceeding of 15th International Conference on Transparent Optical Networks (ICTON),* 1–4. doi: 10.1109/ICTON.2013.6602808

Aziz, M. F., Buraidah, M. H., Careem, M. A., and Arof, A. K. (2015). PVA based gel polymer electrolytes with mixed iodide salts (K^+I^- and $Bu_4N^+I^-$) for dye sensitized solar cell application. *Electrochimica Acta, 182*, 217–223

Aziz, M. F., Noor, I. M., Buraidah, M. H., Careem, M. A., and Arof, A. K. (2013b). PVA–based gel polymer electrolytes doped with $(CH_3)_4NI/KI$ for application in dye–sensitized solar cells. *Proceeding of 15th International Conference on Transparent Optical Networks (ICTON)*, 1–4, doi: 10.1109/ICTON.2013.6602906

Aziz, M. F., Noor, I. M., Sahraoui, B., and Arof, A. K. (2014). Dye sensitized solar cells with PVA–KI–EC–PC gel electrolytes. *Optical and Quantum Electronics, 46*(1), 133–141

Bandara, T. M. W. J., Dissanayake, M. A. K. L., Albinsson, I., and Mellander, B. E. (2011). Mobile charge carrier concentration and mobility of a polymer electrolyte containing PEO and $Pr_4N^+I^-$ using electrical and dielectric measurements. *Solid State Ionics, 189*(1), 63–68

Bandara, T. M. W. J., and Mellander, B. E. (2011). Evaluation of mobility, diffusion coefficient and density of charge carriers in ionic liquids and novel electrolytes based on a new model for dielectric response, In Kokorin, A., *Ionic Liquids: Theory, Properties, New Approaches* : INTECH Open Access Publisher

Barber, P., Balasubramanian, S., Anguchamy, Y., Gong, S., Wibowo, A., Gao, H., Ploehn, H. J., and Zur Loye, H.–C. (2009). Polymer composite and nanocomposite dielectric materials for pulse power energy storage. *Materials, 2*(4), 1697–1733

Bhattacharya, B., Lee, J. Y., Geng, J., Jung, H.–T., and Park, J.–K. (2009). Effect of cation size on solid polymer electrolyte based dye sensitized solar cells. *Langmuir, 25*(5), 3276–3281

Bipp, H., and Kieczka, H. (2000). Formamides. In Elvers, B., *Ullmann's Encyclopedia of Industrial Chemistry*: Wiley–VCH Verlag GmbH & Co. KGaA

Blehn, G. F., and Ernsberger, M. L. (1948). Polyvinyl Alcohol as an Emulsifying Agent. *Industrial & Engineering Chemistry, 40*(8), 1449–1453

Bourdon, J. (1965). Spectral sensitization of chemical effects in solids. *The Journal of Physical Chemistry, 69*(3), 705–713

Brinkman, E., van der Does, L., and Bantjes, A. (1991). Poly(vinyl alcohol)–heparin hydrogels as sensor catheter membranes. *Biomaterials, 12*(1), 63–70

Buraidah, M. H., and Arof, A. K. (2011). Characterization of chitosan/PVA blended electrolyte doped with NH_4I. *Journal of Non–Crystalline Solids, 357*(16–17), 3261–3266

Buraidah, M. H., Teo, L. P., Majid, S. R., and Arof, A. K. (2010). Characteristics of TiO_2/solid electrolyte junction solar cells with redox couple. *Optical Materials, 32*(6), 723–728

Cahen, D., Hodes, G., Grätzel, M., Guillemoles, J. F., and Riess, I. (2000). Nature of photovoltaic action in dye sensitized solar cells. *The Journal of Physical Chemistry B, 104*(9), 2053–2059

Cao, Y., Zhang, J., Bai, Y., Li, R., Zakeeruddin, S. M., Grätzel, M., and Wang, P. (2008). Dye sensitized solar cells with solvent–free ionic liquid electrolytes. *The Journal of Physical Chemistry C, 112*(35), 13775–13781

Chen, Y. T., Chuang, Y. C., Su, J. H., Yu, H. C., and Chen–Yang, Y. W. (2011). High discharge capacity solid composite polymer electrolyte lithium battery. *Journal of Power Sources, 196*(5), 2802–2809

Chowdari, B., and Wang, W. (2000). (Eds), *Solid State Ionics, Materials and Devices* : World Scientific

Croce, F., Appetecchi, G. B., Mustarelli, P., Quartarone, E., Tomasi, C., and Cazzanelli, E. (1998). Investigation of ion dynamics in $LiClO_4$/EC/PC highly concentrated solutions by ionic conductivity and DSC measurements. *Electrochimica Acta, 43*(10–11), 1441–1446.

Deraman, S. K., Subban, R. H. Y., and Nor Sabirin, M. (2012). Ionic conductivity of PVC–NH_4I–EC proton conducting polymer electrolytes. A*dvanced Materials Research*, 545, 312–316

Dissanayake, M. A. K. L., Thotawatthage, C. A., Senadeera, G. K. R., Bandara, T. M. W. J., Jayasundera, W. J. M. J. S. R., and Mellander, B. E. (2012). Efficiency enhancement by mixed cation effect in dye sensitized solar cells with PAN based gel polymer electrolyte. *Journal of Photochemistry and Photobiology A, Chemistry, 246*, 29–35

Ericson, H., Svanberg, C., Brodin, A., Grillone, A. M., Panero, S., Scrosati, B., and Jacobsson, P. (2000). Poly(methyl methacrylate)–based protonic gel electrolytes, a spectroscopic study. *Electrochimica Acta, 45*(8–9), 1409–1414

Every, H. A., Zhou, F., Forsyth, M., and MacFarlane, D. R. (1998). Lithium ion mobility in poly(vinyl alcohol) based polymer electrolytes as determined by ^{7}Li NMR spectroscopy. *Electrochimica Acta, 43*(10–11), 1465–1469

Flory, P. J. (1944). Network structure and the elastic properties of vulcanized rubber. *Chemical reviews, 35*(1), 51–75

Garca–Coln, L., Del Castillo, L., and Goldstein, P. (1989). Theoretical basis for the Vogel–Fulcher–Tammann equation. *Physical Review B, 40*(10), 7040

Gerischer, H., and Tributsch, H. (1968). Elektrochemische untersuchungen zur spektralen sensibilisierung von ZnO‐Einkristallen. *Berichte der Bunsengesellschaft für physikalische Chemie, 72*(3), 437–445

Grätzel, M. (1999). Mesoporous oxide junctions and nanostructured solar cells. *Current Opinion in Colloid & Interface Science*, 4(4), 314–321

Grätzel, M. (2001). Photoelectrochemical cells. *Nature,* 414(6861), 338–344

Grätzel, M. (2003). Dye sensitized solar cells. *Journal of Photochemistry and Photobiology C, Photochemistry Reviews*, *4*(2), 145–153

Grondin, J., Rodriguez, D., and Lassègues, J. C. (1995). Proton conducting polymer electrolyte–The Nylon$_{6–10}$/H_3PO_4 blends. *Solid State Ionics, 77*, 70–75

Han, S.–h., and Gu, X.–h. (2008). The application of grafting modification on PVA in textile sizing. *Journal of Wuhan University of Science and Engineering, 8,* 010

Hauffe, K., Danzmann, H., Pusch, H., Range, J., and Volz, H. (1970). New experiments on the sensitization of zinc oxide by means of the electrochemical cell technique. *Journal of the Electrochemical Society, 117*(8), 993–999

Hayashi, T., and Moriya, T. (1976). *Aqueous composition containing acrylic or butadiene polymers*. Patent No: US 3996181 A, United State

Hema, M., Selvasekarapandian, S., Arunkumar, D., Sakunthala, A., and Nithya, H. (2009a). FTIR, XRD and ac impedance spectroscopic study on PVA based polymer electrolyte doped with NH_4X (X = Cl, Br, I). *Journal of Non–Crystalline Solids, 355*(2), 84–90

Hema, M., Selvasekarapandian, S., Hirankumar, G., Sakunthala, A., Arunkumar, D., and Nithya, H. (2010). Laser Raman and ac impedance spectroscopic studies of PVA,NH_4NO_3 polymer electrolyte. *Spectrochimica Acta Part A, Molecular and Biomolecular Spectroscopy, 75*(1), 474–478

Hema, M., Selvasekerapandian, S., Hirankumar, G., Sakunthala, A., Arunkumar, D., and Nithya, H. (2009b). Structural and thermal studies of PVA,NH_4I. *Journal of Physics and Chemistry of Solids, 70*(7), 1098–1103

Herrmann, W. O., and Wolfram, H. (1928). *Process for the preparation of polymerized vinyl alcohol and its derivatives*. Patent No: US 1672156 A, United State

Holomb, R., Xu, W., Markusson, H., Johansson, P., and Jacobsson, P. (2006). Vibrational spectroscopy and ab initio studies of lithium bis(oxalato)borate (LiBOB) in different solvents. *The Journal of Physical Chemistry A, 110*(40), 11467–11472

Hou, W.–H., Chen, C.–Y., Wang, C.–C., and Huang, Y.–H. (2003). The effect of different lithium salts on conductivity of comb–like polymer electrolyte with chelating functional group. *Electrochimica Acta, 48*(6), 679–690

Ileperuma, O. A., Asoka Kumara, G. R., Yang, H.–S., and Murakami, K. (2011). Quasi–solid electrolyte based on polyacrylonitrile for dye sensitized solar cells. *Journal of Photochemistry and Photobiology A, Chemistry, 217*(2–3), 308–312

Jacob, M. M. E., and Arof, A. K. (2000). FTIR studies of DMF plasticized polyvinyledene fluoride based polymer electrolytes. *Electrochimica Acta, 45*(10), 1701–1706

Jyothi, N. K., Kumar, K. V., and Murthy, P. N. (2014). FTIR, XRD and DC conductivity studies of proton conducting gel polymer electrolytes based on polyacrylonitrile (PAN), I*nternational Journal of ChemTech Research*, 6(13), 5214–5219

Kadir, M., Majid, S., and Arof, A. (2010). Plasticized chitosan–PVA blend polymer electrolyte based proton battery. *Electrochimica Acta*, *55*(4), 1475–1482

Kalaignan, G. P., Kang, M.–S., and kang, Y. S. (2006). Effects of compositions on properties of PEO–KI–I_2 salts polymer electrolytes for DSSC. *Solid State Ionics, 177*(11–12), 1091–1097

Karan, N. K., Pradhan, D. K., Thomas, R., Natesan, B., and Katiyar, R. S. (2008). Solid polymer electrolytes based on polyethylene oxide and lithium trifluoro– methane sulfonate (PEO–$LiCF_3SO_3$), Ionic conductivity and dielectric relaxation. *Solid State Ionics, 179*(19–20), 689–696.

Karmakar, A., and Ghosh, A. (2012). Dielectric permittivity and electric modulus of polyethylene oxide (PEO)–$LiClO_4$ composite electrolytes. *Current Applied Physics, 12*(2), 539–543.

Karuppasamy, K., Antony, R., Alwin, S., Balakumar, S., and Sahaya Shajan, X. (2015). A review on PEO based solid polymer electrolytes (SPEs) complexed with LiX (X= Tf, BOB) for rechargeable lithium ion batteries. *Materials Science Forum, 807*, 41–63

Kelly, C. A., Farzad, F., Thompson, D. W., Stipkala, J. M., and Meyer, G. J. (1999). Cation–controlled interfacial charge injection in sensitized nanocrystalline TiO_2. *Langmuir, 15*(20), 7047–7054

Khiar, A. S. A., and Arof, A. K. (2010). Conductivity studies of starch–based polymer electrolytes. *Ionics, 16*(2), 123–129

Kufian, M. Z., Aziz, M. F., Shukur, M. F., Rahim, A. S., Ariffin, N. E., Shuhaimi, N. E. A., Majid, S. R., Yahya, R., and Arof, A. K. (2012). PMMA–LiBOB gel electrolyte for application in lithium ion batteries. *Solid State Ionics, 208*, 36–42

LaBlance, S. J. (2003). *Method of making furniture, and furniture made thereby*. Patent No US: 20010045768 A1, United State

Lanza, V., and Herrmann, D. (1958). The density dependence of the dielectric constant of polyethylene. *Journal of Polymer Science, 28*(118), 622–625

Lee, K.–M., Suryanarayanan, V., and Ho, K.–C. (2009). High efficiency quasi–solid–state dye sensitized solar cell based on polyvinyidene fluoride–co–hexafluoro propylene containing propylene carbonate and acetonitrile as plasticizers. *Journal of Photochemistry and Photobiology A, Chemistry, 207*(2–3), 224–230

Leones, R., Esperança, J. M. S. S., Pawlicka, A., de Zea Bermudez, V., and Silva, M. M. (2015). Polymer electrolyte based on DNA and N,N,N–trimethyl–N–(2–hydroxyethyl)ammonium bis(trifluoromethylsulfonyl)imide. *Journal of Electroanalytical Chemistry, 748*, 70–75

Li, L., and Hsieh, Y.–L. (2005). Ultra–fine polyelectrolyte fibers from electrospinning of poly(acrylic acid). *Polymer, 46*(14), 5133–5139

Lim, C.–S., Teoh, K. H., Liew, C.–W., and Ramesh, S. (2014). Capacitive behavior studies on electrical double layer capacitor using poly (vinyl alcohol)–lithium perchlorate based polymer electrolyte incorporated with TiO_2. *Materials Chemistry and Physics, 143*(2), 661–667

Lim, Y.–J., An, Y.–H., and Jo, N.–J. (2012). Polystyrene–Al_2O_3 composite solid polymer electrolyte for lithium secondary battery. *Nanoscale Research Letters, 7*(1), 1–6

Linford, R. G. (1988). *Experimental technique for studying polymer electrolytes*. In *Solid State Ionics*, Singapore: World Scientific

Lischka, U., Wietelmann, U., and Wegner, M. (1999). *Lithium bisoxalatoborate used as conducting salt in lithium ion batteries,* Patent No: DE19829030C1, German

Liu, S., Liu, W., Liu, Y., Lin, J.–H., Zhou, X., Janik, M. J., Colby, R. H., and Zhang, Q. (2010). Influence of imidazolium–based ionic liquids on the performance of ionic polymer conductor network composite actuators. *Polymer International, 59*(3), 321–328

MacDonald, G. A., Lager, T. M., Machurick, M. A., and Sorenson, J. P. (1999). *Flexible polymer packaging bag with easy–open end seal feature*. Patent No. US 5967665 A, United State

Macdonald, J. R., and Johnson, W. B. (2005). Fundamentals of impedance spectroscopy. In Barsoukov, E., and Macdonald, J. R., (2nd edition), *Impedance spectroscopy :Theory, experiment, and applications* (pp. 1–26). John Wiley & Sons, Inc

Malathi, J., Kumaravadivel, M., Brahmanandhan, G. M., Hema, M., Baskaran, R., and Selvasekarapandian, S. (2010). Structural, thermal and electrical properties of PVA–$LiCF_3SO_3$ polymer electrolyte. *Journal of Non–Crystalline Solids, 356*(43), 2277–2281

Maurya, K. K., Srivastava, N., Hashmi, S. A., and Chandra, S. (1992). Proton conducting polymer electrolyte, II poly ethylene oxide+NH_4l system. *Journal of Materials Science, 27*(23), 6357–6364

Mohamad, A., Haliman, H., Sulaiman, M., Yahya, M., and Ali, A. (2008). Conductivity studies of plasticized anhydrous PEO–KOH alkaline solid polymer electrolyte. *Ionics, 14*(1), 59–62

Mohamad, A., Mohamed, N., Alias, Y., and Arof, A. (2002). Studies of alkaline solid polymer electrolyte and mechanically alloyed polycrystalline Mg_2Ni for use in nickel metal hydride batteries. *Journal of Alloys and Compounds, 337*(1), 208–213

Mohamed, N. S., and Arof, A. K. (2004). Conductivity studies of $LiCF_3SO_3$–doped and DMF–plasticized PVDF–based solid polymer electrolytes. *Physica Status Solidi (a), 201*(14), 3096–3101

Morita, R., Honda, R., and Takahashi, Y. (2000). Development of oral controlled release preparations, a PVA swelling controlled release system (SCRS), I. Design of SCRS and its release controlling factor. *Journal of Controlled Release, 63*(3), 297–304

Moseley, P. T., and Garche, J. (2014). *Electrochemical Energy Storage for Renewable Sources and Grid Balancing*: Elsevier

Moser, J. (1887). Notiz über die Verstärkung photoelectrischer Ströme durch optische Sensibilisierung. *Monatshefte für Chemie*, *8*, 373

Namba, S., and Hishiki, Y. (1965). Color Sensitization of Zinc Oxide with Cyanine Dyes. *The Journal of Physical Chemistry, 69*(3), 774–779

Nelson, R. (1965). Minority Carrier Trapping and Dye Sensitization. *The Journal of Physical Chemistry, 69*(3), 714–718

Noor, I. S., Majid, S. R., and Arof, A. K. (2013). Poly(vinyl alcohol)–LiBOB complexes for lithium–air cells. *Electrochimica Acta, 102*, 149–160

Noor, I. S. M., Majid, S. R., Arof, A. K., Djurado, D., Claro Neto, S., and Pawlicka, A. (2012). Characteristics of gellan gum–$LiCF_3SO_3$ polymer electrolytes. *Solid State Ionics, 225,* 649–653

O'regan, B., and Grätzel, M. (1991). A low–cost, high–efficiency solar cell based on dye sensitized colloidal TiO_2 films. *nature, 353*(6346), 737–740

Osman, Z., and Arof, A. K. (2003). FTIR studies of chitosan acetate based polymer electrolytes. *Electrochimica Acta, 48*(8), 993–999

Osman, Z., Isa, K. B. M., Othman, L., and Norlida, K. (2011). Studies of ionic conductivity and dielectric behavior in polyacrylonitrile based solid polymer electrolytes. *Defect and Diffusion Forum*, 312, 116–121

Pandey, K., Asthana, N., Dwivedi, M. M., and Chaturvedi, S. K. (2013). Effect of plasticizers on structural and dielectric behaviour of [PEO+ $(NH_4)_2C_4H_8(COO)_2$] polymer electrolyte. *Journal of Polymers, 2013,* 12

Park, N.–G., Chang, S.–H., van de Lagemaat, J., Kim, K.–J., and Frank, A. J. (2000). Effect of cations on the open–circuit photovoltage and the charge–injection efficiency of dye sensitized nanocrystalline rutile TiO_2 Films. *Bulletin–Korean Chemical Society, 21*(10), 985–988

Parthasarathy, M., Pillai, V. K., Mulla, I. S., Shabab, M., and Khan, M. I. (2007). 'All–solid–state' electrochemistry of a protein–confined polymer electrolyte film. *Biochemical and Biophysical Research Communications, 364*(1), 86–91

Perera, K., and Dissanayake, M. (2006). Conductivity variation of the liquid electrolyte, EC,PC,LiCF. *Sri Lankan Journal of Physics, 7*, 1–5

Peter, L. M. (2007). Dye sensitized nanocrystalline solar cells. *Physical Chemistry Chemical Physics, 9*(21), 2630–2642

Petrowsky, M., and Frech, R. (2008). Concentration dependence of ionic transport in dilute organic electrolyte solutions. *The Journal of Physical Chemistry B, 112*(28), 8285–8290

Ping, Z. H., Nguyen, Q. T., Chen, S. M., Zhou, J. Q., and Ding, Y. D. (2001). States of water in different hydrophilic polymers–DSC and FTIR studies. *Polymer, 42*(20), 8461–8467

Pramod, K. S., Kang–Wook, K., Nagarale, R. K., and Hee–Woo, R. (2009). Preparation, characterization and application of ionic liquid doped solid polymer electrolyte membranes. *Journal of Physics D, Applied Physics, 42*(12), 125101

Pramod, K. S., Nagarale, R. K., Pandey, S. P., Rhee, H. W., and Bhaskar, B. (2011). Present status of solid state photoelectrochemical solar cells and dye sensitized solar cells using PEO–based polymer electrolytes. *Advances in Natural Sciences, Nanoscience and Nanotechnology, 2*(2), 023002

Rahman, M. Y. A., Salleh, M. M., Talib, I. A., and Yahaya, M. (2004). Effect of ionic conductivity of a PVC–$LiClO_4$ based solid polymeric electrolyte on the performance of solar cells of ITO/TiO_2/PVC–$LiClO_4$/graphite. *Journal of Power Sources, 133*(2), 293–297

Rajendran, S., and Uma, T. (2000). Characterization of plasticized PMMA–$LiBF_4$ based solid polymer electrolytes. *Bulletin of Materials Science, 23*(1), 27–29

Rajkumar, T., and Ranga Rao, G. (2008). Investigation of hybrid molecular material prepared by ionic liquid and polyoxometalate anion. *Journal of Chemical Sciences, 120*(6), 587–594

Ramesh, S., and Wong, K. C. (2009). Conductivity, dielectric behaviour and thermal stability studies of lithium ion dissociation in poly(methyl methacrylate)–based gel polymer electrolytes. *Ionics, 15*(2), 249–254

Ramesh, S., Yahaya, A., and Arof, A. (2002). Dielectric behaviour of PVC–based polymer electrolytes. *Solid State Ionics, 152*, 291–294

Ramya, C. S., Savitha, T., Selvasekarapandian, S., and Hirankumar, G. (2005). Transport mechanism of Cu–ion conducting PVA based solid–polymer electrolyte. *Ionics, 11*(5–6), 436–441

Reddy, M. J., Sreekanth, T., and Rao, U. V. S. (1999). Study of the plasticizer effect on a (PEO+$NaYF_4$) polymer electrolyte and its use in an electrochemical cell. *Solid State Ionics, 126*(1–2), 55–63

Redmond, G., and Fitzmaurice, D. (1993). Spectroscopic determination of flatband potentials for polycrystalline titania electrodes in nonaqueous solvents. *The Journal of Physical Chemistry, 97*(7), 1426–1430

Reger, D., Goode, S., and Ball, D. (2009). *Chemistry, principles and practice*: Cengage Learning

Rofaiel, A., Ellis, J. S., Challa, P. R., and Bazylak, A. (2012). Heterogeneous through–plane distributions of polytetrafluoroethylene in polymer electrolyte membrane fuel cell gas diffusion layers. *Journal of Power Sources, 201*, 219–225

Said, S. M., Zulkifli, A. Z. S., Kamarudin, M. A., Mainal, A., Subramanian, B., and Mohamed, N. S. (2015). Polymer electrolyte liquid crystal system for improved optical and electrical properties. *European Polymer Journal, 66*, 266–272

Shi, Y., Wang, Y., Zhang, M., and Dong, X. (2011). Influences of cation charge density on the photovoltaic performance of dye sensitized solar cells, lithium, sodium, potassium, and dimethylimidazolium. *Physical Chemistry Chemical Physics, 13*(32), 14590–14597

Shuhaimi, N. E. A., Teo, L. P., Woo, H. J., Majid, S. R., and Arof, A. K. (2012). Electrical double–layer capacitors with plasticized polymer electrolyte based on methyl cellulose. *Polymer Bulletin, 69*(7), 807–826

Shukla, N., and Thakur, A. (2009). Role of salt concentration on conductivity optimization and structural phase separation in a solid polymer electrolyte based on PMMA–$LiClO_4$. *Ionics, 15*(3), 357–367

Sim, L. N., Majid, S. R., and Arof, A. K. (2012). FTIR studies of PEMA/PVdF–HFP blend polymer electrolyte system incorporated with $LiCF_3SO_3$ salt. *Vibrational Spectroscopy, 58*, 57–66

Singh, K. P., and Gupta, P. N. (1998). Study of dielectric relaxation in polymer electrolytes. *European Polymer Journal, 34*(7), 1023–1029

Singh, K. P., Singh, R. P., and Gupta, P. N. (1995). Polymer based solid state electrochromic display device using PVA complex electrolytes. *Solid State Ionics, 78*(3–4), 223–229

Singh, P. K., Bhattacharya, B., Mehra, R. M., and Rhee, H.–W. (2011). Plasticizer doped ionic liquid incorporated solid polymer electrolytes for photovoltaic application. *Current Applied Physics, 11*(3), 616–619

Singh, P. K., Kim, K.–W., Park, N.–G., and Rhee, H.–W. (2008a). Mesoporous nanocrystalline TiO_2 electrode with ionic liquid–based solid polymer electrolyte for dye–sensitized solar cell application. *Synthetic Metals, 158*(14), 590–593

Singh, P. K., Kim, K.–W., and Rhee, H.–W. (2008b). Electrical, optical and photoelectrochemical studies on a solid PEO–polymer electrolyte doped with low viscosity ionic liquid. *Electrochemistry Communications, 10*(11), 1769–1772

Snaith, H. J. (2010). Estimating the maximum attainable efficiency in dye–sensitized solar cells. *Advanced Functional Materials, 20*(1), 13–19

Somani, P. R., Marimuthu, R., Viswanath, A. K., and Radhakrishnan, S. (2003). Thermal degradation properties of solid polymer electrolyte (poly(vinyl alcohol)+phosphoric acid)/methylene blue composites. *Polymer Degradation and Stability, 79*(1), 77–83

Song, J., Wang, Y., and Wan, C. (1999). Review of gel–type polymer electrolytes for lithium–ion batteries. *Journal of Power Sources, 77*(2), 183–197

Subba Reddy, C. V., Han, X., Zhu, Q.–Y., Mai, L.–Q., and Chen, W. (2006). Dielectric spectroscopy studies on (PVP+PVA) polyblend film. *Microelectronic Engineering, 83*(2), 281–285

Subban, R., Ahmad, A., Kamarulzaman, N., and Ali, A. (2005). Effects of plasticiser on the lithium ionic conductivity of polymer electrolyte PVC–$LiCF_3SO_3$. *Ionics, 11*(5–6), 442–445

Sumathipala, H. H., Hassoun, J., Panero, S., and Scrosati, B. (2007). High performance PEO–based polymer electrolytes and their application in rechargeable lithium polymer batteries. *Ionics, 13*(5), 281–286

Świergiel, J., Płowaś, I., Grembowski, J., and Jadżyn, J. (2015). Stokes–Einstein–Nernst relation in dilute electrolyte solutions of lithium perchlorate in polyethylene glycols (200, 300, 400, and 600). *Journal of Chemical and Engineering Data,* 60(12), 3588-3593.

Sydney, U. o. (2009). Retrieved from https,//scilearn.sydney.edu.au/fychemistry/ calculators/ lattice_energy.shtml

Teo, L. P., Buraidah, M. H., Nor, A. F. M., and Majid, S. R. (2012). Conductivity and dielectric studies of Li_2SnO_3. *Ionics, 18*(7), 655–665

Thomas, P., Ernest Ravindran, R. S., and Varma, K. B. R. (2012). Dielectric properties of Poly(methyl methacrylate)(PMMA)/$CaCu_3Ti_4O_{12}$ composites. *Proceedings of the 10th International Conference on the Properties and Applications of Dielectric Materials (ICPADM),* 1–4. doi:10.1109/ICPADM.2012.6319009

Thomas, S., Deepak, T., Anjusree, G., Arun, T., Nair, S. V., and Nair, A. S. (2014). A review on counter electrode materials in dye sensitized solar cells. *Journal of Materials Chemistry A, 2*(13), 4474–4490

Thünemann, A. F. (2000). Dielectric relaxation of polyacrylonitrile in its pristine and cyclized stage. *Macromolecules, 33*(5), 1790–1795

Tipton, A. L., Lonergan, M. C., Ratner, M. A., Shriver, D. F., Wong, T. T. Y., and Han, K. (1994). Conductivity and dielectric constant of PPO and PPO–based solid electrolytes from Dc to 6 GHz. *The Journal of Physical Chemistry, 98*(15), 4148–4154

Trang, T., Lee, D., and Kim, J. (2013). Enhancing the ionic transport of PEO–based composite polymer electrolyte by addition of TiO_2 nanofiller for quasi–solid state dye–sensitized solar cells. *Metals and Materials International, 19*(6), 1369–1372

Tripathi, S., Mehrotra, G. K., and Dutta, P. K. (2009). Physicochemical and bioactivity of cross–linked chitosan–PVA film for food packaging applications. *International Journal of Biological Macromolecules, 45*(4), 372–376

Tsubomura, H., Matsumura, M., Nomura, Y., and Amamiya, T. (1976). Dye sensitised zinc oxide, aqueous electrolyte, platinum photocell. *Nature,* 261, 402–103

Van Schalkwijk, W., and Scrosati, B. (2002). *Advances in lithium–ion batteries*: Springer Science & Business Media

Walsh, D., and Zoller, P. (1995). *Standard pressure volume temperature data for polymers*: CRC Press

Wang, S., Qiu, W., Li, T., Yu, B., and Zhao, H. (2006). Properties of lithium bis (oxalato) borate (LiBOB) as a lithium salt and cycle performance in $LiMn_2O_4$ half cell. *International Journal of Electrochemical Science, 1*, 250–257

Wang, Z. S., Kawauchi, H., Kashima, T., and Arakawa, H. (2004). Significant influence of TiO_2 photoelectrode morphology on the energy conversion efficiency of N719 dye–sensitized solar cell. *Coordination chemistry reviews*, 248(13), 1381–1389.

Watson, D. F., and Meyer, G. J. (2004). Cation effects in nanocrystalline solar cells. *Coordination Chemistry Reviews, 248*(13–14), 1391–1406

Weissermel, K., and Arpe, H. (1978). I*ndustrial Organic Chemistry, Important Raw Materials and Intermediates*, Germany: Wiley–VCH Verlag GmbH

Wright, P. V. (1975). Electrical conductivity in ionic complexes of poly(ethylene oxide). *British Polymer Journal, 7*(5), 319–327

Xiaomei, L., Xinli, Z., Kequan, L., Xiaodan, Z., Jianming, Y., Yiqiang, W., Sha, L., and Shoulu, Y. (2012). PVA wood adhesive modified with sodium silicate cross–linked copolymer. *Proceedings of the International Conference on Biobase Material Science and Engineering (BMSE)*, 108–111. doi:10.1109/BMSE.2012. 6466192

Xu, K., Zhang, S., Poese, B. A., and Jow, T. R. (2002). Lithium bis (oxalato) borate stabilizes graphite anode in propylene carbonate. *Electrochemical and Solid–State Letters, 5*(11), A259–A262

Xu, K., Zhang, S. S., Lee, U., Allen, J. L., and Jow, T. R. (2005). LiBOB, Is it an alternative salt for lithium ion chemistry? *Journal of Power Sources, 146*(1–2), 79–85

Xu, W., and Angell, C. A. (2001). Weakly coordinating anions, and the exceptional conductivity of their nonaqueous solutions. *Electrochemical and Solid–State Letters, 4*(1), E1–E4

Xu, W., Shusterman, A. J., Videa, M., Velikov, V., Marzke, R., and Angell, C. A. (2003). Structures of orthoborate anions and physical properties of their lithium salt nonaqueous solutions. *Journal of the Electrochemical Society, 150*(1), E74–E80

Yang, C. R., Perng, J. T., Wang, Y. Y., and Wan, C. C. (1996). Conductive behaviour of lithium ions in polyacrylonitrile. *Journal of Power Sources, 62*(1), 89–93

Yang, R. Y., Chen, H. Y., and Lai, F. D. (2012). Performance degradation of dye–sensitized solar cells induced by electrolytes. *Advances in Materials Science and Engineering*, Volume 2012, Article ID 902146, 4 pages

Yella, A., Lee, H.–W., Tsao, H. N., Yi, C., Chandiran, A. K., Nazeeruddin, M. K., Diau, E. W.–G., Yeh, C.–Y., Zakeeruddin, S. M., and Grätzel, M. (2011). Porphyrin–sensitized solar cells with cobalt (II/III)–based redox electrolyte exceed 12 percent efficiency. *Science, 334*(6056), 629–634

Yin, Y., Zhou, J., and Zhou, X. (2009). Preparation and characterization of mediator doped PEO/$LiAlO_2$/SiO_2 solid polymer electrolyte. *ECS Transactions, 19*(30), 1–8

Yoshikawa, M., Ooi, T., and Izumi, J. I. (1999). Alternative molecularly imprinted membranes from a derivative of natural polymer, cellulose acetate. *Journal of Applied Polymer Science, 72*(4), 493–499

Young, N. P., Devaux, D., Khurana, R., Coates, G. W., and Balsara, N. P. (2014). Investigating polypropylene–poly(ethylene oxide)–polypropylene triblock copolymers as solid polymer electrolytes for lithium batteries. *Solid State Ionics, 263*, 87–94

Yu, H., Wu, J., Fan, L., Xu, K., Zhong, X., Lin, Y., and Lin, J. (2011). Improvement of the performance for quasi–solid–state supercapacitor by using PVA–KOH–KI polymer gel electrolyte. *Electrochimica Acta, 56*(20), 6881–6886

Zafer, C., Ocakoglu, K., Ozsoy, C., and Icli, S. (2009). Dicationic bis–imidazolium molten salts for efficient dye sensitized solar cells, Synthesis and photovoltaic properties. *Electrochimica Acta, 54*(24), 5709–5714

Zaidi, S. J. (2009). Research trends in polymer electrolyte membranes for PEMFC. In Zaidi, S.J., and Matsuura, T., *Polymer membranes for fuel cells* (pp. 7–25): Springer

Zgârian, R. G., Tihan, G. T., Kajzar, F., Rău, I., Pawlicka, A., and Mîndroiu, M. V. (2015). Chromophore doped DNA based solid polymer electrolyte for electrochromic devices. *Arabian Journal of Chemistry,* 1–8, http,//dx.doi.org/10.1016/j.arabjc.2015.08.007

LIST OF PUBLICATIONS AND PAPER PRESENTED

Publications

1. I.S. Noor, S.R. Majid, A.K. Arof, Poly(vinyl alcohol)–LiBOB complexes for lithium–air cells, *Electrochimica Acta*, 102 (2013) 149–160. (ISI/SCOPUS Cited Publication) [Impact Factor = 4.803]

2. A.K. Arof, S. Amirudin, S.Z. Yusof, I.M. Noor, A method based on impedance spectroscopy to determine transport properties of polymer electrolytes, *Physical Chemistry and Chemical Physics*, 16 (2014) 1856–1867. (ISI/SCOPUS Cited Publication) [Impact Factor = 4.449]

3. Mimi Hayati Abdul Rahaman, Mayeen Uddin Khandaker, Ziaul Raza Khan, Mohd Zieauddin Kufian, Ikhwan Syafiq Mohd Noor, Abdul Kariem Arof, Effect of gamma irradiation on poly(vinyledenedifluoride)–lithium bis(oxalato)borate electrolyte, *Physical Chemistry and Chemical Physics*, 16 (2014) 11527. (ISI/SCOPUS Cited Publication). [Impact Factor = 4.449]

4. I.S.M. Noor, S.R. Majid, A.K. Arof, D. Djurado, S. Claro Neto, A. Pawlicka, Characteristics of gellan gum–$LiCF_3SO_3$ polymer electrolytes, *Solid State Ionics*, 225 (2012) 649–653.(ISI/SCOPUS Cited Publication) [Impact Factor = 2.380]

5. M.F. Aziz, I.M. Noor, B. Sahraoui, A.K. Arof, Dye sensitized solar cells with PVA–KI–EC–PC gel electrolytes, *Optical and Quantum Electronics*, 46 (2014) 133–141. (ISI/SCOPUS Cited Publication). [Impact Factor = 1.290]

6. I.A. Fadzallah, I.M. Noor, M.A. Careem, A.K. Arof, Investigation of transport properties of chitosan–based electrolytes utilizing impedance spectroscopy, *Ionics*, (2016) DOI: 10.1007/s11581-016-1687-0 (ISI/SCOPUS Cited Publication). [Impact Factor = 2.119]

7. M.F. Aziz, I.M. Noor, M.H. Buraidah, M.A. Careem, A.K. Arof, PVA–based gel polymer electrolytes doped with $(CH_3)_4NI/KI$ for application in dye–sensitized solar cells, *15th International Conference on Transparent Optical Networks (2013)* art. no. 6602906. (ISI/SCOPUS Cited Publication).

8. J. Jaglarza, K. Marszalek, R. Duraj, I.M. Noor, A.K. Arof, N. Wolska, Z. Sofiani, Elastic scattering phenomena in thin polymer layers, *Materials Today: Proceedings*, 3S(2016) S57–S64. (ISI/SCOPUS Cited Publication).

Paper Presented

1. I.M. Noor, N.A. Mat Nor, N.R. Ramli, N. Aziz, R.M. Taha, A.K. Arof, Utilization of saffron (*Crocus sativus L.*) as sensitizer in dye–sensitized solar cells, *International Symposium New Tendencies of Developing Fundamental and Applied Physics: Problems, Achievements, Prospectives*, Tashkent, Uzbekistan, 10 and 11 November 2016. (International)

2. I.M. Noor, L. Shamsuddin, A.K. Arof, Perovskite solar cells using polymer electrolytes, *14th International Conference on Frontiers of Polymers and Advanced Materials (ICFPAM 2016)*, Daejeon, South Korea, 31 October to 4 November 2016. (International)

3. I.M. Noor, L. Shamsuddin, A.K. Arof, Perovskite solar cell using PVA based polymer electrolyte as electrons medium transport, *International Conference on Functional Materials (ICFM 2016)*, Tirunelveli, Tamilnadu, India, 7–10 September 2016. (International)

4. I.M. Noor, A.K. Arof, An improved method to determine transport properties of gel polymer electrolyte that can be represented by a series connection of a resistor and leaky capacitor, *5th International Conference on Functional Materials and Devices (ICFMD 2015)*, Johor Bahru, Malaysia, 4–6 August 2015. (International)

5. I.M. Noor, A.A.A. Kariem, N.A. Mat Nor, N. Aziz, R.M, Taha, A.K. Arof, Application of saffron as dye materials in dye sensitized solar cells, *5th International Conference on Functional Materials and Devices (ICFMD 2015)*, Johor Bahru, Malaysia, 4–6 August 2015. (International)

6. I.M. Noor, M.A.A. Shahrom, B. Sahraoui, A.K. Arof, PVdF–HFP complexes Mg triflate gel polymer electrolyte and application in electrical double layer capacitor, *13thInternational Conference on Frontiers of Polymers and Advanced Materials (ICFPAM 2015)*, Marrakesh, Morocco, 30 March to 2 April 2015. (International)

7. I.M. Noor, M.A. Careem, A.K. Arof, Dye sensitized solar cells with poly(vinyl alcohol) based gel polymer electrolyte containing lithium bis(oxalato)borate salt *XIV International Symposium on Polymer Electrolyte 2014 (ISPE14)*, Geelong, Australia, 24–29 August 2014. (International)

8. I.M. Noor, S.R. Majid, A.K. Arof, Electrical properties of gellan gum–lithium triflate solid polymer electrolyte with ionic liquid, *International Conference on Science & Engineering of Materials (ICSEM 2014)*, Greater Noida, India, 6–8 January 2014. (International)

9. I.M. Noor, M.H. Buraidah, B. Sahraoui, A.K. Arof, Effect of butyl– and pentyl–quinolinium bromide in dye sensitized solar cells applications, *12th International Conference on Frontiers of Polymers and Advanced Materials (ICFPAM 2013)*, Auckland, New Zealand, 8–13 December 2013. (International)

10. M.F. Aziz, I.M. Noor, M.H. Buraidah, M.A. Careem, A.K. Arof, PVA–based gel polymer electrolytes doped with $(CH_3)_4NI/KI$ for application in dye–sensitized solar cells, *15th International Conference on Transparent Optical Networks (ICTON 2013)*, Cartagena, Spain, 23–27 June 2013. (International)

11. I.M. Noor, S.R. Majid, A.K. Arof, Effect of ionic liquid on electrical properties of gellan gum–lithium triflate solid polymer electrolyte, *4th International Conference on Functional Materials and Devices (ICFMD 2013)*, Penang, Malaysia, 8–11 April 2013. (International)

12. M.F. Aziz, I.M. Noor, B. Sahraoui, A.K. Arof, Dye sensitized solar cells with PVA–KI–EC–PC gel electrolytes, *13th International Conference on Advanced Materials for Photonics, Sensing And Energy Conversion Energy Applications (AMPSECA)*, El Jadida, Morocco, 5–7 December 2012. (International)